NANOCOMPOSITES BASED ON BLENDS OF POLYSTYRENE

A THESIS SUBMITTED TO
THE GRADUATE SCHOOL OF NATURAL AND APPLIED SCIENCES
OF
MIDDLE EAST TECHNICAL UNIVERSITY

BY

ALİ SİNAN DİKE

IN PARTIAL FULFILLMENT OF THE REQUIREMENTS
FOR
THE DEGREE OF DOCTOR OF PHILOSOPHY
IN
POLYMER SCIENCE AND TECHNOLOGY

JUNE 2011

Approval of the thesis:

NANOCOMPOSITES BASED ON BLENDS OF POLYSTYRENE

submitted by **ALİ SİNAN DİKE** in partial fulfillment of the requirements for the degree of **Doctor of Philosophy in Polymer Science and Technology, Middle East Technical University** by,

Prof. Dr. Canan Özgen   _____
Dean, Graduate School of **Natural and Applied Sciences**

Prof. Dr. Necati Özkan   _____
Head of Department, **Polymer Science and Technology**

Prof. Dr. Ülkü Yılmazer   _____
Supervisor, **Chemical Engineering Dept., METU**

Examining Committee Members:

Prof. Dr. Erdal Bayramlı   _____
Chemistry Dept., METU

Prof. Dr. Ülkü Yılmazer   _____
Chemical Engineering Dept., METU

Prof. Dr. Cevdet Kaynak   _____
Metallurgical and Materials Engineering Dept., METU

Prof. Dr. Göknur Bayram   _____
Chemical Engineering Dept., METU

Assist. Prof. Dr. Güralp Özkoç   _____
Chemical Engineering Dept., Kocaeli University

Date: June 14, 2011

I hereby declare that all information in this document has been obtained and presented in accordance with academic rules and ethical conduct. I also declare that, as required by these rules and conduct, I have fully cited and referenced all material and results that are not original to this work.

Name, Last name : Ali Sinan Dike

Signature

ABSTRACT

NANOCOMPOSITES BASED ON BLENDS OF POLYSTYRENE

Dike, Ali Sinan

PhD, Department of Polymer Science and Technology

Supervisor: Prof. Dr. Ülkü Yılmazer

June 2011, 189 pages

Due to brittleness of polystyrene, PS, its usage area is restricted. To solve this problem and expand the usage area of PS, it can be blended and impact modified with an elastomeric material. In this study, the decrease in the modulus and tensile strength imparted by impact modification was overcome by reinforcing this mixture by incorporating organoclays and producing nanocomposites.

This study consists of two parts. In the first part of this study three different types of aliphatic elastomeric materials and three different types of organoclays were used and their effects on the morphology, mechanical, thermal, and rheological properties of PS were investigated. Lotader AX8900, Lotader AX8840 and Lotader 2210 were chosen as the aliphatic elastomeric compatibilizers; and Cloisite® 15A, Cloisite® 25A and Cloisite® 30B were chosen as the organoclays. Organoclay content was kept at 2% and elastomer content was kept at 5% throughout the first part of the study.

In the second part of this study, an aromatic elastomer; Styrene-Butadiene-Styrene rubber, SBS, was chosen as the elastomeric compatibilizer and maleic anhydride was grafted onto SBS rubber at different ratios. Grafting was made by means of a co-rotating twin screw extruder. Cloisite® 30B was used as the organoclay. In order to investigate the effects of organoclay addition on the

properties of the PS and PS / Elastomer blends, PS / Elastomer blends were also prepared and their properties were also investigated. Clay content was varied between 0% and 4%, and the elastomer content was varied between 0% and 40% throughout the second part of the study. All samples were prepared by a co-rotating twin screw extruder, followed by injection molding at appropriate conditions.

In order to investigate the state of dispersion and the basal spacings of the organoclays in the PS matrix, XRD analyses were carried out. No significant improvement was observed on the basal spacing of the nanocomposites prepared in the first part of the study, but nanocomposites prepared in the second part of the study exhibited intercalated or exfoliated structures.

In order to investigate the average domain sizes of the elastomeric phases, SEM analyses were carried out. To remove the elastomeric phase from the PS matrix, etching was done with n-Heptane in an ultrasonic bath at room temperature. Average domain sizes increased as the elastomer content increased in the binary blends and ternary nanocomposites.

In order to investigate the flow behaviour of the raw materials and the samples prepared throughout this study, MFI tests were carried out. In the first part of the study, addition of elastomer and organoclay decreased the MFI values, as expected. Although both PS and elastomeric materials used in the second part of the study have similar MFI values, samples prepared with these materials exhibited higher MFI values than both of the polymers.

In order to investigate the effects of the compatibilizer type, organoclay type, and concentration of materials on the mechanical properties of the prepared samples, tensile and unnotched Charpy impact tests were performed. Due to incompatibility of the elastomeric phase with the PS matrix, no significant improvement was observed in tensile properties of the nanocomposites prepared in the first part of this study. In the second part of the study, the aromatic elastomers enhanced the intercalation / exfoliation of clay layers resulting in higher tensile strength, modulus, elongation at break and impact strength with respect to neat PS.

In order to observe the effects of organoclay and elastomer addition on the thermal properties of blends and nanocomposites prepared in this study, Differential Scanning Calorimetry analyses were done. By this analysis, glass transition temperature, T_g was measured. Elastomer addition increased the T_g of the samples, whereas organoclay addition did not affect the T_g significantly.

Keywords: Polystyrene, maleic anhydride, organoclay, nanocomposites, extrusion

ÖZ

POLİSTİREN ALAŞIMLARI BAZLI NANOKOMPOZİTLER

Dike, Ali Sinan

Doktora, Polimer Bilim ve Teknolojisi

Tez Yöneticisi: Prof. Dr. Ülkü Yılmazer

Haziran 2011, 189 sayfa

Polistirenin (PS) kırılganlığı nedeni ile kullanım alanı sınırlıdır. Bu sorunu çözmek ve polistirenin kullanım alanını genişletmek için PS elastomerik bir malzeme ile karıştırılabilir ve darbe dayanımı modifiye edilebilir. Bu çalışmada, darbe modifikasyonu nedeni ile Young modülü ve gerilme dayanımında meydana gelen azalmanın üstesinden bu karışıma organokil ilave edilip ve nanokompozit üretip karışımı güçlendirerek gelindi.

Bu çalışma iki kısımdan oluşur. Çalışmanın ilk kısmında üç farklı alifatik elastomerik malzeme ve üç farklı organokil kullanıldı ve onların polistirenin yapısal, mekanik, termal ve reolojik özellikleri üzerindeki etkileri incelendi. Lotader AX8900, Lotader AX8840 ve Lotader 2210 alifatik elastomerik uyumlaştırıcılar olarak seçildi ve Cloisite ® 15A, Cloisite ® 25A ve Cloisite ® 30B organokil olarak seçildi. Çalışmanın ilk kısmının tamamında organokil miktarı 2% ve elastomer miktarı 5% olarak korundu.

Çalışmanın ikinci kısmında aromatik bir elastomer, Stiren-Bütadien-Stiren kauçuğu; SBS, elastomerik uyumlaştırıcı olarak seçildi ve SBS kauçuğu üzerine değişik oranlarda maleik anhidrit aşılandı. Aşılama vidaları aynı yönde dönen çift vidalı ekstruder yardımı ile yapıldı. Organokil olarak Cloisite® 30B kullanıldı.

Organokilin PS ve PS / Elastomer alaşımları üzerindeki etkilerini incelemek için PS / Elastomer alaşımları da hazırlandı ve onların özellikleri de incelendi. Çalışmanın ikinci kısmının tamamında kil içeriği 0% ile 4% arasında, elastomer içeriği 0% ile 40% arasında değiştirildi. Bütün numuneler uygun koşullarda, vidaları aynı yönde dönen çift vidalı ekstruderde hazırlandı ve ardından enjeksiyonlu kalıplama işlemi uygulandı.

Organokillerin PS matriksi içindeki dağılım durumunu ve kil tabakalarının aralıklarını incelemek için X ışınları kırınımı analizleri yapıldı. Çalışmanın ilk kısmında hazırlanan nanokompozitlerin tabaka aralıklarında önemli bir artış gözlenmedi fakat çalışmanın ikinci kısmında hazırlanan nanokompozitler araya girmiş ve yapraklanmış yapılar sergilediler.

Elastomerik fazların ortalama alan boyutlarını incelemek için taramalı elektron mikroskopu analizleri yapıldı. Elastomerik fazı PS matriksinden uzaklaştırmak için ultrasonik banyoda oda sıcaklığında n-Heptan ile aşındırma yapıldı. İkili alaşımlar ve üçlü nanokompozitlerin elastomer içeriği arttıkça ortalama alan boyutu büyüdü.

Bu çalışmada kullanılan hammadde ve hazırlanan numunelerin akış davranışlarını incelemek için eriyik akış indeksi testi uygulandı. Çalışmanın ilk kısmında elastomer ve organokil ilavesi eriyik akış indeksi değerlerini beklenildiği şekilde düşürdü. Çalışmanın ikinci kısmında kullanılan PS ve elastomerik malzemeler benzer eriyik akış indeksi değerlerine sahip olmalarına ragmen bu malzemelerle hazırlanan numuneler bu malzemelerin her ikisinden daha yüksek eriyik akış indeksi değeri sergilediler.

Uyumlaştırıcı tipi, organokil tipi ve malzemelerin konsantrasyonunun hazırlanan malzemelerin mekanik özellikleri üzerindeki etkilerini incelemek için çekme ve çentiksiz Charpy darbe testleri yapıldı. Elastomerik fazın PS matriksi ile uyumsuzluğu nedeni ile çalışmanın ilk kısmında hazırlanan nanokompozitlerin gerilme özelliklerinde önemli bir artış gözlenmedi. Çalışmanın ikinci kısmında aromatik elastomerler kil tabakalarını araya girmiş / yapraklanmış hale getirerek daha yüksek gerilme dayanımı, modül, kopmada uzama ve darbe dayanımı değerlerine sebep oldu.

Organokil ve elastomer ilavesinin bu çalışmada hazırlanan alaşım ve nanokompozitlerin ısısal özellikleri üzerindeki etkilerini incelemek için Diferansiyel Taramalı Kalorimetri Analizi yapıldı. Bu analiz yoluyla camsı geçiş sıcaklığı, T_g ölçüldü. Elastomer ilavesi örneklerin camsı geçiş sıcaklığını arttırdı fakat organokil ilavesi camsı geçiş sıcaklığını önemli derecede etkilemedi.

Anahtar Kelimeler: Polistiren, maleik anhidrit, organik kil, nanokompozitler, ekstrüzyon

To the light of the life.

ACKNOWLEDGEMENTS

TABLE OF CONTENTS

LIST OF TABLES

LIST OF FIGURES

FIGURES

xix

NOMENCLATURE

A_i Area of a domain in SEM analysis, μm^2

A_0 Initial cross sectional area, mm^2

d   Interlayer spacing, Å

d_{av} Average domain size, nm

D   Distance between grips of tensile test specimen, mm

D   Extruder barrel diameter, mm

E   Young's Modulus, MPa

F   Instantaneous load, N

L   Extruder barrel length, mm

L   Total length of impact test specimen, mm

L   Overall length of tensile test specimen, mm

L_c Capillary tube length, mm

L_0 Initial gauge length, mm

n   Order of diffraction peak

n   Rabinowitsch correction factor

n_i Number of domains analyzed in SEM analysis

Q   Volumetric flow rate, $mm^3.s^{-1}$

R_c Capillary tube radius, mm

T   Thickness of tensile and impact test specimen, mm

T_g Glass Transition Temperature, ºC

T_m Melting Temperature, ºC

T_c Crystallization Temperature, ºC

W   Width of narrow section of tensile test specimen, mm

Greek Letters

σ Engineering stress, MPa

σ_m Tensile strength, MPa

ε Engineering strain, mm/mm

θ Scattering angle, º

λ Wavelength, nm

η_i Melt viscosity of component i, Pa.s

ϕ_i	Volume fraction of component i
η_{hv}	Melt viscosity of high viscosity component i, Pa.s
ϕ_{hv}	Volume fraction of high viscosity component i
η_{lv}	Melt viscosity of low viscosity component, Pa.s
ϕ_{lv}	Volume fraction of low viscosity component i
Γ	Apparent shear rate, s^{-1}
Y	True shear rate, s^{-1}
μ	Viscosity of Newtonian fluids, Pa.s
τ_{wall}	Shear stress at tube wall, Pa
ΔP	Pressure drop across capillary tube, Pa

Abbreviations

CEC	Cation Exchange Capacity
DSC	Differential Scanning Calorimetry
DTA	Differential Thermal Analysis
E-BA-GMA	Ethylene-b-Butyl Acrylate-b-Glycidyl Methacrylate
GMA	Glycidyl Methacrylate
ISO	International Organization for Standardization
MAH	Maleic Anhydride
MFI	Melt Flow Index
MMT	Montmorillonite
MT2EtOH	Methyl, tallow, bis-2-hydroxyethyl quaternary ammonium
OH	Hydroxyl
OPS	Poly (styrene-co-vinyloxazolin)
PA12	Polyamide 12
PA66	Polyamide 66
PMMA	Poly (methyl methacrylate)
PS	Polystyrene
SAXS	Small Angle X-Ray Scattering
SBS	Styrene-Butadiene-Styrene
SBSgMAH	Maleic Anhydride grafted Styrene-Butadiene-Styrene
SEM	Scanning Electron Microscopy
TEM	Transmission Electron Microscopy
TG	Thermogravimetry

WAXS	Wide Angle X-Ray Scattering
XRD	X-Ray Diffraction
15A	Cloisite® 15A
25A	Cloisite® 25A
30B	Cloisite® 30B
2MHTL8	Di-methyl, hydrogenated tallow, 2-ethylhexyl quaternary ammonium
2M2HT	Di-methyl, di-hydrogenated tallow quaternary ammonium

CHAPTER 1

INTRODUCTION

Composite materials are engineered materials made from two or more constituent materials with significantly different physical or chemical properties which remain separate and distinct on a macroscopic level within the finished structure.

Composite materials are made up of individual materials referred to as constituent materials. There are two categories of constituent materials: matrix and reinforcement. At least one portion of each type is required. The matrix material surrounds and supports the reinforcement materials by maintaining their relative positions. The reinforcements impart their special mechanical and physical properties to enhance the matrix properties. A synergism produces material properties unavailable from the individual constituent materials, while the wide variety of matrix and strengthening materials allows the designer of the product or structure to choose an optimum combination.

Polymers are widely used as matrix materials for producing composites, which are lightweight materials with high strength and modulus values. Since their processing is relatively simple and does not require very high temperatures and pressures, polymers are preferred as matrix materials. Beside this, problems associated with the degradation of the reinforcement material during manufacture are less significant for polymer matrix composites -PMC's- than for composites with other matrices, such as ceramic and metal. Design flexibility, variety of processing techniques for producing PMC parts and relative cheapness of polymers with respect to other materials are also advantages of these materials.

Nanocomposites are a class of plastic compounds containing well dispersed and exfoliated nanofillers such as nanoclays. Nanocomposites exhibit unique performance profiles such as stiffness/impact balance or transparent barrier

properties. Due to the structural properties gained by well dispersion of the nanosized fillers, nanocomposites possess highly improved mechanical, thermal, physical, and barrier properties when compared to pristine polymer and conventional composites [1].

Layered silicates are widely used in nanocomposites as inorganic fillers, and they have high aspect ratios. Material properties improve significantly in the case of well dispersion of the silicate layers throughout the polymer matrix owing to interaction of the filler and polymer.

Montmorillonite which belongs to the general family of 2:1 layered silicates is the most commonly used smectite clay in nanocomposites. The structure of montmorillonite consists of an octahedral alumina sheet between two tetrahedral silica sheets. The layer thickness of the crystal structure is around 1 nm, and the lateral dimensions of these layers may be in the range of 30 nm to several microns or larger [2]. Natural montmorillonite is a quite hydrophilic material, thus it is incompatible with many hydrophobic engineering polymers. So the layered silicates are not easily dispersed in most polymers. In order to overcome this problem, a simple cation exchange process is applied to montmorillonite to make the clay organophilic.

Polystyrene (PS) is one of the most widely used kinds of plastic and made from the aromatic monomer styrene, a liquid hydrocarbon that is commercially manufactured from petroleum by the chemical industry. PS is a brittle thermoplastic material and used in disposable cutlery, plastic models, CD and DVD cases, and smoke detector housings. Products made from foamed polystyrene are used in many applications, for example packing materials, insulation, and foam drink cups.

In order to provide well dispersion of organoclay in polystyrene matrix, a third material may be used in nanocomposites, called compatibilizer. There are many studies in the literature that emphasize the effect of the compatibilizer on dispersion of organoclay in the polymer matrix [3-13].

In order to prepare nanocomposites three main processes are used: In-situ intercalative polymerization method, solution intercalation method and melt intercalation method. Among these methods, melt intercalation method is relatively simple and more environmentally-friendly than the others, because of the absence of organic solvents. Thus, it is the mostly used method for commercial applications [14]. In melt intercalation method, above the glass transition or melting temperature of the polymer matrix, the molten polymer chains diffuse into the clay galleries leading to three types of structures. If the clay platelets remain as large stacks and no polymer chains get inserted between the layers, the material is called "conventional composite". The polymer chains may be inserted between the clay layers without deteriorating the well ordered structure of the particles, and these types of composites are called as "intercalated" nanocomposites. In "exfoliated" nanocomposites, the clay particles are completely dispersed in the polymer matrix. In this study, nanocomposites were prepared by melt intercalation method [15-16]. A co-rotating twin screw extruder was used for preparing nanocomposites.

The aim of this study is to investigate the effects of compatibilizer type, organoclay type, and grafted maleic anhydride ratio on the morphology, mechanical, thermal and rheological properties of polystyrene. Three types of compatibilizers, terpolymer of ethylene–methyl acrylate–glycidyl methacrylate (E-MA-GMA), copolymer of ethylene-glycidyl methacrylate (E-GMA), and terpolymer of ethylene–n-butyl acrylate–maleic anhydride (E-nBA-MAH), and organoclays, Cloisite® 15A, Cloisite® 25A and Cloisite® 30B were used during the first stage of the experiments. Then, SBS, 1% maleic anhydride grafted SBS, and 2% maleic anhydride grafted SBS were used as compatibilizers and Cloisite® 30B was used as the organoclay during the second stage of the experiments.

In first stage, PS/compatibilizer blends containing 5%, 10% or 15% compatibilizer and PS/organoclay nanocomposites containing 2% organoclay were prepared. Then, ternary nanocomposites containing 5% compatibilizer and 2% organoclay were produced by means of a co-rotating twin screw extruder.

In second stage, maleic anhydride was grafted onto SBS at 1% w/w and 2% w/w ratios. Then, PS/SBS, PS/ SBS-g-MA (1%) and PS/ SBS-g-MA (2%) blends were prepared by melt compounding method. Finally, PS/SBS/Clay, PS/SBSgMA

(1%)/Clay and PS/SBS-g-MA(2%)/Clay nanocomposites were prepared by melt compounding method. In order to characterize the nanocomposites, all standard test specimens were prepared by injection molding.

Transmission Electron Microscopy (TEM) and X-Ray Diffraction (XRD) analyses were performed in order to observe the dispersion of the organoclay in the matrix. Scanning Electron Microscopy (SEM) analysis was performed to observe the dispersion of elastomeric phase and effects of organoclay on domain sizes. Thermal characterization of the nanocomposites was performed by Differential Scanning Calorimetry (DSC). Flow properties were determined with Melt Flow Index (MFI) measurements, viscosity of the raw materials were observed at different shear rates by capillary viscometer. Mechanical characterization of the nanocomposites was performed by tensile and impact tests.

CHAPTER 2

BACKGROUND

2.1 Composites

A composite is a material which is made up of two or more distinct materials differing in form or composition on a macroscale. A familiar composite is concrete, which is basically made up of sand and cement. Many common materials can be classified as composites. Materials are combined with each other to produce new materials that exhibit the positive characteristics of both of their components.

Composites usually consist of matrix and reinforcement phases. Matrix phase is the continuous part of the composite. This phase acts as a binder, which holds components together, and the main load-bearing constituent, so it governs the mechanical properties of the materials. Reinforcement phase is dispersed in the continuous phase. The final properties of the composites depend on not only the properties of each phase but also on the relative amounts of the constituents, the geometry of the dispersed phase which includes the shape, particle size, orientation and dispersion of reinforcing material, as well as on the reinforcement-matrix interface [17].

Classification of composites can be made according to the matrix material that they are made up of. The matrix can be metal, ceramic, polymer, etc. In composites with metal matrix, reinforcement improves specific stiffness, strength, abrasion resistance, creep resistance, thermal conductivity and dimensional stability. Also, their resistance to degradation, non-flammability and operating temperatures can be enhanced by organic fluids. In ceramic matrix composites, fibers are incorporated into the matrix to preserve the high processing temperature and the composites have inherent resilience to oxidation and deterioration [17].

2.1.1 Polymer Matrix Composites

In composite manufacturing, polymers are widely used as the matrix material. Polymer matrix composites contain inorganic and organic additives. These additives have certain geometries, such as fibers, flakes, spheres and particulates. Polymers have many advantages over other types of matrix materials. They are preferred because of their lightweight, and the processing cost is low.

As matrix materials, polymers can be classified into two categories depending on the behavior upon heating: thermoplastics and thermosets. Although thermoplastics can be repeatedly softened and reshaped by heat, thermosets can not be reshaped once cure reaction has been completed. Thermoplastics have two dimensional (linear or branched) structure and they are soluble in appropriate solvents. However, thermosets have three dimensional network structures and due to crosslinks between main chains they are insoluble.

2.2 Nanocomposites

The nanocomposite term can be defined as a two-phase material in which one of the phases is dispersed in the second one at a nanometer (10^{-9}m) level. Polymer nanocomposites are mineral-filled plastics that contain relatively small amounts (usually <10% w/w) of nanometer-sized inorganic particles [18]. Because of their enhanced thermal and mechanical properties, low permeability and flammability values they are widely used in automotive, aerospace, telecommunication, housing, coating, electronic and packing industries [19].

Nanocomposites can be classified depending on how many dimensions of the dispersed particles are in the nanometer range: Isodimensional, two-dimensional and one-dimensional.
A nanoparticle is called as isodimensional if three dimensions of nanoparticle are in the order of nanometers. Spherical silica nanoparticles are one example of this group. When two dimensions of the nanoparticle are in the nanometer scale and the third is larger, it is called as two-dimensional nanoparticle and it forms an

elongated structure, such as nanotubes or whiskers. The third type of nanoparticle is the one-dimensional nanoparticle and in this type, the nanoparticle has a very high aspect ratio owing to a few nanometer thickness, to hundreds to thousands nanometers of length. Graphite, carbon oxides, metal phosphates, clays and layered silicates are some examples of fillers used in producing nanocomposites [2].

This study is based on the polymer-layered silicate nanocomposites which belong to this third class.

2.2.1. Polymer – Clay Nanocomposites

Polymer - clay nanocomposite can be defined as a polymer or copolymer having dispersed exfoliated individual platelets obtained from an intercalated layered material [20]. Over the past decade, polymer – clay nanocomposites have attracted considerable interest in both academia and industry, owing to their outstanding mechanical properties like stiffness, strength, and modulus with only a small amount of the nanoadditives. This is caused by the large surface area to volume ratio of nanoadditives when compared to micro- and macro-additives [21].

2.2.2. Layered Silicates

In order to enhance the physical properties of a polymeric matrix or to lower the cost, fillers are used. These fillers are divided into two groups: High aspect ratio fillers and low aspect ratio fillers. Mica, glass fibers, clay minerals and carbon nanotubes belong to the high aspect ratio group and talc, kaolin, glass spheres belong to the low aspect ratio group.

Layered silicates belong to the structural group of 2:1 phyllosilicates, which is an undergroup of smectites. Natural clay minerals such as montmorillonite, hectorite and saponite and synthetic layered minerals like fluorohectorite, laponite or magadiite belong to this group [22]. Crystal lattices of clay minerals are generated by a combination of tetrahedral and octahedral sheets. In order to form 2:1 layered silicates, a natural stacking of those tetrahedral and octahedral sheets occurs in specific ratios and modes. Silica is the main component of a tetrahedral

sheet, while octahedral sheet comprises various elements such as Al, Mg, and Fe. Those sheets are arranged as 1 nm thin layers, with an octahedral sheet sandwiched between two tetrahedral silica sheets. Structure of 2:1 layered silicates is shown in Figure 2.1.

Stacks with a regular van der Walls gap in between them, that are called the interlayer, basal spacing or the gallery, are formed by the regular organization of the layers. Negative charges are generated by isomorphic substitution within the layers (for example, Al^{3+} replaced by Mg^{2+} or by Fe^{2+} or Mg^{2+} replaced by Li^{+}) and they are counterbalanced by alkali or alkaline earth cations situated in the interlayer [23]. The cations are generally hydrated and the negative charge is quantified as the cation-exchange capacity and it is usually in the range from 80 to 150 meq/100g for smectites [22].
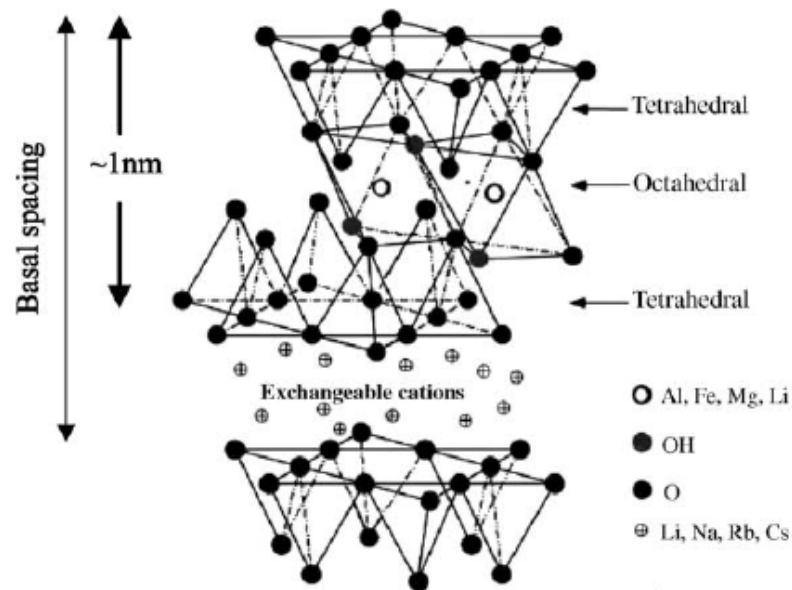
Figure 2.1 Structure of 2:1 layered silicates [23]

The phyllosilicate 2:1 layer clays include mica, smectite, vermiculite, and chlorite. Smectite group can be further divided into montmorillonite (MMT), saponite and hectorite species [24]. Their chemical formulas are shown in Table 2.1 [25]

Table 2.1 Chemical formulas of commonly used smectite type layered silicates

Layered Silicate	General Formula*
Montmorillonite	$M_x(Al_{4-x}Mg_x)Si_8O_{20}(OH)_4$
Saponite	$M_xMg_6(Si_{8-x}Al_x)O_{20}(OH)_4$
Hectorite	$M_x(Mg_{6-x}Li_x)Si_8O_{20}(OH)_4$

*M = monovalent cation; x = degree of isomorphous substitution.

2.2.3 Montmorillonite

Montmorillonite consists of two-dimensional layers where a central octahedral sheet of alumina or magnesia is fused to two external silica tetrahedra. Each layer is separated from other layers by van der Waals gaps, which are called galleries. The basal spacing is of the order of 1 nm. These layers form stacks with a regular van der Waals gap in between them, which is called interlayer. Isomorphic substitution within the layers, such as Al^{3+} replaced by Mg^{2+}, generates negative charges. These negative charges are counterbalanced by alkali or alkaline earth cations situated in the interlayer [26].

2.2.4. Types of Nanocomposite Structures

Depending on the components used, synthesizing methods, strength of the interfacial interactions and the clay loading directly affect the structure of the polymer–layered silicate nanocomposite. It is not always possible to end with a nanocomposite when the organoclay is mixed with a polymer, the dispersion of the clay platelets should be in the nanometer range. Nanocomposites have much higher surface area for polymer filler interaction compared to conventional composites [27].

According to the structure of dispersed clay platelets in the polymer matrix, the composites can be categorized into three main groups; phase separated composites (conventional composite), intercalated nanocomposites, and

exfoliated nanocomposites. Types of nanocomposite structures are shown in Figures 2.2, 2.3 and 2.4.
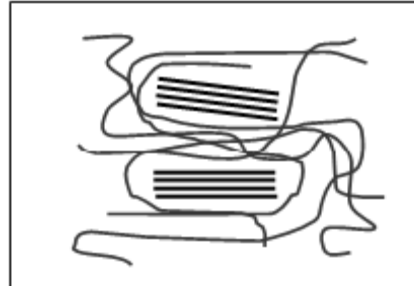
Figure 2.2 Schematic representation of conventional composites
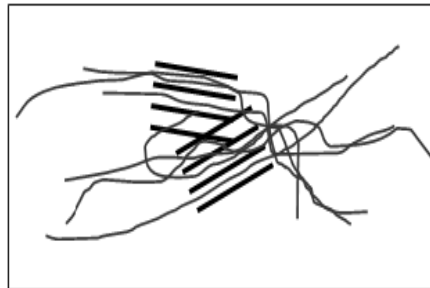
Figure 2.3 Schematic representation of intercalated nanocomposites
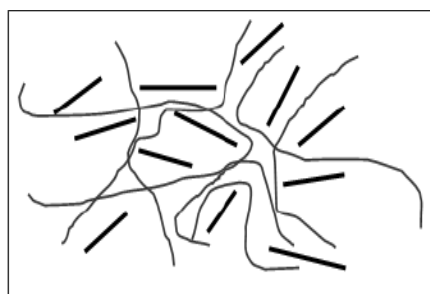
Figure 2.4 Schematic representation of exfoliated nanocomposites

If the polymer and clay are incompatible, the clay platelets remain as large stacks and no polymer chains get inserted between the layers. In this type of structures, the clays are called tactoids and the properties of the composite stay in the same

range as those of traditional conventional composites with poor properties (Figure 2.2). Intercalated structures (Figure 2.3) are formed when polymer chains are inserted between the silicate layers, while the stacking order remains the same as microcomposites. This leads to an expansion of the interlayer spacing by less than 20-30 Å. When the clay layers are completely pushed apart to create a disordered array and they are uniformly dispersed in the continuous polymer matrix, the composite is considered to be exfoliated or delaminated. As a result of this delamination, the silicate sheets lose their geometry leading to a larger surface area with improved properties (Figure 2.4). However, fully exfoliated structure is rarely seen in practice. Instead, partially exfoliated and partially intercalated structures can be seen more often [16].

2.2.5 Nanocomposite Preparation Techniques

In order to prepare nanocomposites, several methods were proposed so far. They are based on three different methods; in-situ intercalative polymerization technique, solution intercalation technique and melt intercalation technique. In this study melt intercalation technique was used.

2.2.5.1 In-Situ Polymerization

In-situ polymerization is one of the methods used to synthesize polymer-clay nanocomposites. Nowadays, it is the conventional process used to synthesize thermoset-clay nanocomposites [28]. The modified layered silicate is swollen by a liquid monomer or a monomer solution. The monomer migrates into the galleries of the layered silicate, so that the polymerization can occur within the intercalated sheets. The polymerization reaction leads to the delamination of the clay [28]. The polymerization reaction can be carried out by heat, radiation or a suitable initiator. This process is schematically illustrated in Figure 2.5.
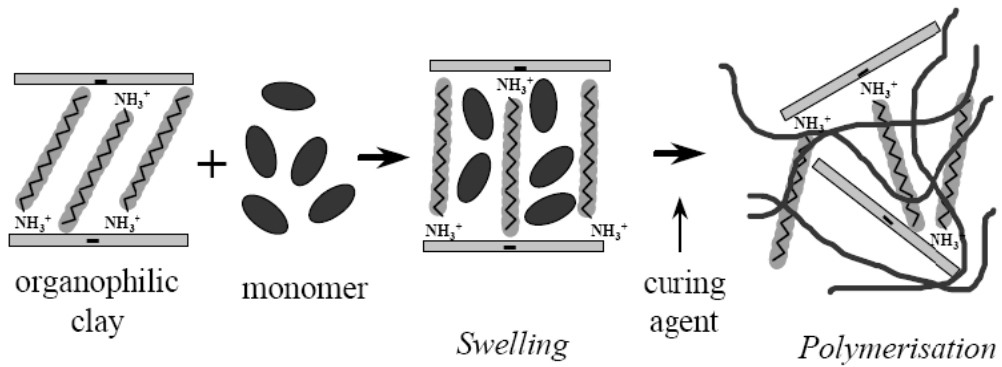
Figure 2.5 Schematic representation of in-situ polymerization [28]

2.2.5.2 Solution Method

It is well known that such layered silicates, owing to the weak forces that stack the layers together can be easily dispersed in an adequate solvent [29]. Then, the polymer dissolved in the solvent, is added to the solution and intercalates between the clay layers. The last step consists of removing the solvent by evaporation under vacuum. Nanocomposites, based on untreated clays can also be synthesized using this approach [28]. This process is schematically illustrated in Figure 2.6.
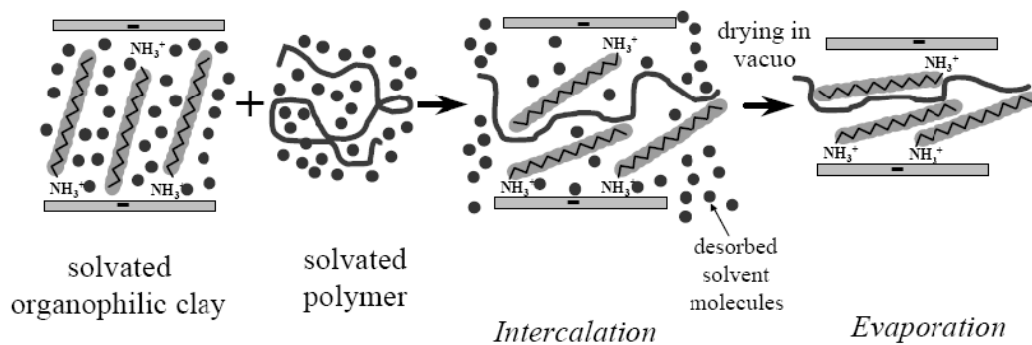
Figure 2.6 Schematic representation of the intercalation of the polymer by solution method [28]

2.2.5.3 Melt Intercalation Method

In this method, the layered silicate is mixed with the polymer matrix in the molten state. Under these conditions, if the layer surfaces are sufficiently compatible with the chosen polymer, the polymer can crawl into the interlayer surface to form either an intercalated or an exfoliated nanocomposite. This process is schematically illustrated in Figure 2.7. In this technique, no solvent is required [29]. Due to its great potential in industrial applications, the melt intercalation process has become increasingly popular.
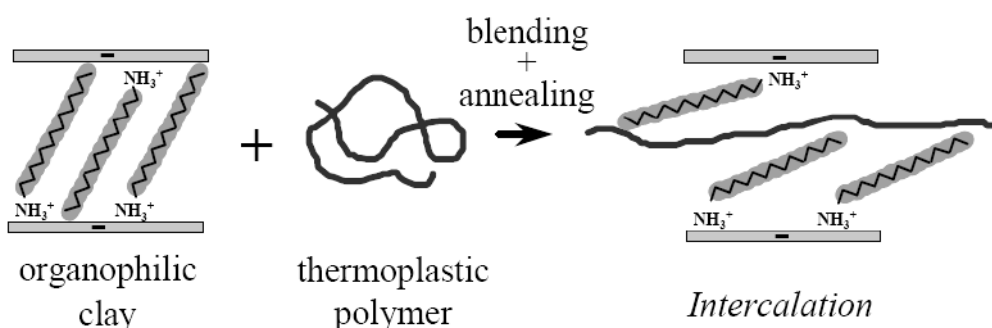
Figure 2.7 Schematic representation of melt intercalation process [28]

2.3 General Properties and Applications of Polystyrene

Polystyrene belongs to the group of standard thermoplastics that also includes polyethylene, polypropylene and polyvinylchloride. Because of its special properties, polystyrene can be used in an extremely wide range of applications [30]. Polystyrene is a versatile polymer whose principal characteristics include transparency, ease of coloring, and processing and low cost [31]. Polystyrene is usually available in general purpose or crystal, high impact and expanded grades. It is a linear polymer that in principle can be produced in syndiotactic and atactic forms. The mechanical and rheological behaviour of polystyrene is predominantly determined by its average molecular weight; the strength improves with increasing chain length but the melt viscosity increases as well making processing difficult [30].

Commercial polystyrene is an amorphous material with a molecular weight between 100,000 and 400,000. At temperatures sufficiently below glass transition temperature (T_g) and at low deformations, the material obeys Hooke's law of elasticity under external stress. Above its T_g, polystyrene is a viscoelastic melt. It is called viscoelastic, because the polymeric material displays both a viscous and an elastic response to shear stress, depending on the rate and the temperature of the test. Also, there are two main factors that influence the viscous and the elastic behavior of the product, namely molecular weight and molecular weight distribution [32].

Due to brittle characteristics of polystyrene, the main development directions were aimed at copolymerization of styrene with polar comonomers such as methacrylates or maleic anhydride and as impact modified with different rubbers or styrene-butadiene block copolymers, which will be discussed later. It is a linear polyethylene chain with laterally attached phenyl rings, being responsible for the enhanced glass transition temperature and high refractive index. Polystyrene has two different structures according to the side of the chain on which the phenyl groups are attached. Syndiotactic polystyrene has phenyls groups that are attached to the alternating sides of the polymer chain, whereas atactic polystyrene has no order. Their chemical structures are shown in Figure 2.8. Stiffness, brilliance, gloss and hardness are the main characteristics of this material [31].
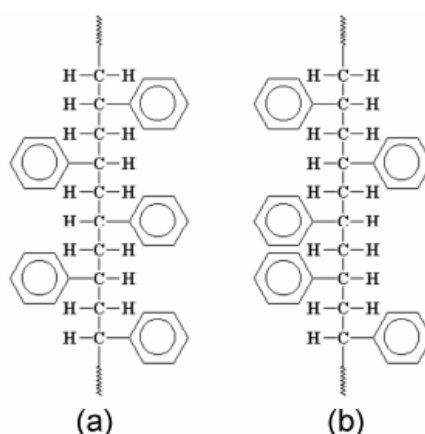
Figure 2.8 Chemical structure of (a) Syndiotactic PS (b) Atactic PS

2.3.1 Polymerization of Styrene

Styrene is almost unique in the extent of its ability to undergo spontaneous polymerization simply by heating the monomer without the aid of chemical initiator. Polystyrene was first produced commercially in 1938 by the Dow Chemical Company. The first polymerization process involved loading cans of styrene into an oven and allowing them to spontaneously polymerize to high conversion. Today, most polystyrene is manufactured via continuous free radical bulk polymerization with the aid of a suitable initiator [33].

Free-radical polymerization is a rapid reaction which consists of the sequence of events, namely initiation, propagation, and termination [34]. Free-radical polymerization is initiated by the action of free-radicals i.e., electrically neutral species with an unshared electron. Free radicals for the initiation are usually generated by the thermal decomposition of organic peroxides or azo compounds [35]. Their effect on polymerization is to increase the rate of reaction and at the same time, to decrease the molecular weight of the polymer. These compounds are readily homolytically cleaved by heat or ultraviolet light to produce free radicals. Benzoyl peroxide is a typical and widely used initiator and it is useful in the temperature range of 60°C-90°C [36]. Polymerization steps are schematically shown in Figure 2.9.
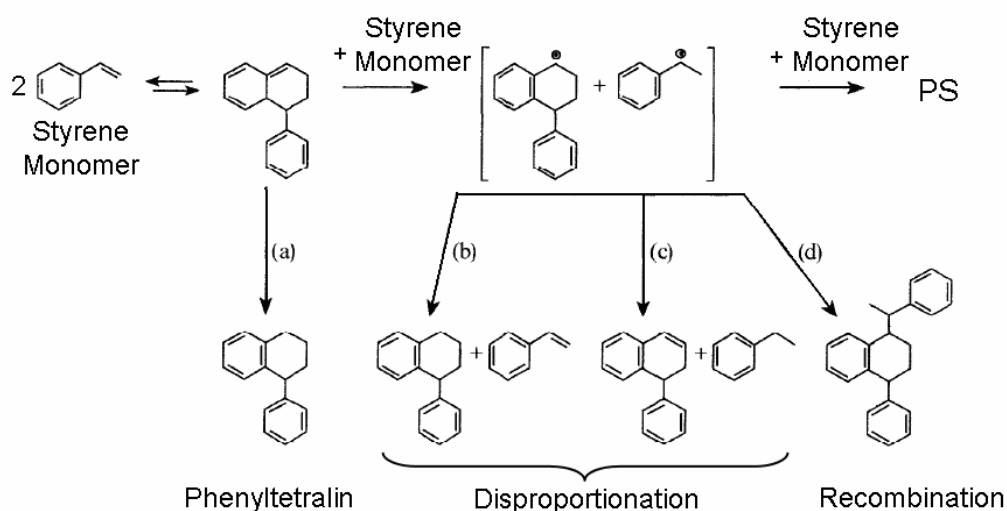
Figure 2.9 Schematic representation of polymerization of styrene [32]

2.4 Rubber Toughening

Toughened polymers represent a large area of scientific and technological concern. In fact, with the gradual penetration of plastics in areas traditionally dominated by metals and ceramics, new polymeric materials, both thermoplastics and thermoset resins, have been developed for increasingly demanding applications. These materials are able to provide the right combination of lightness and mechanical performance over a wide range of temperatures. In many instances, a good balance between stiffness and tougheness is required but most of the as synthesized polymers which exhibit adequate rigidity are characterized by brittleness and low resistance to crack propagation [37, 38, 39].

Two different approaches have emerged, both with their own potential and weakness. One is to synthesize new homo or copolymers, based on novel monomers as in the case of polycarbonates, polysulphones and polyether-ketones. The second approach consists of modifying existing polymers through the addition of a second polymeric component, a route generally referred to as "blending". Such a method presents the distinctive advantage of being, in general, more economically attractive, since the development of new synthetic methods is a long and costly process [40].

An excellent example of the blending approach is provided by rubber toughening in which a small amount of rubber, typically between 5 and 20 % by weight, is incorporated as a disperse phase into a rigid plastic matrix. The resulting blend is characterized by a considerably higher fracture toughness than the parent polymer; there is an inevitable reduction in the modulus and tensile strength but these losses are far outweighed by the improvement in fracture toughness. This approach has been proven to be very successful and a wide variety of plastics toughened in this way are now commercially available. Among the best known examples are high impact polystyrene (HIPS), and polyvinylchloride (PVC); other plastics which have been toughened using this technology include polymethylmethacrylate (PMMA), polypropylene (PP), polycarbonate (PC), Nylons and, most recently, thermosetting resins such as epoxies, polyimides and unsaturated polyesters [41, 42].

In the case of rubber toughened thermoplastics, an essential condition to achieve satisfactory results is that the rubbery phase must be finely and homogeneously dispersed within the matrix; furthermore the rubbery particles must be adequately bonded to the matrix. To this end, the rubber must possess a solubility parameter sufficiently different from that of the matrix polymer to ensure a fine second phase dispersion but close enough to promote adequate adhesion of the particles to the matrix. Such stringent requirements strongly limit the choice of possible rubber tougheners for a given polymer matrix. To overcome this limitation, the concept of compatibilizing agents in the form of block or graft copolymers has been developed and succesfully applied in a wide number of actual cases [43, 44].

Essentially, a suitable block or graft copolymer whose segments are chemically equivalent to the blend components is added. Atter the blending process, such a copolymer locates preferentially at the interphase, thus promoting a better dispersion of the second component and an improved adhesion between the phases. The behaviour of small amounts of compatibilizer in an immiscible blend has been described as that of a classic emulsifying agent, similar to the soap molecules at an oil-water interface [45]. The success of the use of block or graft copolymers (and in some instances also random copolymers) as compatibilizers accounts for many of the large number of commercially available blends, e.g. HIPS and ABS. The renewed interest towards the reactive melt processing, i.e. reactive extrusion (REX) and reactive injection moulding (RIM), is also due to the recent achievements in the development of copolymer compatibilizers. Moreover, when the thermoplastic matrix is able to crystallize, further factors must be taken into account such as the structure and size of spherulites and lamellar crystals, the spherulite grow rate and the nucleation process, which are all affected by the presence of the dispersed soft phase [46-49].

The toughening of thermosetting resins poses different, yet equally challenging issues. Generally, a critical step towards the preparation of a toughened thermosetting blend is to start from a single-phase homogeneous reactants mixture prior to the curing process. For this reason, the rubbers usually employed are low molecular weight liquids and are miscible enough to dissolve in the resin prepolymer. However, the elastomeric phase separates out during the curing process, giving rise to fine and homogeneous dispersion of the second

17

component in the resin matrix. The phase separation process is of paramount importance in these systems and depends on both kinetic and thermodynamic factors. The understanding of these factors and the ability to control them to obtain the desired morphology of the materials represent one of the main goals of the research efforts in this area. As for thermoplastics, also in the case of thermosetting blends, a certain degree of chemical interaction between the resin and the rubber modifier is required to improve the interfacial adhesion and hence to achieve an effective toughening. Such reactions generally involve the end-groups of the rubber modifier whose functionality is adjusted according to the chemical nature of the matrix resin.

Concurrently with the development of novel tougheners and of more sophisticated technologies to produce multicomponent polymer blends with balanced end-properties, a large amount of efforts has been spent to elucidate the mechanisms of fracture in these complex systems. This in an attempt to be able to control the very many factors which play a role in the fracture behaviour of toughened plastics. Alter more than twenty years of extensive research in this area we may say that we are still far from a complete understanding of the whole phenomenon but very significant advances have been achieved especially in the case of blends based on rubber modifiers. In fact, it is now well established that rubber particles with low moduli act as stress concentrators in both thermoplastic and thermoset resins, enhancing shear yielding and/or crazing in the matrix, depending on its molecular architecture. In particular, in the case of thermosets, the crazing mechanism does not operate, while one important process is the initiation and growth of multiple localized shear yield deformations in the matrix. In addition, a cavitation process occurring either in the rubber particles or at the particle-matrix interface often plays a key role. Once formed, these voids grow and so dissipate energy; at the same time they lower the stress required to initiate shear yielding in the matrix thus promoting more extensive plastic deformation [50].

2.4.1 Factors Affecting Rubber Toughening

There are a number of factors that influence the amount of toughening obtained by the use of additives and fillers. Most of these factors have been experimentally

18

determined, however, recent mechanical modeling has improved our understanding of these important toughening mechanisms.

In rubber-toughened plastics, the matrix plays an important role in determining the overall toughness. Some matrices tend to craze because of low entanglement density [51]. Massive crazing induced by rubber particles is clearly observed in high impact polystyrene. In crazing polymers, high molecular weight is needed to stabilize crazes. Highly entangled polymers tend to deform via shear banding. High molecular weight matrices are, in general, tougher than their low-molecular counterparts. Shear banding is clearly observed in lightly crosslinked epoxies. In the case of epoxies, lower crosslink density produces a more "toughenable" polymer upon rubber addition.

Rubber particle size has been studied by a number of investigators [52-54]. Rubber particles over 5 microns in diameter are often too large to interact with the stress field at the crack tip. Rubber particles under 100 nm in diameter appear to be too small to cavitate effectively. Without the cavitation of the rubber particles, subsequent matrix shear bending in the presence of a triaxial stress field at the crack tip is very unlikely.

The effect of rubber concentration on toughness has been studied by a large number of researchers [55-60]. Some have attributed a minimum amount of rubber needed to an interparticle distance effect (mostly semicrystalline plastics while others have shown a linear increase in toughness with rubber content. At high rubber content the toughness decreases presumably due to the fact that there is less matrix available for massive shear banding or crazing.

The type of rubber has been shown to be important by a number of researchers [61-63]. For example, in nylon, the type of rubber has been shown to be more important than the interparticle distance. The effect of the type of rubber has been often associated with the caviational strength of the rubber particle. However, it is important to note that the blend morphology and matrix-particle interphase regions may also change.

Rubber particle strength has also been examined [64-66]. A number of investigators have shown that epoxies containing microvoids are as tough their rubber-modified counterparts. However, these micro-voided materials are much more difficult to process than conventional rubber-toughened polymers and the microvoid modification has only been applied to a few number of matrices. Therefore, the utility of the microvoided polymer concept is limited however, the study of these systems do challenge our understanding of the role of rubber-particle cavitation resistance.

The role of the rubber particle-matrix interface has been studied by a few groups with mixed results [67-69]. Some researchers have found that strengthening the interface improves toughness, others have shown that a diffuse interphase region improves toughness, while others have shown that the interphase region can control the amount of matrix dilation around the rubber particles.

The role of the particle morphology has been studied by a number of researchers [70-71] Bucknall et al. [70] have studied the role of a salami type microstructure in rubber-toughened polystyrene. Lovell et al. [71] have studied the effect of multilayered core-shell latex particles on toughening PMMA. There appears to be advantages over the simple on phase particles.

The role of blend morphology in rubber-toughened plastics has also been studied [72-73]. Clearly, the rubber phase has to be uniformly distributed for improved toughness. However, there may be an advantage of having segregation on a microscopic scale as shown by Bagheri et al. [72] and by Qian et al. [73].

In summary, there are a number of variables to consider when developing toughened plastics and their interrelationships remain an area of active study

2.4.2 Impact Modification of Polystyrene

To increase the impact strength of the polystyrene, significant investigations have been made on the concept of impact modification of polystyrene by blending it with various types of low-modulus, rubbery polymers. Through the development of reactive extrusion techniques, impact modification of polystyrene involves polymer

blending and compatibilization with rubbery polymers containing polar or reactive functionalities. Compatibility is defined as the ability of the rubber modifier to disperse itself into the polymer matrix to form stable rubber particle dispersions with reduced interfacial tension and improved adhesion.

Rubber modified polystyrene exhibits higher impact strength than polystyrene by preventing crazes from developing into cracks. The rubber particles constitute the dispersed phase in the polymer matrix. Generally, small dispersed particles enhance the stress concentration while larger ones stop the growth of cracks. In order to establish this mechanism, a well defined adhesion of the rubber particles to the matrix is required [74, 75]. Rubber particles dissipate impact energy by transforming it into deformation of themselves, eventually by the formation of voids in the rubber phase itself. Difference between the formation of crazes after mechanical impact for brittle materials and rubber toughened materials is shown in Figure 2.10. When the toughened material is subjected to uni-axial stress, the localized stress nearby a rubber particle is magnified by the local stress concentration effect of the particle. The matrix will yield locally in response to this localized stress field, thus avoiding a brittle failure of the material [32].
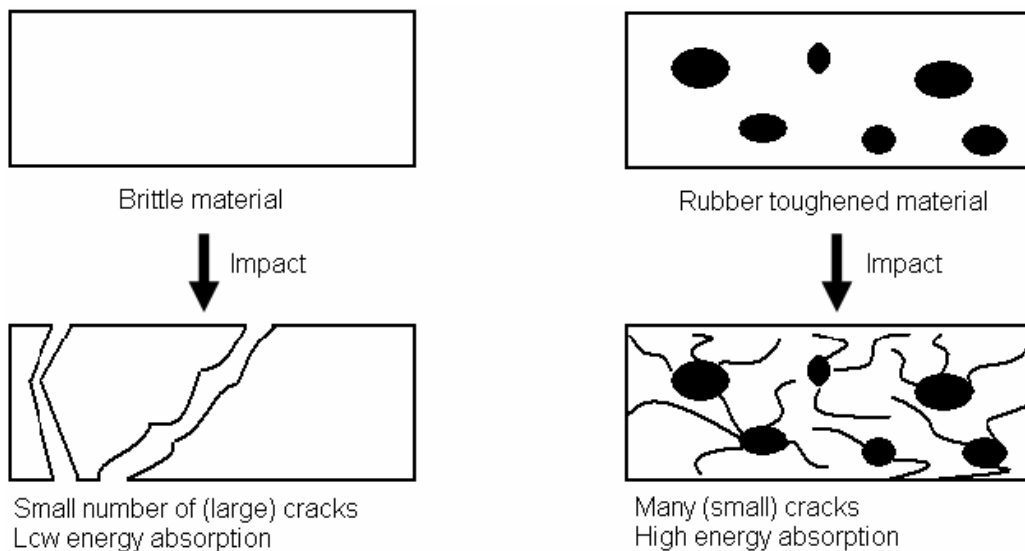
Figure 2.10 Craze formation after mechanical impact [32].

2.4.3 High Impact Polystyrene

High impact polystyrene, which is called as HIPS, is a rubber modified polystyrene thermoplastic. In the process of HIPS, polybutadiene (PB) phase is dissolved in styrene monomer followed by free radical polymerization. Thus, some of the growing styrene polymer chains graft on to the polybutadiene rubber. The chemical structure of HIPS is shown in Figure 2.11
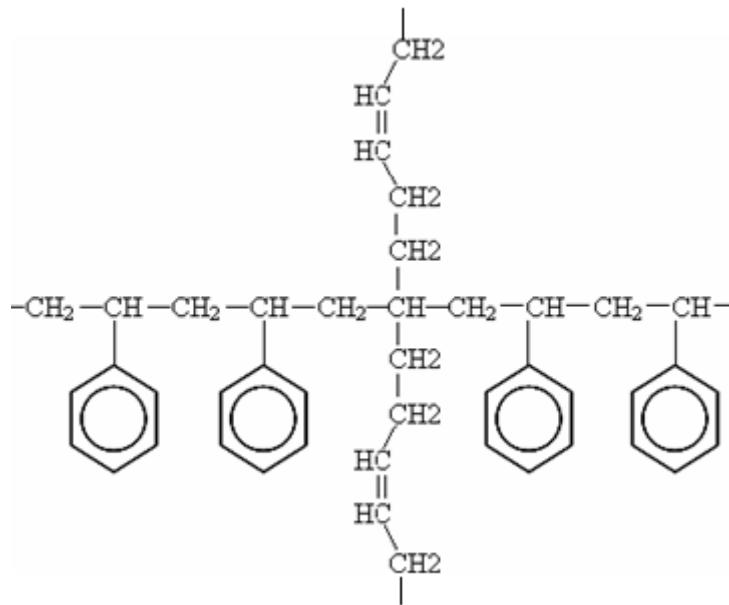
Figure 2.11 Chemical structure of HIPS [76]

Polystyrene homopolymer is preferred for its clarity, rigidity and dimensional stability. In addition to these properties, HIPS is valued for its high impact strength compared to polystyrene. However, HIPS has some disadvantages such as poor high temperature properties, poor oxygen barrier properties, relatively low ultraviolet light stability and low chemical resistance [77]. PS and PB homopolymers do not mix and PB branches form little globs. But these little globs are always tied to the PS phase and act to absorb energy when the polymer gets hit with something [76].

The tensile strength of HIPS increases with decreasing temperature and increasing strain rate. This is an expected characteristic of a rubber toughened system. On the other hand, elongation at break value decreases as the

temperature drops and the deformation rate increases. Temperature has a significantly greater effect on the mechanical properties of HIPS when compared the effect of deformation rate.

2.4.4 Styrene Block Copolymers as Impact Modifiers

Block copolymers, which are compatible with the polymer matrix are used for the impact modification of polystyrene. Compatibility is directly related with the ability of the rubber phase to disperse itself uniformly to reduce interfacial tension and to improve adhesion [78]. There are various types of block copolymers used for impact modification, but commercially available styrene-rubber-styrene block copolymers, in which the outer styrene blocks serve to anchor the middle rubber block, are preferred.

Because of their ability to form distinct styrene (hard phase) and diene (rubber phase) domains with well defined morphologies, styrene block copolymers have useful properties. To achieve this, requires an unusual degree of control over the polymerization, which must yield discrete blocks of a uniform and controlled size. Most styrene containing block copolymers are manufactured using anionic polymerization technique. However, the most important disadvantage of this method is the costly polymerization chemistry because of the stringent requirements for monomer and solvent purity.

Order of impact modification depends on the molecular weight of the rubber block and the rubber particle size used in the PS matrix. As the molecular weight of rubber block increases, viscosity also increases leading to larger size of dispersed particles. Thus, with increasing size of the dispersed particles, impact strength increases.

2.5 Polymer Processing

In order to obtain different products, various polymer processing methods like extrusion, pultrusion, injection molding, resin transfer molding, compression molding, tubular film blowing, fiber spinning and calendering are applied. However, extrusion and injection molding are the two basic processing steps in

the polymer industry. In this study, extrusion and injection molding are used to prepare the nanocomposite samples.

2.5.1 Extrusion

Extrusion is defined as continuously forcing a molten material through a shaping device. Extruders are the most common machines in the plastics processing industry. They permit multiple process steps in a single machine, including melting, metering, mixing, reacting, side-stream addition, and venting. Schematic diagram of an extrusion process is given in Figure 2.12.
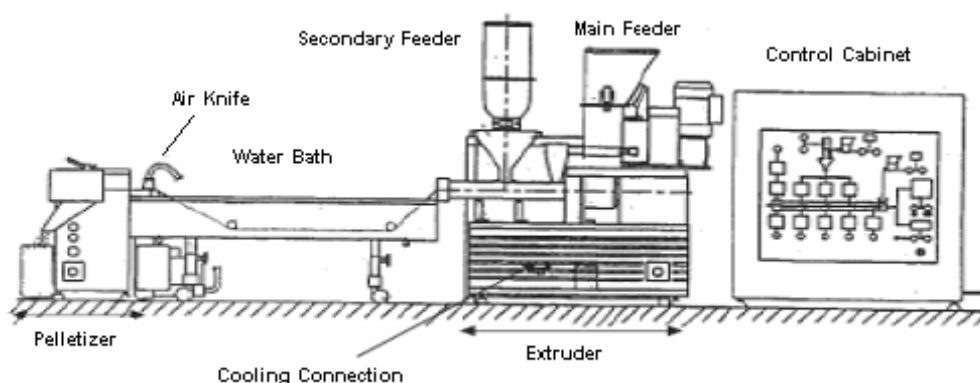
Figure 2.12 Schematic drawing of extrusion process

There are three main extruder types; the screw extruder, the ram extruder and the drum or disk extruder. Polymers that have high melting points like PTFE and UHMWPE can be processed by ram extruders [79]. In a screw extruder, which is used in this study, two screws rotate in a cylinder; the rotation of the screws creates a pumping action.

Twin-screw extruders may have either two co-rotating or counter-rotating screws in the barrel. The screws rotate in the same direction in co-rotating twin-screw extruders, while they rotate in the opposite direction in counter-rotating twin-screw extruders. Twin-screw extruders are suitable for processing materials which are hard to feed because of its positive displacement characteristics in the intermeshing region. Maximum positive displacement is provided by

counterrotating twin-screw extruders which makes them the primary choice for profile extrusion, whereas co-rotating twin-screw extruders are utilized for applications like compounding, mixing, devolatization and chemical reaction because of the complex flow in the intermeshing region where good mixing and compounding characteristics are required. Good mixing, devolatization properties and good control over residence time are the advantages of twin-screw extruders [80].

Drag flow is the operating principle of single screw extruders. The material is transmitted to the end of the extruder by the help of the screws. The polymer is prevented from sticking on the walls of the barrel. On the other hand, the rotating action of the screws helps the material be pushed down in counter-rotating, fully intermeshing extruders. Both positive displacement and drag flow are effective in co-rotating, fully intermeshing extruders. Some of the positive displacement occurs in the intermesh area as the polymer is dragged along the extruder in the rest of the barrel circumference [81]. Conveying characteristics of extruder can be seen in Figure 2.13.
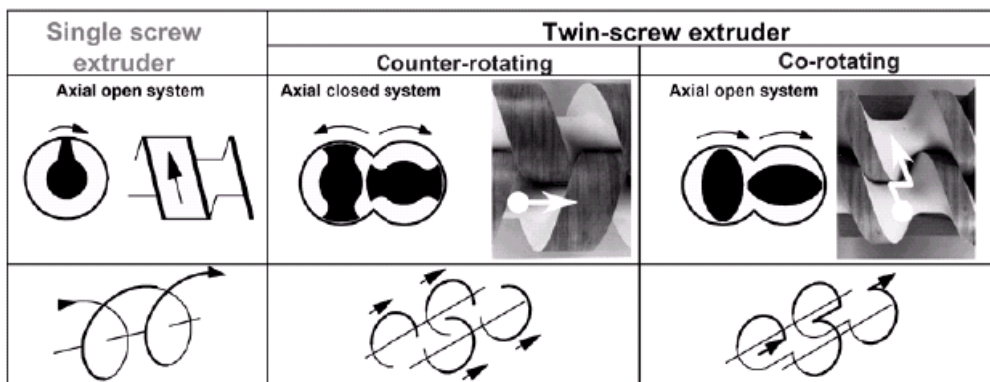
Figure 2.13 Extruder conveying characteristics [81]

2.5.2 Injection Molding

Injection molding is one of the most common processing methods for plastics. It is used to produce finished articles which range from household appliances to automobile bumpers. Also, it is one of the most important polymer flow processes

due to the significant fraction of the total industrial output of plastics that is injection molded [82].

The basic steps or stages of injection molding process are shown in Figure 2.14. The solid plastic is melted, and the melt is injected into the mold under high pressure. In order to solidify the article the mold is cooled. Finally, the mold is opened and the article is ejected [82].

| Plastic is molten | → | Molten plastic is injected into the mold | → | Mold is cooled | → | Article is removed from mold |
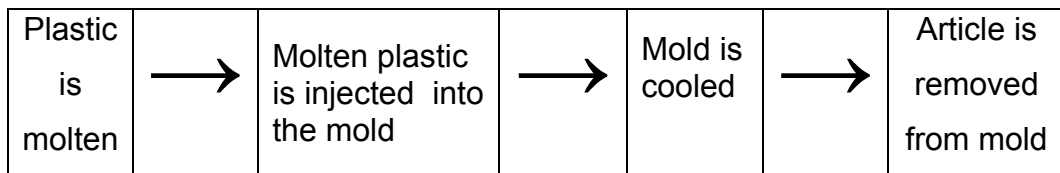
Figure 2.14 Stages in the injection molding process

The original injection molding machines were based on the pressure die casting technique for metals. The first machine is reported to have been patented in the United States in 1872, specifically for use with cellulose. This was an important invention, but probably before its time, because in the following years very few developments in injection molding processes were reported, and it was not until the 1920s, in Germany, that a renewed interest was taken in the process. The first German machines were very simple pieces of equipment and relied totally on manual operation. The next major development in injection molding, i.e. the introduction of hydraulically operated machines, did not occur until the late 1930s when a wide range of thermoplastics started to become available. In 1950s a new generation of equipment was developed. These machines catered more closely for the particular properties of polymer melts, and modern machines are of the same basic design, although of course the control systems are much more sophisticated nowadays [83].

Although the process of injection molding is very simple, injection molding machines and molds are very costly due to the high pressure needed for injection of the thermoplastic melt and the associated complex controls [84].

The injection molding process is a simple cycling operation consisting of three steps; filling, packing and cooling. Firstly, polymer melt is pushed forward through a nozzle to a cooled cavity of a closed mold which gives the shape to the plastic. After waiting for a sufficient time for the plastic part to solidify, the mold opens and the part is removed. The pressure exerted on the polymer melt by the screw section is kept constant during the filling step. In the packing step, the pressure builds up and it is maintained very high during the cooling stage to minimize shrinkage and shape changes [82]. The temperature of the melt is controlled by the temperature control system of the injection unit, but it may also be affected by the injection speed and by the level of back pressure, and it should be kept above the melting temperature of the polymer. However, the thermoplastic must be cooled under pressure below glass transition temperature and melting before the opening of the mold, followed by part ejection [85].

2.6 Polymer Characterization

In order to determine the properties of the newly developed materials and the applications for which the materials can be used, some analyses are required. During this study, morphological, rheological, mechanical and thermal analyses are performed on the prepared samples.

2.6.1 Morphological Characterization

X-ray diffraction (XRD) and transmission electron microscopy (TEM) analyses are widely used to determine the dispersion of clay particles in polymer matrix. Informations obtained from TEM and XRD analyses are complementary for each other.

2.6.1.1 X-ray Diffraction (XRD)

The method of X-ray diffraction and scattering is one of the oldest and most widely used techniques available for investigating the orderly arrangements of atoms and molecules of the polymer structures. X-rays are electromagnetic radiation of very short wavelength (0.01 to 100 nm), produced when an electron hits a piece of metal in an evacuated tube. A beam of x rays incident to a material

is partly absorbed and partly scattered, and the rest is transmitted unmodified. Diffraction occurs as waves interact with a regular structure whose repeat distance is about the same as the wavelength [86]

The peaks in an X-ray diffraction pattern are directly related to the atomic distances. Figure 2.15 shows the two scattering planes of atoms, which may be either due to two consecutive clay layers or other crystallographic planes of the layers themselves that are separated by the interplanar spacing.
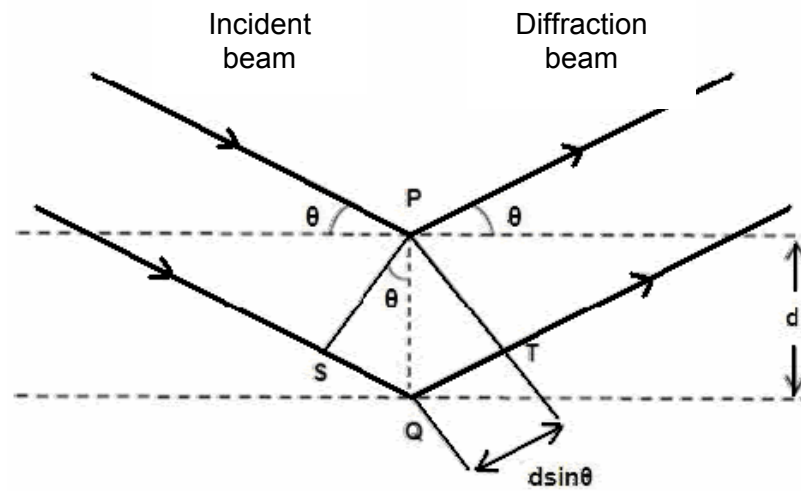
Figure 2.15 Diffraction of X-rays by planes of atoms [17]

For a given set of lattice plane with an inter-plane distance of d (Å), the condition for a diffraction peak to occur can be simply written as the following equation, which is the Bragg's law:

$$n.\lambda = 2.d.\sin\theta \qquad\qquad (2.1)$$

In the equation, λ (Å) is the wavelength of the x-ray, θ (°) is the scattering angle, and n is an integer representing the order of the diffraction peak [87].

2.6.1.2 Transmission Electron Microscopy (TEM)

The disappearance of peaks in XRD analysis results does not always mean that clay platelets are exfoliated. There are many factors affecting XRD results of layered silicates such as concentration and orientation of the clay, sampling problems and poor calibration of XRD instruments. Thus, TEM analysis is complimentary to the XRD analysis. By TEM analysis, qualitative understanding of the internal structure, distribution of the various phases and views of the defect structure through direct visualization at levels down to atomic dimensions can be achieved.

Transmission electron microscopy (TEM) is an imaging technique whereby a beam of electrons is focused onto a specimen causing an enlarged version to appear on a fluorescent screen or layer of photographic film, or to be detected by a charge-coupled device (CCD) camera [88].

The wavelength of electrons is dependent on their energy, thus it can be tuned by adjustment of accelerating fields, and can be much smaller than that of light, yet the electrons can still interact with the sample due to their electrical charge. Electrons are generated by a process known as thermionic discharge in the same manner as the cathode in a cathode ray tube, or by field emission; they are then accelerated by an electric field and focused by electrical and magnetic fields onto the sample. The electrons can be focused onto the sample providing a resolution far better than is possible with optical microscopes, and with improved depth of vision. Details of a sample can be enhanced in optical microscopy by the use of stains; similarly with electron microscopy, compounds of heavy metals such as lead or uranium can be used to selectively deposit heavy atoms in the sample and enhance structural detail, the dense electron clouds of the heavy atoms interacting strongly with the electron beam. The electrons can be detected using a photographic film, or fluorescent screen among other technologies [88]. Modern TEMs are often equipped with specimen holders that allow the user to tilt the specimen to a range of angles in order to obtain specific diffraction conditions, and apertures placed below the specimen allow the user to select electrons diffracted in a particular direction [88].

2.6.1.3 Scanning Electron Microscopy (SEM)

In SEM analysis, the surface of a specimen to be examined is scanned with an electron beam, and the reflected (or back-scattered) beam of electrons is collected, and then displayed at the same scanning rate on a cathode ray tube. The image on the screen, which may be photographed, represents the surface features of the specimen. The surface must be electrically conductive; therefore a very thin metallic surface coating must be applied to nonconductive materials. Magnifications ranging from 10 to in excess of 50000 diameters are possible [17].

SEM is limited to a surface view only. It does not provide information about the interior of the specimen, but the surface can be monitored as black and white images which can be fitted to a x-ray instrument and elemental analysis can be made. Also, the images can be used to make accurate conclusion about the morphology of the polymer systems.

2.6.2 Mechanical Characterization

Due to their desirable mechanical properties at low cost compared to other materials, polymers are widely used in many applications. Thus, mechanical properties of polymers can be taken into consideration as most important properties among all physical and chemical properties. There are various number of mechanical tests and testing instruments in order to investigate the properties of polymers such as tensile test, impact test and flexural test.

2.6.2.1 Tensile Test

Tensile tests are performed in order to measure the force required to break a specimen and the extent to which the specimen elongates to that breaking point. The test is applied according to standardized testing method [89]. According to this standard, the specimens are rectangular or in the shape of dogbone, as seen in Figure 2.16.

The ends of the specimen are clamped into the jaws of the testing machine and the jaws are separated by the application of a known force. Since the specimen is

pulled up, it elongates or breaks when the load applied is higher than the load which the specimen can resist. Tensile test provides a stress-strain diagram, which is used to determine the tensile modulus. Stress-strain tests not only give the modulus and an indication of the strength of the material but also toughness which is an indication of the energy that a material can absorb before breaking [90]. Area under linear part of the stress-strain curve gives information on the resilience of the material tested. Whole area under stress-strain curve gives information on the toughness of the material tested.
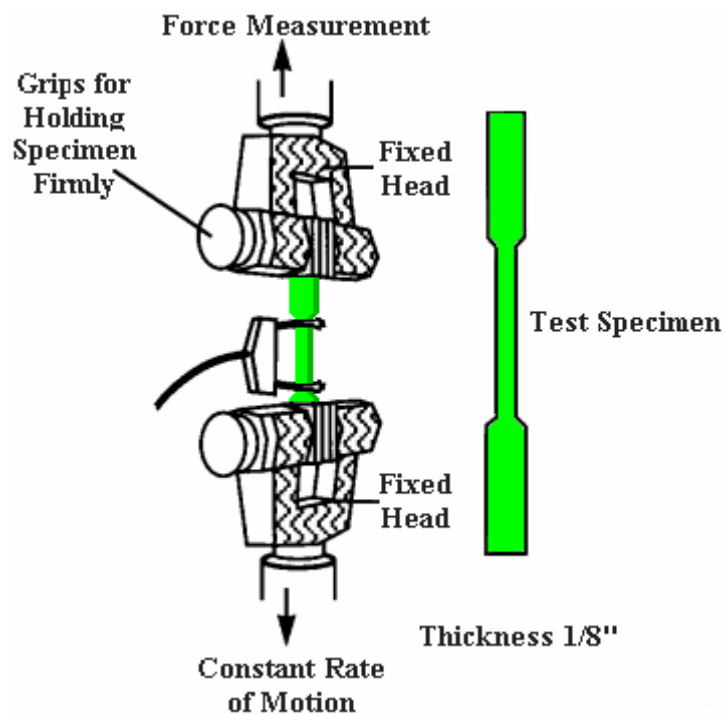
Figure 2.16 Tensile specimen and tensile test procedure [91]

There are several types of stress-strain curves which represent the different material properties. Some of them are shown in Figure 2.17.
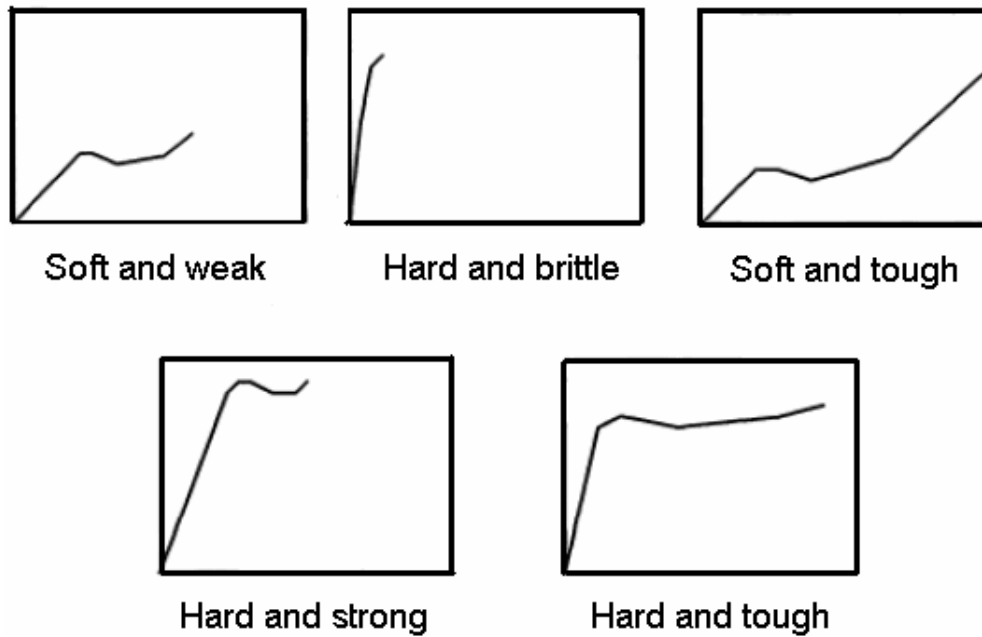
Figure 2.17 Different types of stress-strain curves

2.6.2.2 Impact Test

Impact tests measure the energy required for failure when a standard specimen receives a rapid stress loading. The impact strength of a polymer can be measured employing a number of techniques including the Izod and the Charpy tests [34]. For both the Izod and Charpy tests, a hammer-like weight strikes a specimen and the energy-to-break is determined from the loss in the kinetic energy of the hammer. Other variations include the falling ball or dart test, whereby the energy-to-break is determined from the weight of the ball and the height from which it is dropped. Figure 2.18 shows the schematical drawing of Charpy impact test.
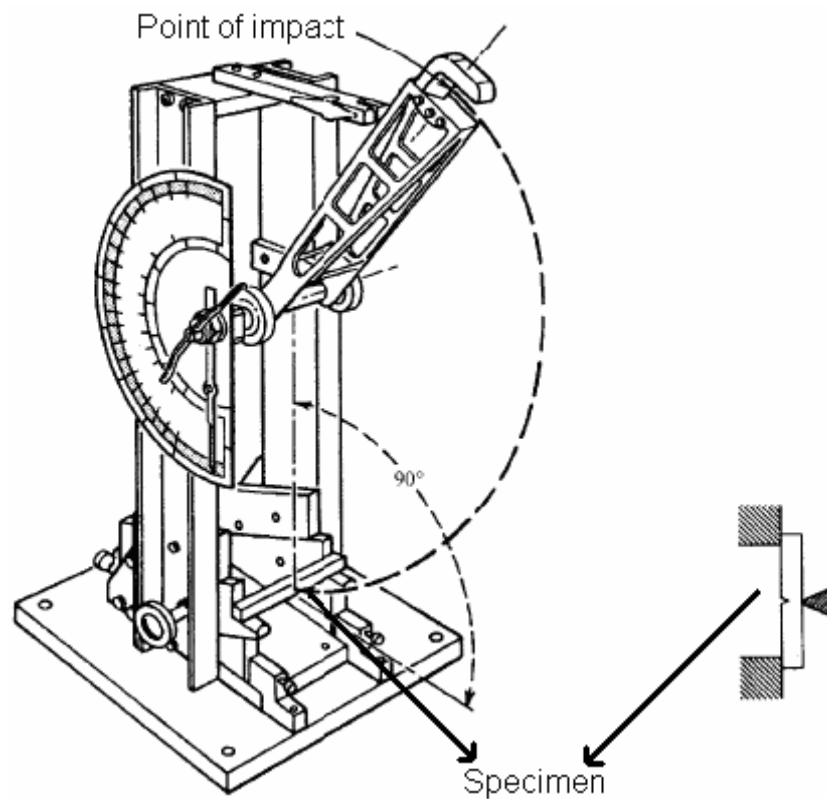
Figure 2.18 Charpy impact test [92]

2.6.3 Rheological Characterization

Rheology is the science of the deformation and flow of matter. It is concerned with the response of materials to applied stress. That response may be irreversible viscous flow, reversible elastic deformation, or a combination of the two. Viscoelastic materials show both flow and elasticity.

2.6.3.1 Capillary Viscometry

The viscosity of Newtonian fluids can be measured by using capillary viscometer. This method measures the time taken for a defined quantity of fluid to flow through a capillary with known diameter and length. It consists of a very small, cylindrical tube and a liquid or viscous melt is forced through the capillary by imposing a pressure drop. The very small diameter of the tube, the very large length to diameter ratio minimizes entrance and exit effects and ensures a fully developed velocity profile [93].

2.6.3.2 Melt Flow Index (MFI)

The melt index is not an intrinsic or fundamental property of a polymer. It is rather a conventional property of a polymer for expressing important flow characteristics [94]. The melt index, also known as melt flow rate, test measures the rate of extrusion of a thermoplastic material through an orifice of standard diameter under prescribed conditions of temperature and load [95]. The weight of the material extruded during the specified time is the melt index expressed in grams per ten minutes.

Melt flow index apparatus resembles a ram extruder in which a reciprocating piston pushes the material forward through the die. The mode of its operation is discontinuous. The polymers that are sensitive to moisture absorption have to be predried to eliminate the inaccuracies in the melt index values due to bubble formation in the polymer melt. Schematical drawing of MFI apparatus is shown in Figure 2.19
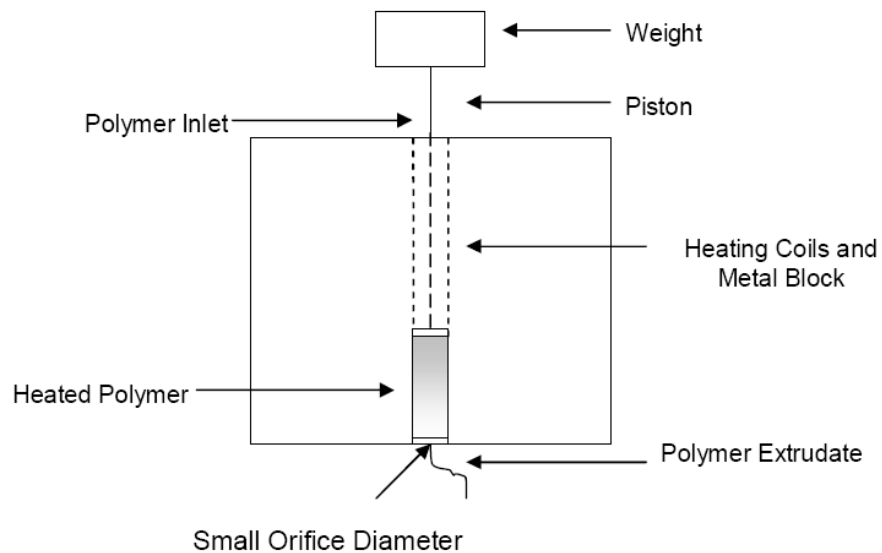
Figure 2.19 MFI Apparatus [96]

Melt flow indices are generally in the ranges of 0.1 to 50. Although the actual test time can be between 15 s and several minutes, it is expressed as the flow that would take place in a 10 min period. It is based on the effect of polymer molecular weight on relaxation times, the normal stress effects in extrusion and kinetic energy losses at the entrance and exit of the tubes during Poiseuille flow [97].

2.6.4 Thermal Characterization

In order to monitor the physical or chemical change of a sample when it is temperature changed various kinds of analytical techniques are used. Thermogravimetry (TGA), differential thermal analysis (DTA), and differential scanning calorimetry (DSC) are the three principal thermo-analytical methods. In this study, T_g of the nanocomposites was studied with DSC analysis.

2.6.4.1 Differential Scanning Calorimetry (DSC)

The differential scanning calorimeter (DSC) is the instrument that has dominated the field of thermal analysis in the past decade. The term DSC was coined in 1963 at Perkin-Elmer to describe a new thermal analyzer they had developed [98]. It measures heat flows and temperatures associated with exothermic and endothermic transitions. The ease with which important properties such as transitions, heat capacity, reaction, and crystallization kinetics are characterized has made DSC widely used in the plastics laboratory [99].

In DSC analysis, two identical small sample pans are instrumented to operate at the same temperature and can be programmed up or down in temperature at the same rate. A sample is placed in one, and the other is left empty. Instrumentation is provided to measure the electrical power necessary to keep the two sample pans at the same temperature. If a temperature is encountered at which the sample undergoes a change of phase or state, more or less power will be needed to keep the sample pan at the same temperature as the reference pan (depending on whether the reaction is exothermic or endothermic). Since power is the value being recorded, the area under the peak is the electrical equivalent of the heat of the reaction. To measure heat capacity in this calorimeter, the sample pan and reference pan are first brought to some temperature and then heated at some

constant rate. Since the reference pan is empty, it will require a smaller amount of electrical power to achieve this rate [100]. A typical DSC curve is shown in Figure 2.20.
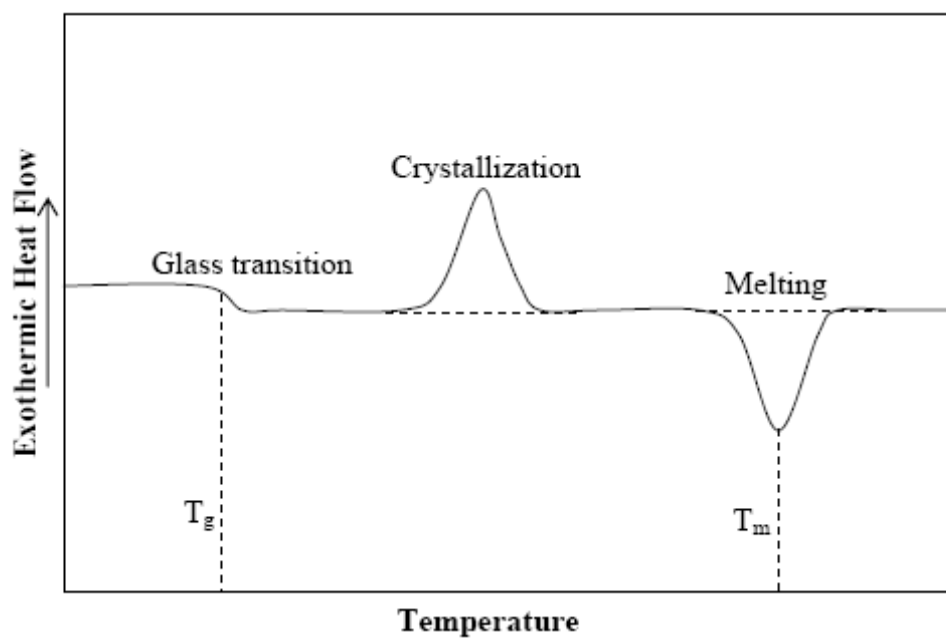
Figure 2.20 DSC thermogram [101]

2.7 Previous Studies

Park et. al. [102] processed PS/organoclay nanocomposites in the presence of poly(styrene-co-vinyloxazolin) (OPS). They found out that the arrangement of the organic modifier between the clay layers affects the dispersion of layers. Lateral bilayer type arrangement results in exfoliated structures, whereas intercalated structures are obtained with paraffinic monolayer type arrangement.

Zhang et al. [103] synthesized PS-clay nanocomposites by γ-radiation technique using four different modified clays. Three of the modified clays were reactive while one was non-reactive. With the reactive modified clays, exfoliated structures were obtained whereas with the nonreactive clay intercalated structure was obtained. The thermal properties of nanocomposites prepared by reactive clay were greatly

enhanced due to the chemical bond formed between the clay and the chains of polystyrene.

Xie et al. [104] prepared polystyrene-clay nanocomposites by suspension polymerization of styrene monomer in the presence of organo-MMT and investigated the effects of organo-MMT concentration and alkyl chain lengths of surfactants on the properties of polystyrene-clay nanocomposites. The optimum organoclay content to yield the best improvement in thermal properties was 5 wt. %. The alkyl chain length of surfactant affected the properties of the nanocomposites as well. With the surfactant possessing the highest chain length, the nanocomposite with the highest glass transition temperature was obtained.

Tanoue et. al. [105] showed that the dispersion of silicate layer for PS/organoclay nanocomposites are tremendously affected by the screw rotation speed, namely the degree of shear. Poly(styrene-co-vinyloxazolin) (OPS) was used as an additional material which enhanced the mechanical properties. It was demonstrated that as the screw rotation increases the distance between the clay platelets, increases for PS/OPS/organoclay ternary systems and fully exfoliated structures were obtained at 70 – 100 rpm speeds.

Tomova et al. [106] indicated that end group configuration is important for the interfacial adhesion and morphology formation in binary polyamide/elastomer blends and in ternary PA 6/PA 66/maleated elastomer blends obtained by melt mixing in a Brabender single screw extruder. The domain size of elastomeric phase was found to be 1 μm for PA 6, whereas it was 4-7 μm for PA 66. It was attributed to difunctionality of PA 66 that enables it to react twice per chain with the maleated elastomer.

Gelfer et al. [107] demonstrated that due to the higher compatibility of organoclay with PMMA than PS matrix, the organoclay concentrated on PMMA phase and at the interphase in PS/PMMA blends. Since PS and PMMA are immiscible polymers, they form separated phases, however, with the addition of organoclay it was found that the average domain size reduces drastically which is the indication of the compatibilization effect of the organoclay. This compatibility is attributed to

the interaction between the polymer matrix and the surfactant, rather than the interaction between polymer matrix and clay surface.

Doh and Cho [108] investigated the effects of various o-MMT structures on the properties of PS-MMT nanocomposites. The nanocomposite containing benzyl-unit similiar to styrene monomer in o-MMT exhibited the highest decomposition temperature. It was concluded that structural affinity between styrene monomer and the organic group of modififed clay is an important factor affecting the structure and properties of the nanocomposites.

Gilman et al. [109] prepared nanocomposites using modified fluorohectorite and montmorillonite by melt intercalation. TEM image of PS-fluorohectorite confirmed that it is a neatly intercalated structure. TEM image for the PS-MMT nanocomposite showed that it contained both intercalated and delaminated MMT layers. Cone calorimetry results showed that the PS-fluorohectorite had no effect on the peak heat release rate whereas PS-MMT hybrid had a 60% reduction in peak heat release rate compared to pure polystyrene. It was also observed that degree of dispersion of the silicate layers affects the flammability properties of the nanocomposites.

Lepoittevin et al. [110] focused on a new approach; masterbatch route to prepare poly (ε-caprolactone)-montmorillonite nanocomposites. Masterbatch route was simply the combination of in-situ polymerization and melt intercalation methods. At the same clay content, the Young's modulus of the nanocomposites prepared by the masterbatch method was higher than that of the ones prepared by melt intercalation. By applying the new method, an intercalated structure was obtained even with native Na-MMT rather than a microcomposite.

Fu et al. synthesized [111] PS-clay nanocomposites by direct dispersion of organically modified clay in styrene monomer followed by free-radical polymerization.The organoclay contained a vinyl benzyl group in the structure. The XRD and TEM results revealed that the clay layers were exfoliated in the PS matrix. It was concluded that vinyl benzyl group of the surfactant is effective in exfoliating MMT in PS matrix.

Zhang et al. [112] reported the first example of clay that contains a carbocation and its use to prepare PS-clay nanocomposites. The nanocomposite was prepared by emulsion polymerization and its mixed intercalated-exfoliated structure was established by XRD and TEM. Both the clay and its nanocomposite showed outstanding thermal stability. It was deduced that this new organically-modified clay may be useful for the preparation of materials which must be processed at temperatures which are above the thermal stability limit of the common ammonium substituted clays.

CHAPTER 3

EXPERIMENTAL

3.1 Materials

3.1.1 Polymer Matrix

In this study, polystyrene matrix with a trade name of Lacqrene® 1960N was used. It was purchased from TOTAL Petrochemicals and supplied in the form of pellets in 25 kg polyethylene bags. Properties of Lacqrene® 1960N given by the supplier are in Table 3.1.

Table 3.1 Properties of polystyrene (Lacqrene® 1960N) [113]

Property	Method	Unit	Value
Rheological			
Melt Flow Index (200 ^{o}C – 5 Kg	ISO 1133 H	g/10min	30
Density	ISO 1183	g/cm^3	1.05
Thermal			
Vicat Softening Point 10N (T increase = 50°C/h)	ISO 306A50	^{o}C	105
Vicat Softening Point 50N (T increase = 50°C/h)	ISO 306B50	^{o}C	101
HDT unannealed under 1.8 MPa	ISO 75-2A	^{o}C	84
HDT annealed under 1.8 MPa	ISO 75-2A	^{o}C	96
Mechanical			
Unnotched Charpy impact strength	ISO 179/1eU	kJ/m^2	6
Tensile strength at break	ISO 527-2	MPa	35

Table 3.1 Properties of polystyrene (Lacqrene® 1960N) [113] (continued)

Elongation at break	ISO 527-2	%	2.5
Tensile Modulus	ISO 527-2	MPa	3200
Flexural Modulus	ISO 178	MPa	2900
Hardness	ISO 2039-2		L 70
Electrical			
Dielectric strength	---	kV/mm	135
Surface resistivity	ISO IEC 93	Ohm	$>10^{14}$
Miscalleneous			
Mold shrinkage	---	%	0.4-0.7
Water absorption	ISO 62	%	<0.1

3.1.2 Organoclays

Three different natural montmorillonites modified with a quaternary ammonium salt were used in this study as filler. These organoclays, namely Cloisite® 15A, Cloisite® 25A, and Cloisite® 30B, were purchased from Southern Clay Products, Texas-U.S.A. They are all additives for plastics to improve various plastic physical properties, such as mechanical, thermal, and barrier properties.

3.1.2.1 Cloisite® 15A

The cation of Cloisite® 15A is dimethyl, dehydrogenated tallow, quaternary ammonium and the anion is chloride. Figure 3.1 shows the chemical structure of organic modifier of Cloisite® 15A. Physical properties obtained from manufacturer are listed in Table 3.2.
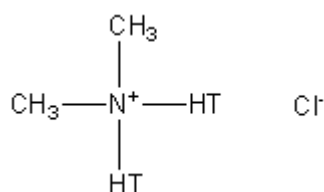
Figure 3.1 Chemical structure of organic modifier (2M2HT$^+$) and anion (Cl$^-$) of Cloisite® 15A.

2M : Dimethyl

HT : Hydrogenated Tallow (Alkyl chain), (~65% C18; ~30% C16; ~5% C14)

Table 3.2 Physical properties of Cloisite® 15A

Properties	Cloisite® 15A
Organic Modifier (1)	2M2HT
Modifier Concentration	125 meq/100g clay
% Moisture	< 2%
% Weight Loss on Ignition	43%
<u>Typical Dry Particle Sizes:</u>	10% less than: 2µ
(microns, by volume)	50% less than: 6µ
	90% less than: 13µ
Color	Off white
Loose Bulk Density, lbs/ft^3	10.79
Packed Bulk Density, lbs/ft^3	18.64
Specific Gravity, g/cc	1.66
d- spacing (X-Ray)	31.5Å

3.1.2.2 Cloisite® 25A

The organic modifier of Cloisite® 25A is dimethyl, hydrogenated tallow, 2-ethylhexyl quaternary ammonium and its anion is methyl sulfate. Figure 3.2 shows the chemical structure of the cation of Cloisite® 25. Table 3.3 summarizes the physical properties of Cloisite® 25 .

CH$_3$

CH$_3$—N$^+$—CH$_2$—CH—CH$_2$—CH$_2$—CH$_2$—CH$_3$

HT

CH$_2$

CH$_3$

OH   O

S

O   O$^-$
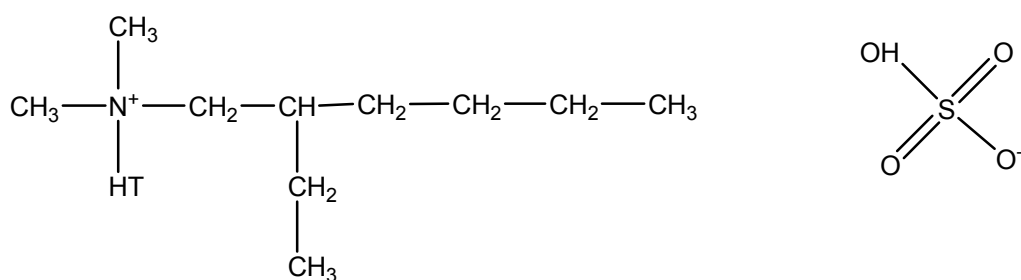
Figure 3.2 Chemical structure of organic modifier (2MHTL8$^+$) and anion (methyl sulfate) of Cloisite® 25A

2MHTL8: dimethyl, hydrogenated tallow, 2-ethylhexyl quaternary ammonium

HT: Hydrogenated Tallow (~65% C18; ~30% C16; ~5% C14)

Table 3.3 Physical properties of Cloisite® 25A

Properties	Cloisite® 25A
Organic Modifier	2MHTL8
Modifier Concentration	95 meq/100g clay
% Moisture	< 2%
% Weight Loss on Ignition	34%
Typical Dry Particle Sizes:	10% less than: 2μ
(microns, by volume)	50% less than: 6μ
	90% less than: 13μ
Color	Off white
Loose Bulk Density, lbs/ft^3	12.08
Packed Bulk Density, lbs/ft^3	20.48
Specific Gravity, g/cc	1.87
d- spacing (X-Ray)	18.6Å

3.1.2.3 Cloisite® 30B

Cloisite® 30B is treated with methyl, tallow, bis-2-hydroxyethyl, quaternary ammonium by manufacturer. The anion of this clay is chloride ion. The chemical structure of organic modifier is shown in Figure 3.3. The physical properties of Cloisite® 30B are given in Table 3.4.

$$CH_3 \!-\! N^+ \!-\! T$$

with
$$CH_2 \!-\! CH_2 \!-\! OH$$
$$CH_2 \!-\! CH_2 \!-\! OH$$
$$Cl^-$$
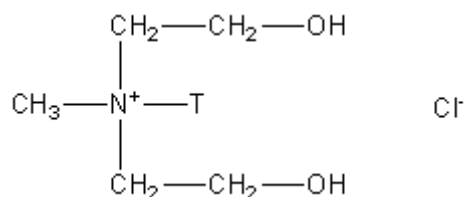
Figure 3.3 Chemical structure of organic modifier (MT2EtOH⁺) and anion (Cl⁻) of Cloisite® 30B

MT2EtOH: methyl, tallow, bis-2-hydroxyethyl, quaternary ammonium
T : tallow (~65% C18; ~30% C16; ~5% C14)

Table 3.4 Physical properties of Cloisite® 30B

Properties	Cloisite® 30B
Organic Modifier	MT2EtOH
Modifier Concentration	90 meq/100g clay
% Moisture	< 2%
% Weight Loss on Ignition	30%
Typical Dry Particle Sizes:	10% less than: 2μ
(microns, by volume)	50% less than: 6μ
	90% less than: 13μ
Color	Off white
Loose Bulk Density, lbs/ft³	14.25
Packed Bulk Density, lbs/ft³	22.71
Specific Gravity, g/cc	1.98
d- spacing (X-Ray)	18.5Å

3.1.3 Compatibilizers

Both aliphatic and aromatic elastomers used in this study are also known as impact modifiers and have compatibilization capability. Therefore, in this study the terms compatibilizer, elastomer and impact modifier are used in the same sense.

In the first part of this study Lotader® AX8900; a terpolymer of Ethylene–Methyl Acrylate–Glycidyl Methacrylate (E-MA-GMA) , Lotader® AX8840; a copolymer of Ethylene–Glycidyl Methacrylate (E-GMA), and Lotader® 2210; a terpolymer of Ethylene–nButyl Acrylate–Maleic Anhydride (E-nBA-MAH), were chosen as the compatibilizers. They were purchased from Arkema Inc., France. The reason for choosing Lotader® resins as compatibilizer was that, they are highly compatible with various thermoplastics including polyethylene, owing to their reactivity, crystallinity and melt fluidity characteristics. Moreover, these resins have high thermal stability during processing.

Lotader® AX8900 and Lotader® AX8840 contain glycidyl methacrylate (GMA) monomer as the reactive group which enables the polymer to react with substances such as hydroxyl (OH) containing materials, carboxylic acids (COOH), and amines. The chemical structure of Lotader® AX8900 and Lotader® AX8840 are given in Figure 3.4 and Figure 3.5, and Table 3.5 gives the specifications of both resins.
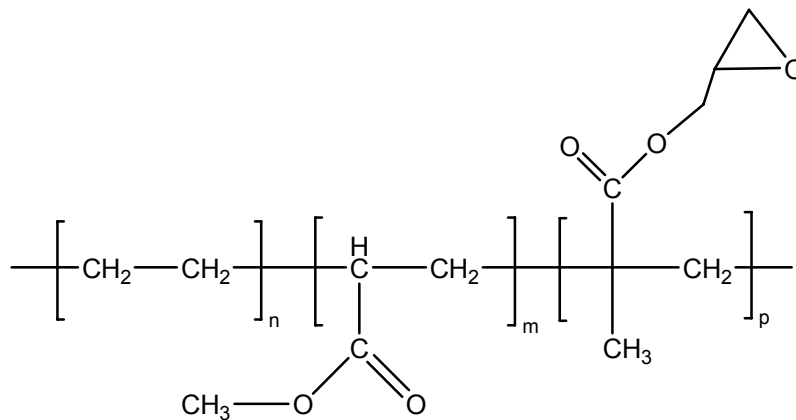
Figure 3.4 Chemical structure of Lotader® AX8900 (E-MA-GMA)
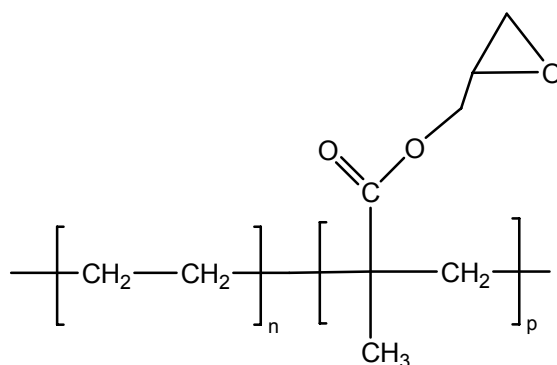
Figure 3.5 Chemical structure of Lotader® AX8840 (E-GMA)

Table 3.5 Specifications of Lotader® AX8900 and Lotader® AX8840

	Unit	Lotader® AX8900	Lotader® AX8840
Type of Polymer		E-MA-GMA	E-GMA
Methyl Acrylate Content	wt %	25	0
Glycidyl Methacrylate Content	wt%	8	8
Melt Index (190°C, 2.1kg,ASTM 1238)	g/10min.	6	5
Melting Point (DSC)	°C	60	105
Vicat Softening Point (ASTM1525-1kg)	°C	< 40	87
Tensile Strength at Break (ASTM D638)	MPa	4	8
Elongation at Break (ASTM D638)	%	1100	420
Hardness Shore A (ASTM D2240)	-	70	92

Lotader® 2210 is different from the other two resins, since it contains maleic anhydride (MAH) monomer, instead of the GMA monomer, as the reactive group. The acrylic ester group of this terpolymer decreases the crystallinity and modifies the mechanical properties. The reactive group, MAH, increases adhesion onto polar substrates and helps formation of chemical bonds with substrates such as metals. Chemical structure and specifications of Lotader® 2210 are given in Figure 3.6 and Table 3.6.
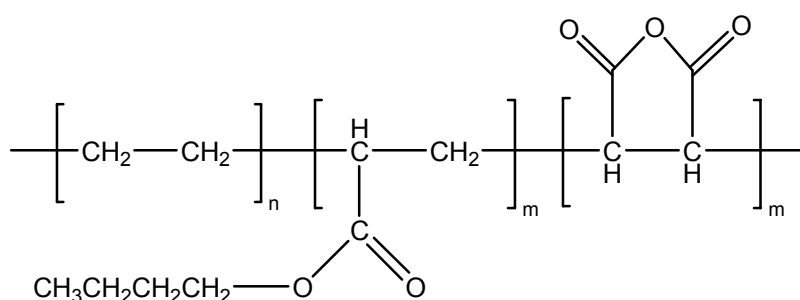
Figure 3.6 Chemical structure of Lotader® 2210 (E-nBA-MAH)

Table 3.6 Specifications of Lotader® 2210

	Unit	**Lotader® 2210**
Type of Polymer		E-nBA-MAH
Butyl Acrylate Content	wt %	8
Maleic Anhydride Content	wt%	2.6
Melt Index (190°C, 2.1kg,ASTM 1238)	g/10min.	3
Melting Point (DSC)	°C	107
Vicat Softening Point (ASTM1525-1kg)	°C	80
Tensile Strength at Break (ASTM D638)	MPa	12

Table 3.6 Specifications of Lotader® 2210 (continued)

Elongation at Break (ASTM D638)	%	600
Hardness Shore D (ASTM D2240)	-	46

In the second part of this study, styrene-butadiene-styrene (SBS) rubber with a trade name of Elastron D was used. It was purchased from Elastron Kimya A.Ş. and supplied in the form of pellets. Properties of Elastron D given by the supplier are in Table 3.7.

Table 3.7 Properties of SBS rubber (Elastron D) [114]

Property	Unit	Value
Hardness	Shore A - D	20A – 65D
Density	g/cm^3	>0.89
Working temperature (max)	^{o}C	65
Working temperature (min)	^{o}C	-30
Solvent resistance	---	Poor
Motor oil resistance	---	Poor
Acid-Base resistance	---	Good
UV-Ozone stability	---	Medium

In order to modify SBS rubber used in the second part of this study, 1% (w/w) or 2% (w/w) maleic anhydride was grafted by means of an extruder. Predefined amounts of maleic anhydride and SBS rubber were manually premixed and then this mixture was fed into the extruder.

3.1.4 Maleic Anhydride

Maleic anhydride (2,5-Furandione) used in this study was purchased from Sigma-Aldrich Chemicals Co. Chemical structure and some basic properties of maleic anhydride are given in Figure 3.7 and Table 3.8 respectively.
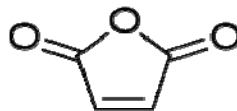
Figure 3.7 Chemical structure of maleic anhydride

Table 3.8 Properties of Maleic Anhydride [115]

Property	Unit	Value
Molecular weight	g/mol	98.06
Appearance		White powder

3.2 Experimental Set-Up

3.2.1 Melt Blending

In this study, a co-rotating twin screw extruder was used in order to obtain ternary nanocomposites. The model of extruder is Thermoprism TSE 16 TC with L/D = 24. The screw diameter and the twin bore diameter of the extruder are 15.6 mm and 16 mm respectively. It has a barrel length of 384 mm. In addition to these, maximum screw speed and maximum torque that can be achieved are 500 rpm and 12 Nm. It is possible to set barrel zones and die temperatures, screw speed and feed flow rate of main-feeder and side-feeder by using control panel with this extruder which allows us to perform several experiments with different process parameters. Figures 3.8 and 3.9 show the extruder and its screw configuration that was used for this study.

Figure 3.8 Thermo Prism TSE 16 TC twin screw extruder

Figure 3.9 Screw Configuration of Thermo Prism TSE 16 TC twin screw extruder

During the extrusion process, temperature profile of the hopper, the mixing zones and the die, the screw speed, and the total flow rate of feed were constant in all

experiments. Process temperatures were 200, 200, 200, 200 ,200 °C for the hopper, the three mixing zones and the die, respectively. The screw speed and total flow rate of feed were kept constant at 150 rpm and 25 g/min throughout the experiments. In order to obtain the desired compositions, inlet flow rate of the main-feeder and the side-feeder were calibrated before each extrusion run. The molten product obtained from the extruder barrel was cooled by passing through a water bath, whose temperature was continuously controlled. At the end of the water bath, a blower was placed in order to remove the water from the product surface, and finally the product was collected in plastics bags after passing through the pelletizer.

3.2.2 Injection Molding

After the extrusion, the specimens were injection molded by DSM Xplore laboratory scale micro injection molding equipment. The photograph of this equipment can be seen in Figure 3.10. It consists of a mold on the left hand side and a pressure cylinder on the right hand side, where a nozzle is connected to the mold. The maximum pressure limit of this machine is 16 bars.

Figure 3.10 Injection Molding Machine

Before molding the samples, the pellets were put into the cylinder with a spoon. After waiting for three minutes for the material to melt, the melt was injected into the mold with a maximum pressure of 13 bars. In each molding operation, two

specimens were obtained, one of which had the shape of a dogbone, whereas the other one was the sample of the impact test with a rectangular shape. During the molding process, the melt and mold temperatures were set to 200 and 30°C, respectively for all the samples.

3.3 Experimental Procedure

Firstly, compatibilizers and clays were dried at appropriate temperatures in order to get rid of the moisture. Drying conditions were determined by considering the melting point of the raw materials. Table 3.9 shows the drying conditions.

Table 3.9 Drying conditions

Materials	Drying Temperature (°C)	Drying Time (h)
PS	-	-
Lotader® AX8900	40	12-15
Lotader® AX8840		
Lotader® 2210		
Elastron D		
Cloisite® 15A	120	12-15
Cloisite® 25A		
Cloisite® 30B		

Secondly, compatibilizer and PS were manually premixed at predefined ratios. PS+Compatibilizer mixture was fed from the main feeder of the extruder, and clay was fed from the side feeder of the extruder.

Thirdly, all extruded blends and nanocomposites were dried overnight at 80 $^\circ$C. Then, injection molding was done.

Flowchart of the experimental procedure and characterization of the nanocomposites are shown in Figure 3.11.

```
                        ┌─────────────────────┐
                        │       Drying        │
                        │  of Raw Materials   │
                        └─────────────────────┘
                                  ⇩
                        ┌─────────────────────┐
                        │ Melt Blending by Twin│
                        │   Screw Extruder    │
                        └─────────────────────┘
                                  ⇩
                        ┌─────────────────────┐
                        │  Injection Molding  │
                        │       220°C         │
                        └─────────────────────┘
                                  ⇩
   ┌──────────────┐     ┌─────────────────────┐     ┌──────────────┐
   │ Morphological│ ⇦   │   Characterization  │  ⇨  │   Thermal    │
   │Characterizaton│    │         of          │     │Characterization│
   │(SEM, XRD, TEM)│    │   Nanocomposites    │     │    (DSC)     │
   └──────────────┘     └─────────────────────┘     └──────────────┘
                      ⇙                     ⇘
   ┌──────────────┐                         ┌──────────────┐
   │ Rheological  │                         │  Mechanical  │
   │Characterizaton│                        │Characterization│
   │              │                         │              │
   │Melt Flow Index│                        │ Tensile Test │
   │Capillary Viscometer│                   │ Impact Test  │
   └──────────────┘                         └──────────────┘
```
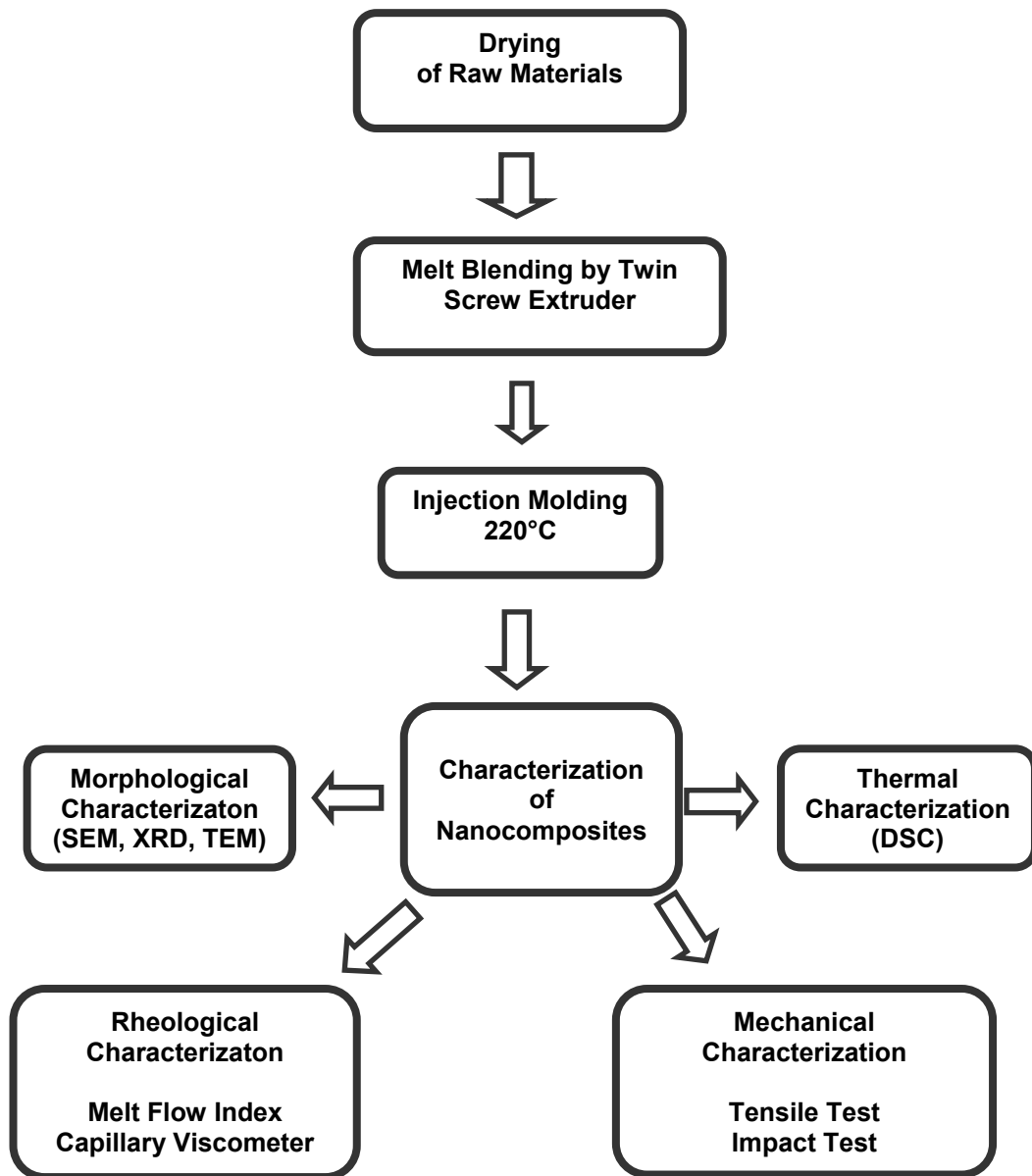
Figure 3.11 Flowchart of experimental procedure and characterization

Compositions of all samples prepared for this study are shown in Table 3.10

Table 3.10 Compositions of all the samples

Set	Composition	Concentration wt %		
		PS	**Elastomer**	**Organoclay**
1	PS	100	-	-
PS/Organoclay Compositions				
2	PS+15A	98	-	2
3	PS+25A	98	-	2
4	PS+30B	98	-	2
5	PS+30B	96	-	4
PS/Compatibilizer Compositions				
6	PS+SBS	95	5	-
7	PS+SBS	90	10	-
8	PS+SBS	85	15	-
9	PS+SBS	75	25	-
10	PS+SBS	60	40	-
11	PS+SBSgMAH (1%)	95	5	-
12	PS+SBSgMAH (1%)	90	10	-
13	PS+SBSgMAH (1%)	85	15	-
14	PS+SBSgMAH (1%)	75	25	-
15	PS+SBSgMAH (1%)	60	40	-
16	PS+SBSgMAH (2%)	95	5	-
17	PS+SBSgMAH (2%)	90	10	-
18	PS+SBSgMAH (2%)	85	15	-
19	PS+SBSgMAH (2%)	75	25	-
20	PS+SBSgMAH (2%)	60	40	-
Ternary Compositions				
21	PS+8900+15A	93	5	2
22	PS+8840+15A	93	5	2
23	PS+2210+15A	93	5	2
24	PS+8900+25A	93	5	2
25	PS+8840+25A	93	5	2

Table 3.10 Compositions of all the samples (continued)

26	PS+2210+25A	93	5	2
27	PS+8900+30B	93	5	2
28	PS+8840+30B	93	5	2
29	PS+2210+30B	93	5	2
30	PS+SBS+30B	93	5	2
31	PS+SBS+30B	88	10	2
32	PS+SBS+30B	83	15	2
33	PS+SBS+30B	73	25	2
34	PS+SBS+30B	58	40	2
35	PS+SBS+30B	91	5	4
36	PS+SBS+30B	86	10	4
37	PS+SBS+30B	81	15	4
38	PS+SBS+30B	76	20	4
39	PS+SBS+30B	71	25	4
40	PS+SBSgMAH (1%)+30B	93	5	2
41	PS+SBSgMAH (1%)+30B	88	10	2
42	PS+SBSgMAH (1%)+30B	83	15	2
43	PS+SBSgMAH (1%)+30B	73	25	2
44	PS+SBSgMAH (1%)+30B	58	40	2
45	PS+SBSgMAH (2%)+30B	93	5	2
46	PS+SBSgMAH (2%)+30B	88	10	2
47	PS+SBSgMAH (2%)+30B	83	15	2
48	PS+SBSgMAH (2%)+30B	73	25	2
49	PS+SBSgMAH (2%)+30B	58	40	2
50	PS+SBSgMAH (2%)+30B	91	5	4
51	PS+SBSgMAH (2%)+30B	86	10	4
52	PS+SBSgMAH (2%)+30B	81	15	4
53	PS+SBSgMAH (2%)+30B	76	20	4
54	PS+SBSgMAH (2%)+30B	71	25	4

3.4 Characterization of the Specimens

In order to investigate the effects of the composition of raw materials, compatibilizer type and organoclay type on the final properties of the nanocomposites, morphological, thermal, flow, and mechanical analyses were carried out.

3.4.1 Morphological Analysis

3.4.1.1 X-Ray Diffraction (XRD) Analysis

The composites containing organoclay were analyzed by using a RIGAKU D/MAX 2200/PC X-Ray diffractometer that generates a voltage of 40kV and current 40 mA from Cu Kα radiation source (λ= 1.5418). The diffraction angle 2θ was scanned from 1° to 10° with scanning rate of 1°/min and a step size of 0.02°. Bragg's law was used to calculate the distance between the silicate layers. The samples for X-Ray diffraction analysis were obtained from injection molded specimens.

3.4.1.2 Scanning Electron Microscopy (SEM) Analysis

Scanning electron microscopy (SEM) analysis was performed by a JEOL JSM-6400 low voltage scanning electron microscope. The impact fracture surfaces were etched in an ultrasonic bath for 15 minutes at 30 $^{\circ}$C, by using n-heptane to dissolve the elastomeric phase. Before SEM photographs were taken, the fractured surfaces were coated with a thin layer of gold in order to obtain a conductive surface. SEM photographs were taken for each specimen at x250 and x1500 magnifications. This analysis was used to observe the dispersion of the elastomeric phase and investigate the failure mechanism of the nanocomposites and blends.

3.4.1.3 Transmission Electron Microscopy (TEM) Analysis

For TEM analysis, sections of 70 nm in thickness were cryogenically cut with a diamond polymer knife at a temperature of -100°C for PS/organoclay binary and

PS/elastomer/organoclay ternary nanocomposites. These samples were examined by a Fei Transmission Electron Microscope at an acceleration rate of 80 kV in METU, Central Laboratory . All samples were trimmed parallel to the molding direction.

3.4.2 Thermal Analysis

3.4.2.1 Differential Scanning Calorimetry (DSC) Analysis

The glass transition temperature measurements of the samples were carried out under nitrogen atmosphere by using Perkin Elmer Diamond differential scanning calorimeter. They were heated from 20°C to 350°C with a heating rate of 20°C/min. Sufficient amount of samples were cut from dry tensile bars and placed in aluminum DSC pans. Changes in T_g values were examined for selected compositions to see the effects of clay content, compatibilizer content and the type of the compatibilizer. Due to steric hindrance effect of the phenyl group in the backbone of polystyrene, it is an amorphous material and no crystallinity was detected.

3.4.3 Mechanical Analysis

Tensile tests and impact tests were performed at room temperature. At least five samples were used for each composition set and average and standard deviation values of the test results were recorded.

3.4.3.1 Tensile Tests

Tensile tests were performed for each composition according to ASTM D638M-91a (Standard Test Method for Tensile Properties of Plastics) [89], by using a Lloyd LR 30 K Universal Testing machine. The shape and dimensions of the specimens are given in Figure 3.12 and Table 3.11 respectively.
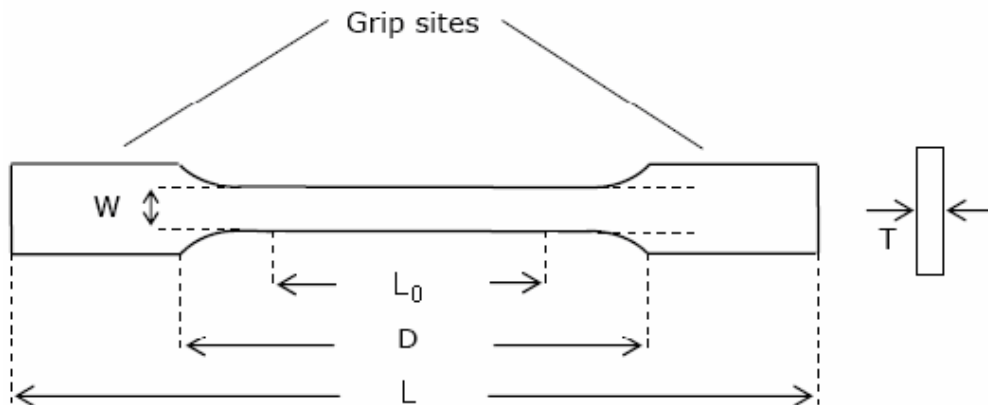
Figure 3.12 ASTM Tensile test specimen

Table 3.11 Dimensions of tensile test specimen

Symbol	Specimen Dimensions (mm)
W, Width of narrow section	5
D, Distance between grips	50
L, Total length of specimen	30
L$_0$, Gauge length of specimen	75
T, Thickness of specimen	2.1

The crosshead speed was calculated as 3 mm/min, based on the gauge length of 30 mm and strain rate of 0.1 min^{-1}. The test was performed by pulling the specimens until it fails. Stress and strain data were obtained from the mechanical testing device and tensile strength, tensile modulus, strain at yield and strain at break values were determined by using these graphs.

3.4.3.2 Impact Test

In order to perform unnotched charpy impact tests, samples with dimensions of 80x10x4 mm were used with the Ceast Resil Impactor. Its photograph is shown in Figure 3.13. All of the tests were performed at room temperature. At least five samples were used for each composition set and the average and standard deviation values were calculated.

Figure 3.13 Ceast Resil Impact Tester

3.4.4 Flow Characteristics

3.4.4.1 Melt Flow Index (MFI) Test

Melt flow index (MFI) test was performed according to ASTM D1238-79 using an Omega Melt Flow Indexer. The measurements were carried out at 200 °C with a load of 2.16 kg. The weight of the sample passing through the die in 10 min, defined as melt index, was determined for all compositions. At least five measurements were done for each sample to get accurate results. The results were recorded as grams/10 min. The melt flow index machine used in this study is shown in Figure 3.14.

Figure 3.14 Omega Melt Flow Indexer

3.4.4.2 Capillary Viscometry

The apparent shear viscosity of the raw materials PS, SBS, SBSgMAH (1%) and SBSgMAH (2%) were measured by using LCR Series capillary rheometer. The experiments were performed at 200°C and in the range of shear rate from 1.37 to 412 (1/s). The dimensions of the die were: 30.48 mm capillary length, 0.762 mm capillary diameter.

CHAPTER 4

RESULTS AND DISCUSSION

4.1 Morphological Analyses

4.1.1 X-Ray Diffraction (XRD) Analysis

XRD analysis has been widely used to analyze the dispersion state of an organoclay in the polymer matrix and the interlayer spacing of the silicate layers. The patterns obtained from the analysis are used for the characterization of the structure of nanocomposites by using the 2theta peak, which is used for the calculation of the distance between the silicate layers according to Bragg's law. The intercalation of polymer chains between the silicate layers results in an increase in the interlayer spacing. For intercalated structures, the characteristic peak tends to shift to a lower angle due to the expansion of the basal spacing [116]. Although the layer spacing increases, there still exists an attractive force between the layers to stack them in an ordered structure. Change in intensity and the shape of the basal reflections is another evidence that specifies the intercalation of polymer chains [25].

On the other hand, peaks disappear in the XRD pattern of exfoliated polymer nanocomposites due to completely dispersed clay platelets in the matrix. XRD results may indicate the dispersion state of the clay platelets in the polymer matrix but they should not be used as the only evidence for delamination or exfoliation. Because of low organoclay loading, X-ray beams may hit to a non-uniformly dispersed region of the sample. The features of the local microstructures from TEM give useful information on the overall picture that is drawn from XRD results [117]. Thus, XRD and TEM analyses should be evaluated together to obtain more

accurate information about the dispersion state of the organoclays in the polymer nanocomposites.

In order to obtain exfoliated structures, interaction between the clay surface and the polymer should be high. Viscosity and other shear elements such as screw speed and screw configuration also affect the clay dispersion.

The XRD diffraction pattern of the organoclays Cloisite ® 30B, 15A and 25A used in this study and the pattern of each composition are shown separately in Appendix A. The basal spacing values of all the compositions are shown in Table 4.1. The basal spacing of the organoclays 30B, 15A and 25A were found as 18.1 Å, 31.5 Å / 12.4 Å and 18.7 Å respectively. The secondary peak d_{002} in Cloisite ® 15A is due to unmodified clay, since it coincides with the d-spacing of unmodified clay.

Table 4.1 XRD results of all compositions

Composition	1st Peak		2nd Peak	
	2theta (°)	d_{001} (Å)	2theta (°)	d_{002} (Å)
Organoclays				
Cloisite ® 30B	4.88	18.1	---	---
Cloisite ® 15A	2.80	31.5	7.10	12.4
Cloisite ® 25A	4.72	18.7	---	---
PS/Organoclay Nanocomposites				
PS+30B (2%)	6.00	14.7	---	---
PS+15A (2%)	2.87	30.7	5.56	15.9
PS+25A (2%)	3.28	26.9	5.62	15.7
PS+30B (4%)	6.12	14.4	---	---
PS/2% Organoclay/5% Aliphatic Elastomer Nanocomposites				
PS + 2210 + 30B	6.20	14.3	---	---
PS + 8840 + 30B	6.23	14.2	---	---
PS + 8900 + 30B	2.09	42.3	6.24	14.2
PS + 2210 + 15A	2.79	31.7	5.15	17.2
PS + 8840 + 15A	2.57	34.4	5.10	17.3

Table 4.1 XRD results of all compositions (continued)

PS + 8900 + 15A	2.36	37.4	4.52	19.6
PS + 2210 + 25A	3.13	28.2	5.67	15.6
PS + 8840 + 25A	2.83	31.2	5.37	16.5
PS + 8900 + 25A	2.56	34.5	---	---
PS/2% Cloisite ® 30B/SBS Nanocomposites				
PS + SBS (5%) + 30B	2.66	33.2	5.55	15.9
PS + SBS (10%) + 30B	5.85	15.1	---	---
PS + SBS (15%) + 30B	5.50	16.1	---	---
PS + SBS (25%) + 30B	5.55	15.9	---	---
PS + SBS (40%) + 30B	6.25	14.1	---	---
PS/2% Cloisite ® 30B/1% SBSgMAH Nanocomposites				
PS + SBSgMAH (5%)+ 30B	2.93	30.2	5.83	15.2
PS + SBSgMAH (10%)+ 30B	2.93	30.2	5.85	15.1
PS + SBSgMAH (15%)+ 30B	3.02	29.3	6.03	14.7
PS + SBSgMAH (25%)+ 30B	6.17	14.3	---	---
PS + SBSgMAH (40%)+ 30B	6.76	13.1	---	---
PS/2% Cloisite ® 30B/2 % SBSgMAH Nanocomposites				
PS + SBSgMAH (5%)+ 30B	2.42	36.5	5.92	14.9
PS + SBSgMAH (10%)+ 30B	2.54	34.8	5.93	14.9
PS + SBSgMAH (15%)+ 30B	2.50	35.3	6.00	14.7
PS + SBSgMAH (25%)+ 30B	2.26	39.1	6.38	13.9
PS + SBSgMAH (40%)+ 30B	6.56	13.5	---	---
PS/4% Cloisite ® 30B/SBS Nanocomposites				
PS + SBS (5%) + 30B	2.22	39.8	5.89	15.0
PS + SBS (10%) + 30B	1.99	44.4	5.87	15.1
PS + SBS (15%) + 30B	1.99	44.4	5.77	15.3
PS + SBS (20%) + 30B	1.94	45.5	5.65	15.6
PS + SBS (25%) + 30B	1.94	45.5	5.65	15.6
PS/4% Cloisite ® 30B/2 % SBSgMAH Nanocomposites				
PS + SBSgMAH (5%)+ 30B	2.22	39.8	5.90	15.0
PS + SBSgMAH (10%)+ 30B	2.28	38.7	6.08	14.5

Table 4.1 XRD results of all compositions (continued)

PS + SBSgMAH (15%)+ 30B	1.99	44.4	6.17	14.3
PS + SBSgMAH (20%)+ 30B	2.02	43.7	6.20	14.3
PS + SBSgMAH (25%)+ 30B	6.23	14.2	---	---

XRD patterns of binary polystyrene/organoclay nanocomposites are given in Figure 4.1. The basal spacing of the silicate layers in binary nanocomposites decreased with respect to the basal spacing of layers in original powders of Cloisite ® 15A and Cloisite ® 30B. The change in the d_{001} interlayer spacing of the binary nanocomposite containing PS/Cloisite® 15A is not significant. However, due to insertion of the PS chains between unmodified layers, the second peak is shifted to the left. There are many parameters which may affect exfoliation of clay layers such as polarity, shear intensity of the extruder, initial d-spacing value, organoclay stability and surfactant packing density. Because of absence of polar groups on its modifier, Cloisite® 15A has the most hydrophobic surface and the highest initial d-spacing value among the organoclays used in this study. Attraction between platelets in Cloisite ® 15A is relatively low due to high interlayer spacing, and diffusion of polymer chains into these layers might be easier. Thus, it is expected that interaction between non-polar polystyrene matrix and Cloisite® 15A should be higher than other organoclays used in this study. In spite of this high interaction, other factors restrict the exfoliation of the clay platelets. Cloisite ® 15A has two long aliphatic tails and these tails restricted the access of polymer chains to the clay surface. Because of these alkyl chains, the interaction between the platelets of Cloisite ® 15A and polymer chains could not be overcome.

Cloisite ® 30B has the most hydrophilic surface among the organoclays used in this study because of –OH groups on its organic modifier. Therefore, its dispersion is poor in the highly non-polar PS matrix.

However, in Cloisite ® 25A the d_{001} peak of the powder increased from 18.7 Å to 26.9 Å upon compounding with PS. Also, another peak appeared at 15.7 Å. This is probably due to unintercalated clay layers of Cloisite ® 25A
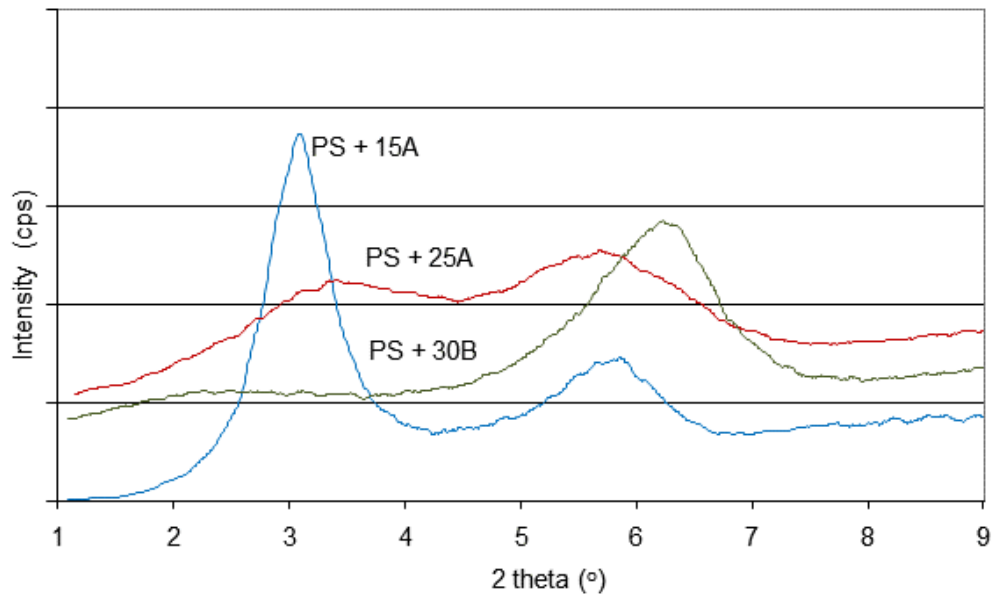
Figure 4.1 XRD patterns of nanocomposites containing 2wt% organoclay

The intercalation of polystyrene chains into silicate layers or exfoliation of silicate layers was tried to be achieved by adding a third component to the PS/organoclay binary nanocomposites. Figures 4.2, 4.3 and 4.4 show the XRD patterns of nanocomposites containing 2% organoclay and 5% elastomer. In order to obtain exfoliated or intercalated structures, clay surface and polymer matrix should have high interaction. Polystyrene is a non-polar polymer, thus it is difficult to obtain exfoliation in polystyrene. To overcome this problem, a third component, compatibilizer having high interaction both clay and polymer matrix, should be used.
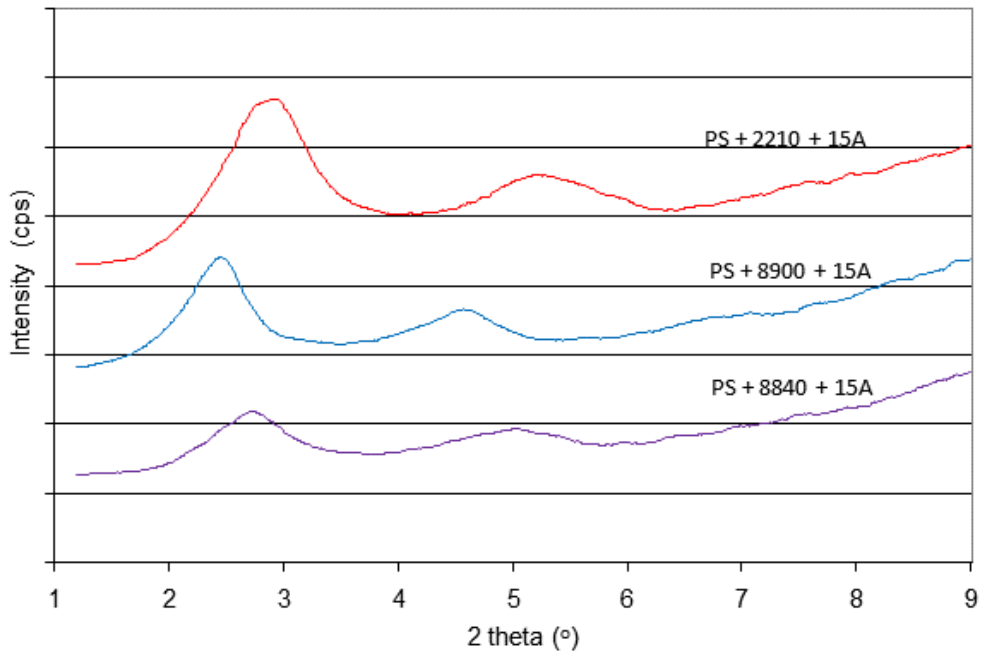
Figure 4.2 XRD patterns of nanocomposites containing 2wt% Cloisite ® 15A and 5wt% elastomer
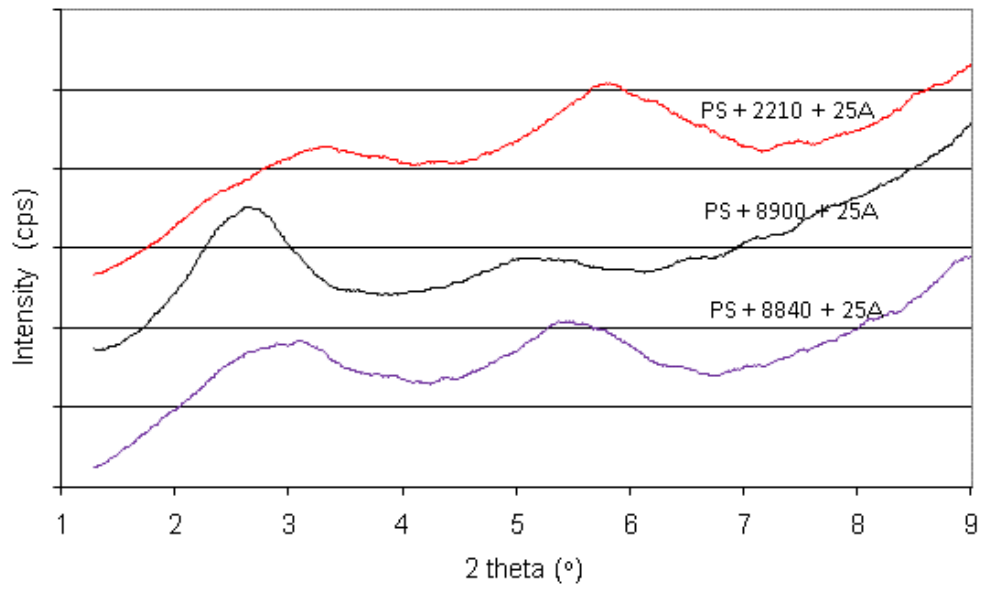
Figure 4.3 XRD patterns of nanocomposites containing 2wt% Cloisite ® 25A and 5wt% elastomer
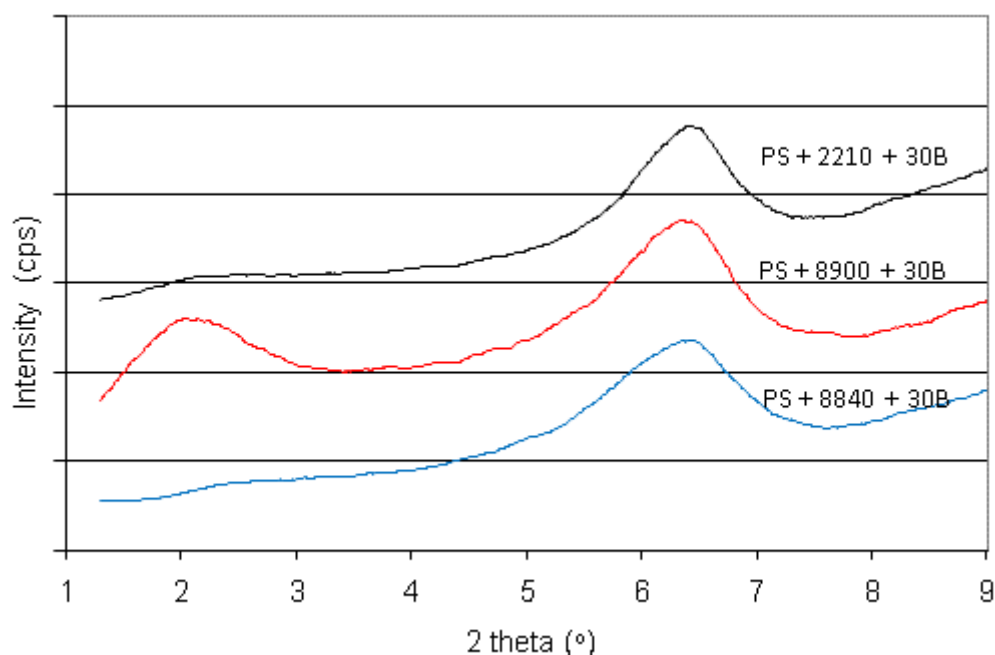
Figure 4.4 XRD patterns of nanocomposites containing 2wt% Cloisite ® 30B and 5wt% elastomer

To accomplish this work, materials which might be compatible with organoclays and polystyrene matrix were used. Lotader® AX8900 is a terpolymer of Ethylene – Methyl Acrylate – Glycidyl Methacrylate (E-MA-GMA), Lotader® AX8840 is a Copolymer of Ethylene – Glycidyl Methacrylate (E-GMA) and Lotader® 2210 is a terpolymer of Ethylene – nButyl Acrylate –Maleic Anhydride (E- nBA-MAH). All of the compatibilizers used in this study have functional groups. However, none of these compatibilizers significantly helped exfoliation of silicate layers, as observed from Table 4.1 and Figures 4.2 through 4.5.

When the effects of organoclay content and elastomer type on the dispersion of silicate layers are investigated, very little enhancement can be observed in the basal spacing of these ternary nanocomposites. Besides, in some cases the diffraction peak shifted to the right, indicating a decrease in the basal spacing. Increasing clay content had no positive effect on the intercalation or exfoliation of silicate layers. The interaction between the functional groups of elastomeric materials and hydroxyl groups on the clay surface may be weakened due to heat treatment or the decomposition of organic modifier, so that some portion of the

ammonia salts may have exuded from the clay gallery, leading to a decrease in interlayer spacing. [118]

Another reason of the collapse in basal spacing may be explained by the applied high pressure during the injection molding process. In the injection molding process, molten polymer is injected from barrel to the mold by applying about 10 bars of pressure. High pressure may also cause the reduction in the basal spacing of silicate layers.

These set of compatibilizers i.e. Lotaders 2210, AX8900 and AX8840 were not highly effective in intercalating and/or exfoliating these organoclays. It is thought that these compatibilizers are aliphatic, whereas PS is aromatic, therefore these compatibilizers were incompatible with PS. Thus, different aromatic based compatibilizers, Styrene-Butadiene-Styrene (SBS) and maleic anhydride grafted SBS (SBSgMAH) were used in the following section. Grafting of maleic anhydride onto SBS was carried out by means of an extruder and maleic anhydride content of the SBSgMAH was determined by back titration method. Experimental procedure and results of analysis are given in the Appendix D. The aim of grafting maleic anhydride onto SBS is to cause a chemical reaction between the hydroxyl groups of the surface of organoclay and maleic anhydride. Maleic anhydride increases adhesion onto polar substances and allows the creation of chemical bonds.

Figures 4.5, 4.6 and 4.7 show the XRD pattern of nanocomposites containing 2wt% organoclay and different ratios of compatibilizer. In these compositions, pure SBS, 1wt% maleic anhydride grafted SBS and 2wt% maleic anhydride grafted SBS were used as the compatibilizers. As the compatibilizer content increased, peaks in XRD patterns became broader and the intensities decreased. Results showed that increasing these aromatic compatibilizers content causes intercalation and exfoliation of the organoclay layers.
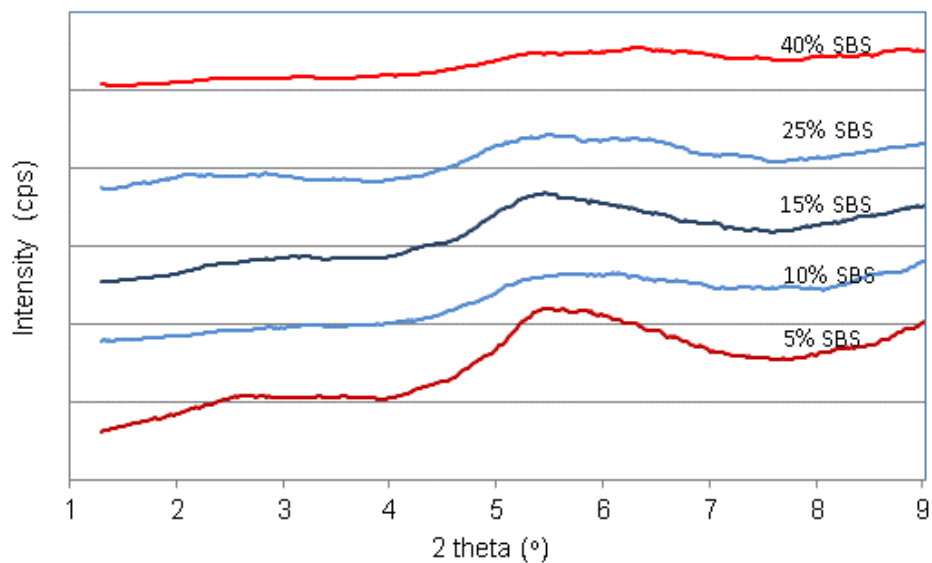
Figure 4.5 XRD patterns of nanocomposites containing 2wt% Cloisite ® 30B and different ratios of pure SBS.
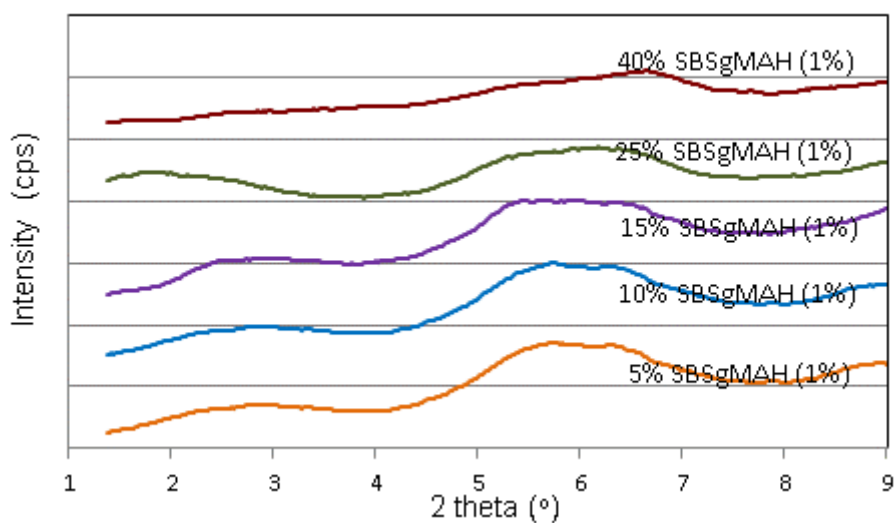
Figure 4.6 XRD patterns of nanocomposites containing 2wt% Cloisite ® 30B and different ratios of 1% maleic anhydride grafted SBS.
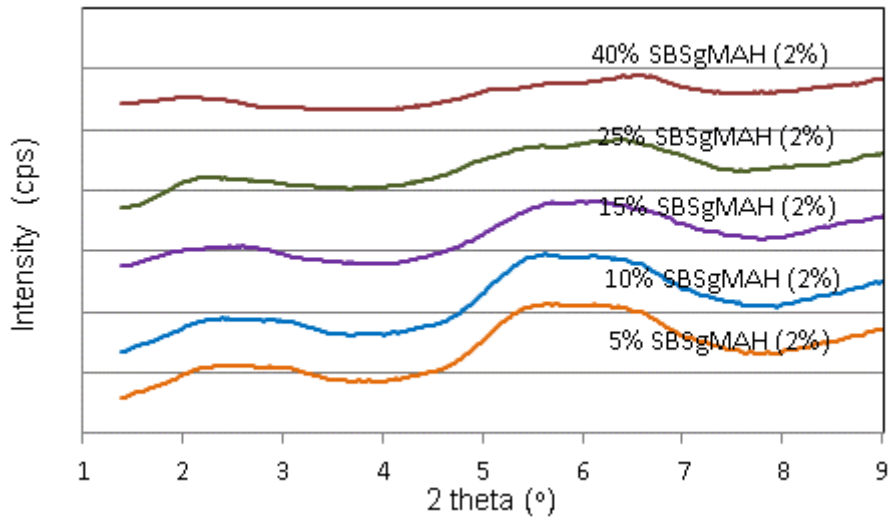
Figure 4.7 XRD patterns of nanocomposites containing 2wt% Cloisite ® 30B and different ratios of 2% maleic anhydride grafted SBS.

Figures 4.8 and 4.9 show the XRD patterns of nanocomposites containing 4wt% Cloisite ® 30B and different ratios of compatibilizers.
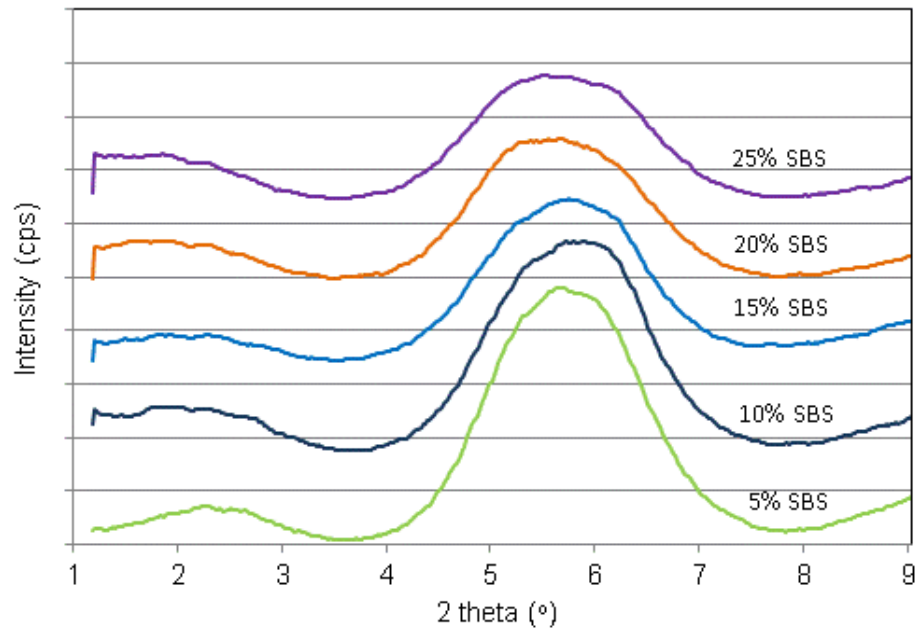
Figure 4.8 XRD patterns of nanocomposites containing 4wt% Cloisite ® 30B and different ratios of pure SBS.
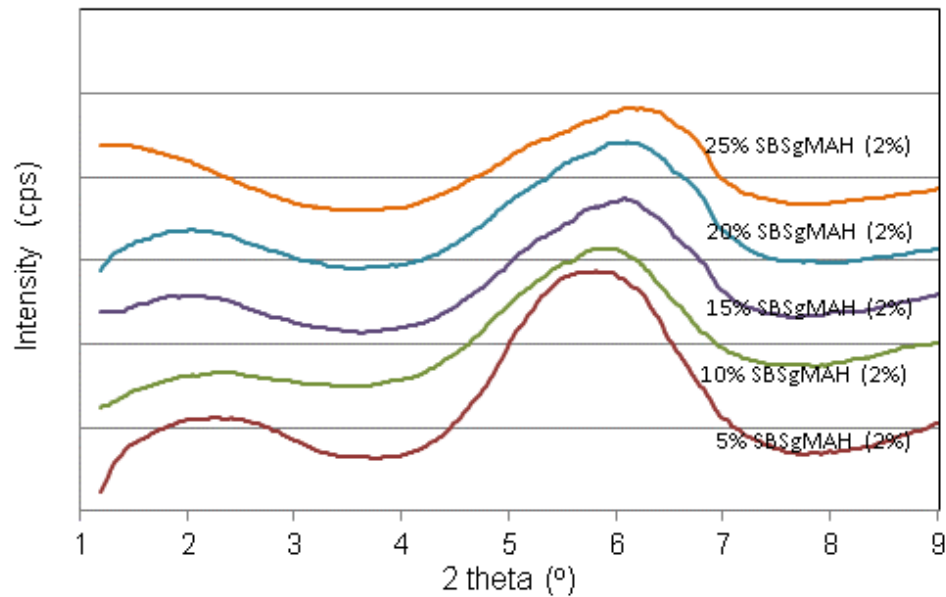
Figure 4.9 XRD patterns of nanocomposites containing 4wt% Cloisite ® 30B and different ratios of 2% maleic anhydride grafted SBS.

Cloisite® 30B has the highest polarity among the organoclays used in this study. Therefore, it is expected to be compatible with polar elastomers. In the second part of the study, Cloisite ® 30B was chosen since the hydroxyl groups in Cloisite ® 30B can react with maleic anhydride. The other two organoclays do not have hydroxyl groups that can react with maleic anhydride.

In ternary nanocomposites, the clay particles are dispersed both in the elastomeric phase and at the interface of polystyrene matrix and elastomer. As shown later in Figures 4.36 - 4.37 the PS matrix has higher viscosity than SBS and SBSgMAH. Thus, it is easier for the SBS and SBSgMAH chains to enter between the clay layers owing to their higher mobility than the PS chains. This is observed in Figures 4.5 through 4.9.

These figures also indicate that the XRD patterns of ternary nanocomposites prepared with SBSgMAH show broader peaks indicating larger interlayer spacing distribution. Thus, it can be said that the elastomer SBSgMAH acts as a better

compatibilizer for PS/Cloisite® 30B nanocomposites, in comparison to Lotader AX8840, Lotader AX8900 and Lotader 2210.

4.1.2 Scanning Electron Microscopy

In order to improve the toughness of brittle polymers, rubbery block copolymers may be used. Dispersion of the rubber phase in the polymer matrix is an important factor that affects the impact strength of materials. SEM analysis can be used to examine the dispersion of elastomeric particles and their size. By SEM analysis, another property, i.e. failure mechanism can also be investigated. In the SEM analysis part of this study, photographs were taken at x250 and x1500 magnifications.

In this study, elastomeric domains were observed when the fractured surfaces of the samples were etched with n-heptane. The effects of both the increase in elastomer content and organoclay addition on the morphology are discussed by the help of the size of these domains.

In order to remove the rubber phase, the fractured surfaces of the samples were etched with n-Heptane before taking SEM photographs. Image J software was used to analyze the dispersion of the rubber phase in the polystyrene matrix. In order to obtain accurate results, about 50-100 domains were analyzed. Average domain size was calculated by using Equations 4.1 and 4.2 where A_i and n_i represent the area and the number of domains that has an area of A_i, respectively.

$$A_{av} = \sum n_i . A_i / \sum n_i \qquad (4.1)$$

$$d_{av} = (A_{av} * 4/\pi)^{0.5} \qquad (4.2)$$

In order to see the effects of n-heptane on the neat PS, etching process was applied on the neat PS in addition to the PS/elastomer binary blends and PS/organoclay/elastomer ternary nanocomposites. Figure 4.10 shows the SEM micrograph of unetched neat PS and Figure 4.11 shows the SEM micrographs of etched neat PS. There is no significant difference between these two figures,

since there were no elastomeric domains to be etched. PS exhibits sharp crack propagation lines due to its brittleness. These sharp lines enhance further propagation of crack and make the PS easier to break with only a small amount of energy.

(a)   (b)
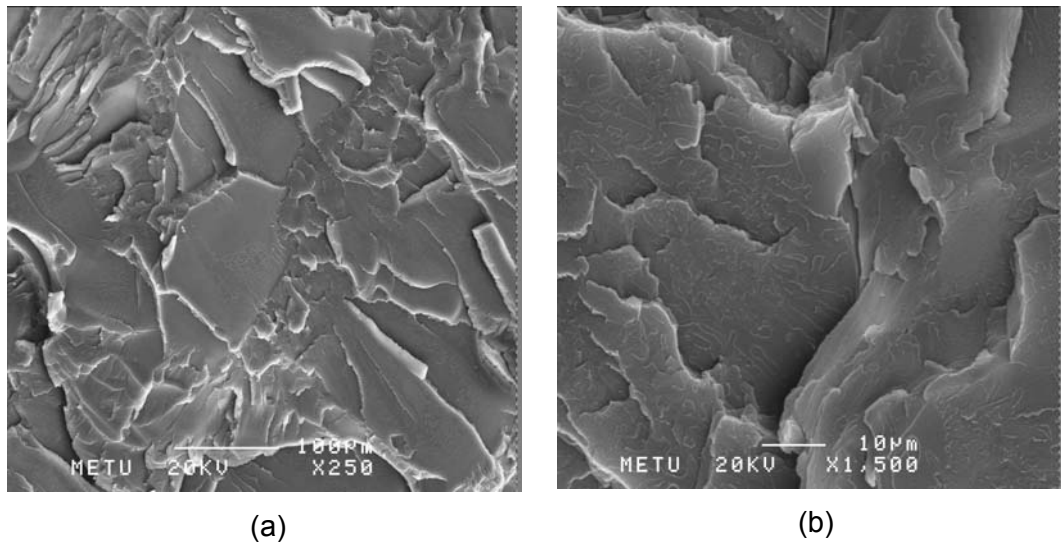
Figure 4.10 SEM micrographs of unetched neat PS with (a) x250 and (b) x1500 magnifications

(a)   (b)
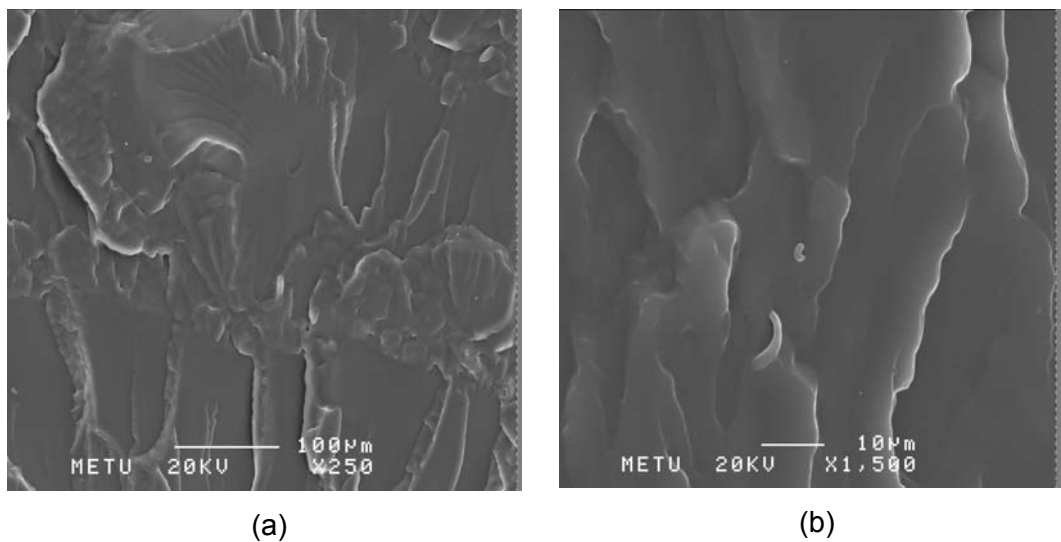
Figure 4.11 SEM micrographs of etched neat PS with (a) x250 and (b) x1500 magnifications

In the first part of this study, nanocomposites were prepared with aliphatic elastomers and three different types of organoclays. Lotader 2210, Lotader AX8840 and Lotader AX8900 were used as elastomers and Cloisite ® 15A, Cloisite ® 25A and Cloisite ® 30B were used as organoclays. Elastomer content was kept at 5% and organoclay content was kept at 2% for all of the compositions. Average domain sizes of these samples are shown in Table 4.2 and SEM images of these samples are shown in Figures 4.12-4.14.

According to the results which are given in Table 4.2, no significant change of the average domain size was observed. This may occur due to incompatibility of the all the three kinds of the elastomers and PS matrix. As explained before, PS contains aromatic phenyl ring, however; all the three kinds of the Lotaders do not.

Table 4.2 Average domain size of the samples containing various kinds of elastomer and various kinds of organoclay

Composition	d_{av} (nm)	Std. Dev.
93% PS + 5% 2210 + 2% 15A	168	15
93% PS + 5% 2210 + 2% 25A	158	17
93% PS + 5% 2210 + 2% 30B	181	18
93% PS + 5% 8840 + 2% 15A	170	16
93% PS + 5% 8840 + 2% 25A	162	17
93% PS + 5% 8840 + 2% 30B	187	20
93% PS + 5% 8900 + 2% 15A	179	17
93% PS + 5% 8900 + 2% 25A	170	16
93% PS + 5% 8900 + 2% 30B	195	19

93% PS + 5% 2210 + 2% 15A 250x	93% PS + 5% 2210 + 2% 15A 1500x
93% PS + 5% 2210 + 2% 25A 250x	93% PS + 5% 2210 + 2% 25A 1500x
93% PS + 5% 2210 + 2% 30B 250x	93% PS + 5% 2210 + 2% 30B 1500x
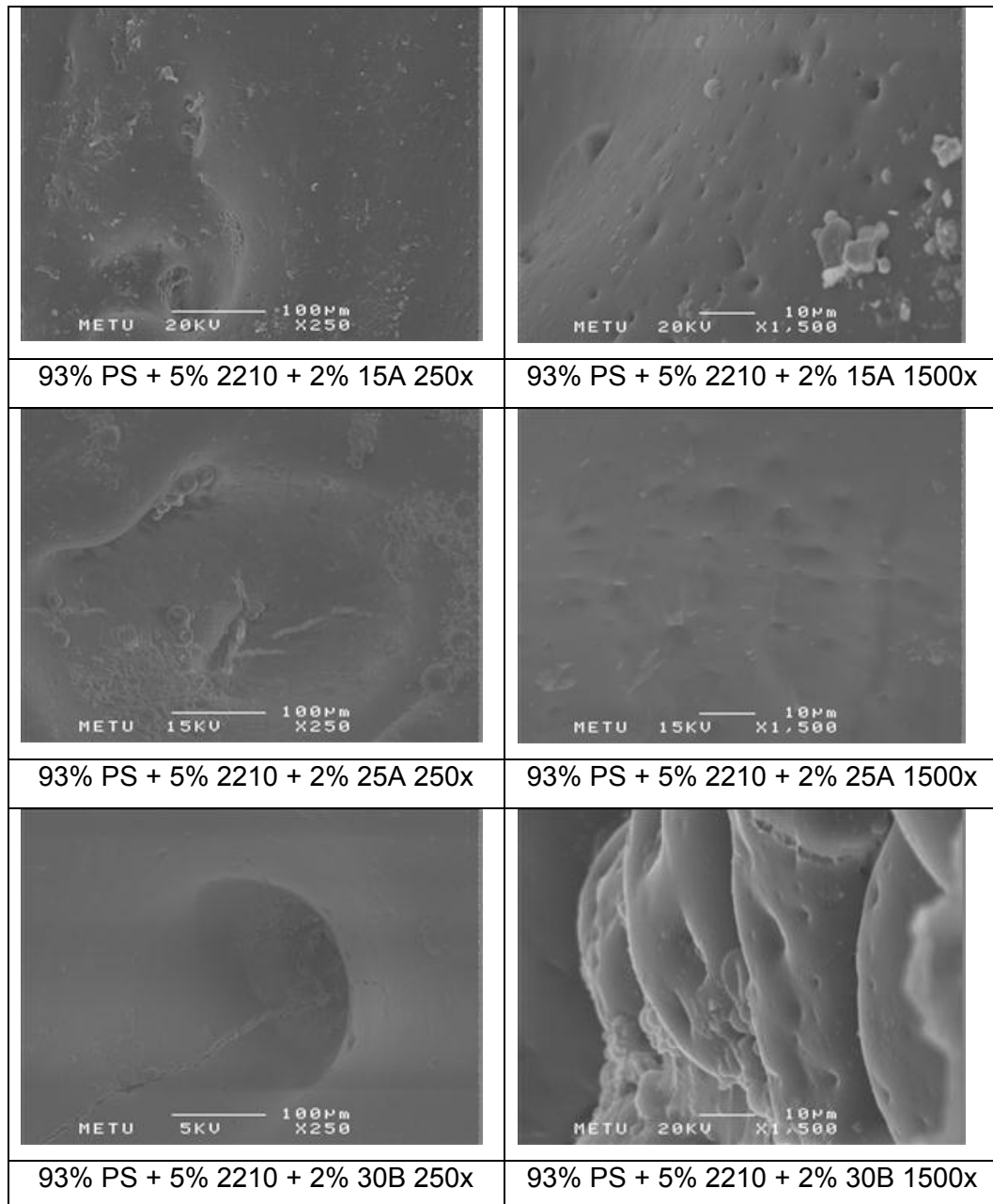
Figure 4.12 SEM micrographs of etched nanocomposites containing 2% organoclay and 5% Lotader 2210 with x250 and x1500 magnifications

93% PS + 5% 8840 + 2% 15A 250x	93% PS + 5% 8840 + 2% 15A 1500x
93% PS + 5% 8840 + 2% 25A 250x	93% PS + 5% 8840 + 2% 25A 1500x
93% PS + 5% 8840 + 2% 30B 250x	93% PS + 5% 8840 + 2% 30B 1500x
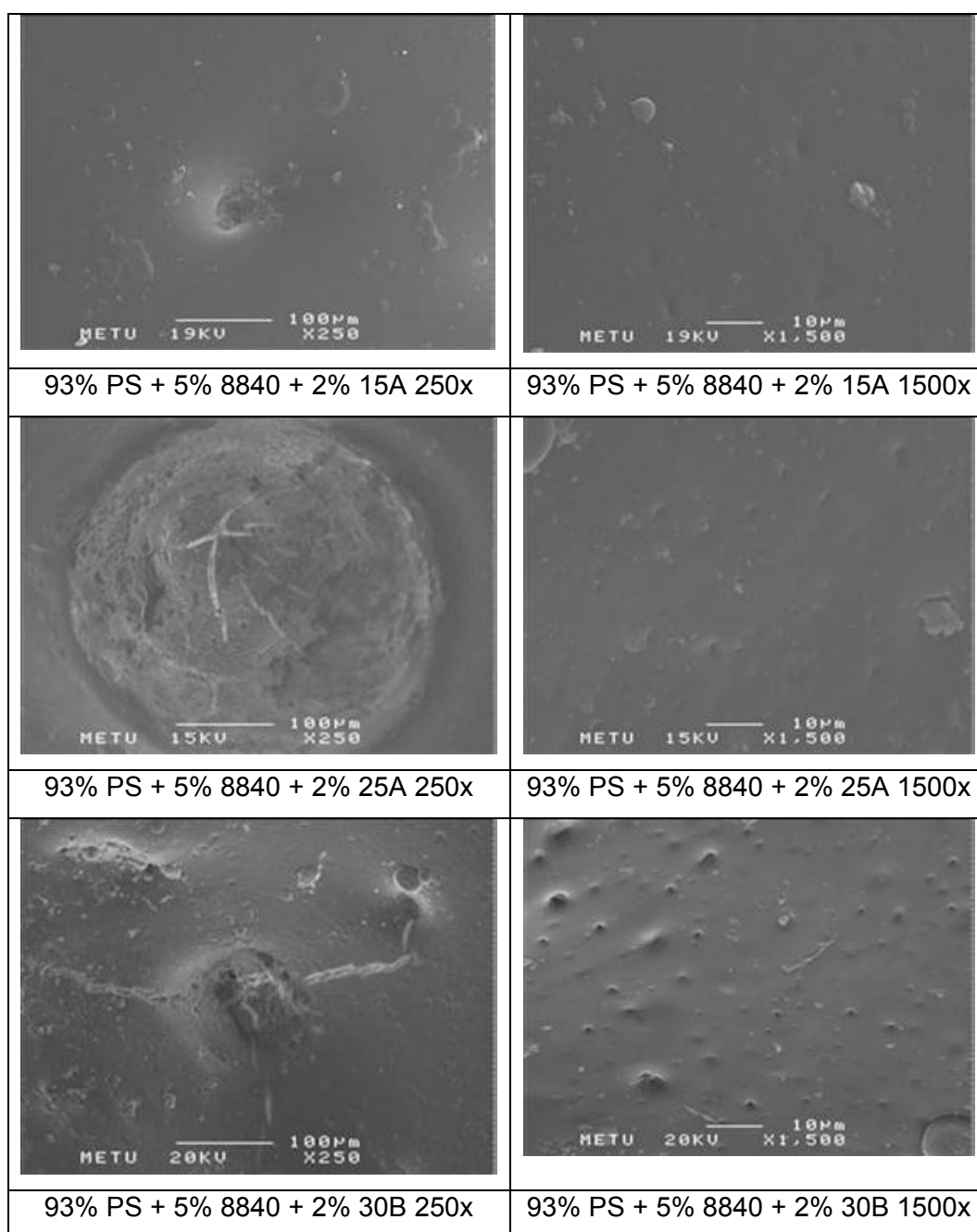
Figure 4.13 SEM micrographs of etched nanocomposites containing 2% organoclay and 5% Lotader AX8840 with x250 and x1500 magnifications

93% PS + 5% 8900 + 2% 15A 250x	93% PS + 5% 8900 + 2% 15A 1500x
93% PS + 5% 8900 + 2% 25A 250x	93% PS + 5% 8900 + 2% 25A 1500x
93% PS + 5% 8900 + 2% 30B 250x	93% PS + 5% 8900 + 2% 30B 1500x
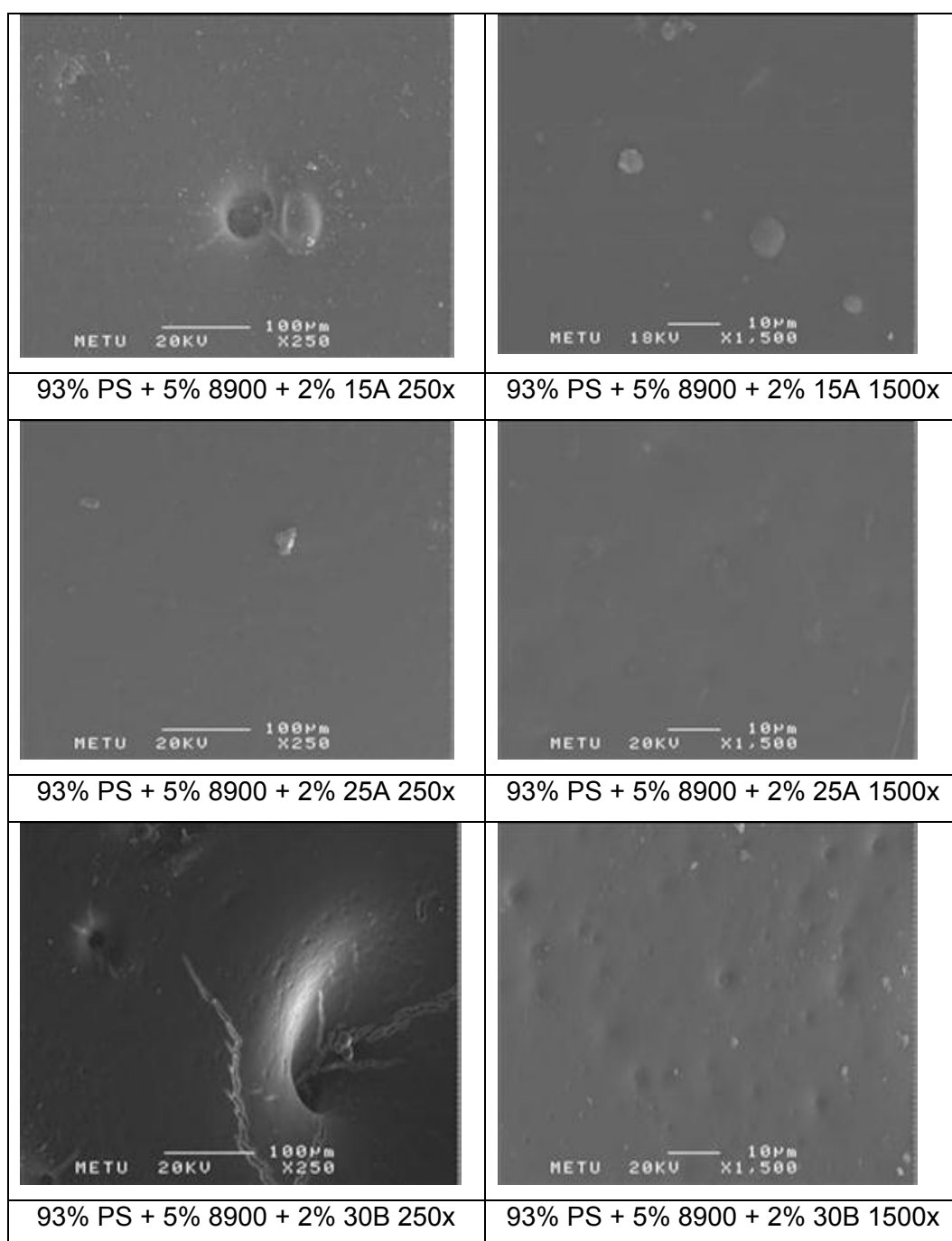
Figure 4.14 SEM micrographs of etched nanocomposites containing 2% organoclay and 5% Lotader AX8900 with x250 and x1500 magnifications

The domain sizes of these set of nanocomposites containing Lotaders 2210, AX8900 and AX8840 as elastomers were not sufficient to impart high impact strength to PS. This may have arisen due to incompatibility of these aliphatic elastomers with PS. Thus, different aromatic based compatibilizers, Styrene-

Butadiene-Styrene (SBS) and maleic anhydride grafted SBS (SBSgMAH) were used in the second part of this study.

The average domain size calculated for all samples prepared with aromatic based elastomers are illustrated in Table 4.3. These domain sizes were calculated from Figures 4.15 through 4.29.

Table 4.3 Average domain size of the samples containing SBS, SBSgMAH (1%) or SBSgMAH (2%) and Cloisite 30B

Composition	d_{av} (nm)	Std. Dev.
Binary Compositions		
95% PS + 5% SBS	176	17
95% PS + 5% SBSgMAH (1%)	180	21
95% PS + 5% SBSgMAH (2%)	193	16
90% PS + 10% SBS	282	29
90% PS + 10% SBSgMAH (1%)	292	35
90% PS + 10% SBSgMAH (2%)	296	34
85% PS + 15% SBS	403	41
85% PS + 15% SBSgMAH (1%)	395	39
85% PS + 15% SBSgMAH (2%)	410	41
75% PS + 25% SBS	510	47
75% PS + 25% SBSgMAH (1%)	525	43
75% PS + 25% SBSgMAH (2%)	532	49
60% PS + 40 % SBS	Co-continuous	---
60% PS + 40 % SBSgMAH (1%)	Co-continuous	---
60% PS + 40 % SBSgMAH (2%)	Co-continuous	---
Ternary Compositions with 2% Cloisite ® 30B		
93% PS + 5% SBS + 2% 30B	354	35
93% PS + 5% SBSgMAH (1%) + 2% 30B	362	32
93% PS + 5% SBSgMAH (2%) + 2% 30B	382	37
88% PS + 10% SBS + 2% 30B	425	41
88% PS + 10% SBSgMAH (1%) + 2% 30B	421	40
88% PS + 10% SBSgMAH (2%) + 2% 30B	416	39

Table 4.3 Average domain size of the samples containing SBS, SBSgMAH (1%) or SBSgMAH (2%) and Cloisite 30B (continued)

83% PS + 15% SBS + 2% 30B	490	45
83% PS + 15% SBSgMAH (1%) + 2% 30B	505	47
83% PS + 15% SBSgMAH (2%) + 2% 30B	467	43
73% PS + 25% SBS + 2% 30B	600	55
73% PS + 25% SBSgMAH (1%) + 2% 30B	601	57
73% PS + 25% SBSgMAH (2%) + 2% 30B	612	53
58% PS + 40% SBS + 2% 30B	Co-continuous	---
58% PS + 40% SBSgMAH (1%) + 2% 30B	Co-continuous	---
58% PS + 40% SBSgMAH (2%) + 2% 30B	Co-continuous	---
Ternary Compositions with 4% Cloisite ® 30B		
91% PS + 5% SBS + 4% 30B	349	33
91% PS + 5% SBSgMAH (2%) + 4% 30B	358	31
86% PS + 10% SBS + 4% 30B	401	44
86% PS + 10% SBSgMAH (2%) + 4% 30B	410	39
81% PS + 15% SBS + 4% 30B	509	47
81% PS + 15% SBSgMAH (2%) + 4% 30B	516	43
76% PS + 20% SBS + 4% 30B	548	49
76% PS + 20% SBSgMAH (2%) + 4% 30B	571	51
71% PS + 25% SBS + 4% 30B	616	54
71% PS + 25% SBSgMAH (2%) + 4% 30B	624	49

In general, Figures 4.15 through 4.19 indicate that, the addition of elastomer, crack propagation lines become shorter and closer to each other and the number of cracks increases. As the amount of elastomer increases, this process becomes more significant. Thus, featureless structure of the PS disappears, indicating an increased amount of energy dissipation during fracture. Beside this, the increasing surface roughness directly affects the toughness of a material. Mechanical test results that will be discussed later verify this argument.

The morphology development of blends during melt mixing comprise processes such as, fluid drops stretching into threads, break-up of the threads into smaller

droplets and coalescence of the droplets into larger ones [78]. In most of the cases, coalescence occurs, although small domains make the system more stable due to the larger surface area created. This is due to the cohesive forces between domains and interfacial mobility of the dispersed phase. Thus, during the coalescence process, that is a result of collision forces, the system becomes un-stabilized and in order to stabilize the blend systems, components of the mixture tend to create a phase structure with a minimum total free energy. Input of energy is required to form these new surfaces and interfaces. When the rate of coalescence and breakdown are balanced, the recombination of the domains is impeded and the equilibrium particle size is achieved [118].

The etched fracture surfaces of the PS/SBS, PS/SBSgMAH (1%) and PS/SBSgMAH (2%) binary blends are shown in Figures 4.15-4.19. An important aspect of the phase morphology is its microstructure. The microstructure of two phase blends may be formed from domains with different shape, size and distribution which are the key factors for achieving desired properties. Droplet matrix morphologies improve the impact properties, fibrillar morphologies result in better tensile properties, blends with lamellar structure enhance barrier properties and co-continuous morphologies show a combination of both components [119, 120].

The domains in PS matrix are formed from dispersed droplets. Table 4.3 and Figures 4.15 – 4.19 show that as the amount of the dispersed phase increases, the average domain size increases and the circular shape of the elastomeric domains become stretched and a less uniform domain distribution is observed. This is related with droplet coalescence during melt mixing, which results in broadening of the domains. Since elastomeric phase has a higher viscosity than PS matrix, its presence increases the viscosity of the blend and the shear stress applied on the clay platelets during extrusion. However, increasing viscosity prevents the dispersion of elastomeric phase into small droplets because the shear stress that is applied on to the material becomes insufficient. So the coalescence rate and domain size increase. This is observed in Table 4.3 which shows that the domain size increases with the elastomer content. Another factor that leads to increase in the coalescence rate with increasing elastomer content

may be attributed to the increase in the number of dispersed domains and therefore the probability of the domains to collide with each other [118, 121].

In this study, PS is the continuous phase according to the general criteria for phase inversion which states that the phase with lower viscosity or higher volume fraction tends to be the continuous phase. With increasing elastomer content, the dispersed morphology turns from dispersed phase structure into a co-continuous structure. As can be seen from Figure 4.19, when the elastomer content is 40% the phase morphology becomes co-continuous.

The concentration where the co-continuous phase morphology becomes observable is called the "phase inversion" point. PS/SBS and PS/SBSgMAH blends exhibit inversion between 25% and 40% content of elastomeric phase.

95% PS + 5% SBS 250x	95% PS + 5% SBS 1500x
95% PS + 5% SBSgMAH (1%) 250x	95% PS + 5% SBSgMAH (1%) 1500x
95% PS + 5% SBSgMAH (2%) 250x	95% PS + 5% SBSgMAH (2%) 1500x
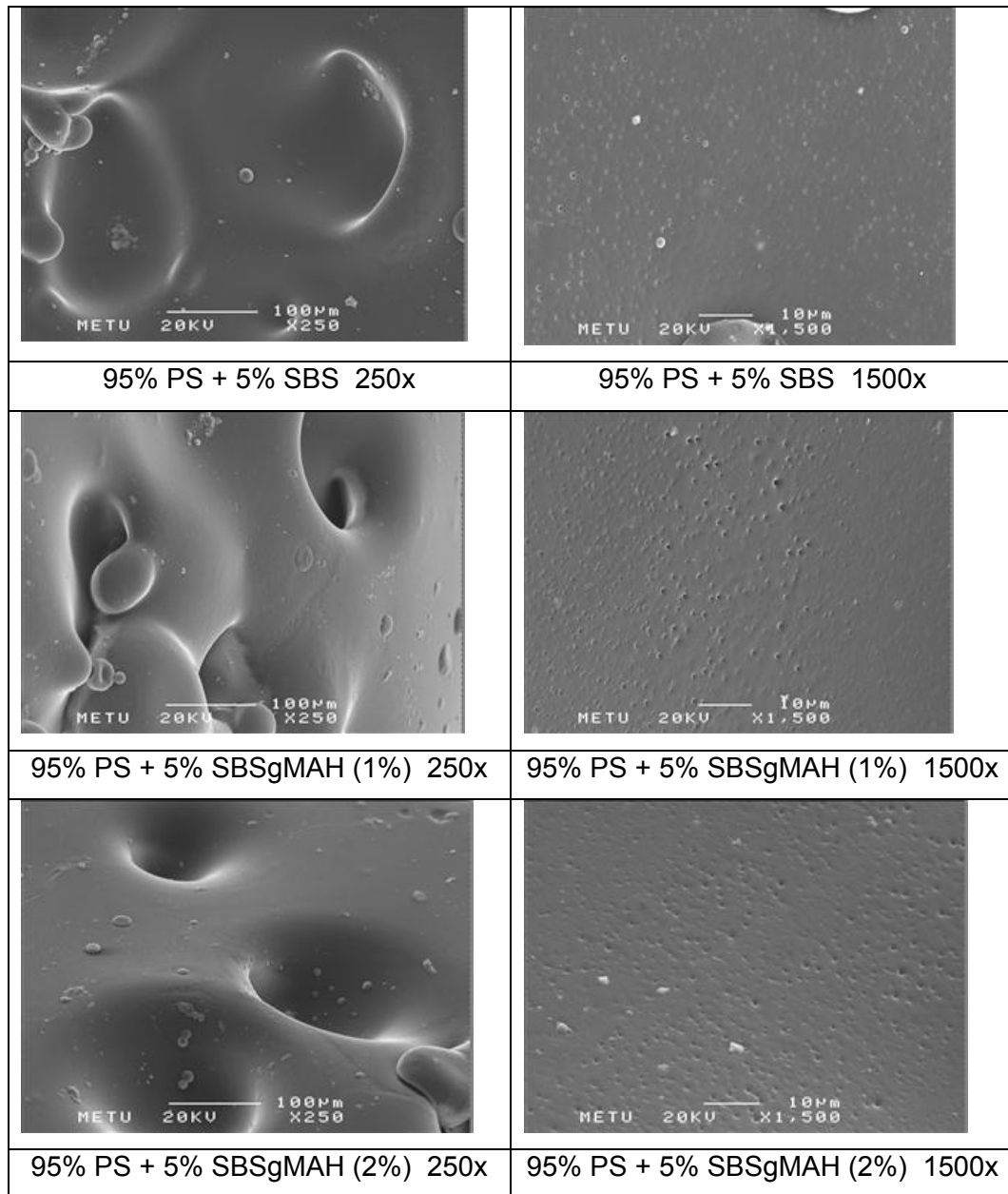
Figure 4.15 SEM micrographs of etched blends containing 5% SBS or SBSgMAH (1%) or SBSgMAH (2%) with x250 and x1500 magnifications

90% PS + 10% SBS 250x	90% PS + 10% SBS 1500x
90% PS + 10% SBSgMAH(1%) 250x	90% PS + 10% SBSgMAH(1%) 1500x
90% PS + 10% SBSgMAH(2%) 250x	90% PS + 10% SBSgMAH(2%) 1500x
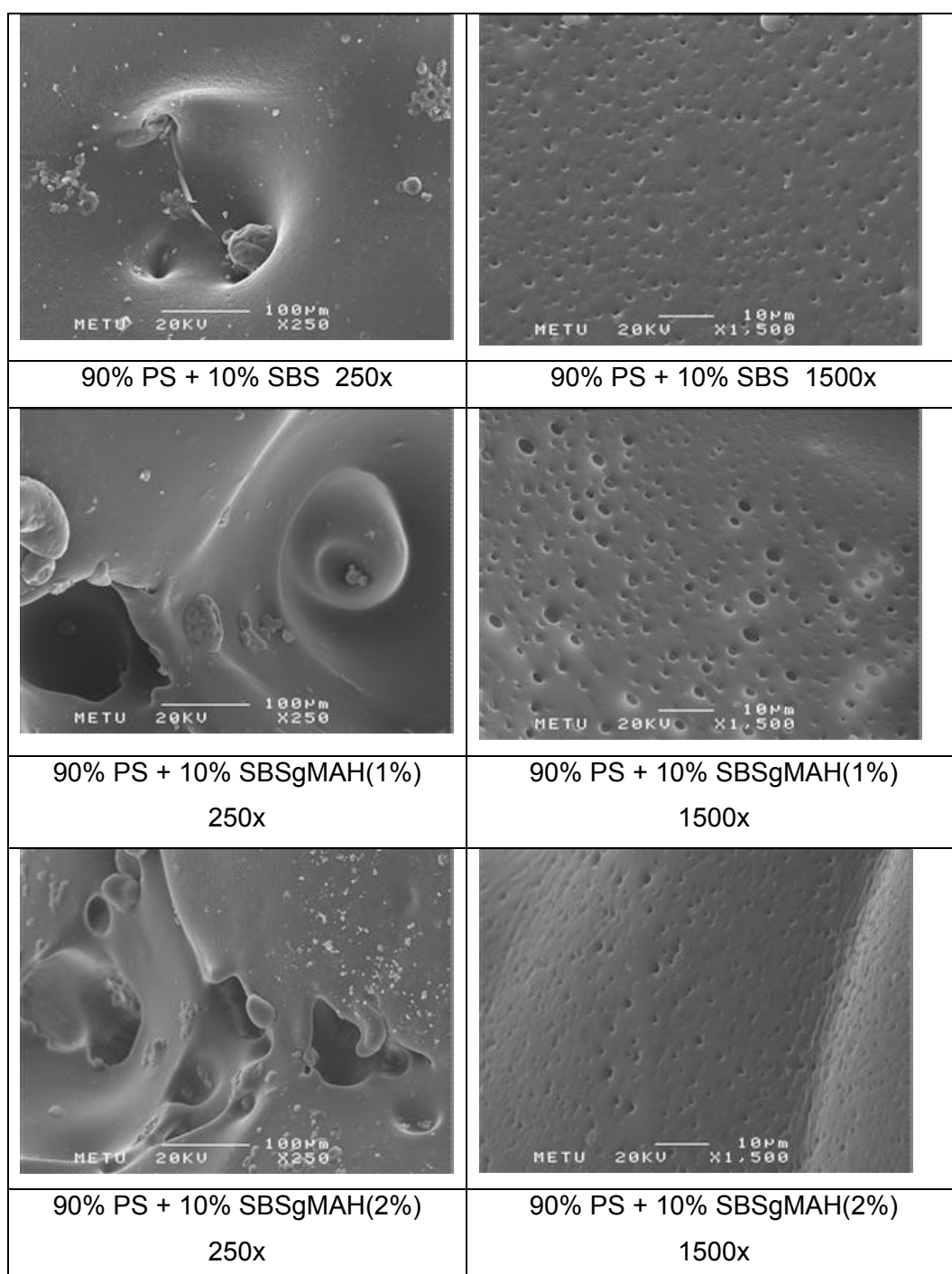
Figure 4.16 SEM micrographs of etched blends containing 10% SBS or SBSgMAH (1%) or SBSgMAH (2%) with x250 and x1500 magnifications

85% PS + 15% SBS 250x	85% PS + 15% SBS 1500x
85% PS + 15% SBSgMAH(1%) 250x	85% PS + 15% SBSgMAH(1%) 1500x
85% PS + 15% SBSgMAH(2%) 250x	85% PS + 15% SBSgMAH(2%) 1500x
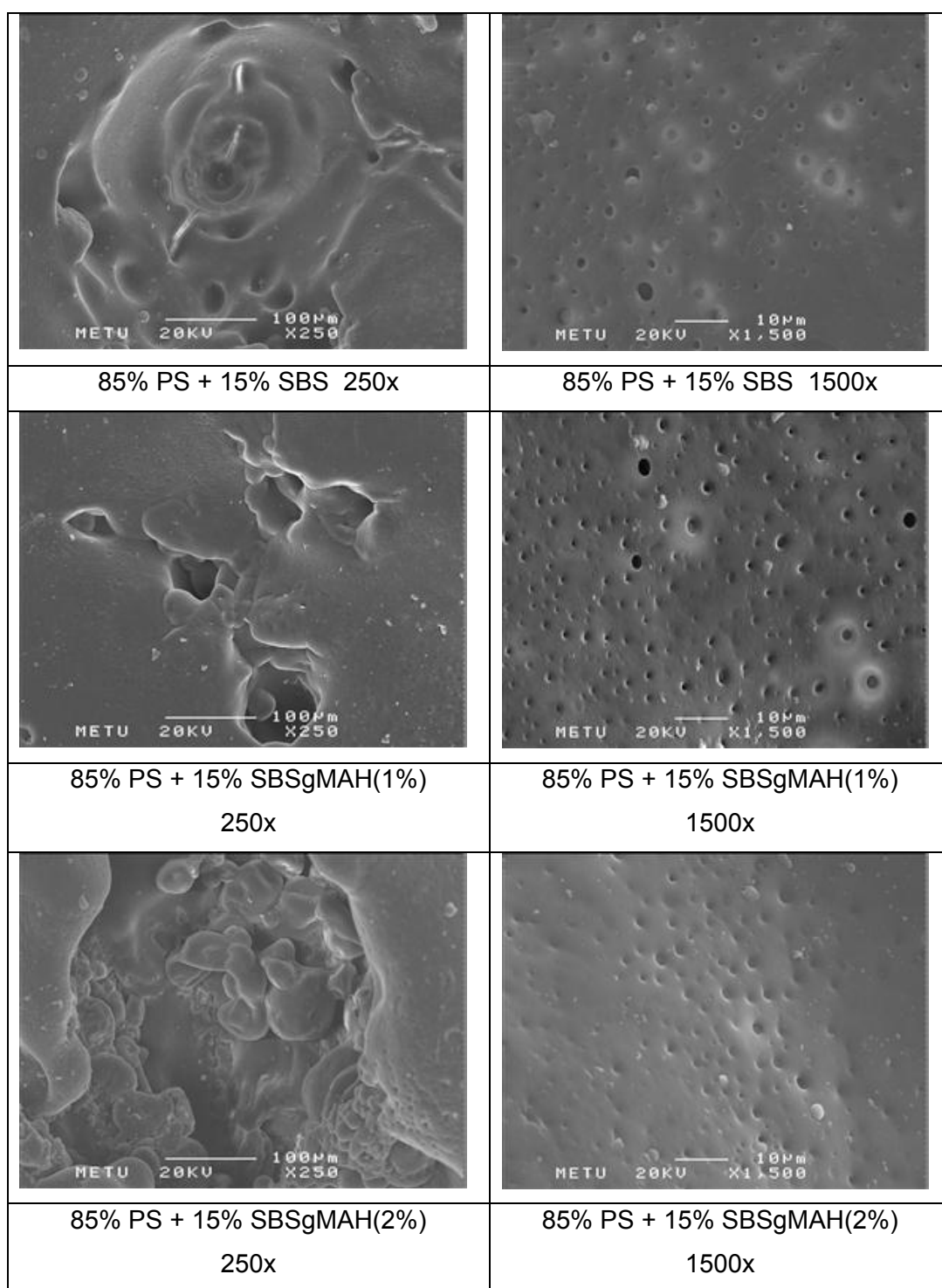
Figure 4.17 SEM micrographs of etched blends containing 15% SBS or SBSgMAH (1%) or SBSgMAH (2%) with x250 and x1500 magnifications

75% PS + 25% SBS 250x	75% PS + 25% SBS 1500x
75% PS + 25% SBSgMAH(1%) 250x	75% PS + 25% SBSgMAH(1%) 1500x
75% PS + 25% SBSgMAH(2%) 250x	75% PS + 25% SBSgMAH(2%) 1500x
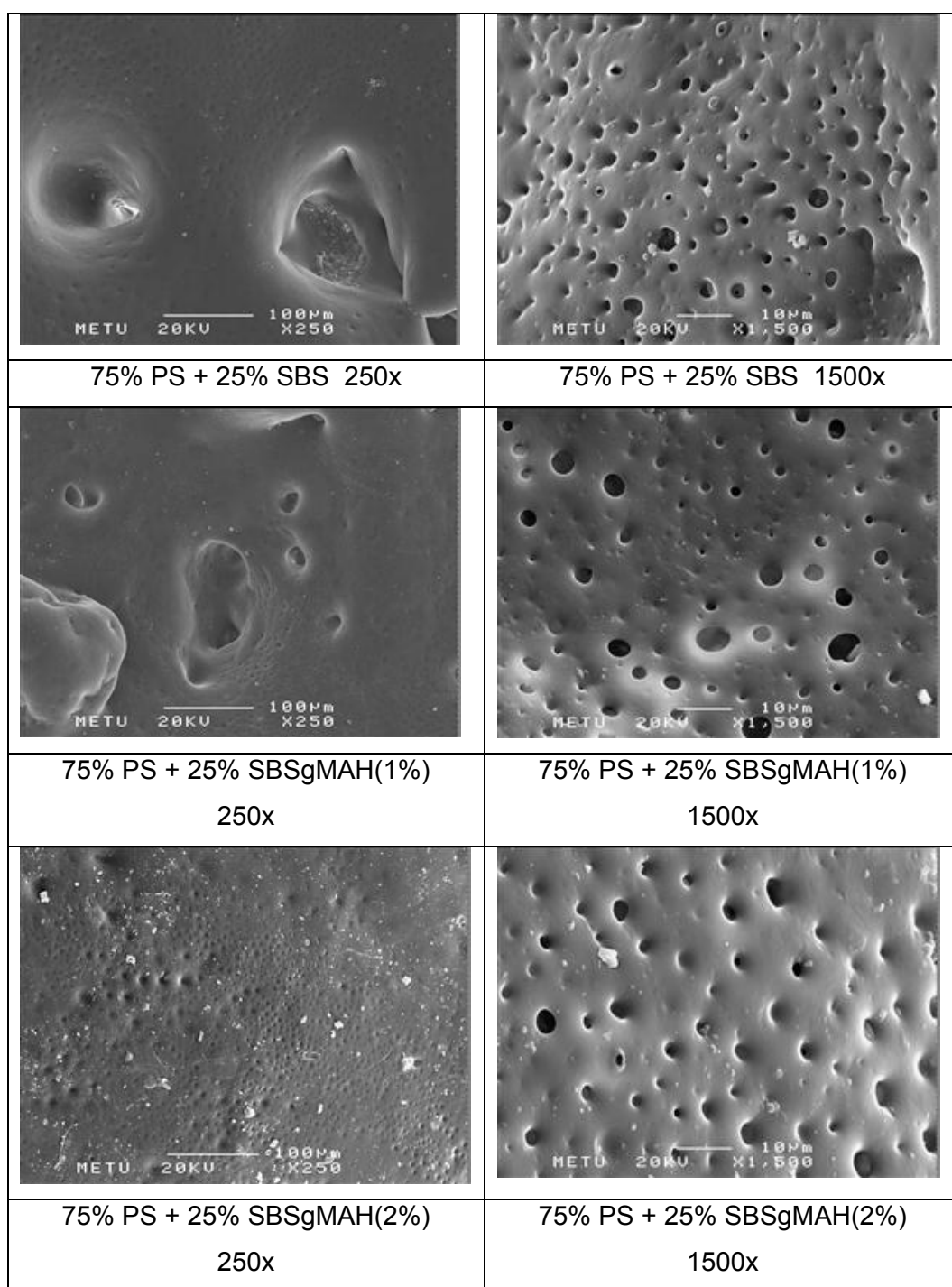
Figure 4.18 SEM micrographs of etched blends containing 25% SBS or SBSgMAH (1%) or SBSgMAH (2%) with x250 and x1500 magnifications

60% PS + 40% SBS 250x	60% PS + 40% SBS 1500x
60% PS + 40% SBSgMAH(1%) 250x	60% PS + 40% SBSgMAH(1%) 1500x
60% PS + 40% SBSgMAH(2%) 250x	60% PS + 40% SBSgMAH(2%) 1500x
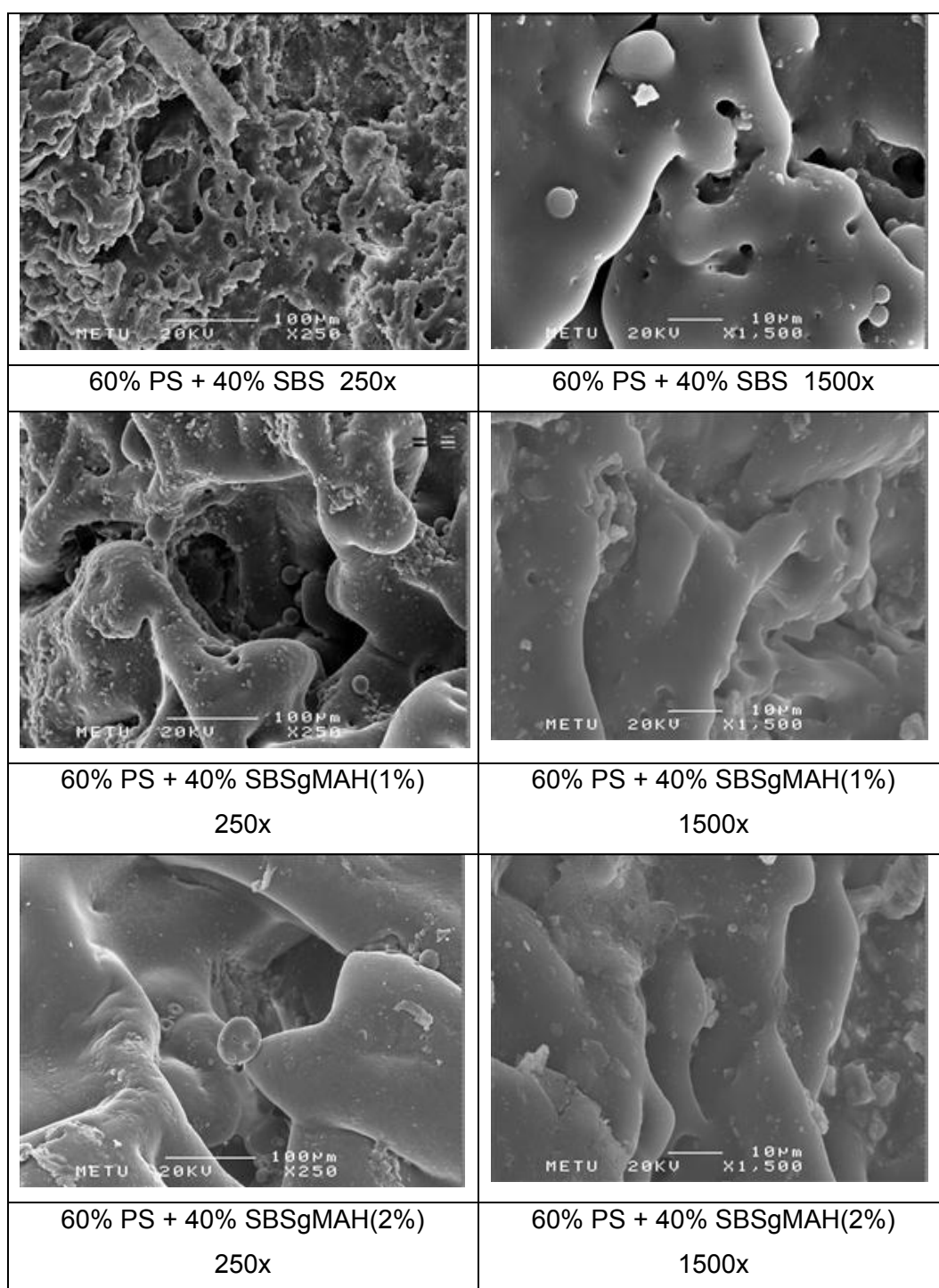
**Figure 4.19** SEM micrographs of etched blends containing 40% SBS or SBSgMAH (1%) or SBSgMAH (2%) with x250 and x1500 magnifications

Figures 4.20 and 4.21 show the etched fracture surface of the ternary nanocomposites containing 2% Cloisite 30B and 5% elastomer or containing 2%

Cloisite 30B and 10% elastomer, respectively. When compared with the average domain sizes of the corresponding binary blends which are about 220 nm and 350 nm, the ternary nanocomposites show an increase in their average domain diameters. If the organoclay particles were completely dispersed in the PS matrix, the clay platelets would suppress the agglomeration of the elastomeric domains [121]. However, in this study, the average domain size increases with organoclay addition, no matter whether it is well dispersed or not, because the clay particles mostly reside at the interphase between PS and elastomeric material. As seen from the results of capillary viscometer analysis, SBS has lower viscosity than PS. Therefore clay particles prefer to localize in the elastomeric phase. Due to filler effect of the clay particles, viscosity of the elastomeric phase increases. Increasing viscosity of the elastomeric phase may cause formation of larger elastomeric domains in the PS matrix.

Table 4.3 and Figures 4.20 - 4.21 show that for the ternary nanocomposites containing SBSgMAH (2%), elastomeric domain sizes were reduced, as expected. This case can be explained by the creation of new bonds due to maleic anhydride. These bonds restrict the increase of elastomeric domain size.

Another property that is observed with the addition of organoclay is the higher number of crack lines. In the case of well dispersed layered silicates, many shorter and closer, circular, nonlinear, cracks are formed simultaneously, and these nonlinear cracks tend to grow until they interfere with each other [122].
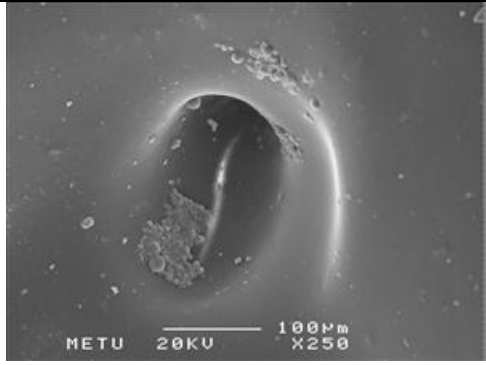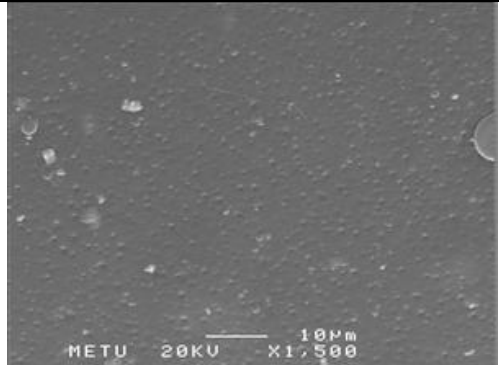
93 % PS + 5 % SBS + 2 % 30B 250x	93 % PS + 5 % SBS + 2 % 30B 1500x
93 % PS + 5 % SBSgMAH (1%) + 2 % 30B 250x	93 % PS + 5 % SBSgMAH (1%) + 2 % 30B 1500x
93 % PS + 5 % SBSgMAH (2%) + 2 % 30B 250x	93 % PS + 5 % SBSgMAH (2%) + 2 % 30B 1500x
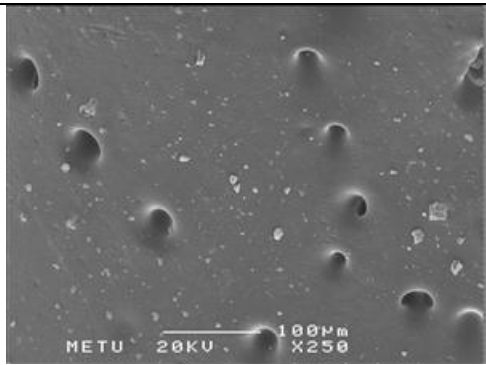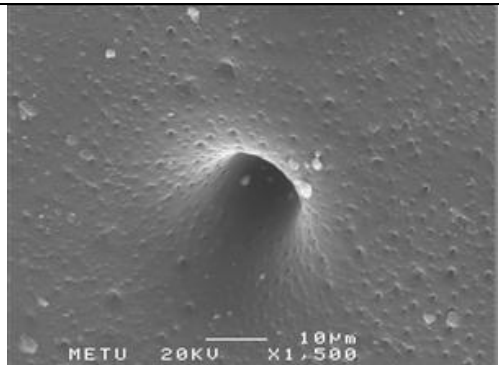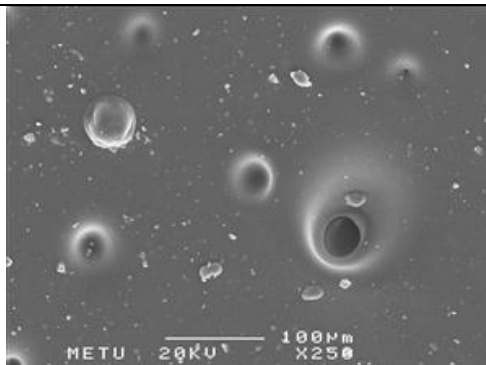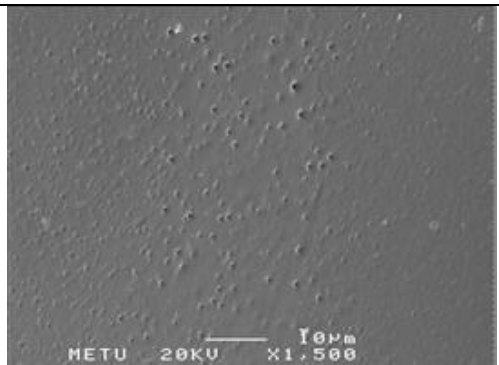
Figure 4.20 SEM micrographs of etched nanocomposites containing 2% Cloisite 30B and 5% SBS or SBSgMAH (1%) or SBSgMAH (2%) with x250 and x1500 magnifications

88 % PS + 10 % SBS + 2 % 30B 250x	88 % PS + 10 % SBS + 2 % 30B 1500x
88 % PS + 10 % SBSgMAH (1%) + 2 % 30B 250x	88 % PS + 10 % SBSgMAH (1%) + 2 % 30B 1500x
88 % PS + 10 % SBSgMAH (2%) + 2 % 30B 250x	88 % PS + 10 % SBSgMAH (2%) + 2 % 30B 1500x
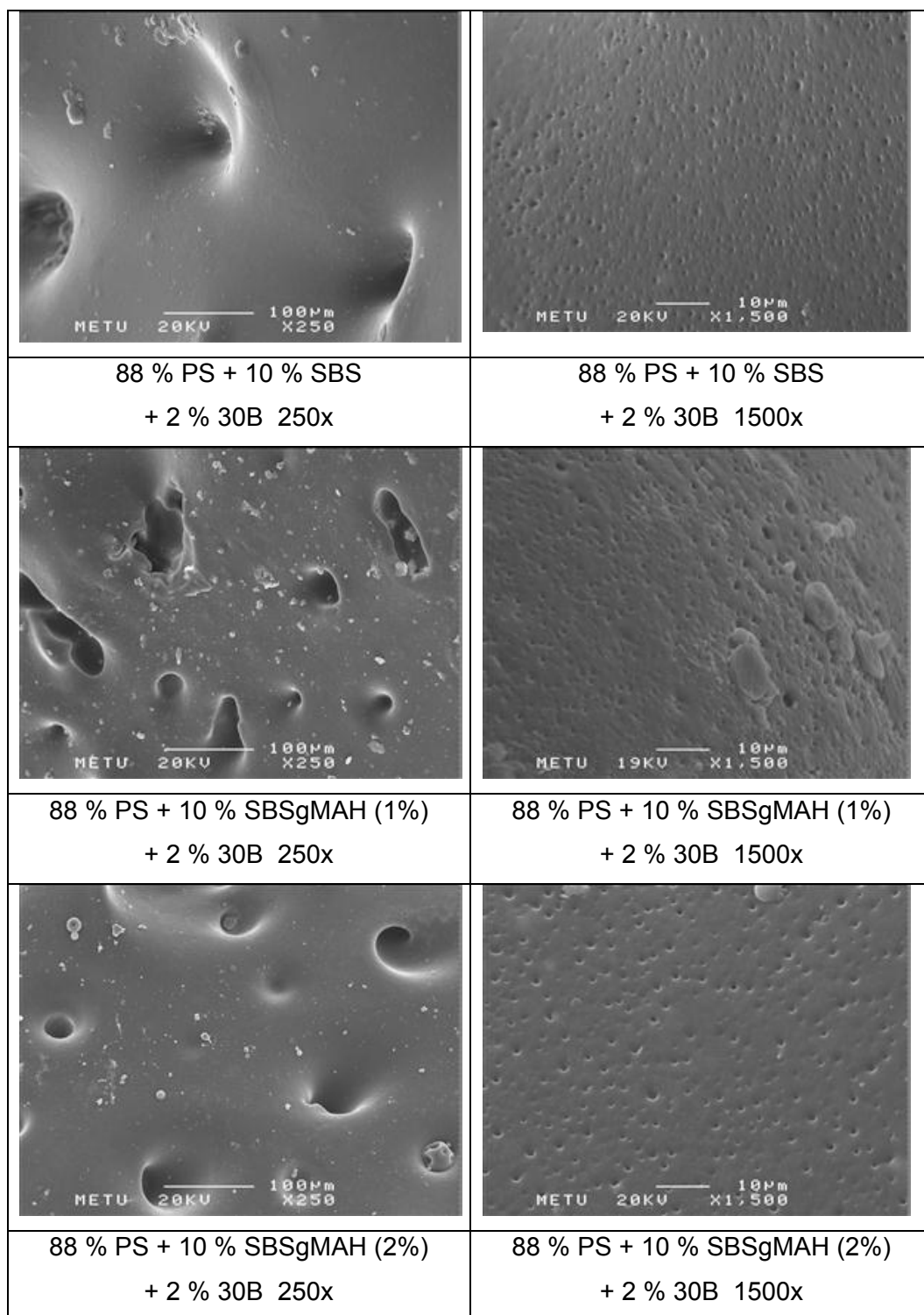
Figure 4.21 SEM micrographs of etched nanocomposites containing 2% Cloisite 30B and 10% SBS or SBSgMAH (1%) or SBSgMAH (2%) with x250 and x1500 magnifications

The etched fracture surface of the ternary nanocomposites containing 15%, 25% and 40% elastomer are shown in Figures 4.22 - 4.24. As in the case of 5% and 10% elastomer containing nanocomposites, the addition of organoclay makes the elastomeric domains larger.

When the SEM micrographs of nanocomposites containing 40% elastomer are considered, the interconnected structure of the minor component can be seen. The entire minor component incorporates into a single continuous phase network inside the PS matrix and a fully co continuous morphology is observed. Since a co-continuous structure is observed at 40% elastomer content, it can be said that the phase inversion occurs between 25% and 40% elastomer content. According to these results, it is obvious that the phase inversion point shifts to lower dispersed phase content with the addition of organoclay. This is an indication of the dispersion of clay layers at the PS-elastomer interphase and also in the elastomer phase. Since clay particles lead to enlargement of the domains, the phase inversion in ternary nanocomposites occurs at lower elastomer content in comparison to binary nanocomposites.

Co-continuous structures exhibit the properties of both of its components, and these components take their part in the load sharing. It is known that PS has a high tensile strength and low impact strength value. On the other hand, elastomeric materials used in this study have low tensile strength and high impact strength values as other elastomeric materials do. Mechanical properties of elastomeric materials are completely opposite to mechanical properties of PS. In this study, co-continuous morphologies obtained between 25% and 40% elastomer content in ternary nanocomposites, led to very high impact strength values as shown later. However, the decrease in the tensile strength values of the nanocomposites cannot be ignored for these compositions.

83 % PS + 15 % SBS + 2 % 30B 250x	83 % PS + 15 % SBS + 2 % 30B 1500x
83 % PS + 15 % SBSgMAH (1%) + 2 % 30B 250x	83 % PS + 15 % SBSgMAH (1%) + 2 % 30B 1500x
83 % PS + 15 % SBSgMAH (2%) + 2 % 30B 250x	83 % PS + 15 % SBSgMAH (2%) + 2 % 30B 1500x
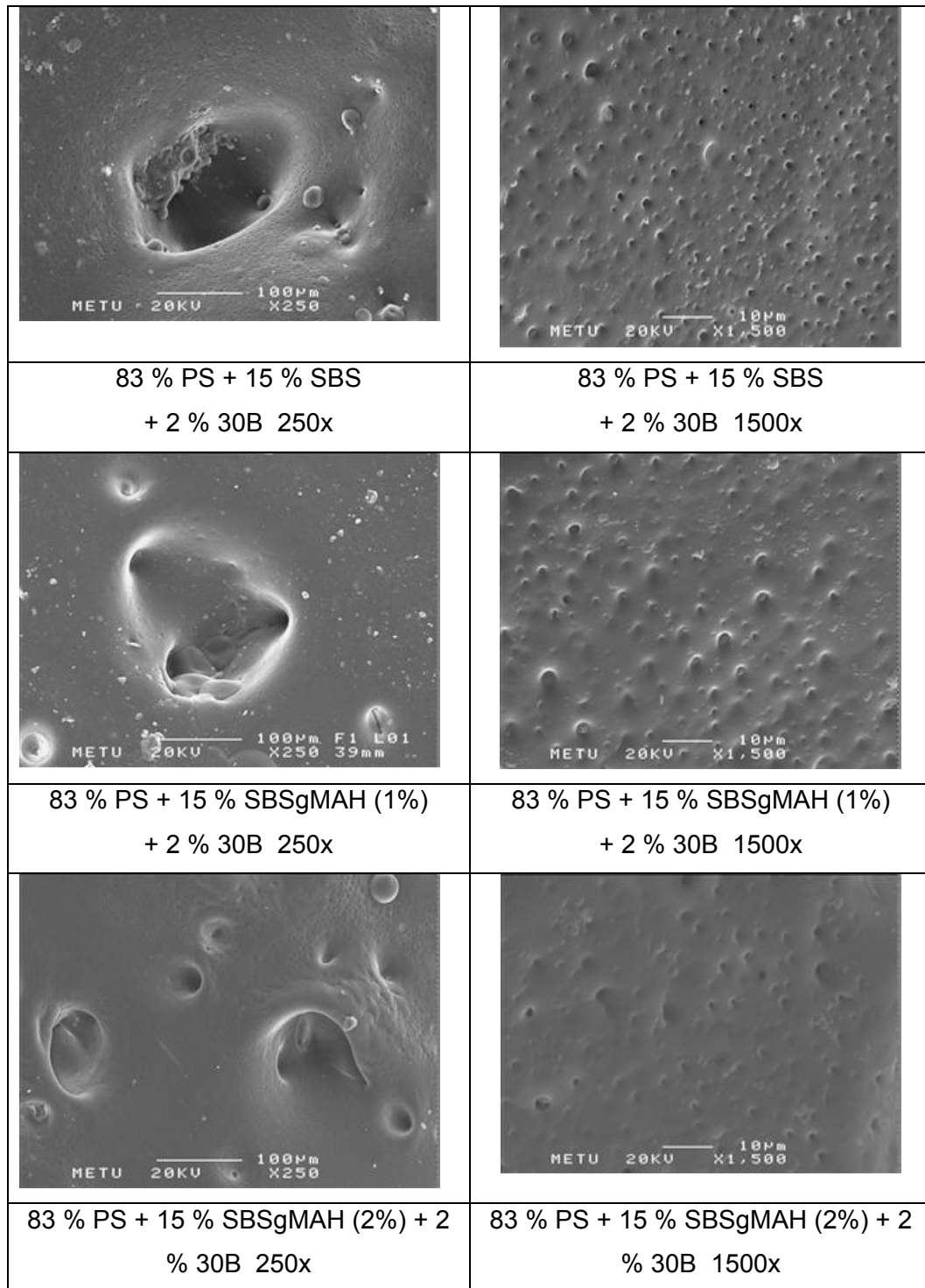
Figure 4.22 SEM micrographs of etched nanocomposites containing 2% Cloisite 30B and 15% SBS or SBSgMAH (1%) or SBSgMAH (2%) with x250 and x1500 magnifications

73 % PS + 25 % SBS + 2 % 30B 250x	73 % PS + 25 % SBS + 2 % 30B 1500x
73 % PS + 25 % SBSgMAH (1%) + 2 % 30B 250x	73 % PS + 25 % SBSgMAH (1%) + 2 % 30B 1500x
73 % PS + 25 % SBSgMAH (2%) + 2 % 30B 250x	73 % PS + 25 % SBSgMAH (2%) + 2 % 30B 1500x
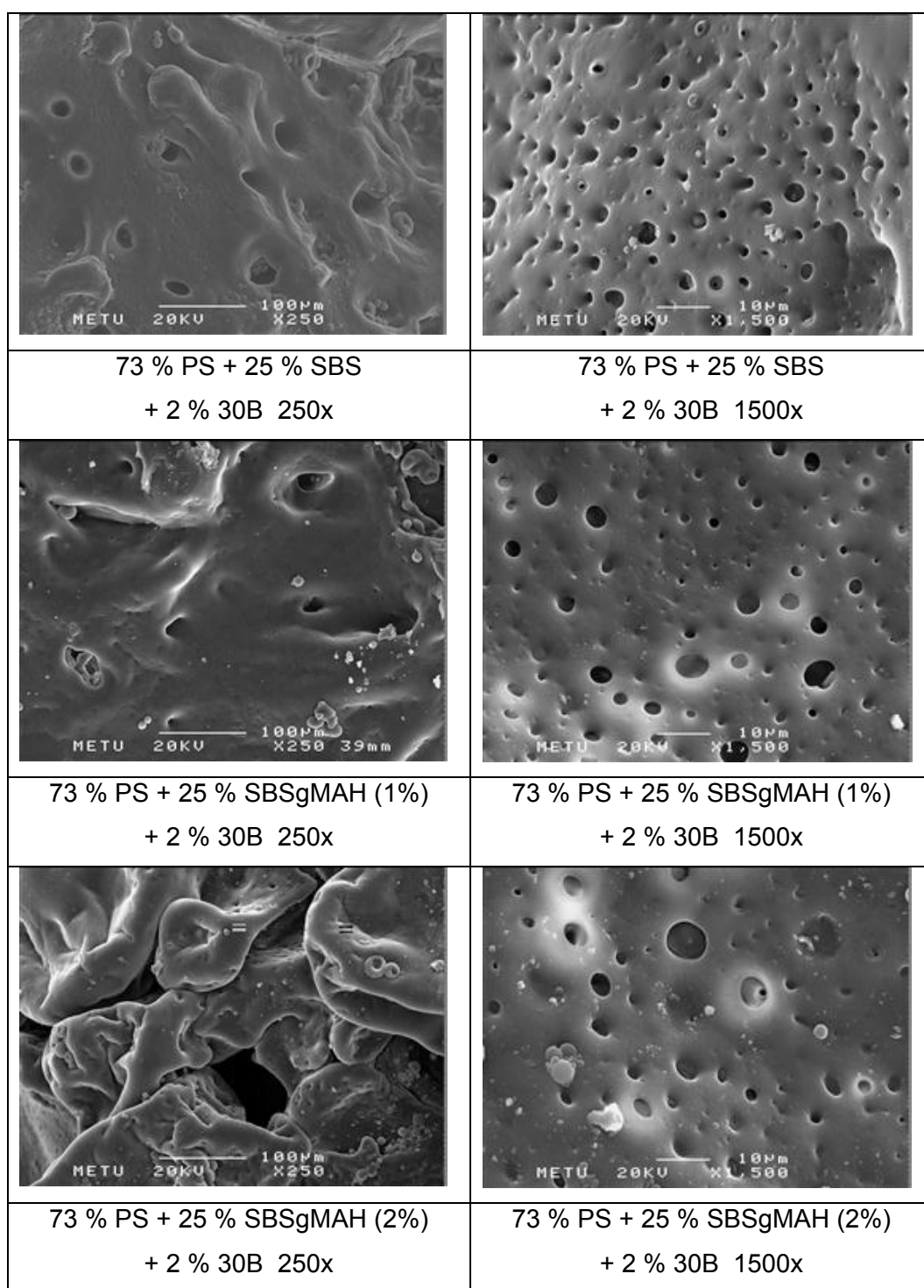
Figure 4.23 SEM micrographs of etched nanocomposites containing 2% Cloisite 30B and 25% SBS or SBSgMAH (1%) or SBSgMAH (2%) with x250 and x1500 magnifications

| 58 % PS + 40 % SBS | 58 % PS + 40 % SBS |
| + 2 % 30B 250x | + 2 % 30B 1500x |

| 58 % PS + 40 % SBSgMAH (1%) | 58 % PS + 40 % SBSgMAH (1%) |
| + 2 % 30B 250x | + 2 % 30B 1500x |

| 58 % PS + 40 % SBSgMAH (2%) | 58 % PS + 40 % SBSgMAH (2%) |
| + 2 % 30B 250x | + 2 % 30B 1500x |
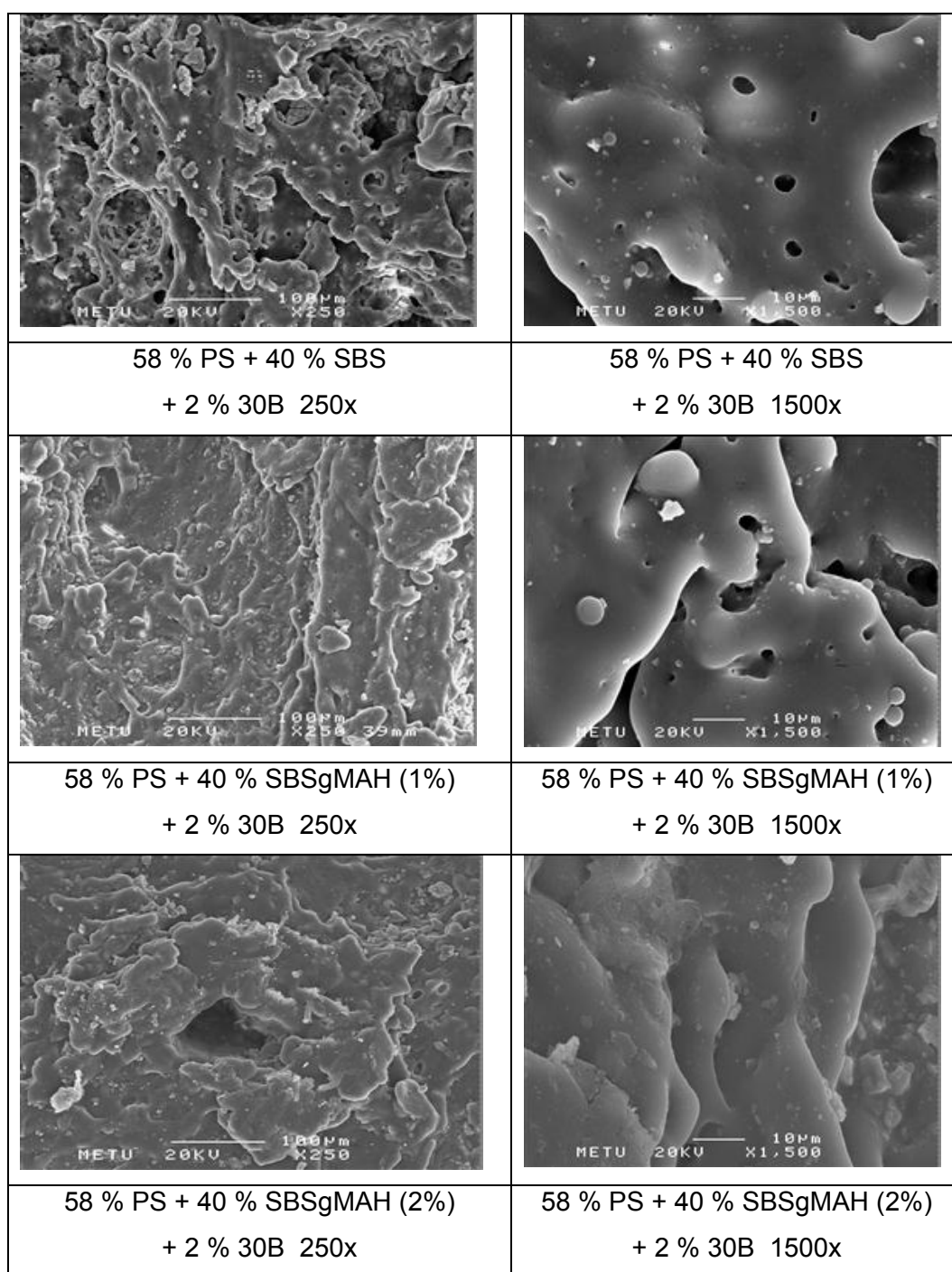
Figure 4.24 SEM micrographs of etched nanocomposites containing 2% Cloisite 30B and 40% SBS or SBSgMAH (1%) or SBSgMAH (2%) with x250 and x1500 magnifications

SEM images of the binary nanocomposites containing 4% organoclay are shown in Figure 4.25. SEM images of the nanocomposites containing 4% organoclay

93

and different amounts of elastomers are shown in Figures 4.26-4.29. Increase in organoclay content results in obtaining larger domains when compared to nanocomposites containing lower amount of organoclay and the same amount of elastomer. These results are summarized in Table 4.3.

| 96 % PS + 4 % 30B 250x | 96 % PS + 4 % 30B 250x |
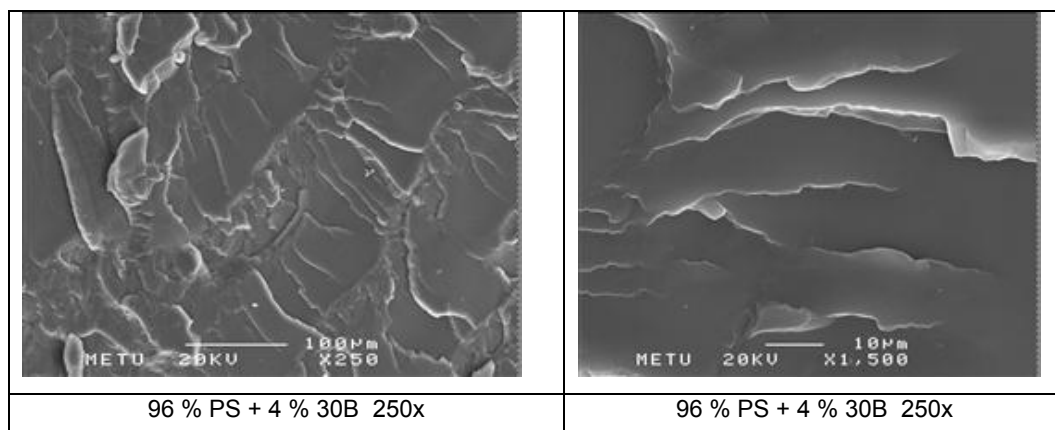
Figure 4.25 SEM micrographs of nanocomposites containing 4% Cloisite 30B with x250 and x1500 magnifications

91 % PS + 5 % SBS + 4 % 30B 250x	91 % PS + 5 % SBS + 4 % 30B 1500x
91 % PS + 5 % SBSgMAH (2%) + 4 % 30B 250x	91 % PS + 5 % SBSgMAH (2%) + 4 % 30B 1500x
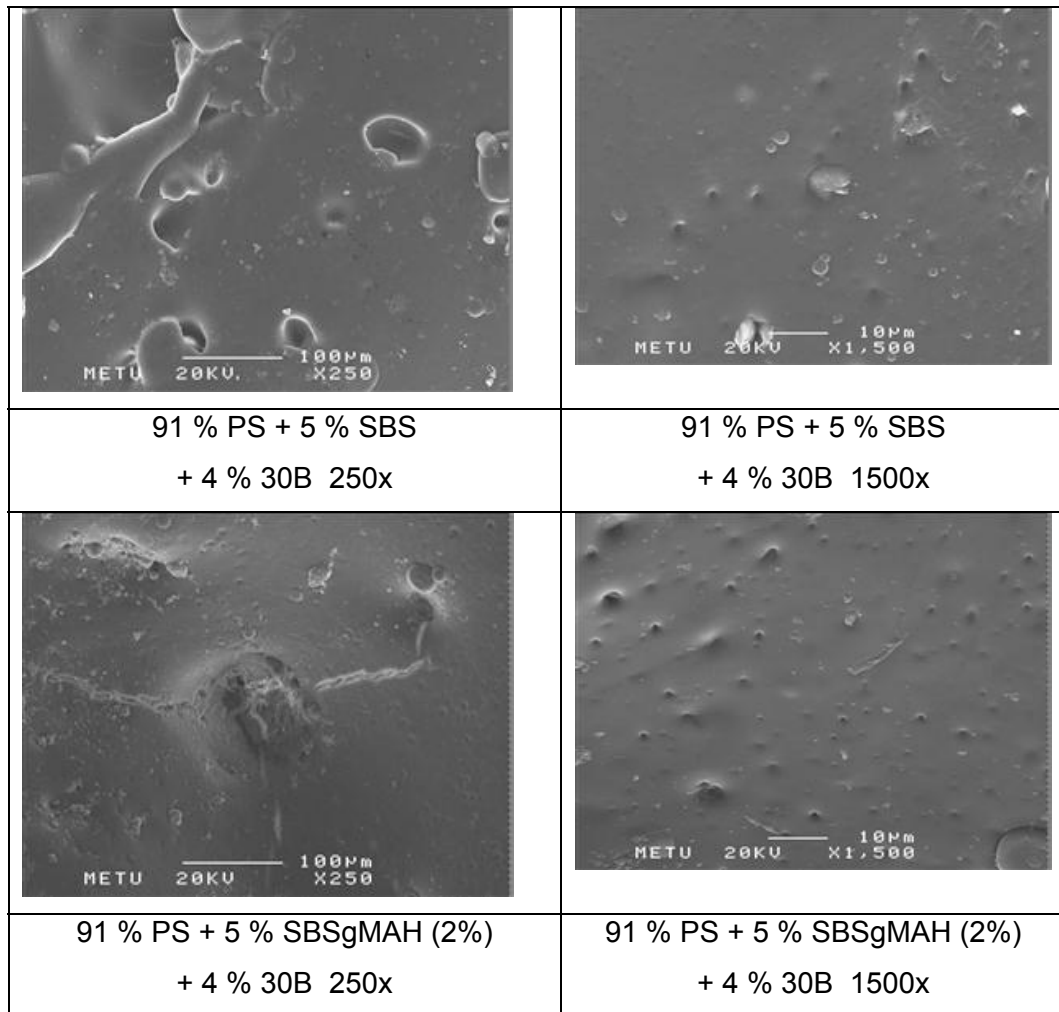
**Figure 4.26** SEM micrographs of etched nanocomposites containing 4% Cloisite 30B and 5% SBS or SBSgMAH (2%) with x250 and x1500 magnifications

86 % PS + 10 % SBS + 4 % 30B 250x	86 % PS + 10 % SBS + 4 % 30B 1500x
86 % PS + 10 % SBSgMAH (2%) + 4 % 30B 250x	86 % PS + 10 % SBSgMAH (2%) + 4 % 30B 1500x
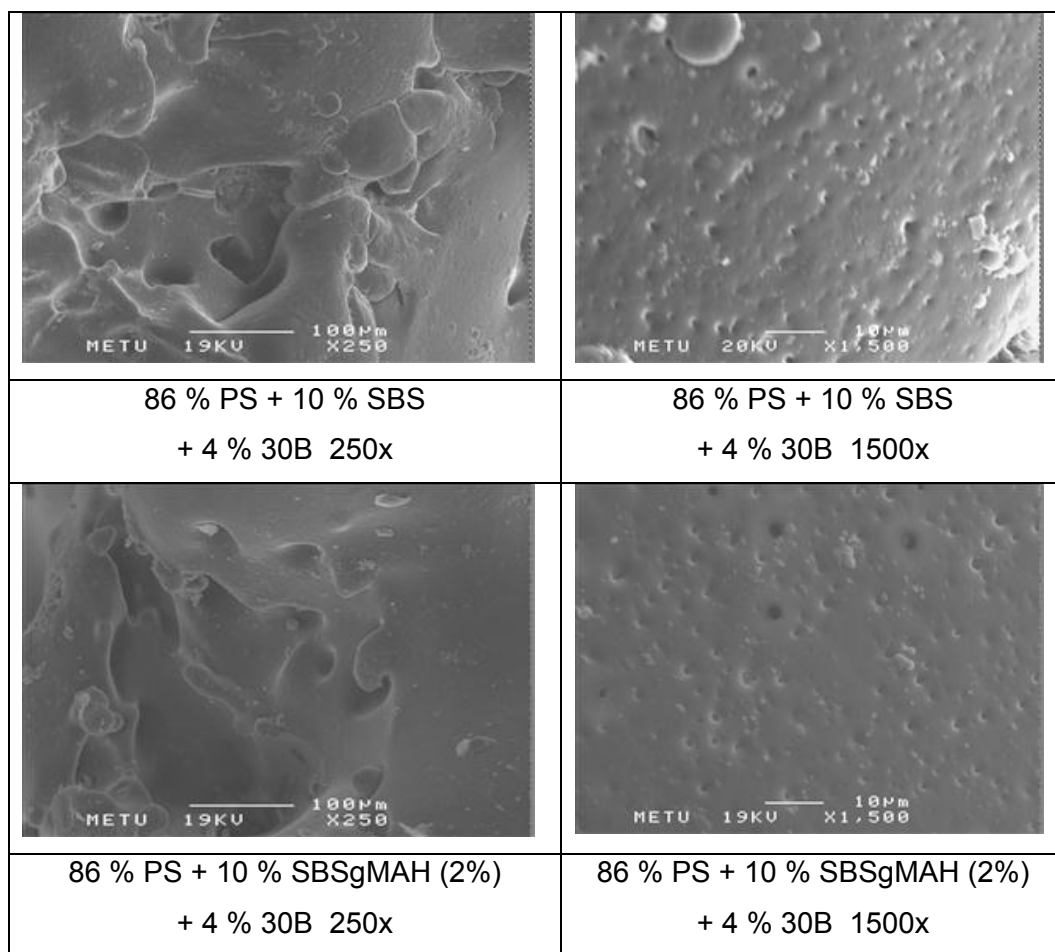
Figure 4.27 SEM micrographs of etched nanocomposites containing 4% Cloisite 30B and 10% SBS or SBSgMAH (2%) with x250 and x1500 magnifications

|	
81 % PS + 15 % SBS + 4 % 30B 250x	81 % PS + 15 % SBS + 4 % 30B 1500x
81 % PS + 15 % SBSgMAH (2%) + 4 % 30B 250x	81 % PS + 15 % SBSgMAH (2%) + 4 % 30B 1500x
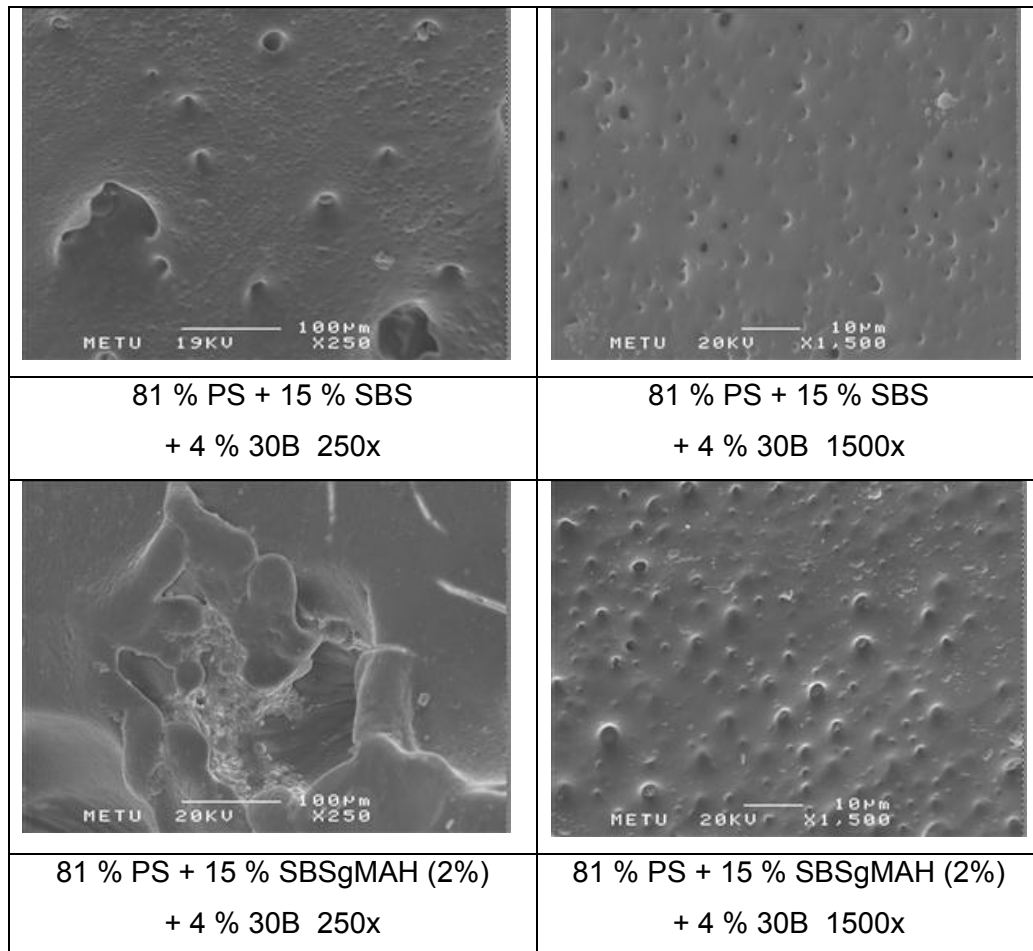
Figure 4.28 SEM micrographs of etched nanocomposites containing 4% Cloisite 30B and 15% SBS or SBSgMAH (2%) with x250 and x1500 magnifications

|	
71 % PS + 25 % SBS + 4 % 30B 250x	71 % PS + 25 % SBS + 4 % 30B 1500x
71 % PS + 25 % SBSgMAH (2%) + 4 % 30B 250x	71 % PS + 25 % SBSgMAH (2%) + 4 % 30B 1500x
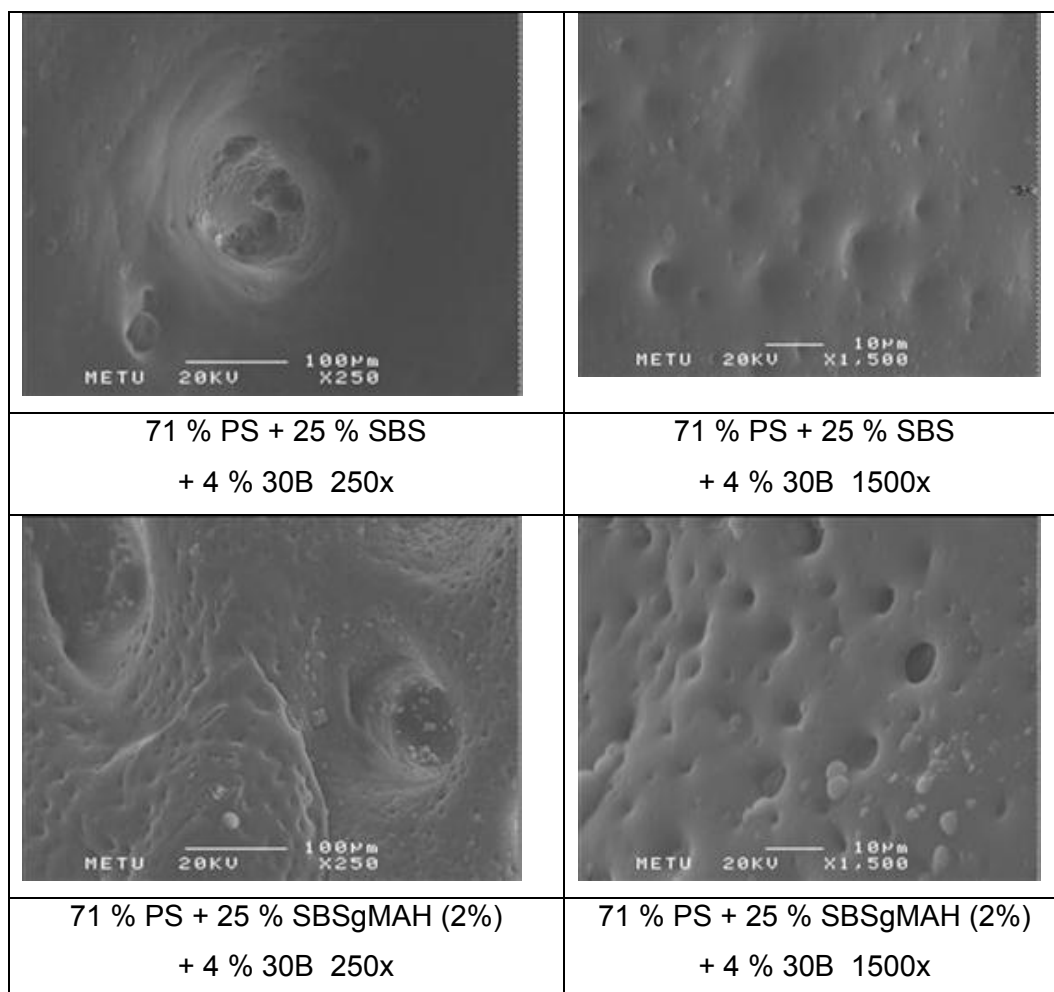
Figure 4.29 SEM micrographs of etched nanocomposites containing 4% Cloisite 30B and 25% SBS or SBSgMAH (2%) with x250 and x1500 magnifications

4.1.3. Transmission Electron Microscopy

In order to investigate the dispersion of organoclays within the polymer matrix, XRD analysis was performed. Although XRD analysis gives information about the dispersion of the organoclays, transmission electron microscopy (TEM) should be used to validate the internal nanometer scale structure and morphology of the nanocomposites. TEM gives the distribution of various phases, through direct visualization. In this study, not only the extent of dispersion of clay layers in nanocomposites was studied, but also the location of the clay particles was detected.

The visible black domains represent the agglomerated clays in TEM images. If the dispersion of clay layers is well, these domains appear as ribbons that indicate the delaminated layers of clay. Beside this, the gray areas represent the PS matrix and white domains represent elastomeric phase which are dispersed in PS matrix.

TEM images of the ternary nanocomposites containing 93% PS/ 2% Cloisite ® 30B/ 5% SBS are shown in Figure 4.30 at different magnifications.

93%PS + 5% SBS + 2% 30B 5 µm scale	93%PS + 5% SBS + 2% 30B 500 nm scale
93%PS + 5% SBS + 2% 30B 100 nm scale	93%PS + 5% SBS + 2% 30B 50 nm scale
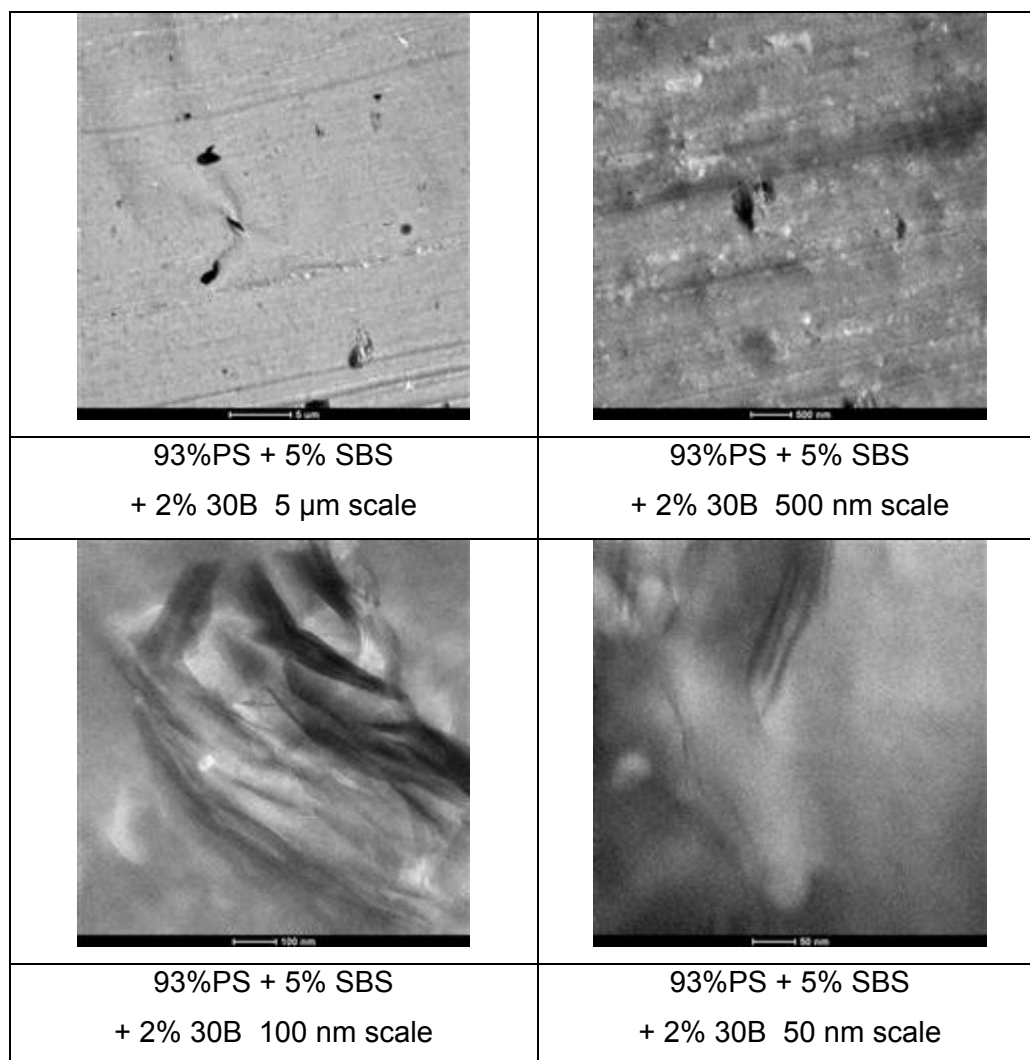
Figure 4.30 TEM micrographs of ternary nanocomposites containing 93 % PS + 5% SBS + 2% Cloisite 30B at different magnifications

As can be seen from the TEM images, the clay particles are localized both at the interphase between the PS and the elastomeric material and inside the domains of elastomeric material. Although domains appear in circular shape in SEM analysis, they appear elliptical in shape in TEM analysis. The reason of this difference may be explained by the cutting direction. The TEM samples were cut parallel to the direction of injection molding, whereas the SEM samples were analyzed perpendicular to this direction.

TEM images of the ternary nanocomposites containing 93% PS/ 2% Cloisite ® 30B/ 5% SBSgMAH (1%) and 93% PS/ 2% Cloisite ® 30B/ 5% SBSgMAH (2%) are shown in Figures 4.31 and 4.32 at different magnifications. When compared to TEM images of nanocomposites containing SBS, it appears that better dispersion of the clay platelets was obtained in the nanocomposites containing maleic anhydride grafted SBS.

93%PS + 5% SBSgMAH (1%) + 2% 30B 1 µm scale	93%PS + 5% SBSgMAH (1%) + 2% 30B 500 nm scale
93%PS + 5% SBSgMAH (1%) + 2% 30B 100 nm scale	93%PS + 5% SBSgMAH (1%) + 2% 30B 100 nm scale
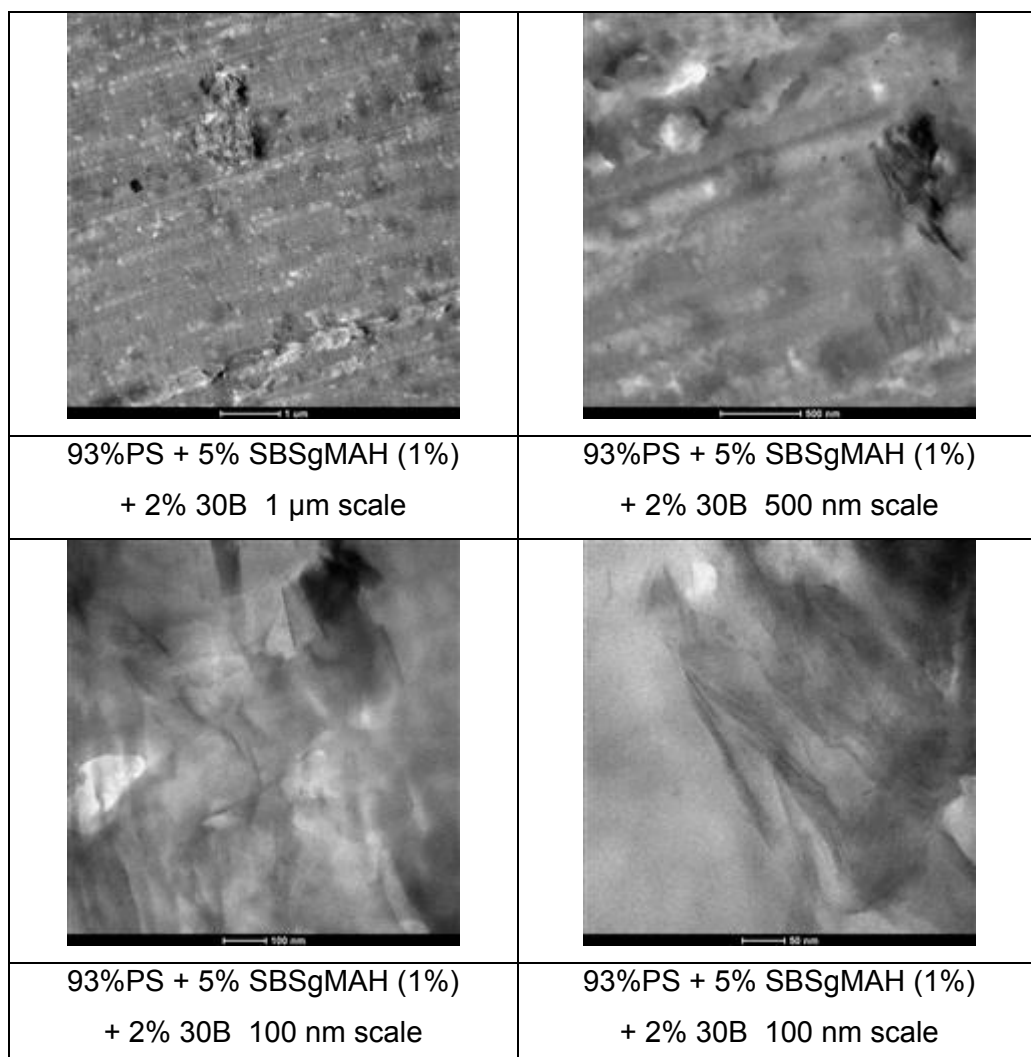
**Figure 4.31** TEM micrographs of ternary nanocomposites containing 93 % PS + 5% SBSgMAH (1%) + 2% Cloisite 30B at different magnifications

| 93%PS + 5% SBSgMAH (2%) + 2% 30B 1 μm scale | 93%PS + 5% SBSgMAH (2%) + 2% 30B 500 nm scale |
| 93%PS + 5% SBSgMAH (1%) + 2% 30B 100 nm scale | 93%PS + 5% SBSgMAH (1%) + 2% 30B 50 nm scale |
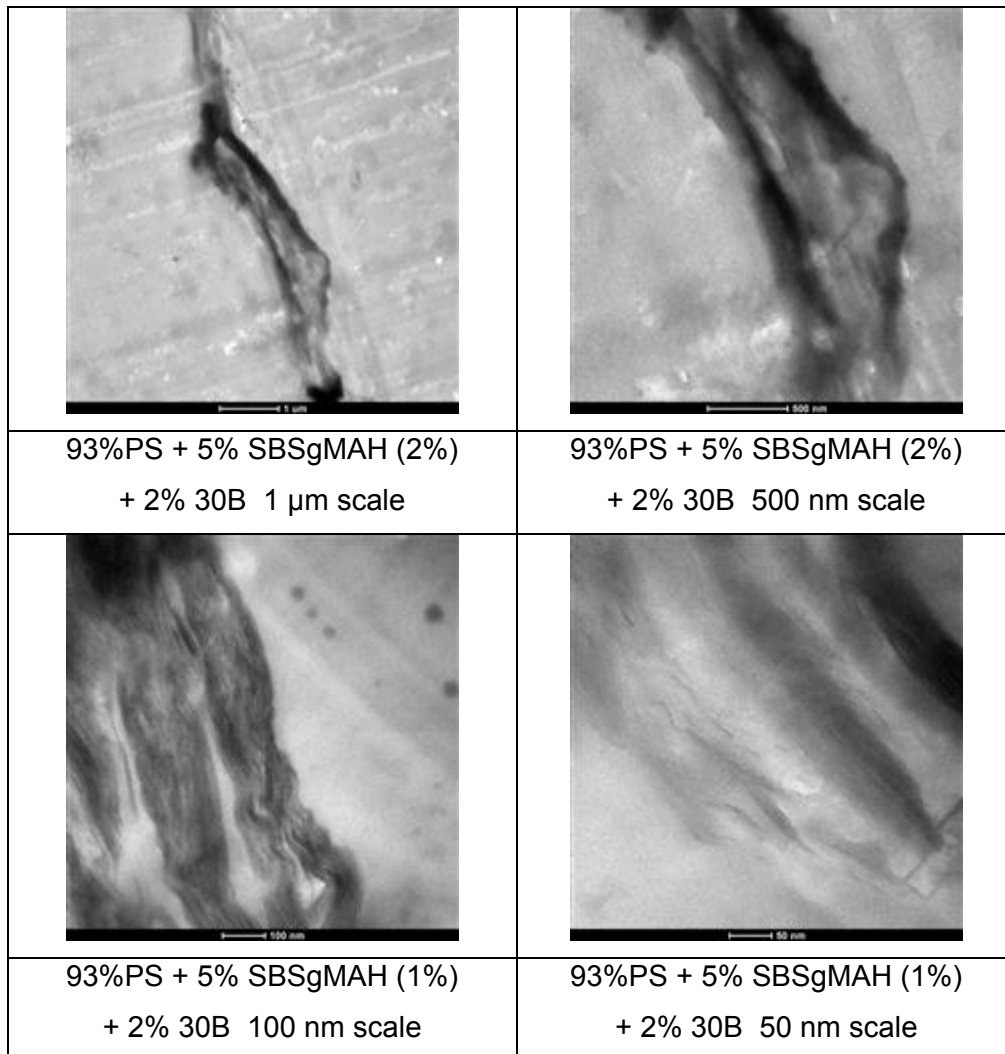
**Figure 4.32** TEM micrographs of ternary nanocomposites containing 93 % PS + 5% SBSgMAH (2%) + 2% Cloisite 30B at different magnifications

TEM images of the ternary nanocomposites containing 73% PS/ 2% Cloisite ® 30B/ 25% SBS, 73% PS/ 2% Cloisite ® 30B/ 25% SBSgMAH (1%) and 73% PS/ 2% Cloisite ® 30B/ 25% SBSgMAH (2%) are shown in Figures 4.33 - 4.35 at different magnifications. It is expected that dispersion state of the organoclays in nanocomposites should increase as the ratio of elastomer to organoclay increases. It can be seen from these images that dispersion of clay layers in nanocomposites containing 25% of elastomer is better than the nanocomposites containing 5% of elastomer. However, exfoliated structures are not observed in any of the samples. The reason for this observation may be the encapsulation of

clay particles by the elastomeric phase and the restricted dispersion of elastomeric phase in the PS matrix. Figures 4.33 – 4.35 also indicate that the dispersion of clay layers gets better as MAH content increases.

73%PS + 25% SBS + 2% 30B 1 μm scale	73%PS + 25% SBS + 2% 30B 500 nm scale
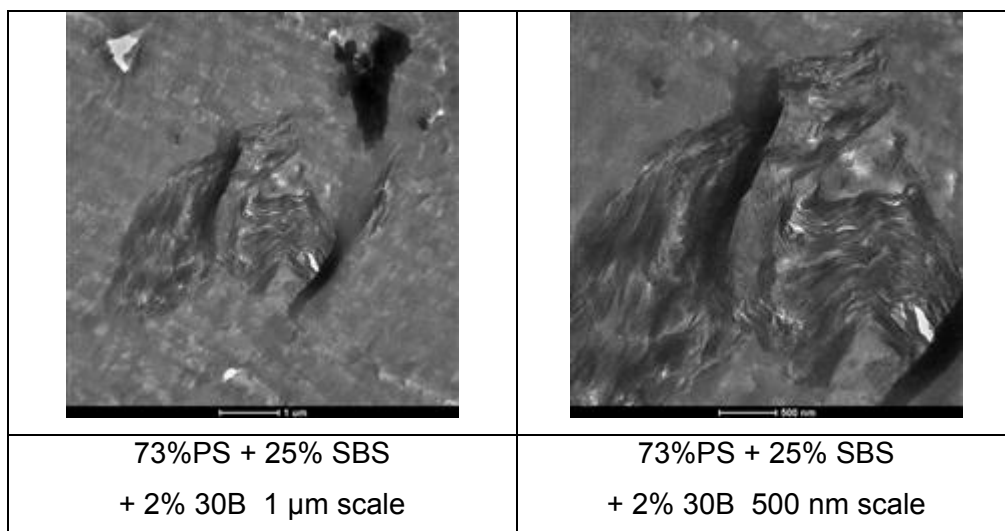
Figure 4.33 TEM micrographs of ternary nanocomposites containing 73 % PS + 25% SBS + 2% Cloisite 30B at different magnifications
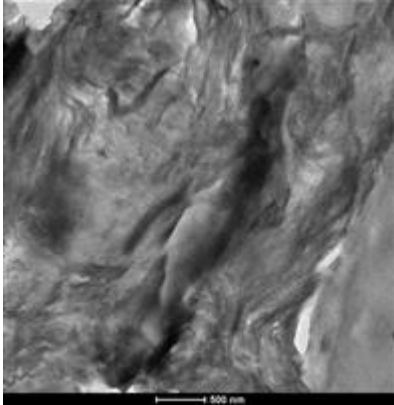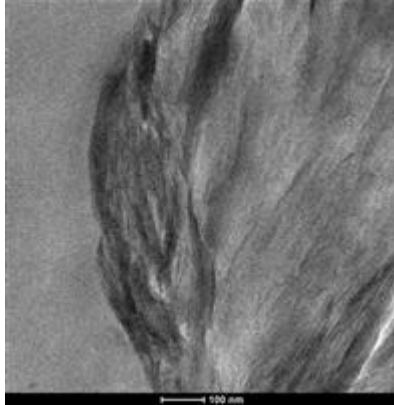
73%PS + 25% SBSgMAH(1%) + 2% 30B 500 nm scale	73%PS + 25% SBSgMAH(1%) + 2% 30B 100 nm scale
73%PS + 25% SBSgMAH(1%) + 2% 30B 50 nm scale	
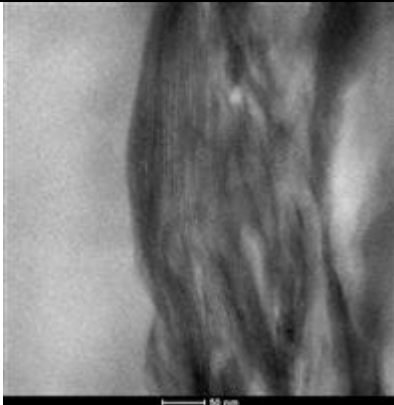
Figure 4.34 TEM micrographs of ternary nanocomposites containing 73 % PS + 25% SBSgMAH (1%) + 2% Cloisite 30B at different magnifications
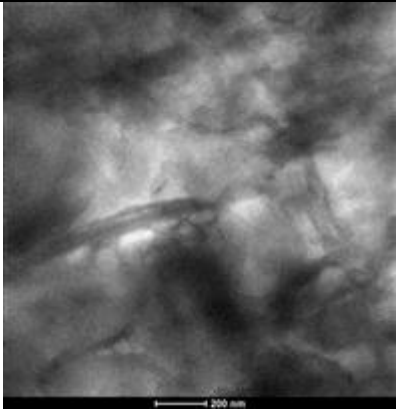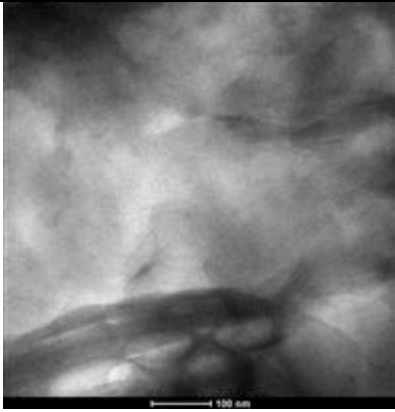
| 73%PS + 25% SBSgMAH(2%) + 2% 30B 200 nm scale	73%PS + 25% SBSgMAH(2%) + 2% 30B 100 nm scale
73%PS + 25% SBSgMAH(2%) + 2% 30B 50 nm scale	
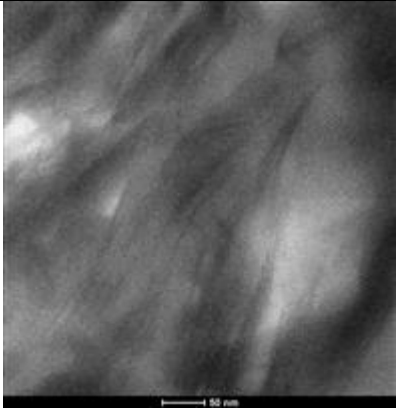
Figure 4.35 TEM micrographs of ternary nanocomposites containing 73 % PS + 25% SBSgMAH (2%) + 2% Cloisite 30B at different magnifications

4.2 Rheological Analyses

4.2.1 Capillary Viscometry

The component which occupies the most space in the mixture tends to act as a continuous phase. However, in order to reduce the energy dissipation, the component having lower viscosity tends to encapsulate the component which is more viscous. Thus, regions in viscosity-composition space where both components will be the continuous phase can be expected. But there is a transition zone where both of the components of the mixture may create

continuous phases. In this case, co-continuous structures may form [123]. This point is called as phase inversion point and the viscosity and volume ratios are the two main factors affecting this point.

In this study, capillary viscometer was used to obtain the melt viscosity values of the raw materials. Measurement of viscosity was made at 200 $^\circ$C. The apparent and Rabinowitsch corrected melt viscosity data of the raw materials used in this study are shown in Figures 4.36 and 4.37, respectively. Data which are used to plot these graphs are shown in Table 4.4. PS has a higher viscosity than SBS. It can be said that viscosity ratio for PS/SBS blends does not change abruptly at high shear rates. The reason for the lower viscosity of SBSgMAH (1%) in comparison to the viscosity of SBSgMAH (2%) is that maleic anhydride acts as a plasticizer at low concentrations. As the maleic anhydride concentration increases, branching occurs and this results in increase in viscosity that is observed in the viscosity of SBSgMAH (2%).
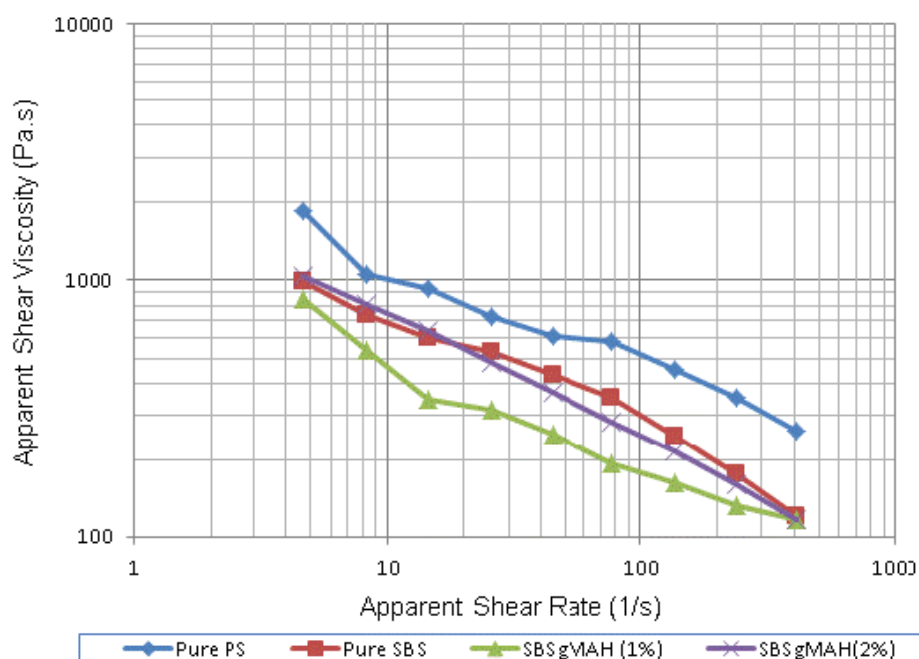
Figure 4.36 Apparent shear viscosities of the raw materials at 200 $^\circ$C at different shear rates.
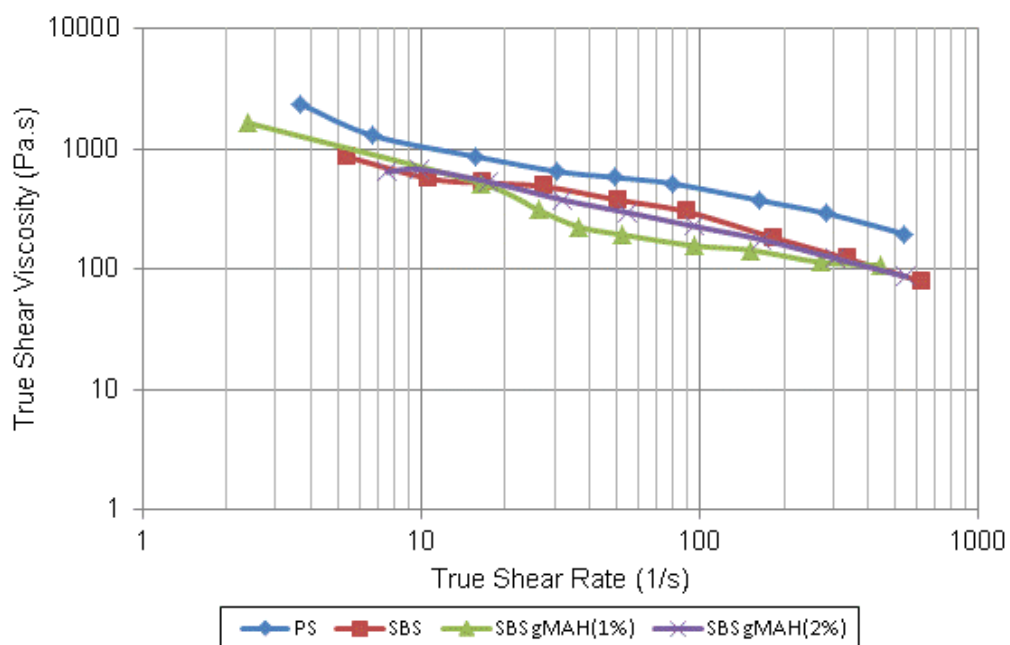
Figure 4.37 True shear viscosities of the raw materials at 200 $^{\circ}$C at different shear rates.

Table 4.4 Apparent melt viscosity data of the raw materials at 200 $^{\circ}$C

Shear Rate (1/s)	PS (Pa.s)	SBS (Pa.s)	SBSgMAH (1%) (Pa.s)	SBSgMAH (2%) (Pa.s)
4.7	1866	997	842	1040
8.3	1051	735	535	812
14.6	930	598	346	637
25.6	724	526	316	478
44.5	607	431	252	366
77.5	580	349	193	281
135.5	452	250	162	217
236.4	352	176	132	160
412.3	259	121	117	116

Table 4.5 True melt viscosity and true shear rate data of the raw materials at 200 °C

PS		SBS		SBSgMAH (1%)		SBSgMAH (2%)	
Shear Rate (1/s)	(Pa.s)	Shear Rate (1/s)	(Pa.s)	Shear Rate (1/s)	(Pa.s)	Shear Rate (1/s)	(Pa.s)
3.7	2355	5.4	865	2.4	1658	7.5	645
6.7	1298	10.6	571	16.5	518	9.8	681
15.6	870	16.6	523	26.3	312	17.3	538
30.7	653	27.4	490	36.8	226	32.3	378
49.7	581	50.8	378	52.2	195	54.7	298
79.2	518	89.6	302	95.1	158	95.3	229
162.9	376	185.3	183	151.3	145	164.8	178
285.1	292	338.6	123	271.1	115	307	123
538.5	198	627.8	79	441.7	109	550.3	87

4.2.2 Melt Flow Index

Melt flow index (MFI) test was performed to investigate the flow behavior of the materials. MFI value depends on many parameters such as viscosity of the material, molecular weight of the material, degree of chain branching, the presence of co-monomers and heat transfer. The tests were performed at 200 °C and 2.16 kg load. No significant change was observed between the MFI values of the raw PS and twice extruded PS, as shown in Table 4.6.

In the first part of this study, nanocomposites were prepared with aliphatic elastomers and different organoclays. Lotader 2210, Lotader AX8840 and Lotader AX8900 were used as the elastomers and Cloisite 15A, Cloisite 25A and Cloisite 30B were used as the organoclays. Elastomer content was kept at 5% and organoclay content was kept at 2% for all of the compositions. MFI values of these samples are shown in Table 4.6. All of the elastomeric materials used in the first part of this study have lower MFI values than PS. Addition of elastomer and organoclay decreased the MFI values, as expected. Since the differences in MFI values are so small, it is difficult to make exact conclusions on the flow properties of these samples.

Binary nanocomposites have lower MFI (higher viscosity) than neat PS, owing to the filler effect of organoclays Rigid fillers are known to increase the viscosity of polymer melts.

Table 4.6 MFI test results of the samples prepared in the first part of this study.

Composition	Concentration		MFI (g/10min)	Standard deviation
	Elastomer (wt %)	Organoclay (wt %)		
PS	---	---	20.2	0.13
PS (extruded twice)	---	---	20.4	0.12
Lotader 2210	100	---	3.6	0.11
Lotader AX8840	100	---	6.1	0.17
Lotader AX8900	100	---	7.6	0.14
PS / Organoclay Binary Nanocomposites				
PS + 15A	---	2	16.6	0.21
PS + 25A	---	2	15	0.14
PS + 30B	---	2	16.9	0.11
PS + 30B	---	4	14.7	0.22
PS / Elastomer / Organoclay Ternary Nanocomposites				
PS + 2210 + 15A	5	2	15.4	0.11
PS + 2210 + 25A	5	2	14.8	0.22
PS + 2210 + 30B	5	2	15.9	0.13
PS + 8840 + 15A	5	2	17.1	0.23
PS + 8840 + 25A	5	2	17.4	0.29
PS + 8840 + 30B	5	2	16.8	0.11
PS + 8900 + 15A	5	2	18.1	0.22
PS + 8900 + 25A	5	2	17.7	0.15
PS + 8900 + 30B	5	2	17.3	0.17

It was concluded from capillary viscometry analysis that PS has higher viscosity than SBS. However, Table 4.7 shows that in MFI tests both of the components have close MFI values. This situation can be explained by the different behavior of the materials under different shear rates, and the nature of capillary measurements and MFI tests. In capillary measurements the shear rate is

constant. However, in MFI test the shear stress is constant and the shear rate varies through the test.

The MFI results of the samples prepared in the second part of this study are given in Table 4.7. Although both PS and SBS have similar MFI values, samples prepared with these materials have higher MFI values than all of the raw materials. In some cases, polymer blends show non-ideal behavior. If two polymers are miscible a maximum can be seen in the MFI values. On the contrary, if the polymers are immiscible a minimum MFI value can be seen.

As seen from the Table 4.7, blends of PS / SBS and PS / SBSgMAH have higher MFI values in comparison to MFI values of pure PS, pure SBS or pure SBSgMAH. This result shows that PS is miscible with both SBS and SBSgMAH. It can also be said from the results in Table 4.7 that maleic anhydride acts as a plasticizer and decreases viscosity, thus it increases MFI values of the samples containing SBSgMAH.

As expected, MFI values of the composites prepared with PS and organoclay are similar. If the clay layers are dispersed totally or polymer chains get inserted between these layers, clay increases the melt viscosity. But, due to poor dispersion of the clay in the PS matrix, decrease in MFI values (increase in viscosity) is small.

Table 4.7 MFI test results of samples prepared in the second part of this study

| Composition | Concentration | | MFI (g/10min) | Std. Dev. |
	Elastomer (wt %)	Organoclay (wt %)		
PS	---	---	20.2	0.13
PS (extruded twice)	---	---	20.4	0.12
SBS	100	---	17.9	0.11
SBSgMAH (1%)	100	---	18.9	0.13
SBSgMAH (2%)	100	---	19.1	0.13

Table 4.7 MFI test results of samples prepared in the second part of this study (continued)

PS / Elastomer Blends				
PS + SBS	5	---	21.9	0.11
PS + SBS	10	---	23.7	0.22
PS + SBS	15	---	25.4	0.13
PS + SBS	25	---	29.5	0.23
PS + SBS	40	---	36.6	0.29
PS + SBSgMAH (1%)	5	---	22.8	0.11
PS + SBSgMAH (1%)	10	---	24.9	0.23
PS + SBSgMAH (1%)	15	---	27.4	0.13
PS + SBSgMAH (1%)	25	---	31.1	0.23
PS + SBSgMAH (1%)	40	---	38.5	0.23
PS + SBSgMAH (2%)	5	---	22.3	0.12
PS + SBSgMAH (2%)	10	---	24.1	0.12
PS + SBSgMAH (2%)	15	---	26.1	0.23
PS + SBSgMAH (2%)	25	---	30.6	0.17
PS + SBSgMAH (2%)	40	---	37.1	0.24
PS / Organoclay Nanocomposites				
PS + 30B	---	2	16.9	0.11
PS + 30B	---	4	14.7	0.22
PS / Elastomer / Organoclay Nanocomposites				
PS + SBS + 30B	5	2	18.4	0.12
PS + SBSgMAH(1%) + 30B	5	2	19.1	0.13
PS + SBSgMAH(2%) + 30B	5	2	18.6	0.12
PS + SBS + 30B	10	2	21.7	0.23
PS + SBSgMAH(1%) + 30B	10	2	23.1	0.13
PS + SBSgMAH(2%) + 30B	10	2	22.2	0.23
PS + SBS + 30B	15	2	25.4	0.14
PS + SBSgMAH(1%) + 30B	15	2	26.3	0.13
PS + SBSgMAH(2%) + 30B	15	2	25.6	0.24
PS + SBS + 30B	25	2	29.8	0.19
PS + SBSgMAH(1%) + 30B	25	2	30.6	0.23

Table 4.7 MFI test results of samples prepared in the second part of this study (continued)

PS + SBSgMAH(2%) + 30B	25	2	29.2	0.16
PS + SBS + 30B	40	2	35.5	0.16
PS + SBSgMAH(1%) + 30B	40	2	36.7	0.15
PS + SBSgMAH(2%) + 30B	40	2	34.9	0.23
PS + SBS + 30B	5	4	17.2	0.13
PS + SBSgMAH(2%) + 30B	5	4	17.4	0.12
PS + SBS + 30B	10	4	20.6	0.13
PS + SBSgMAH(2%) + 30B	10	4	21.1	0.13
PS + SBS + 30B	15	4	23.5	0.12
PS + SBSgMAH(2%) + 30B	15	4	24.6	0.13
PS + SBS + 30B	25	4	28.6	0.17
PS + SBSgMAH(2%) + 30B	25	4	29.2	0.25

Intercalation and exfoliation of the clay platelets require the diffusion of polymer chains into silicate layers or peel away the bottom and top layers as promoted by the application of shear stress and by the polymer adsorption [124]. As viscosity increases, the shear stress applied on the clay platelets also increases and cause separation of the layers. MFI values of the ternary nanocomposites are lower compared to the MFI values of the respective binary blends, since the clay platelets act as fillers and restrict the flow of molten polymer.

4.3 Mechanical Analyses

In this study, tensile and impact tests were performed to evaluate the mechanical properties of the materials. Results of the mechanical tests of all compositions are given in Appendix B.

4.3.1 Tensile Test

In order to investigate the effects of the compatibilizer type, organoclay type, and concentration of materials on the mechanical properties of the prepared samples, tensile and impact tests were performed. Tensile strength, elongation at break

and Young's modulus values were determined from stress-strain curves. Impact energy which is a measure of the work done to fracture a material was determined by the impact test. Tensile properties of the raw materials used in this study are shown in Table 4.8.

Table 4.8 Tensile properties of raw materials

Property	PS (ISO 527)	SBS (ISO 37)
Tensile Strength (MPa)	34.3	4.9
Elongation at break (%)	2	912
Young's modulus (MPa)	1700	2.9

Transparency and relative ease of processing makes PS preferable and it is commonly used in many applications. However, its brittle characteristics restrict its usage area. As seen in Table 4.8, PS has very low elongation at break value which is a sign of brittleness. When PS is subjected to a small deformation, it fails easily. Addition of elastomeric materials is an effective method to overcome this problem. Elastomeric domains absorb the impact energy and restrict the propagation of the cracks. However, addition of elastomeric material results in decreasing the tensile strength and Young's modulus and increasing the elongation at break values of the neat material. Thus, suitable fillers can be used to make the material more rigid and strong. This was one of the goal of this thesis.

In the first part of this study, nanocomposites were prepared with aliphatic elastomers and different organoclays. Lotader 2210, Lotader AX8840 and Lotader AX8900 were used as the elastomers and Cloisite 15A, Cloisite 25A and Cloisite 30B were used as the organoclays. Elastomer content was kept at 5% and organoclay content was kept at 2% in all of the compositions. Effects of montmorillonite type on the tensile properties of PS are shown in Figures 4.38-4.40. There is no significant improvement in the tensile strength and elongation at break values of the neat polymer by producing binary nanocomposites.
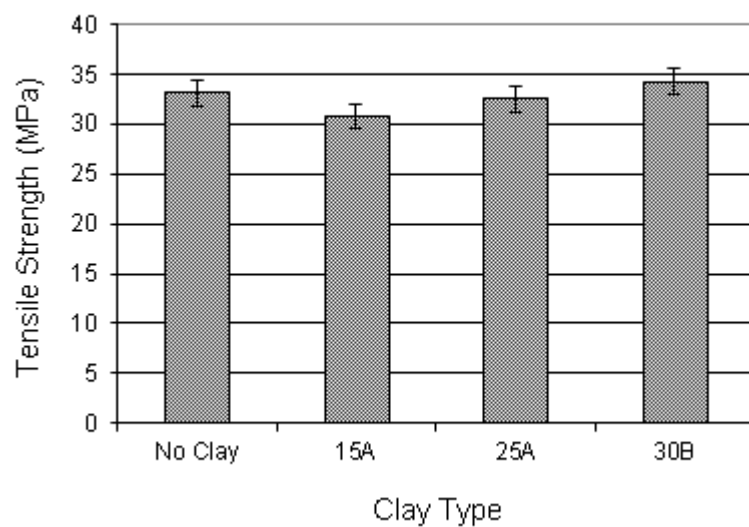
Figure 4.38 Tensile strength of PS / Organoclay (2%) binary nanocomposites
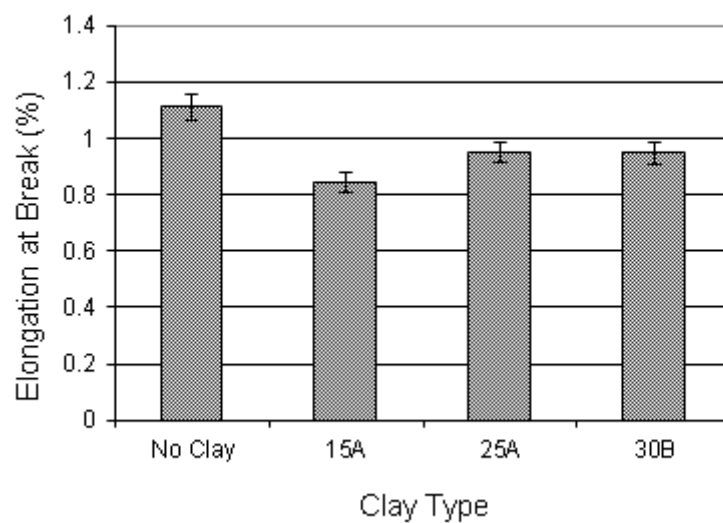

Figure 4.39 Elongation at break of PS / Organoclay (2%) binary nanocomposites
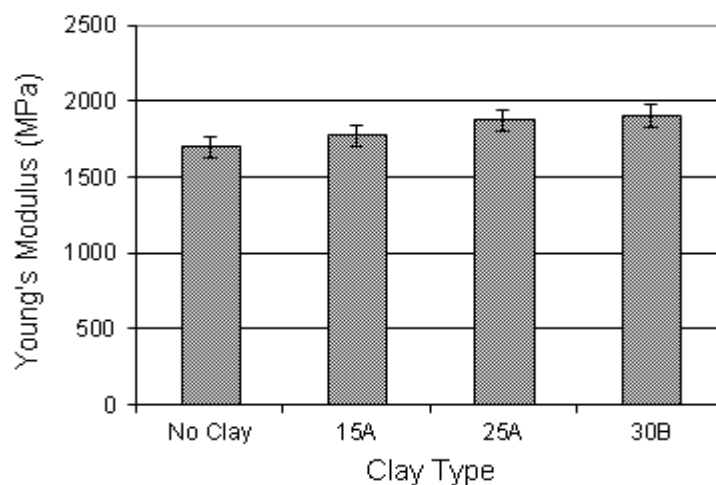
Figure 4.40 Young's modulus of PS / Organoclay (2%) binary nanocomposites

Figures 4.41 – 4.43 show tensile properties of ternary nanocomposites prepared with Lotader 2210, AX8840, AX8900 and Cloisite ® 15A, 25A, 30B. Due to incompatibility of the aliphatic elastomeric phase with the PS matrix, very little improvement was observed in tensile properties of the nanocomposites prepared with these materials.
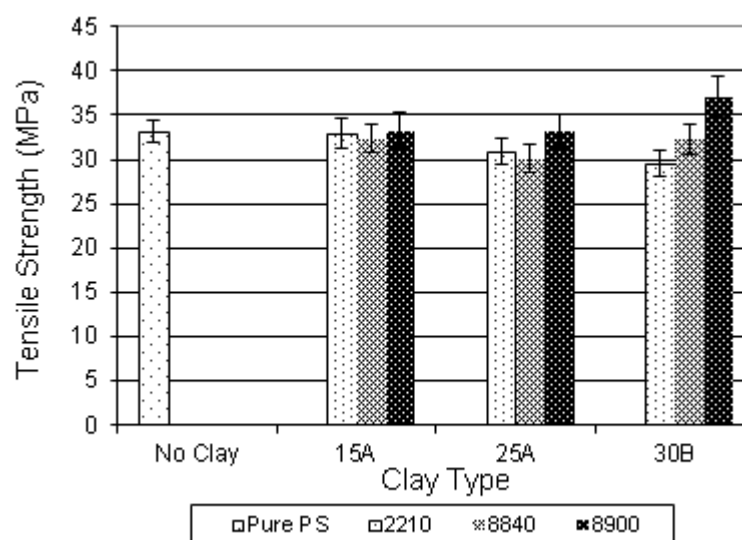
Figure 4.41 Tensile strength of PS / Organoclay (2%) / Elastomer (5%) ternary nanocomposites
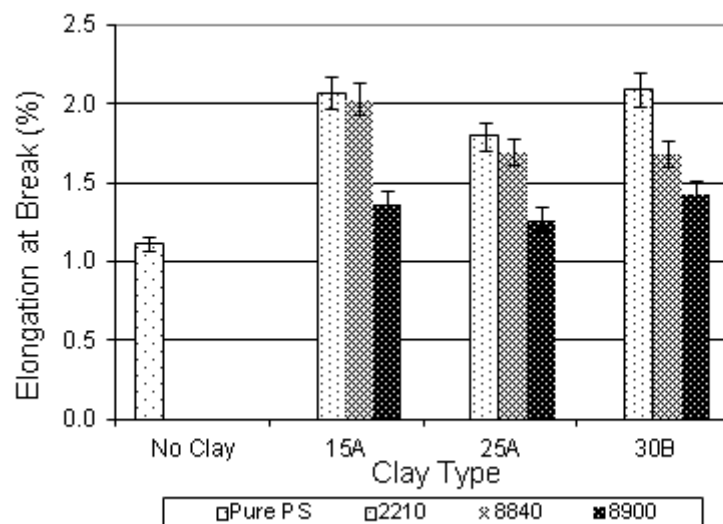
Figure 4.42 Elongation at break of PS / Organoclay (2%) / Elastomer (5%) ternary nanocomposites
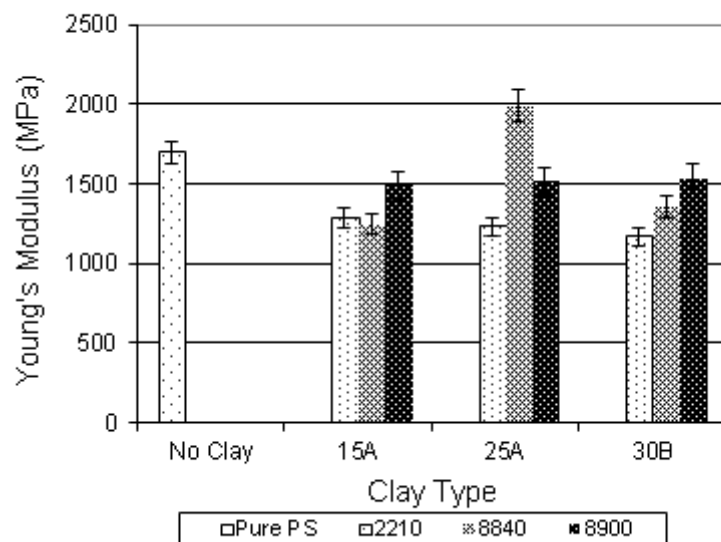
Figure 4.43 Young's modulus of PS / Organoclay (2%) / Elastomer (5%) ternary nanocomposites

Thus, in the second part of this study, an aromatic based elastomer, SBS was chosen and maleic anhydride was grafted onto it. Nanocomposites were prepared with SBS or SBSgMAH and different organoclays. SBS, SBSgMAH (1%) and SBSgMAH (2%) were used as the elastomers and Cloisite ® 30B was used as the organoclay. Elastomer content varied between 5% and 40% and organoclay content was kept at 2% in all of the compositions.

In order to observe the effects of organoclay on the mechanical properties of the PS and the PS/elastomer blends, tensile properties of the PS and PS/elastomer blends were also examined besides the ternary nanocomposites. Figures 4.44 – 4.46 show the tensile properties of PS/SBS and PS/SBSgMAH blends with increasing elastomer content. SBS has lower tensile strength and Young's modulus values compared to pure PS. When they are mixed, elastomeric material imparts dilution effect. While impact energy (as shown later) and elongation at break values increase, tensile strength and Young's modulus values decrease due to this effect.

Selection of proper elastomer and optimum elastomer content are important things to prepare ternary nanocomposites having good mechanical properties. In order to find the proper elastomer and optimum elastomer content, various elastomers have been added to PS at different ratios. Although 5% elastomer addition results in an increase in tensile strength and Young's modulus, it is not enough to obtain the materials with high impact strength (as shown later) which is the aim of this study. Thus, it was decided to increase the elastomer content up to 40%.
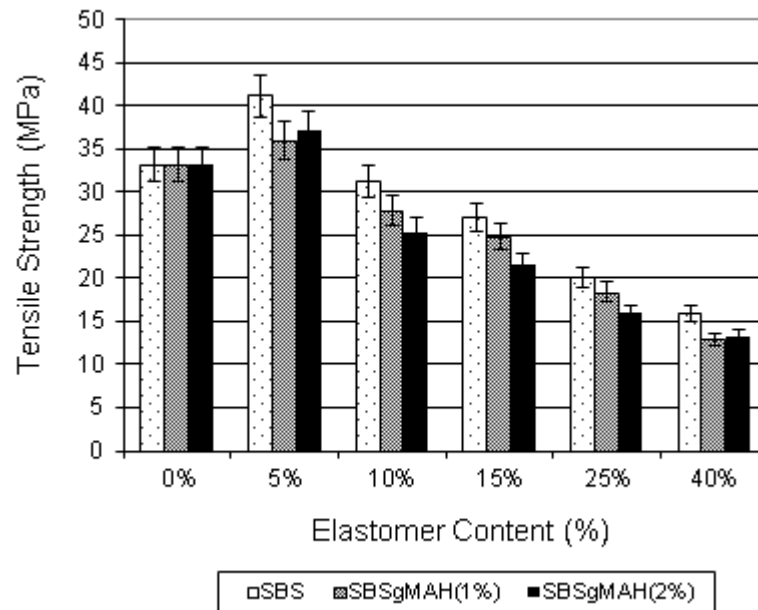
**Figure 4.44** Tensile strength of PS / elastomer binary blends
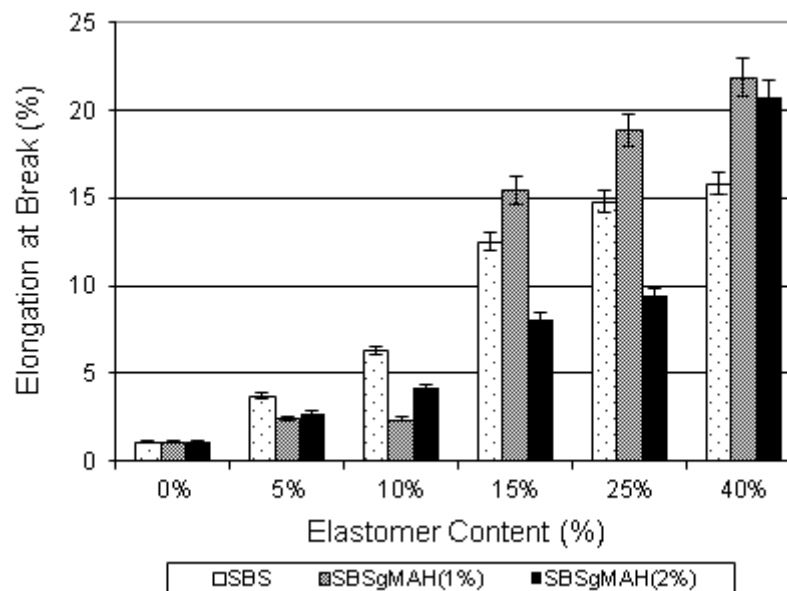
Figure 4.45 Elongation at break (%) of PS / elastomer binary blends
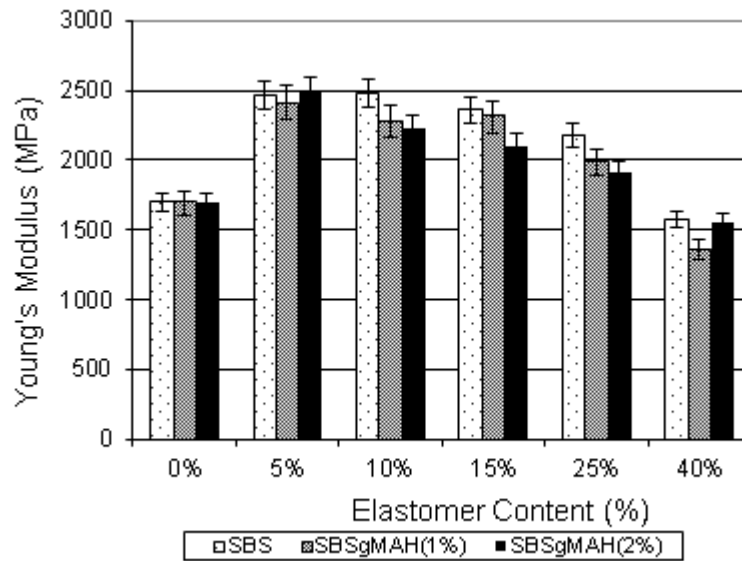
Figure 4.46 Young's modulus (MPa) of PS / elastomer binary blends.

Tensile properties of the ternary nanocomposites containing 2% organoclay and various amounts of elastomer are shown in Figures 4.47 – 4.49. Organoclay addition makes the polymer matrix stiffer due to the high aspect ratio and high rigidity of the silicate layers. Reinforcement effect of the organoclay addition can be explained by the high strength of the clay as well as the increase in the contact area between the organoclay and polymer matrix. Thus, in order to obtain materials having enhanced tensile strength and Young's modulus values, dispersion of organoclay particles must be good. Although clay addition increased tensile strength and Young's modulus values, it decreased elongation at break and impact strength values since organoclay particles can't be elongated as much as the matrix does.

Due to poor dispersion of the silicate layers in the PS matrix, addition of organoclay into PS resulted in slightly lower stiffness and strength in comparison to pure PS. This is observed in the binary nanocomposites.

The data in Figures 4.47 – 4.49 with 0% elastomer content refer to binary composites of Cloisite ® 30B. Although reduction in tensile strength and Young's modulus values is expected with the addition of elastomer, the reverse effect was

observed in ternary nanocomposites. Tensile strength value of the ternary nanocomposites increased while Young's modulus value remained the same. This result can be attributed to the better dispersion of the clay particles in the presence of elastomeric phase as supported with the XRD results. Among all the nanocomposites, the best improvement in the tensile strength value was obtained for the ternary nanocomposites containing 2% Cloisite ® 30B and 5% SBS. The improvement in tensile strength was about 32% with respect to pure PS. The same composition shows 46% improvement in Young's modulus and 270% improvement in elongation at break in comparison to pure PS. Thus, it is observed that ternary nanocomposites can show improvement in all the three properties.
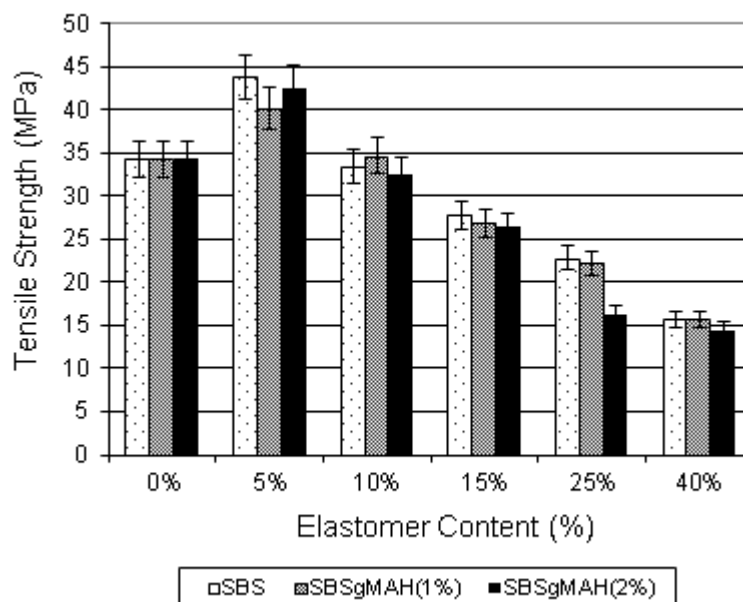

**Figure 4.47** Tensile strength of PS / elastomer / Cloisite 30B (2%) ternary nanocomposites
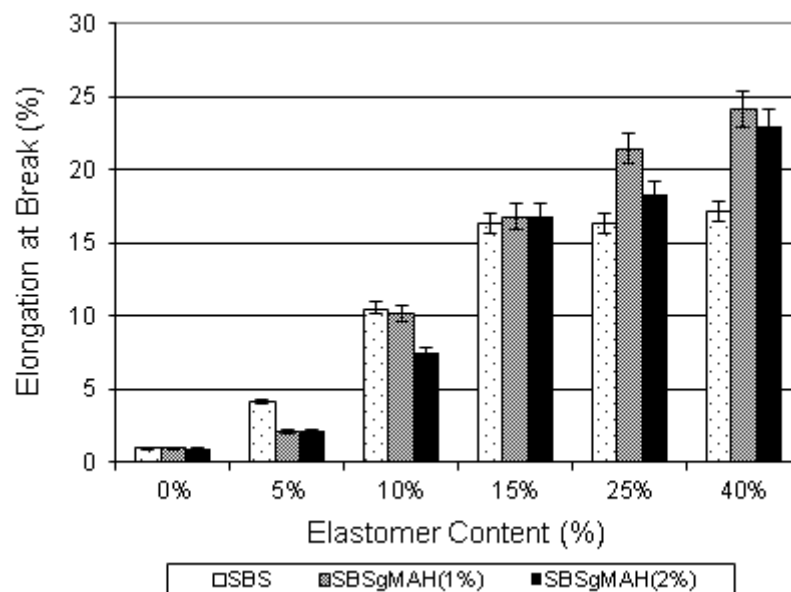
Figure 4.48 Elongation at break of PS / elastomer / Cloisite 30B (2%) ternary nanocomposites
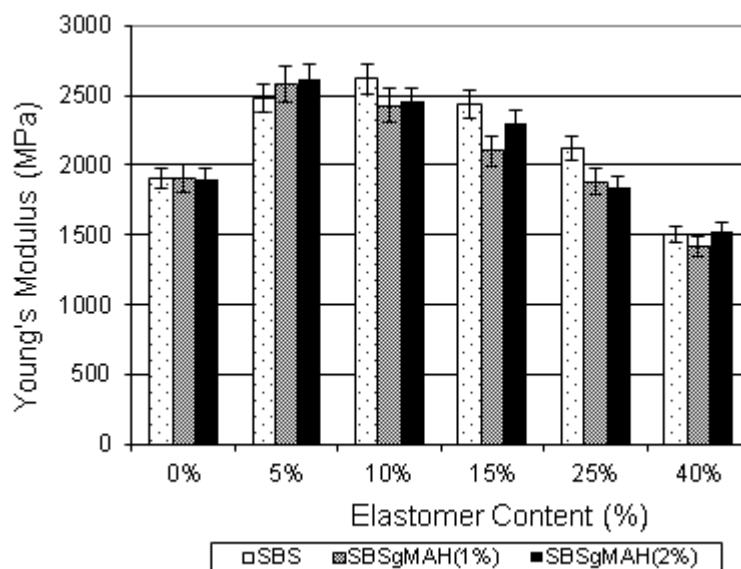

Figure 4.49 Young's modulus of PS / elastomer / Cloisite 30B (2%) ternary nanocomposites

Tensile properties of the nanocomposites containing 4% of organoclay and various amounts of SBS or SBSgMAH (2%) are shown in Figures 4.50 - 4.52. Again synergistic effects are seen in 4% organoclay and 5% elastomer content.

The improvement in the properties of the material with 4% organoclay and 5% SBSgMAH (2%) with respect to neat PS are 44% in tensile strength, 80% in elongation at break and 71% in Young's modulus.
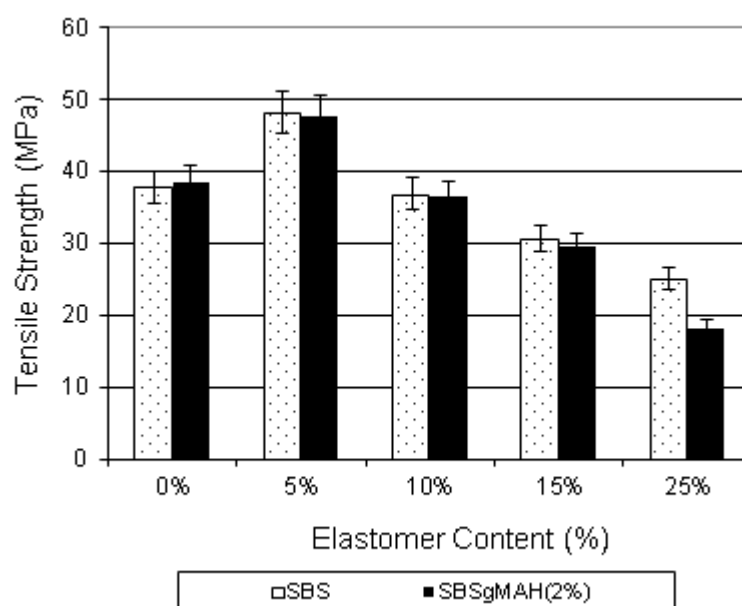

**Figure 4.50** Tensile strength of PS / elastomer / Cloisite 30B (4%) ternary nanocomposites
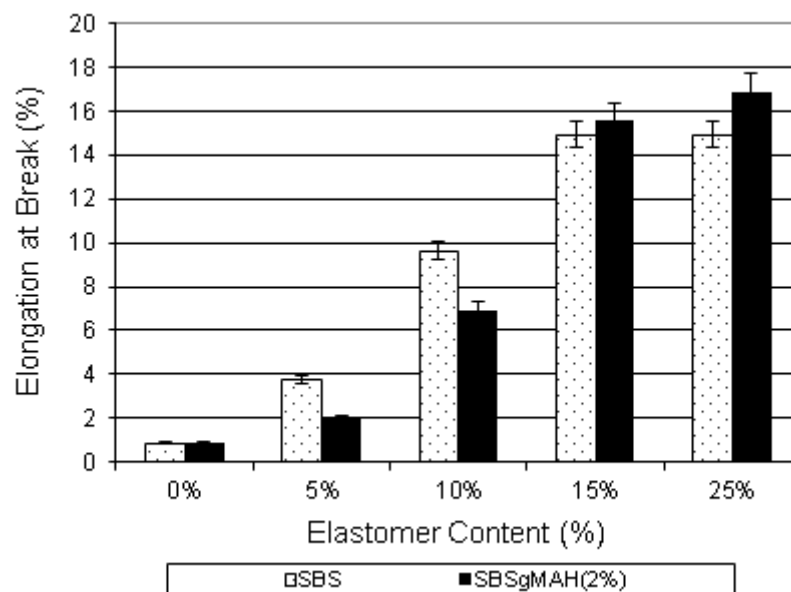
Figure 4.51 Elongation at break of PS / elastomer / Cloisite 30B (4%) ternary nanocomposites
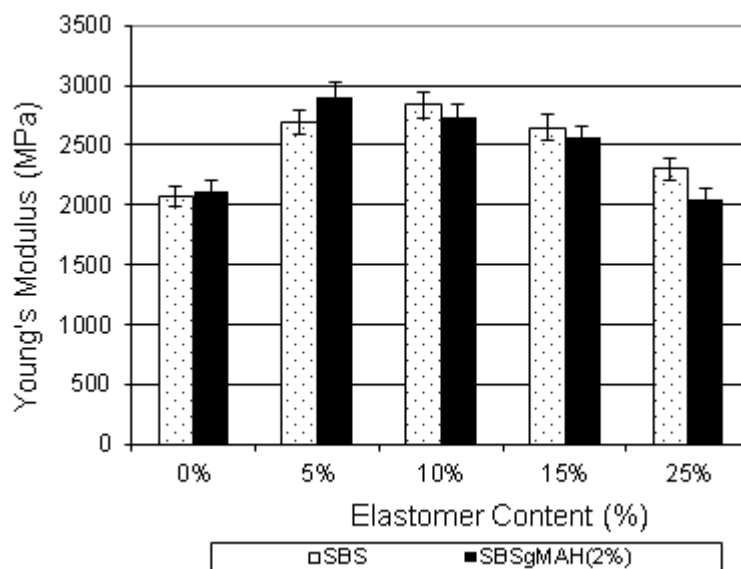

Figure 4.52 Young's modulus of PS / elastomer / Cloisite 30B (4%) ternary nanocomposites

The results obtained so far showed that SBS is compatible with PS and good dispersion of the clay particles improves tensile strength. Although with the addition of 5% elastomer and 4% organoclay improvement was obtained in tensile strength of PS, elongation at break values obtained are still low compared to high impact polystyrene. On the other hand, nanocomposites containing 25% and 40% elastomer have significantly greater elongation at break values than those nanocomposites containing lower amounts of elastomer. Addition of organoclay increases the elongation at break values of nanocomposites having high amounts of elastomer. This increase may be attributed the dispersion of organoclays, which reside at the elastomer and PS interface before phase inversion. After phase inversion, the silicate layers will be distributed more uniformly in both elastomer and PS phases and restrict the crack propagation. Although the elongation at break values of the nanocomposites containing large amounts of elastomer are very high, tensile strength values of these nanocomposites are about half of the nanocomposites containing low amounts of elastomer. Thus, it can be said that the elastomer concentration should be selected according to aim of the use of the material. If the material will be subjected to high tensile stress, nanocomposites containing low amounts of elastomer should be used, if the material will be subjected to high impact, nanocomposites containing high amounts of elastomer should be used.

4.3.2. Impact Test

In order to investigate the effects of elastomer and organoclay addition on the toughness of the materials prepared in this study, unnotched Charpy impact tests were done. Although PS is stiff, its brittleness restricts its use. Thus, it is desired to increase its energy absorbance capacity and prohibit crack propagation when it gets hit with something. High impact polystyrene; HIPS may be a solution to this problem, but production of the HIPS in industrial scale is not suitable due to the difficulty of polymerization of styrene in the presence of polybutadiene. Polybutadiene particles are dispersed in the PS matrix. When HIPS is subjected to an impact force, impact energy is spent for deformation of these domains instead of cracking the PS matrix.

The second method to improve the impact strength of PS is to melt blend it with compatible block co-polymers. Co-polymer should be dispersed uniformly in the PS matrix and adhesion between co-polymer and PS should be good, and interfacial tension should be optimum to obtain improvement in impact strength. Dispersed particle size of the co-polymer is directly related to the improvement of impact strength.

When the impact strength values of the nanocomposites given later are considered, it can be seen that the SEM observations are consistent with the impact test values. Impact strength values of the nanocomposites are directly proportional with the elastomer content.

Impact energy of the materials prepared in this study is shown in Figures 4.53 - 4.56. Clay addition makes the polymer stiffer and may reduce the impact strength. However, addition of clay and elastomer together makes the polymer tougher and increases the impact strength. This situation can be explained by the effect of clay particles on the elastomeric domain sizes. If the elastomer content increases so much, phase inversion occurs and impact strength decreases

In the first part of this study, nanocomposites were prepared with aliphatic elastomers and different organoclays. Lotader 2210, Lotader AX8840 and Lotader AX8900 were used as elastomers and Cloisite 15A, Cloisite 25A and Cloisite 30B were used as organoclays. Elastomer content was kept at 5% and organoclay content was kept at 2% for all of the compositions. Effects of montmorillonite type on the impact strength of PS are shown in Figure 4.53. Among these compositions PS / Cloisite ® 25A / Lotader AX8900 has the highest impact energy value.
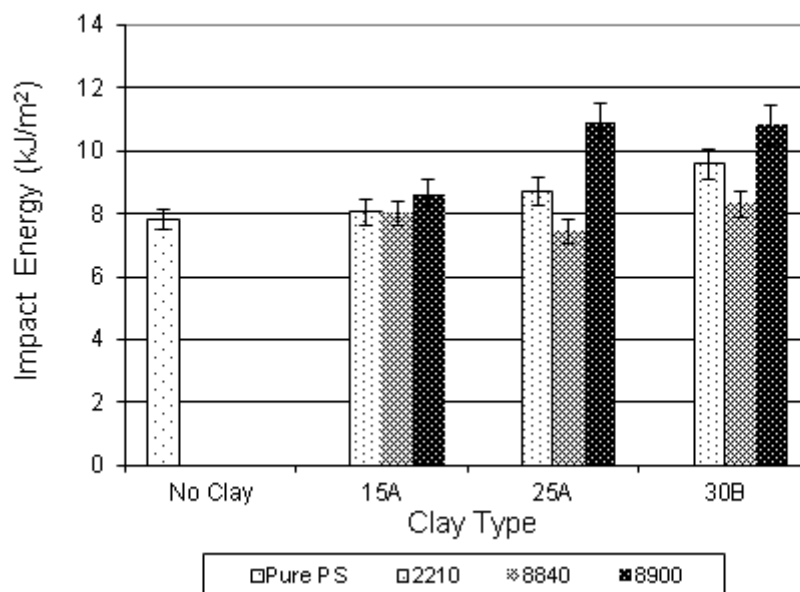
Figure 4.53 Impact energy of PS / Organoclay (2%) / Elastomer (5%) ternary nanocomposites

Average domain size and interdomain distance are important factors that affect the toughening of the materials. The final domain size is controlled by many factors such as; the melt viscosity, melt elasticity of the components, rheological properties, volume fractions of the components, shear stresses and rates, mobility of the interface and surface tension. Small inter-particle distance suppresses craze or crack growth and facilitate the overlap of the stress fields around the adjacent rubber articles. By this way, local shear yielding is promoted and high impact energies are absorbed [119, 122]. However, the size of the domain should not be too small or too big. When there is high adhesion owing to great compatibilization, ultra-fine domains of elastomers are formed and cause low impact strength values, because crack propagation lines progress without touching the elastomer domains. Larger elastomeric domains also influence the toughness of the material negatively, since they form large regions that could not stop the crack propagation. Figure 4.54 shows that in binary blends, the blends containing 15% elastomer have the optimum average domain size resulting in high impact strength without deteriorating the tensile strength values. It also shows that SBSgMAH is better than SBS in improving the impact energy.

126
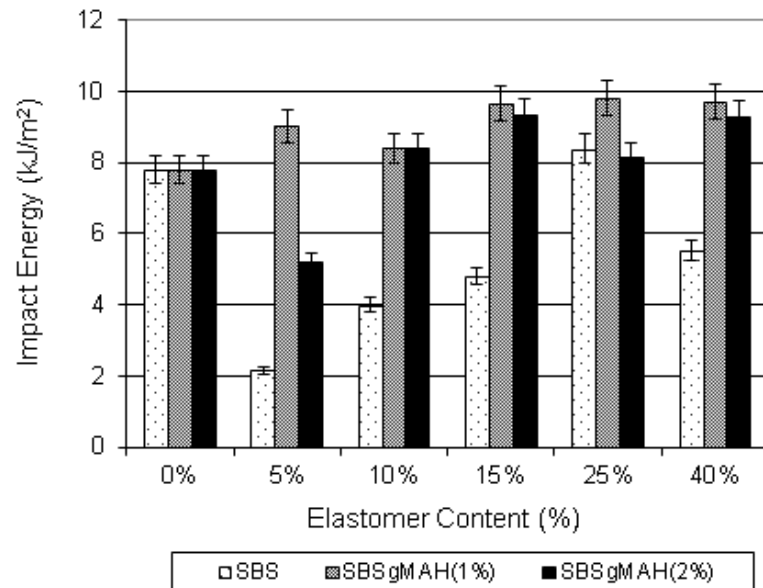
Figure 4.54 Impact energy of PS / Elastomer binary blends

The impact strength of ternary nanocomposites shown in Figure 4.55 – 4.56 indicate that in these materials also, SBSgMAH is better than SBS in improving the impact strength. This may be due to higher interaction provided by SBSgMAH in comparison to SBS. Also, the addition of organoclay further increases the impact strength owing to the crack stopping action of organoclay.
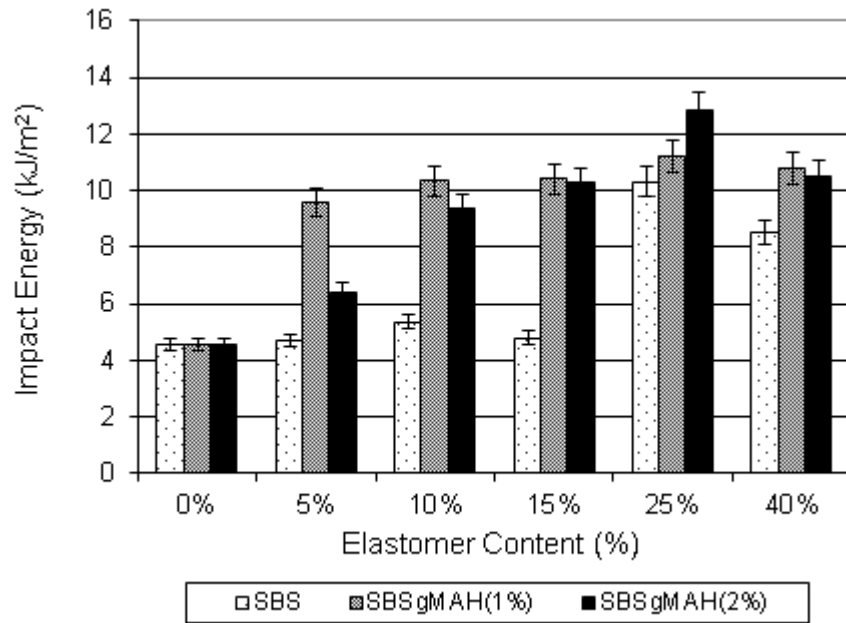
**Figure 4.55** Impact energy of PS / Elastomer / Cloisite 30B (2%) ternary nanocomposites
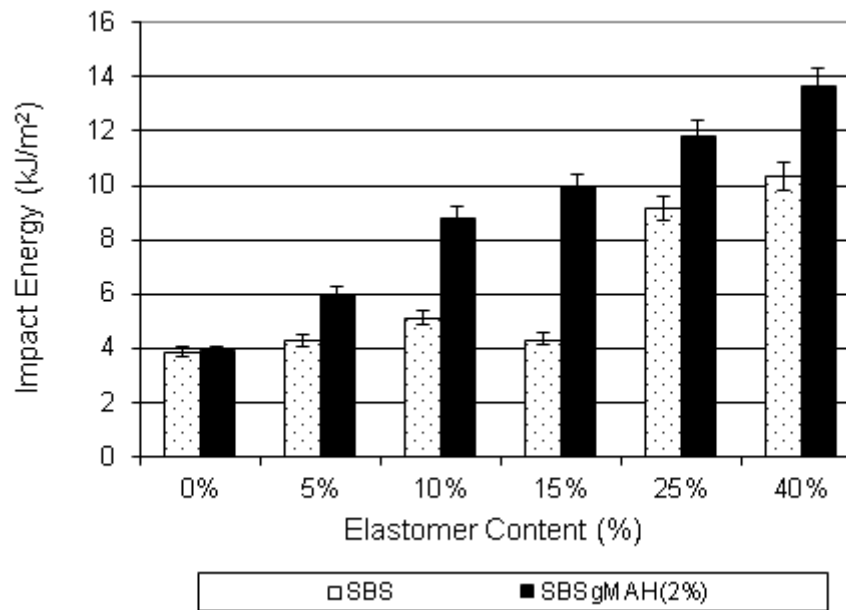
Figure 4.56 Impact energy of PS / Elastomer / Cloisite 30B (4%) ternary nanocomposites

4.4 Thermal Analyses

4.4.1 Differential Scanning Calorimetry

In order to observe the effects of organoclay and elastomer addition on the thermal properties of blends and nanocomposites prepared in this study, Differential Scanning Calorimetry analyses were done. By this analysis, glass transition temperature, T_g was measured and the data obtained are shown in Table 4.7, and the corresponding DSC thermograms are given in Appendix C. Analysis was done between 40 – 260 ^{o}C and heating rate was selected 20 ^{o}C/min to increase the sensitivity and observe the T_g more accurately.

As temperature increases, segmental motion of the polymer chains also increases and it becomes significant above the T_g. Segmental motion of the polymer chains may be prevented by the intercalated or exfoliated clay layers and this may lead to increase in glass transition temperature. Although this idea seems to be logical, no significant change was observed in the glass transition temperature of binary nanocomposites prepared in this study. Thus, it can be said that, organoclay addition does not affect the glass transition temperature significantly.

In addition to this, some fluctuations were observed in the DSC thermograms of the samples containing high amount of elastomer at temperatures above 250 ^{o}C. At first, it may be thought that these fluctuations may have arisen from thermal degradation of the samples. However, much higher temperatures are needed for the degradation of PS. Thus, this thought is incorrect, and it can be said that these fluctuations arose from branching / crosslinking of the elastomeric materials at high temperatures.

If the butadiene domains in SBS mix with the polystyrene chains on a "molecular level", it would be expected that addition of elastomeric material into PS would decrease the glass transition temperature of PS. However, according to the results given in Table 4.9, increasing elastomer content resulted in higher T_g. This result may be due to branching / crosslinking of elastomer that would increase the glass transition temperature. It also indicates that mixing is not achieved at molecular level.

Table 4.9 Results of Differential Scanning Calorimetry Analysis

Composition	Concentration		T_g (^{o}C)
	Elastomer (wt%)	Organoclay (wt%)	
PS	---	---	107.8
PS + 15A	---	2	108.7
PS + 25A	---	2	108.9
PS + 30B	---	2	108.8
PS + 30B	---	4	109.1
PS + 8900 + 30B	5	2	107.3
PS + 8840 + 30B	5	2	107.6
PS + 2210 + 30B	5	2	107.4
PS + SBS	5	---	104.2
PS + SBS	25	---	109.1
PS + SBSgMAH (1%)	5	---	104.4
PS + SBSgMAH (1%)	25	---	109.6
PS + SBSgMAH (2%)	5	---	104.7
PS + SBSgMAH (2%)	25	---	109.8
PS + SBS + 30B	5	2	106.5
PS + SBS + 30B	25	2	108.4
PS + SBS + 30B	5	4	106.8
PS + SBS + 30B	25	4	108.6
PS + SBSgMAH (1%) + 30B	5	2	107.1
PS + SBSgMAH (1%) + 30B	25	2	108.3
PS + SBSgMAH (2%) + 30B	5	2	107.4
PS + SBSgMAH (2%) + 30B	25	2	108.5
PS + SBSgMAH (2%) + 30B	5	4	106.9
PS + SBSgMAH (2%) + 30B	25	4	108.4

CHAPTER 5

CONCLUSIONS

The main disadvantage of PS is its brittleness and it should be eliminated. In this study a novel technique was used to obtain hard and tough PS. It consisted of adding an elastomeric impact modifier to improve toughness, and adding organoclay to increase tensile strength and modulus. This study consists of two parts. In the first part of this study, aliphatic elastomers, Lotader AX8900, AX8840 and 2210 were used as the rubber phase. Blending of the elastomer and PS was done by a co-rotating twin screw extruder. Addition of a rubbery material into PS increases elongation at break and impact strength, while reducing tensile strength and modulus. Thus, organically modified silicates, Cloisite ® 30B, 15A and 25A were used as the organoclays to increase the tensile strength and modulus. The elastomer and organoclay contents were kept at 5% and 2% respectively, and effects of the elastomer and organoclay type on the properties of PS were investigated. Due to incompatibility of the aliphatic elastomers with the PS matrix, no significant improvement was observed in the basal spacing and mechanical properties of these binary and ternary nanocomposites

In the second part of this study, an aromatic elastomer, SBS, was chosen and maleic anhydride was grafted onto it at 1% and 2% ratios. Cloisite ® 30B was chosen as the organoclay. The elastomer content was varied between 0% and 40%, and the organoclay content was varied between 0% and 4%. According to XRD patterns, broader peaks were observed which means larger interlayer spacings. Thus, it can be said that elastomer SBSgMAH acted as a better compatibilizer for PS/Cloisite® 30B nanocomposites, in comparison to Lotader AX8840, Lotader AX8900 and Lotader 2210.

To observe the dispersion of the elastomeric phase which is an important factor affecting the impact strength of the material, etching was done with n-Heptane and the domain sizes of the elastomeric phase were investigated. As observed from SEM analysis, increasing elastomer content resulted in increasing number of

cracks. Besides this, crack lines became shorter and the distance between crack lines decreased. Increasing elastomer content increased the average domain sizes of both binary blends and ternary nanocomposites due to droplet coalescence. Increase of the domain size in the ternary nanocomposites was higher than the domain size of the binary blends with the same elastomer content. This was attributed to the presence of clay particles mostly in the elastomeric phase. Another conclusion which is made from the SEM analysis is the phase inversion point. It was found that phase inversion occurred between 25% and 40% elastomer content.

In order to investigate the rheological and flow properties of the materials, capillary viscometry and melt flow index tests were carried out. PS exhibited a higher viscosity than SBS. It can be said that the viscosity ratio of PS/SBS blends did not change at high shear rates.

All of the elastomeric materials used in the first part of this study exhibited lower MFI values than PS. Addition of elastomer and organoclay decreased the MFI values, as expected. In the second part of the study (with the aromatic elastomers) blends of PS / SBS and PS / SBSgMAH had higher MFI values in comparison to MFI values of pure PS or pure SBS. This result shows that PS is miscible with both SBS and SBSgMAH. Maleic anhydride acted as a plasticizer and decreased viscosity, and increased MFI values of the samples containing SBSgMAH.

If the clay layers are dispersed totally or polymer chains get inserted between these layers, the clay increases the melt viscosity. But in this study, due to poor dispersion of the clay in the PS matrix, decrease in MFI values (increase in viscosity) was small.

When the tensile properties of ternary nanocomposites prepared with Lotader 2210, AX8840, AX8900 and Cloisite ® 15A, 25A, 30B are investigated, no significant improvement was observed in tensile properties of the ternary nanocomposites prepared with these materials. This may due to incompatibility of the aliphatic elastomeric phase with the PS matrix.

Organoclay addition makes the polymer matrix stiffer due to the high aspect ratio and high rigidity of the silicate layers. However, due to poor dispersion of the silicate layers in the PS matrix, addition of organoclay into PS resulted in small increase in stiffness; and the tensile strength was the same as that of pure PS. This was observed in the binary nanocomposites. When the aromatic elastomers were added to the binary composites to produce ternary nanocomposites it was observed that tensile strength and modulus of the ternary nanocomposites increased. This result can be attributed to the better dispersion of the clay particles in the presence of elastomeric phase, as supported with the XRD results. Among all the nanocomposites, the highest improvement in the tensile strength value was obtained for the ternary nanocomposites containing 2% Cloisite ® 30B and 5% SBS. The improvement in tensile strength, modulus and strain at break were about 32%, 46% and 270% respectively with respect to pure PS.

According to impact test results, PS / Cloisite ® 25A / Lotader AX8840 had the highest impact energy value among the all samples prepared in the first part of the study. In the second part of the study, the blends containing 15% elastomer had the optimum average domain size resulting in the high impact strength without deteriorating the tensile strength and modulus values.

When the results of DSC analysis are investigated, no significant changes were observed in the T_g of the samples with the addition of organoclays. Addition of elastomer increased T_g of the samples, unexpectedly. This result was due to branching or crosslinking of the elastomer during extrusion.

REFERENCES

1. Giannelis E.P., "Polymer Layered Silicate Nanocomposites", Advanced Materials, vol.8, 29-35, 1996.

2. Bafna A. A., "Polyethylene-Clay Nanocomposites: Processing-Structure-Property Relationship", Ph.D. Thesis, University of Cincinnati, Ohio, USA, 2004.

3. Hambir S., Bulakh N., and Jog J.P., "Polypropylene / Clay Nanocomposites: Effect of Compatibilizer on the Thermal, Crystallization and Dynamic Behavior", Polymer Engineering and Science, vol.42 No.9, 1800-1807, 2002.

4. Wang K. H., Choi M. H., Koo C. M., Choi Y.S., and Chung I. J., "Synthesis and Characterization of Maleated Polyethylene / Clay Nanocomposites", Polymer, vol.42, 9819-9826, 2001.

5. Li X., "Effect of Blending Sequence on the Microstructure and Properties of PBT/EVA-g-MAH / Organoclay Ternary Nanocomposites". Polymer Engineering and Science, vol.42, No.11,2156-2164, 2002.

6. Gopakumar T.G., Lee J.A., Kontopoulou M., and Parent J.S., "Influence of Clay Exfoliation on the Physical Properties of Montmorillonite / Polyethylene Composites", Polymer, vol. 43, 5483-5491, 2002.

7. Kato M., Okamoto H., Hasegawa N., Tsukigase A. and Usuki A., "Preparation and Properties of Polyethylene-Clay Hybrids", Polymer Engineering and Science, vol.43 No.6, 1312-1316, 2003.

8. Liang G., Xu J., Bao S., and Xu W., "Polyethylene/Maleic Anhydride Grafted Polyethylene/Organic-Montmorillonite Nanocomposites. I. Preparation, Microstructure, and Mechanical Properties", Journal of Applied Polymer Science, vol.91, 3974-3980, 2004.

9. Zhang J., and Wilkie C.A., "Preparation and Flammability of Polyethylene-Clay Nanocomposites", Polymer Degradation and Stability, vol.80, 163-169, 2003.

10. Hotta S., and Paul D.R., "Nanocomposites Formed From Linear Low Density Polyethylene and Organoclays", Polymer, vol.45, 7639-7654, 2004.

11. Zhai H., Xu W., Guo H., Zhou Z., Shen S., and Song Q., "Preparation and Characterization of PE and PE-g-MAH/montmorillonite Nanocomposites", European Polymer Journal, vol. 40, No: 11, 2539-2545, 2004.

12. Morawiec J., Pawlak A., Slouf M., Galeski A., Piorkowska E., Krasnikowa N., "Preparation and Properties of Compatibilized LDPE/Organo-modified Montmorillonite Nanocomposites", European Polymer Journal, vol. 41, 1115-1122, 2005.

13. Zhong Y., and Kee D.D., "Morphology and Properties of Layered Silicate-Polyethylene Nanocomposite Blown Films", Polymer Engineering and Science, 469-477, 2005.

14. Vaia, R.A., Ishii H., and Giannelis E. P., "Synthesis and Properties of two dimensional Nanostructures by Direct Intercalation of Polymer Melts in Layered Silicates." Chemistry of Materials,. 1993, vol. 5: 1694-1696,

15. Dennis, H.R., Hunter D.L., Chang D., Kim S., White J.L., Cho J.W., and Paul D.R., "Effect of Melt Processing Conditions On the Extent of Exfoliation in Organoclay-Based Nanocomposites", Polymer, 2001. 42, 9513-9522

16. Ray, S.S., Okamoto K., and Okamoto M., "Structure-Property Relationship in Biodegradable Poly(butylene succinate)/Layered Silicate Nanocomposites", Macromolecules, 2003. 36: p. 2355-2367

17. Callister W.D., *Material Science and Engineering: An Introduction*, 6th Edition, John Wiley and Sons, Inc.,NY,1997

18. Mani G., Fan Q., Ugbolue S. C., and Yang Y., "Morphological Studies of Polypropylene-Nanoclay", Journal of Applied Polymer Science, Vol. 97, 218-226, 2005

19. Zanetti, M., Lomakin S., and Camino G., "Polymer-Layered Silicate Nanocomposites", Macromolecular Materials and Engineering, 2000. 279: p. 1-9.

20. Utracki L.A. "*Clay Containing Polymeric Nanocomposites*", 1st Edition, Vol.1 Rapra Technology Limited, UK, 2004.

21. Zhang Q., Yu Z., Xie X., and Mai Y., "Crystallization and Impact Energy of Polypropylene/CaCO$_3$ Nanocomposites with Nonionic Modifier", Polymer, vol. 45, 5985-5994, 2004.

22. Kroschwitz J.I., Mark H.F., "Encyclopedia of Polymer Science and Technology", 3rd Ed., Wiley Interscience, Hoboken, N.J., 2003.

23. Ray S.S., and Okamoto M., "Polymer/layered silicate nanocomposites: a review from preparation to processing" Progress in Polymer Science, 28, 1539-1641, 2003.

24. Moore, D.M., and Reynolds R.C., X-ray Diffraction and the Identification and Analysis of Clay Analysis of Clay Minerals, Oxford University Press, Oxford, 1997

25. Alexandre, M., and Dubois P., "Polymer-Layered Silicate Nanocomposites: Preparation, Properties, and Uses of a New Class of Materials",. Materials Science and Engineering, 2000. 28: p. 1-63.

26. Leite, I.F., Soares A. P. S., Carvalho, L. H. Raposo, C. M. O., Malta, O. M. L. and Silva, S. M. L., "Characterization of pristine and purified organobentonites", Journal of Thermal Analysis and Calorimetry, 2010, 100, 563-569.

27. Ray, S.S., and Okamoto M., "New Polylactide / Layered Silicate Nanocomposites;Melt Rheology and Foam Processing", Macromolecular Materials and Engineering, 2003. 288, 936-944.

28. Kornmann, X., "Synthesis and Characterisation of Thermoset-Clay Nanocomposites", Licenciate Thesis, Luleå University of Technology, Sweden 2000.

29. Pavlidou, S.; and Papaspyrides, C.D.; "A review on polymer-layered silicate nanocomposites", Progress in Polymer Science, 33, 12, 1119-1198

30. *"Ullmann's Encyclopedia of Industrial Chemistry"*, 5th edition, VCH Publishers, vol. A21, 617-625, New York, 1992.

31. Ebewele R.O., *"Polymer Science and Technology"*, CRC Press LLC, U.S.A.,2000.

32. Scheirs, J., and Priddy D., *"Modern Styrenic Polymers: Polystyrenes and Styrenic Copolymers"*, John Wiley & Sons. New York, 2003

33. Salamone J.C., "*Polymeric Materials Encyclopedia*", vol. 9, 6806-6813, CRC Press, New York, 1996.

34. Carraher C.E.Jr., *"Seymour/Carraher's Polymer Chemistry: an Introduction"* ,4th Edition, Marcel Dekker Inc., New York, 1996.

35. Rosen S.L., *"Fundamental Principles of Polymeric Materials"*, 2nd edition, John Wiley and Sons, Inc., New York, 1993.

36. *"Encyclopedia of Polymer Science and Technology"*, vol.13,156-200, John Wiley and Sons, Inc., New York, 1971.

37. C.B. Bucknall, "Toughened Plastics", Appl. Sci. Pub., London, 1977.

38. A.J. Kinloch, R. J. Young, "Fracture Behaviour of Polymers", Appl. Sci. Pub., London, 1983.

39. J. M. Margolis, "Advanced Thermoset Composites", Van Nostrand Reinhold Co., New York, N. Y., 1986.

40. M.J. Folkes, P. S. Hope, "Polymer Blends and Alloys", Blackie Academic & Professional, London, 1993.

41. C. K. Riew, A. J. Kinloch, "Toughened Plastics I: Science and Engineering" Advances in Chemistry Series, 233, ACS, Washington, D.C., 1993.

42. C. K. Riew, "Rubber Toughened Plastics", Advances in Chemistry Series, 222, ACS, Washington, DC, 1989.

43. E. Martuscelli, R. Palumbo, M. Kryszewski, "Polymer Blends", Vol. I, Plenum Press, New York, 1980.

44. A. Galeski, E. Martuscelli, M. Kryszewski, "Polymer Blends", Vol. II, Plenum Press, New York, 1984.

45. D.R. Paul, "Polymer Blends ", Vol. 2, D.R. Paul and S. Newman Eds., Academic Press, London, 1978..

46. E. Martuscelli, "Rubber Modification of Polymers: Phase Structure, Crystallization, Processing and Properties in Thermoplastic Elastomers from Rubber-Plastic Blends", S. K. De, A. K. Bhowmick Eds., Ellis Horwood, New York, 1990.

47. E. Martuscelli, "Structure and Properties of Polypropylene-Elastomer Blends in Polypropylene: Structure, Blends and Composites", J. Karger-Kocsis Ed. Chapman and Hall, London, 1995.

48. Z. Bartzak, E. Martuscelli, A. Galeski, "Primary Spherulite Nucleation in Polypropylene-based Blends and Copolymers in "Polypropylene: Structure, Blends and Composites", J. Karger-Kocsis Ed. Chapman and Hall, London, 1995

49. E. Martuscelli, "Relationships Between Morphology, Structure, Composition and Properties in Isotactic Polypropylene Based Blends" in "Polymer Blends and Mixtures", D. J. Walsh, J. S. Higgins, A. Macolmachie, NATO ASI Series, 1984.

50. A. C. Roulin-Moloney, "Fractography and Failure Mechanisms of Polymers and Composites", Elsevier Appl. Sci., London, 1988.

51. Kramer, E. J. Chapter 1 in Advances in Polymer Science, Springer-Verlag: Berlin 1983, vol. 52/53, pp.1-56.

52. Pearson, R. A.; Yee, A. F.; "Influence of particle size and particle size distribution on toughening mechanisms in rubber-modified epoxies" Journal of Materials Science., 1991, 26, 3828.

53. Cigna, G.; Lomellini, P.; Merlotti, "Impact thermoplastics: Combined role of rubbery phase volume and particle size on toughening efficiency." Journal of Applied Polymer Science, 1989, 37(6): 1527-1540

54. Azimi, H. R.; Pearson, R. A.; Hertzberg, R. W. J "Fatigue of rubber-modified epoxies: effect of particle size and volume fraction." Journal of Materials Science 1996, 31(14): 3777-3789

55. Yee, A. F.; Pearson, R. A. "Toughening mechanisms in elastomer-modified epoxies." Journal of Materials Science 1986, 21(7): 2462-2474.

56. Borggreve, R. J. M., Gaymans, R. J.; Schuijer; Ingen Houz, F. "Brittle-tough transition in nylon-rubber blends: effect of rubber concentration and particle size." Polymer 1987 28(9): 1489-1496

57. Hobbs, S. Y.; Bopp, R. C.; Watkins, V. H. "Toughened nylon resins." Polymer Engineering & Science 1983, 23(7): 380-389

58. Wu, S. "A generalized criterion for rubber toughening: The critical matrix ligament thickness." Journal of Applied Polymer Science, 1988, 35(2): 549-561.

59. Bucknall, C.B.; Cote, F.F.; Partridge, I. K. "Rubber toughening of plastics." Journal of Materials Science, 1986, 21(1): 301-306.

60. Muratoglu, O. K.; Argon, A.S.; Cohen, R. E.; Weinburg, M. "Toughening mechanism of rubber-modified polyamides." Polymer, 1995, 36(5): 921-930.

61. Borggreve, R. J. M.; Gaymans, R. J.; Schuijer, "Impact behaviour of nylon-rubber blends: 5. Influence of the mechanical properties of the elastomer." Polymer, 1989, 30(1): 71-77.

62. Dompas, D.; Groeninckx, G. "Toughening behaviour of rubber-modified thermoplastic polymers involving very small rubber particles: 1. A criterion for internal rubber cavitation." Polymer, 1994, 35(22): 4743-4749.

63. Laurienzo, P.; Malinconico, M; Martucelli, E.: Volpe, M. G. "Rubber modification of polybutyleneterephthalate by reactive blending concurrently with polymerization reaction." Polymer, 1991, 30(5): 835-841.

64. Borggreve, R. J. M.; Gaymans, R. J.; Eichenwald, H. M. "Impact behaviour of nylon-rubber blends: 6. Influence of structure on voiding processes; toughening mechanism." Polymer, 1989, 30(1): 78-83.

65. Bagheri, R.; Pearson, R. A. "Role of particle cavitation in rubber-toughened epoxies: 1. Microvoid toughening." Polymer, 1996, 37(20): 4529-4538

66. Lazzeri, A.; Bucknall, C. B.; "Applications of a dilatational yielding model to rubber-toughened polymers." Polymer, 1995, 36(15): 2895-2902.

67. Bagheri;, R.; Pearson, R. A. "Interfacial studies in CTBN-modified epoxies." Journal of Applied Polymer Science, 1995, 58(2): 427-437.

68. Huang, Y.; Kinloch, A. J.; Bertsch, R.; Sibert, A. R. Advances in Chemistry Series, Edited by C. KJ. Riew and A. J. Kinloch, ACS: Washington, D. C. 1993, 233, 189.

69. Chen, T. K.; Jan, Y. H. "Effect of rubber/matrix interfacial modifications on the properties of a rubber-toughened epoxy resin." Polymer Engineering & Science, 1991, 31(8): 577-585.

70. Lovell, P. A., McDonald, J.; Saunders, D. E. J.; Young, R. J. "Studies of rubber-toughened poly(methyl methacrylate): 1. Preparation and thermal properties of blends of poly(methyl methacrylate) with multiple-layer toughening particles." Polymer, 1993, 34(1): 61-69.

71. Bucknall, C. B.; Partridge, I. K. in Toughening of Plastics II, PRI:London 1991, 28/1.

72. Bagheri, R.; Pearson, R. A. "Role of blend morphology in rubber-toughened polymers." Journal of Materials Science, 1996, 31(15): 3945-3954.

73. Qian, J. Y.; Pearson, R. A.; Dimonie, V. L.; Shaffer, O. L.; El-Aasser, M. S. "The role of dispersed phase morphology on toughening of epoxies." Polymer, 1997, 38(1): 21-30.

74. Kramer, E.J., and Krauch H.H., "*Crazing in Polymers*", Springer, Berlin, 1983

75. Bucknall, C.B., "*Toughned Plastics*" Applied Science Publishers, London: 1977.

76. The University of Southern Mississippi, Polystyrene,
http://www.pslc.ws/mactest/styrene.htm.
Last visited on: 15th March 2011.

77. Moore, E.R., "*Encyclopedia of Polymer Science and Engineering*". 1989, New York: John Wiley & Sons.

78. Akkapeddi, M.K., "*Reactive Polymer Blending*" Hanser Gardner Publications, USA: 2001

79. Barry, C. M. F.; Orroth, S. A.; "*Modern Plastics Handbook*", McGraw-Hill, USA, 2000.

80. Shah A., and Gupta M., "Comparison of the Flow in Co-rotating and Counter rotating Twin- Screw Extruders", Antec, 443-447, 2004.

141

81. Anderson P., "*Twin-Screw Extruders*", 83-87, Society of Plastics Engineers.

82. Middleman S., "*Fundamentals of Polymer Processing*", McGraw-Hill, USA, 1977.

83. Crawford R. J., "*Plastics Engineering*", 3rd edition, BH., Oxford, 1998.

84. Tripathi D., "*Practical Guide to Polypropylene*", 1st edition, Rapra Technology Ltd., UK., 2002.

85. Rodriguez, F., Cohen C., Ober C., and Archer A.L., "*Principles of Polymer Systems*": Taylor & Francis. New York, 2003.

86. Kroschwitz J. I., "*Concise Encyclopedia of Polymer Science and Enginering*", Wiley-Interscience Publication, New York, 1990.

87. Jens, A.N., and McMorrow D., "*Elements of Modern X-ray Physics*" John Wiley & Sons, New York 2001.

88. http://en.wikipedia.org/wiki/Transmission_electron_microscope,
Last visited on 15th March 2011.

89. ASTM D638-91a, Standard Test Method for Tensile Properties of Plastics, "*Annual Book of ASTM Standards*", vol.08.01, 174-182, Philadelphia, USA ,1993.

90 Rubin I.I., "*Handbook of Plastic Materials and Technology*", John Wiley & Sons, Inc.,New York, 1990.

91. http://www.matweb.com/reference/tensilestrength.asp
Last visited on 15th March 2011

92 Bower, D.I., "*An Introduction to Polymer Physics*", Cambridge University Press, USA, 2002.

93. Sperling, L.H., "*Introduction to Physical Polymer Science*". 4th ed.,: John Wiley & Sons, New York, 2006.

94 Seymour, R.B., and Carraher, C.E., "*Structure-Property Relationships in Polymers*", Plenum Press, New York, 1984.

95. ASTM D 1238 M-92: Standard Test Methods for Melt Flow Index of Plastics, "*Annual Book of ASTM Standard*s" Vol.08.01, Philadelphia, 1993.

96. Işık, I., "Impact Modified Polyamide-Organoclay Nanocomposites", 2007, PhD Thesis, Middle East Technical University: Ankara, Turkey

97. Rodriguez F., Cohen C., Ober C., and Archer A.L., "*Principles of Polymer Systems*", Taylor & Francis, New York, 2003.

98. Watson, E.S., O'Neill, M.J., Justin, J., and Brenner, N., A "Differential Scanning Calorimeter for Quantitative Differential Thermal Analysis", Analytical Chemistry, 1964, 36, 1233.

99. Lobo, H., Bonilla, J.V., "*Handbook of Plastics Analysis*", Marcel Dekker Inc., New York, 2003.

100. "*Encyclopedia of Polymer Science and Technology: Plastics, Resins, Rubbers, and Fibers*", John Wiley and Sons Inc., New York, 1970.

101. Özkoç, G., "ABS/Polyamide-6 Blends, Their Short Glass Fiber Composites and Organoclay Based Nanocomposites: Processing and Characterization", 2007, PhD Thesis, Middle East Technical University: Ankara, Turkey

102 Park, C.I., Choi W.M., Kim M.H., and Park O.O., "Thermal and Mechanical Properties of Syndiotactic Polystyrene/Organoclay Nanocomposites with Different Microstructures", Journal of Polymer Science: Part B: Polymer Physics, 2004, 42, 1685-1693.

103 Zhang W.A., Chen D.Z., Xu H.Y., Shen X.F., and Fang Y.E., "Influence of Four Different Types of Organophilic Clay on the Morphology and Thermal Properties of Polystyrene/Clay Nanocomposites Prepared by the γ-ray Radiation Technique", European Polymer Journal, 2003, 39, 2323-2328

104 Xie W., Hwu J.M., Jiasng G.J., Buthelezi T.M. and Pan W., "A Study of the Effect of Surfactants on the Properties of Polystyrene-Montmorilllonite Nanocomposites", Polymer Engineering and Science, 2003, 43, 214-222

105 Tanoue, S., Hasook A., Itoh A., Yanou M., Iemoto Y., and Unryu T., "Effect of Screw Rotation Speed on the Properties of Polystyrene/Organoclay Nanocomposites Prepared by a Twin-Screw Extruder", Journal of Applied Polymer Science, 2006, 101, 1165–1173.

106. Tomova D., and Radusch H.J., "Morphology and Properties of Ternary Polyamide 6 / Polyamide 66 / Elastomer Blends", Polymers for Advanced Technologies, 2003, 14, 19-26.

107. Gelfer, M.Y., Song H.H., Liu L., Hsiao B.S., Chu B., Rafailovich M., Si M., and Zaitsev V., "Effects of Organoclays on Morphology and Thermal and Rheological Properties of Polystyrene and Poly(methyl methacrylate) Blends", Journal of Polymer Science Part B Polymer Physics, 2003, 41, 44-54.

108. Doh J.G. and Cho I., "Synthesis and properties of polystyrene-organoammonium montmorillonite hybrid", Polymer Bulletin, 1988. 41: p.511-518,

109. Gilman J.W., Jackson C.L., Morgan A.B., Harris R.H., Manias E., Giannelis E.P., Wuthenow M., Hilton D. And Phillips S.H., "Flammability properties of polymer-layered silicate nanocomposites, polypropylene and polystyrene nanocomposites", Chemistry of Materials, 2000, 12, 1866-1873

110. Lepoittevin B., Pantoustier N., Devalckenaere M., Alexandre M., Calberg C., Jerome R., Henrist C., Rulmont A. And Dubois P., "Polymer/layered silicate nanocomposites by combined intercalative polymerization and melt intercalation: a masterbatch process", Polymer, 2003. 44: p.2033-2040.

111. Fu X., and Qutubuddin S., "Synthesis of polystyrene-clay nanocomposites", Materials Letters, vol.42, 12-15, 2000.

112. Zhang J., and Wilkie C.A., "A carbocation substituted clay and its styrene nanocomposite", Polymer Degradation and Stability, vol.83, 301-307, 2004.

113. Total Petrochemicals, Lacqrene® 1960N, *http://www.totalpetrochemicals.com/en/index.asp.* Last visited on: 15th March 2011.

114. Elastron Kimya A.Ş. Elastron D http://www.elastron.com Last visited on : 15th March 2011

115. Sigma Aldrich Specification Sheet http://www.sigma-aldrich.com Last visited on 15th March 2011.

116. Brindley, G.W., and Brown G., "*Crystal Structures of Clay Minerals and their X-Ray Identification"* Mineralogical Society, London, 1980

117. Vaia, R.A., Klaus D., Kramer E.J., and Giannelis E.P., "Microstructural Evolution of Melt Intercalated Polymer-Organically Modified Layered Silicates Nanocomposites" Chemistry of Materials 1996, 8, 2628-2635

118. Jose, S., Thomas S., Lievana E., and Karger-Kocsis J., "Morphology and Mechanical Properties of Polyamide 12 Blends with Styrene/Ethylene–Butylene/Styrene Rubbers with and without Maleation"*,* Journal of Applied Polymer Science, 2005, 95,1376-1387

119. Wu, S., "Phase Structure and Adhesion in Polymer Blends: A Criterion for Rubber Toughening*",* Polymer, 1985, 26, 1855-1863

120. Verhoogt, H., Willems C.R.J., Dam Van J., and De Boer A.P., "Blends of a Thermotropic LCP and a Thermoplastic Elastomer: II formation and stability of LCP fiber", Polymer Engineering and Science, 1994, 34, 453-460

121. Mert, M., and Yilmazer, U., "Processing and properties of modified polyamide 66-organoclay nanocomposites". Journal of Applied Polymer Science, 2008, 108, 3890-3900.

122. Özden, G., Synthesis and Characterization of Polystyrene Clay Nanocomposites, Chemical Engineering. 2004, MS Thesis, Middle East Technical University: Ankara, Turkey.

123. Paul, D.R., and Barlow J.W., Polymer Blends (or Alloys). Journal of Macromolecular Science Reviews in Macromolecular Chemistry, 1980. 18: 109-168.

124. Lee, K.M., and Han C.D., "Rheology of Organoclay Nanocomposites: Effects of Polymer Matrix/Organoclay Compatibility and the Gallery Distance of Organoclay",. Macromolecules, 2003, 36, 7165-7178

X-RAY DIFFRACTION PATTERNS
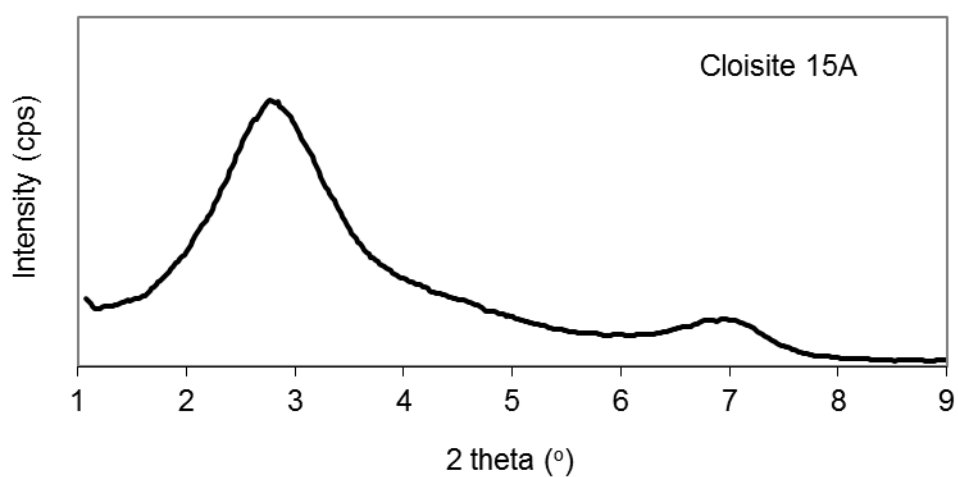
Figure A.1 XRD pattern of Cloisite ® 15A
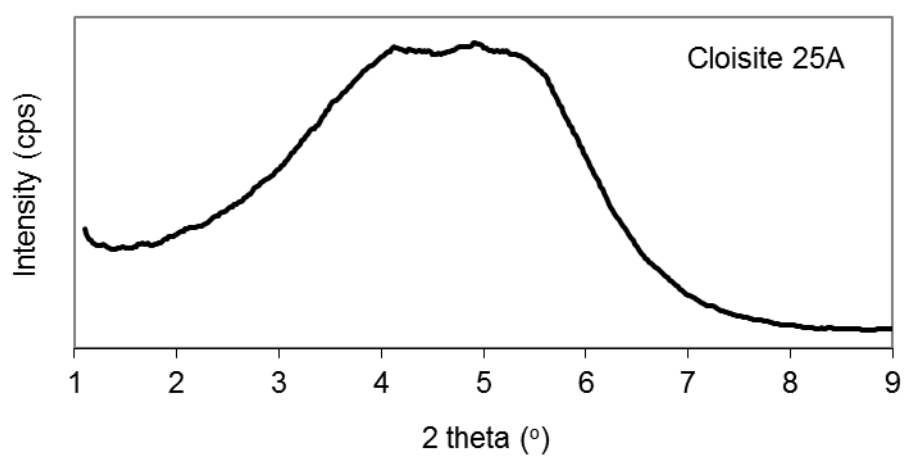
Figure A.2 XRD pattern of Cloisite ® 25A
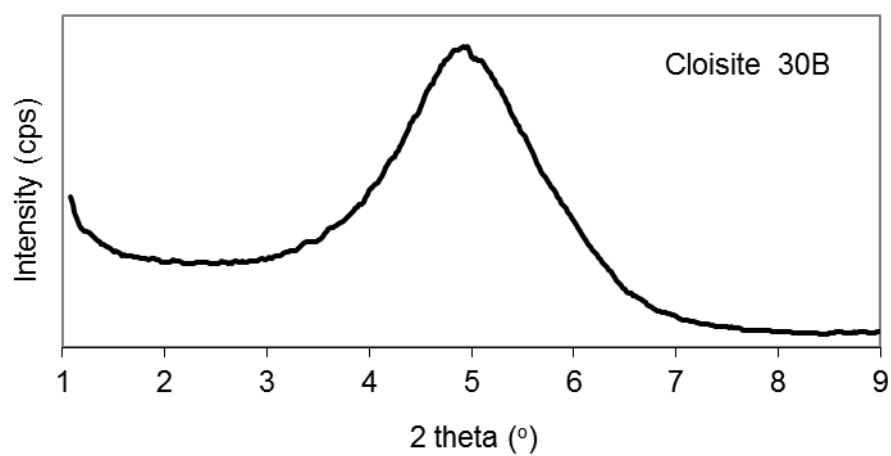
Figure A.3 XRD pattern of Cloisite ® 30B
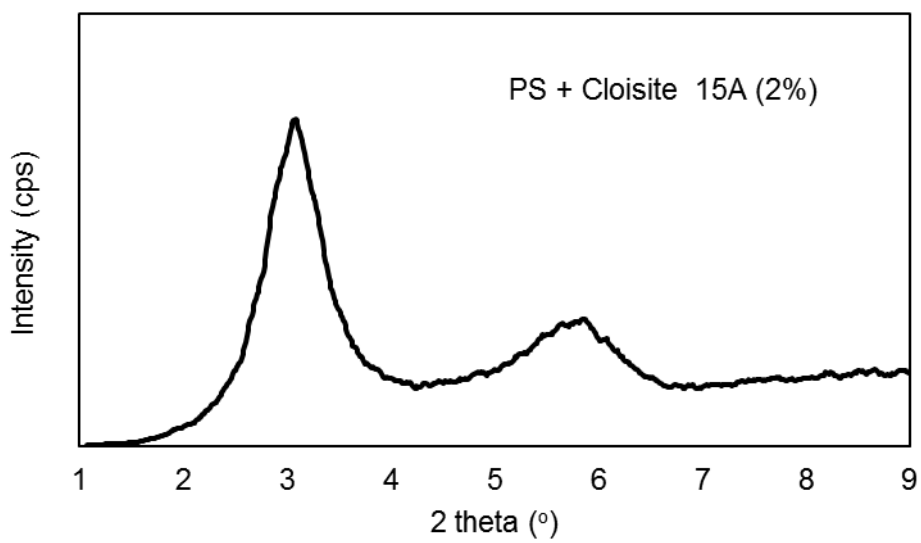
Figure A.4 XRD pattern of PS / Cloisite ® 15A (2%) binary nanocomposites
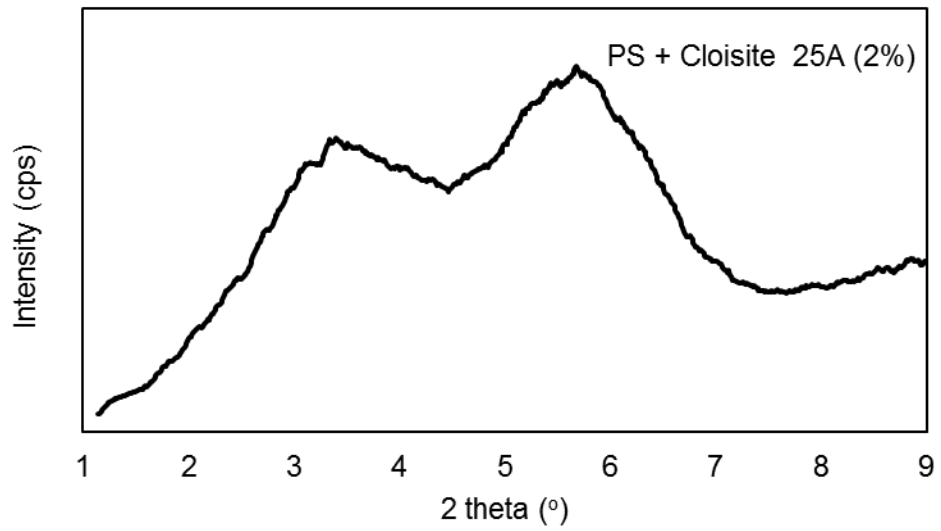
Figure A.5 XRD pattern of PS / Cloisite ® 25A (2%) binary nanocomposites
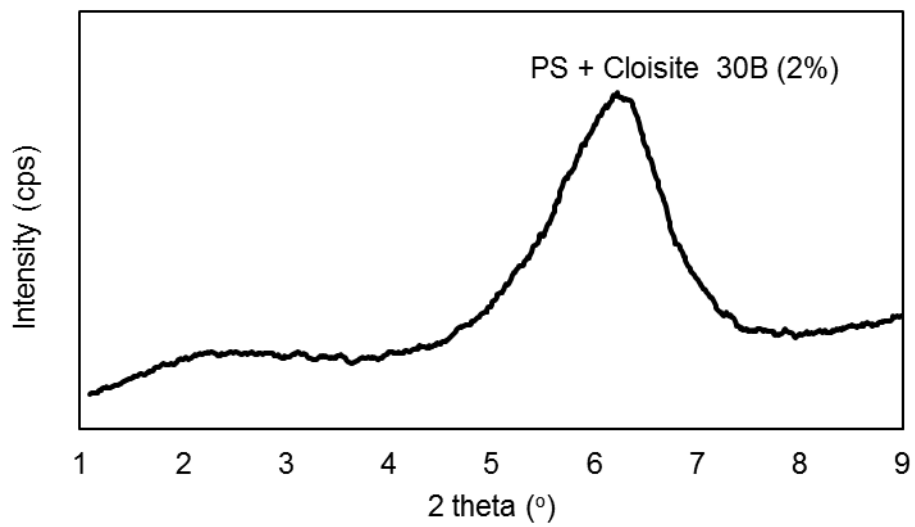
Figure A.6 XRD pattern of PS / Cloisite ® 30B (2%) binary nanocomposites
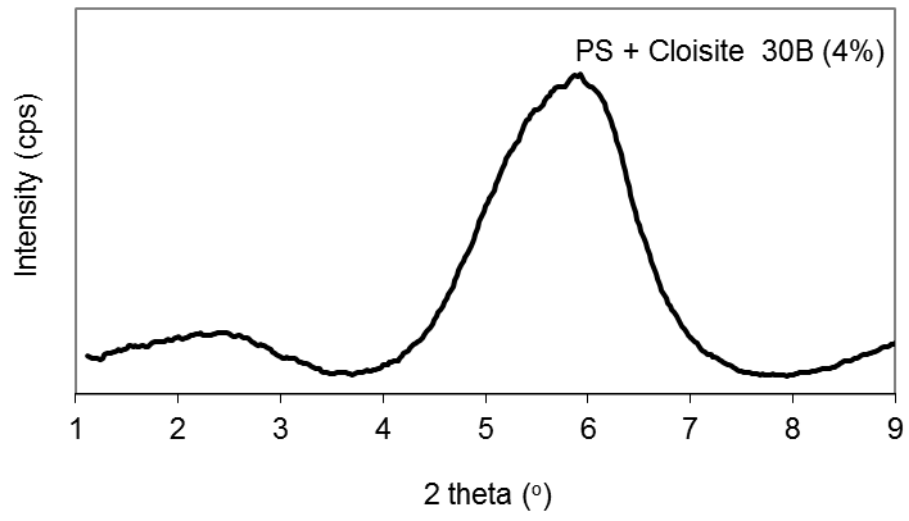
Figure A.7 XRD pattern of PS / Cloisite ® 30B (4%) binary nanocomposites
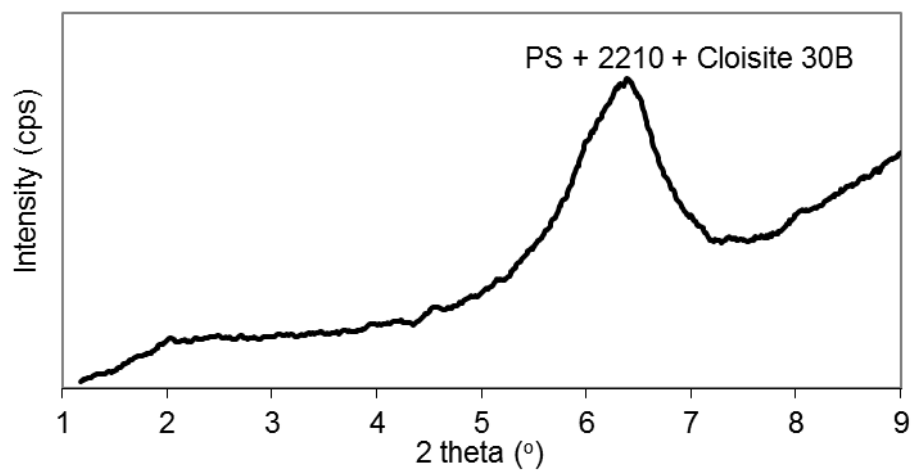
Figure A.8 XRD pattern of PS / Lotader 2210 (5%) / Cloisite ® 30B (2%) ternary nanocomposites
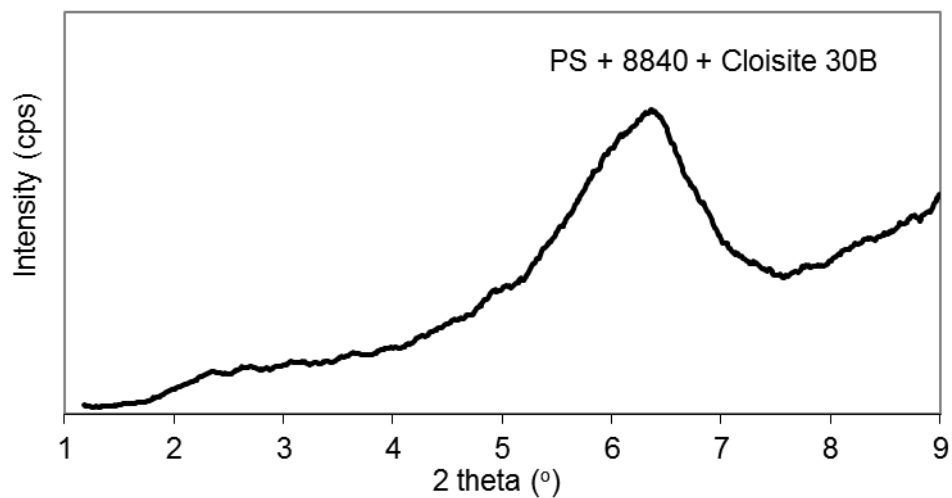
Figure A.9 XRD pattern of PS / Lotader 8840 (5%) / Cloisite ® 30B (2%) ternary nanocomposites
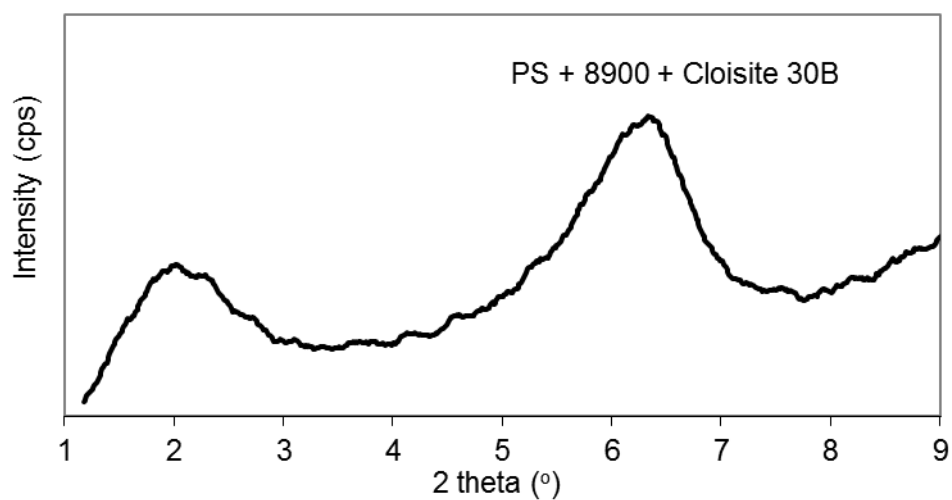
Figure A.10 XRD pattern of PS / Lotader 8900 (5%) / Cloisite ® 30B (2%) ternary nanocomposites
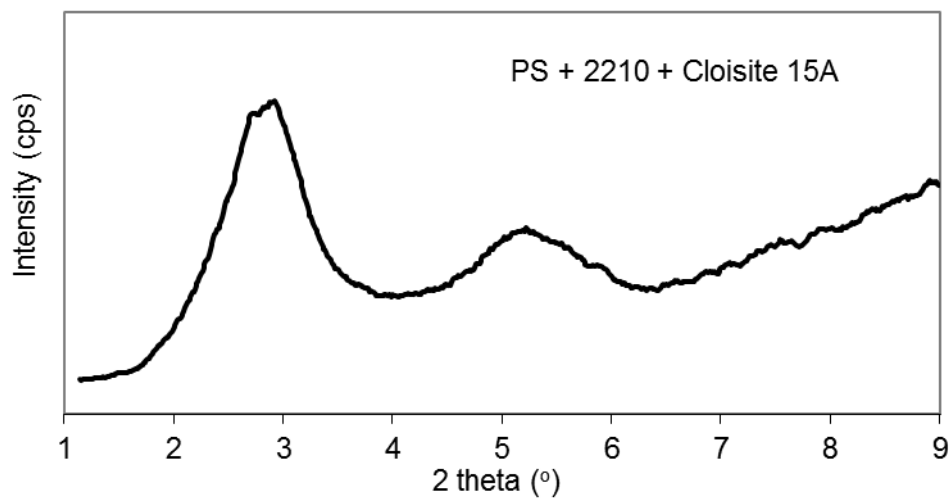
Figure A.11 XRD pattern of PS / Lotader 2210 (5%) / Cloisite ® 15A (2%) ternary nanocomposites
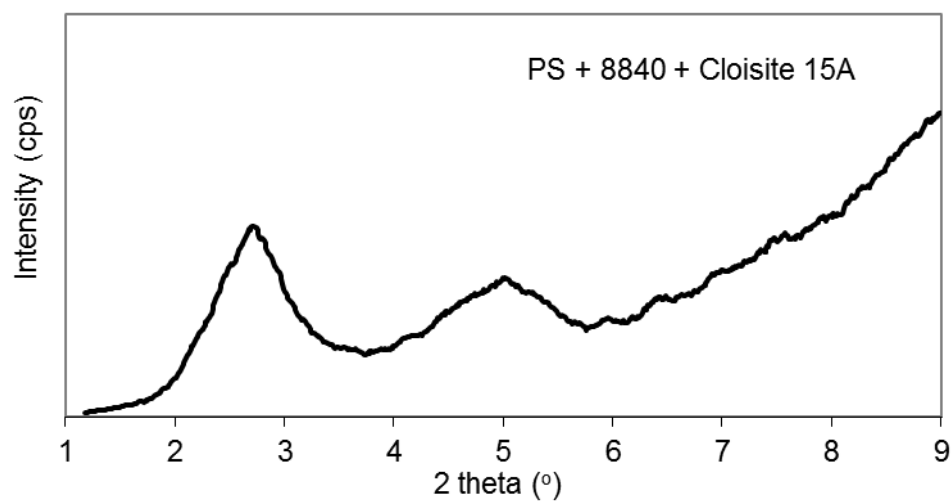

Figure A.12 XRD pattern of PS / Lotader 8840 (5%) / Cloisite ® 15A (2%) ternary nanocomposites
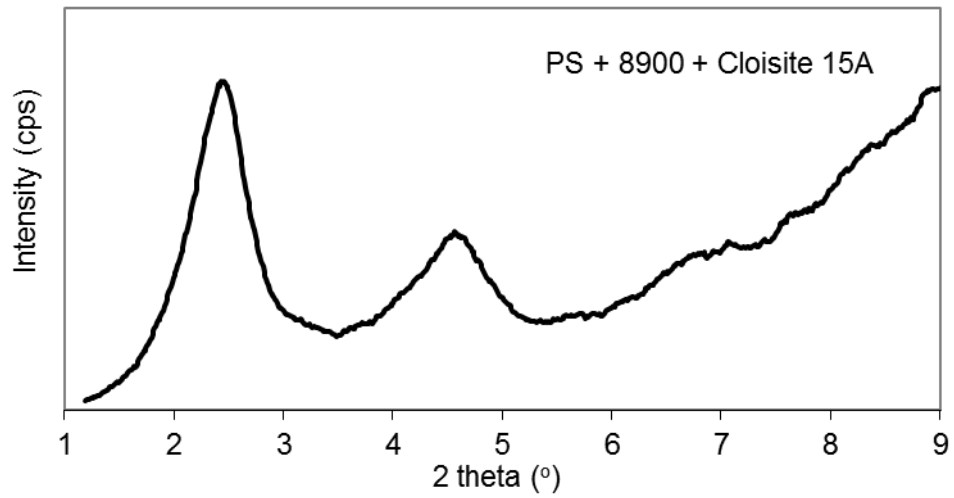
Figure A.13 XRD pattern of PS / Lotader 8900 (5%) / Cloisite ® 15A (2%) ternary nanocomposites
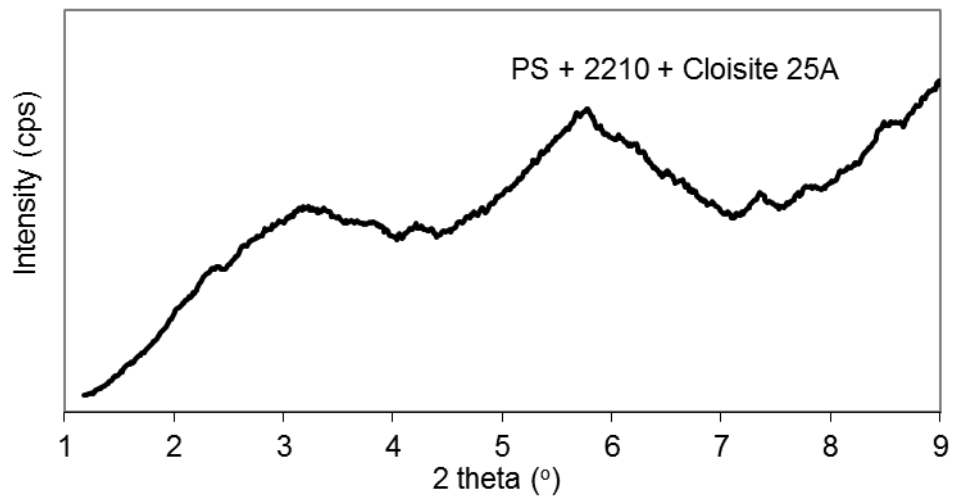
Figure A.14 XRD pattern of PS / Lotader 2210 (5%) / Cloisite ® 25A (2%) ternary nanocomposites
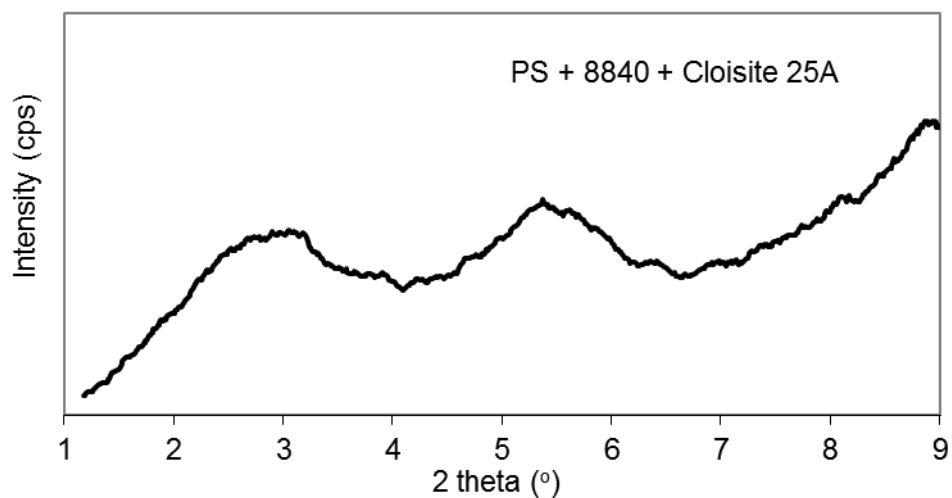
Figure A.15 XRD pattern of PS / Lotader 8840 (5%) / Cloisite ® 25A (2%) ternary nanocomposites
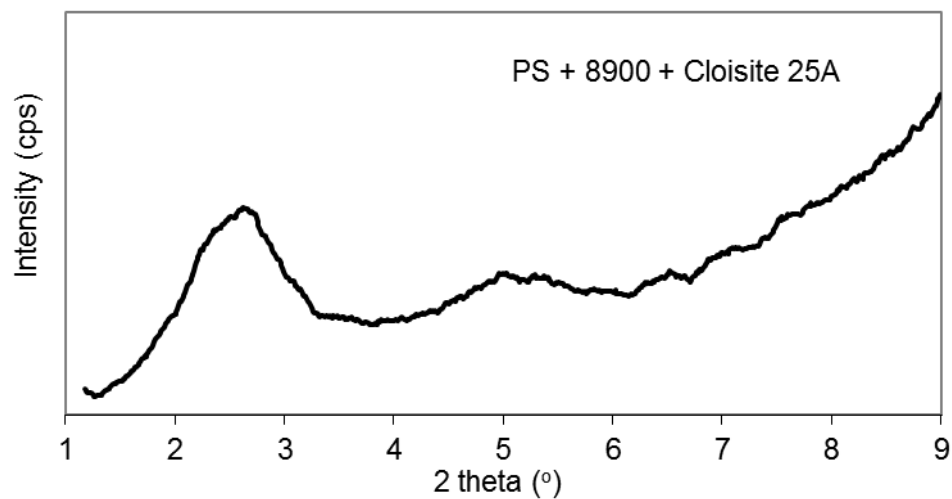
Figure A.16 XRD pattern of PS / Lotader 8900 (5%) / Cloisite ® 25A (2%) ternary nanocomposites
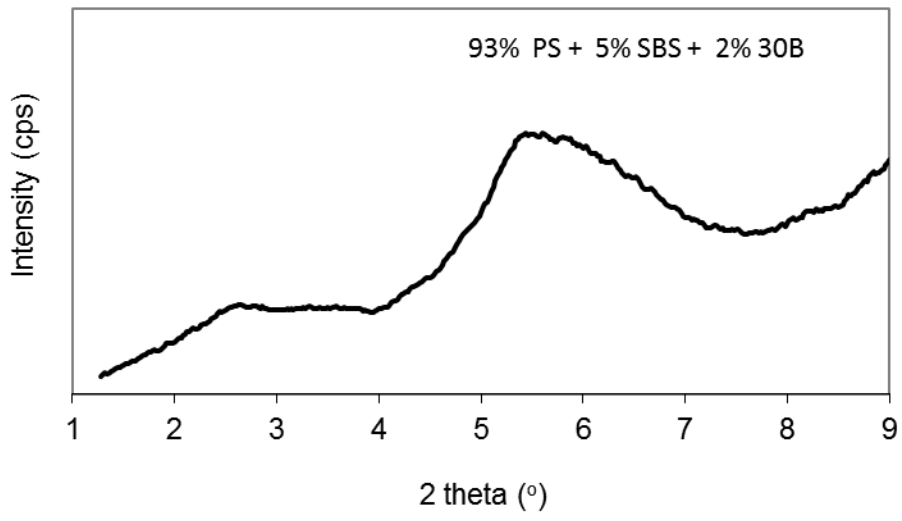
Figure A.17 XRD pattern of PS / SBS (5%) / Cloisite ® 30B (2%) ternary nanocomposites
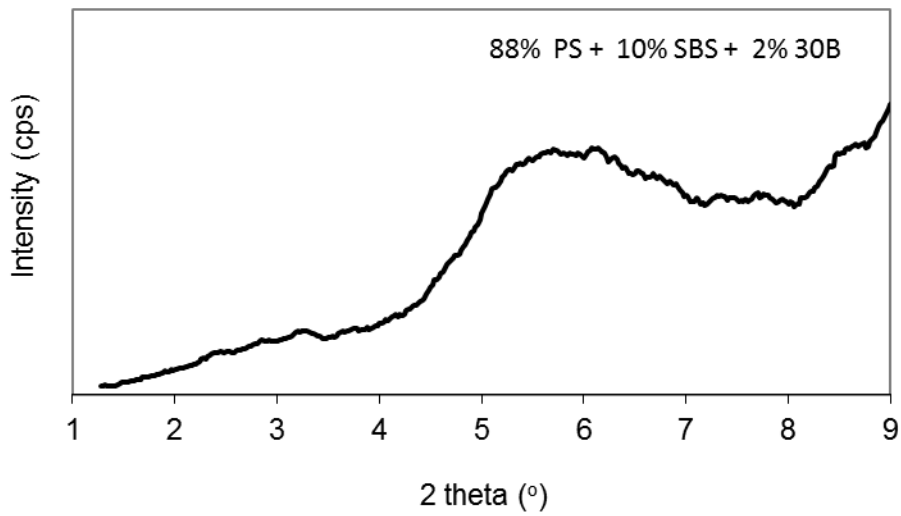
Figure A.18 XRD pattern of PS / SBS (10%) / Cloisite ® 30B (2%) ternary nanocomposites
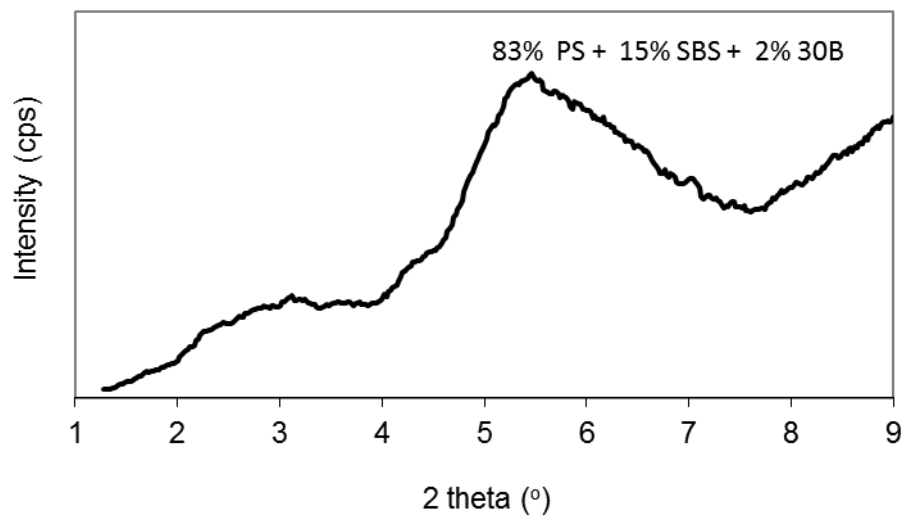
**Figure A.19** XRD pattern of PS / SBS (15%) / Cloisite ® 30B (2%) ternary nanocomposites
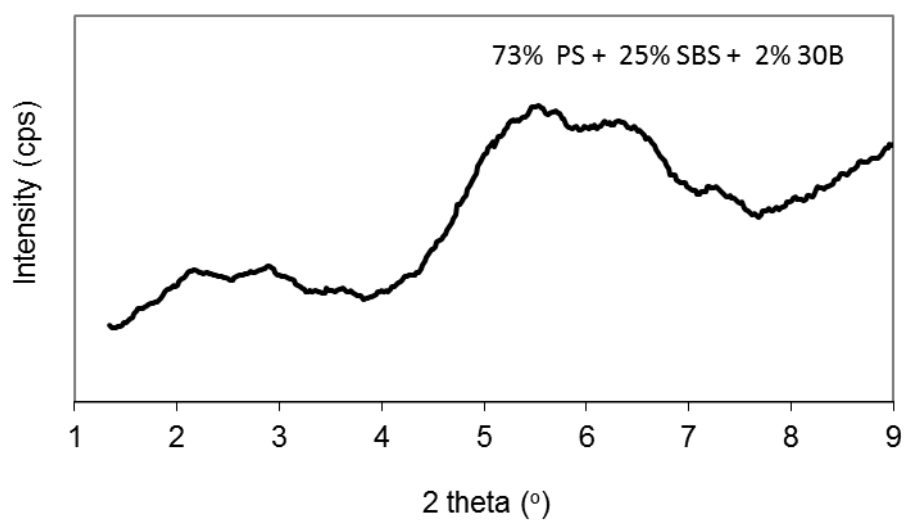
Figure A.20 XRD pattern of PS / SBS (25%) / Cloisite ® 30B (2%) ternary nanocomposites
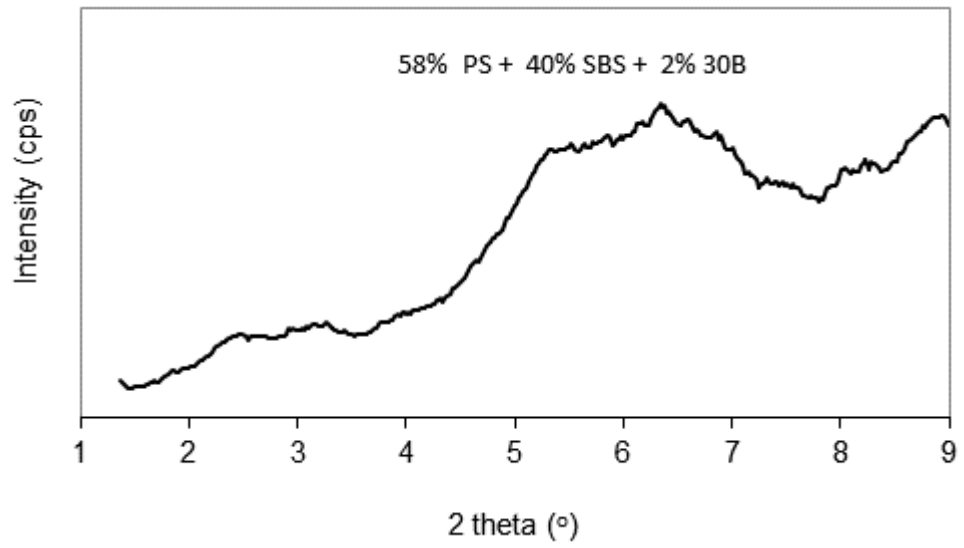
Figure A.21 XRD pattern of PS / SBS (40%) / Cloisite ® 30B (2%) ternary nanocomposites
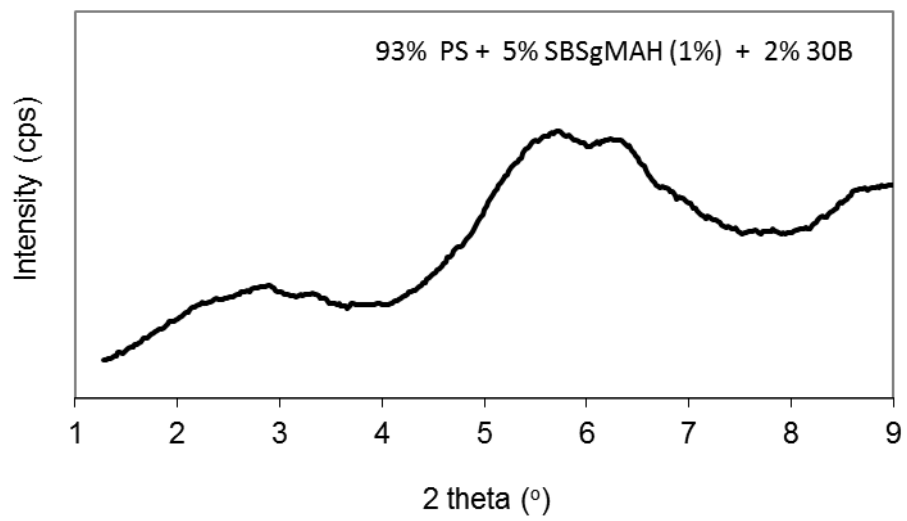
Figure A.22 XRD pattern of PS / 5% SBSgMAH (1%) / Cloisite ® 30B (2%) ternary nanocomposites
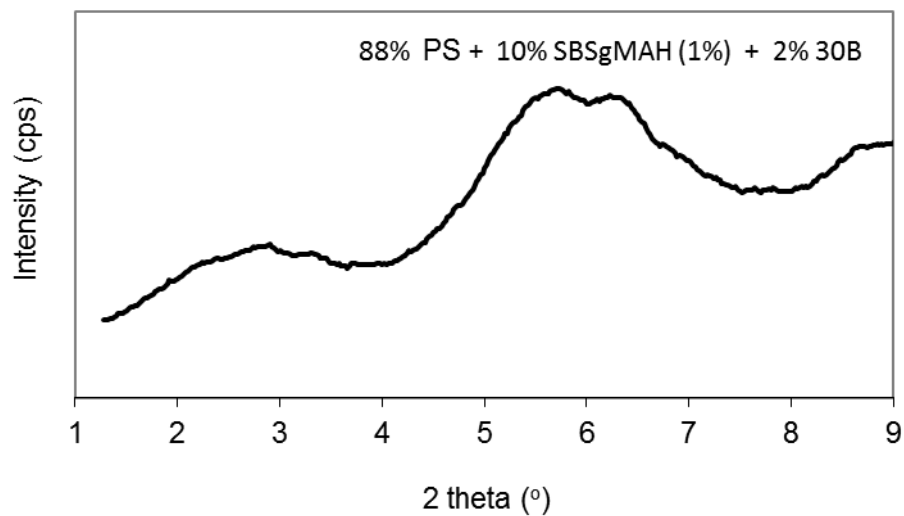
Figure A.23 XRD pattern of PS / 10% SBSgMAH (1%) / Cloisite ® 30B (2%) ternary nanocomposites
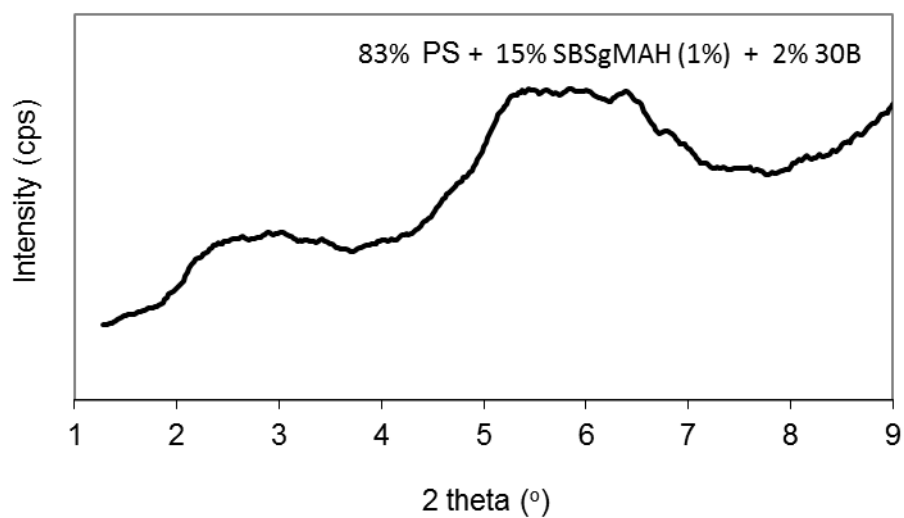

Figure A.24 XRD pattern of PS / 15% SBSgMAH (1%) / Cloisite ® 30B (2%) ternary nanocomposites
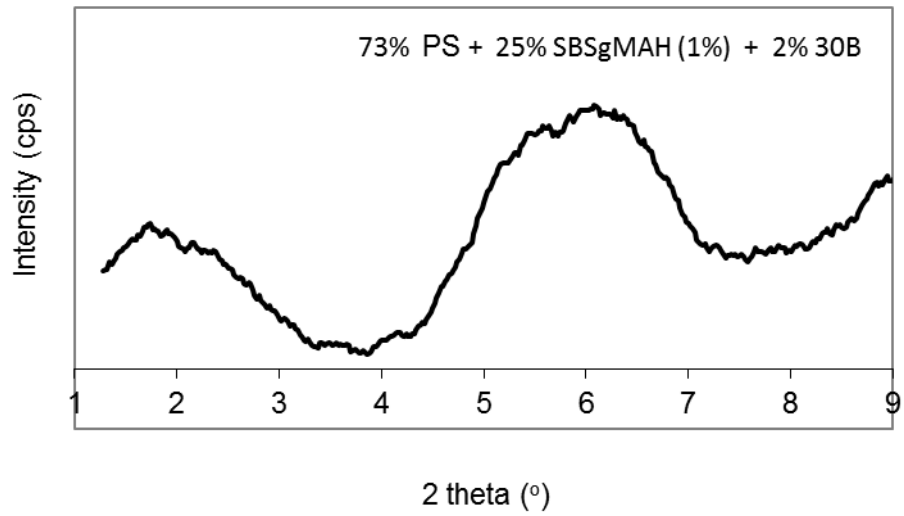
Figure A.25 XRD pattern of PS / 25% SBSgMAH (1%) / Cloisite ® 30B (2%) ternary nanocomposites
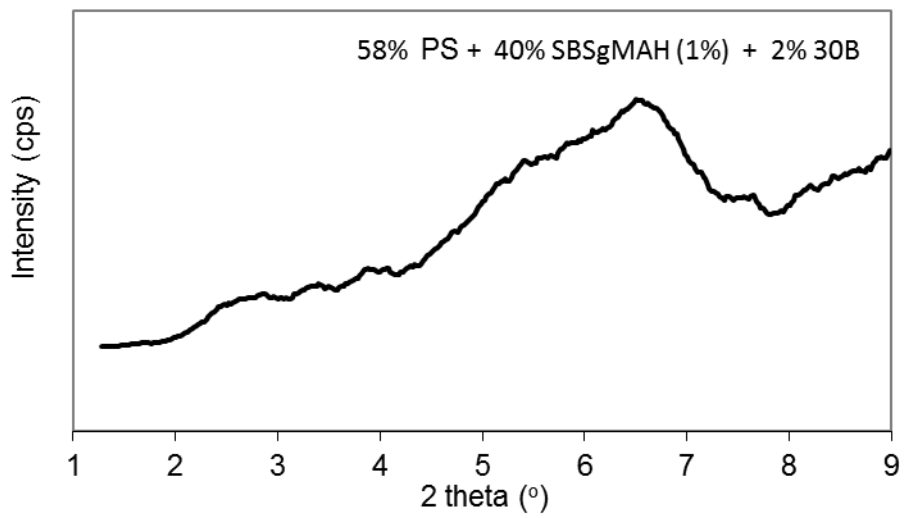
Figure A.26 XRD pattern of PS / 40% SBSgMAH (1%) / Cloisite ® 30B (2%) ternary nanocomposites
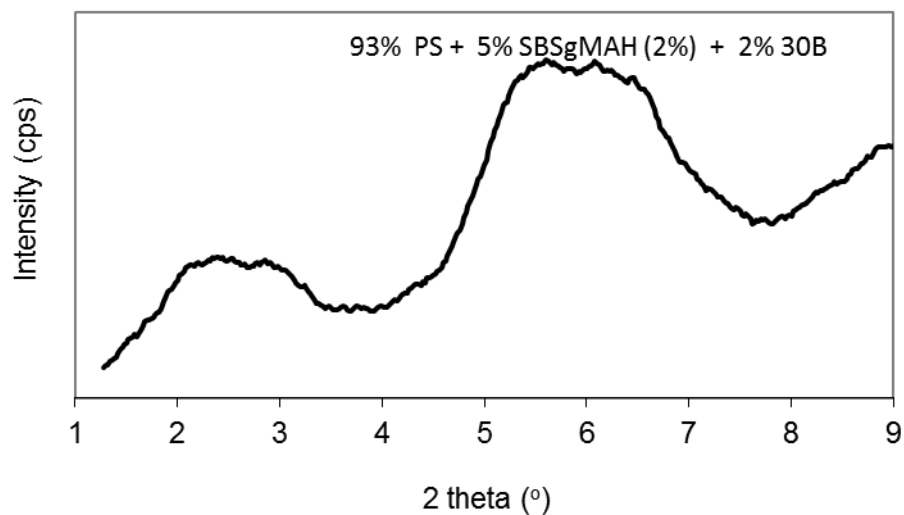
Figure A.27 XRD pattern of PS / 5% SBSgMAH (2%) / Cloisite ® 30B (2%) ternary nanocomposites
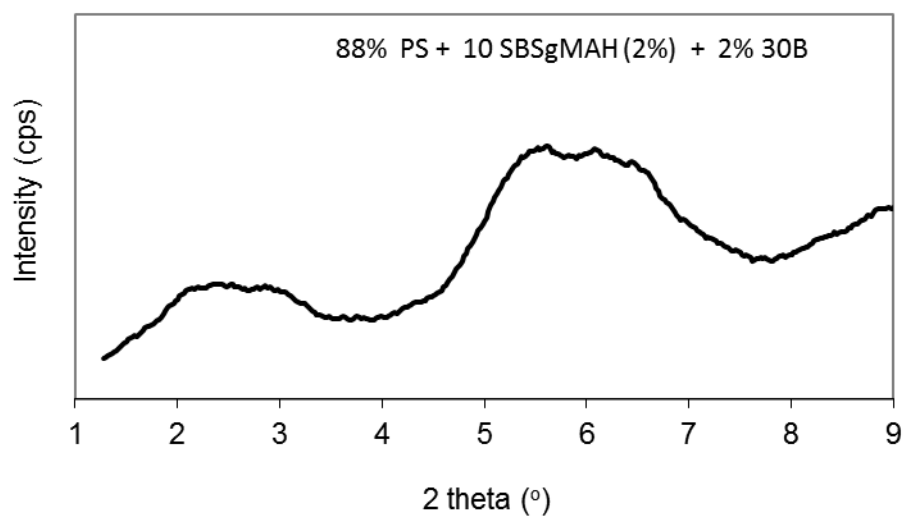
Figure A.28 XRD pattern of PS / 10% SBSgMAH (2%) / Cloisite ® 30B (2%) ternary nanocomposites
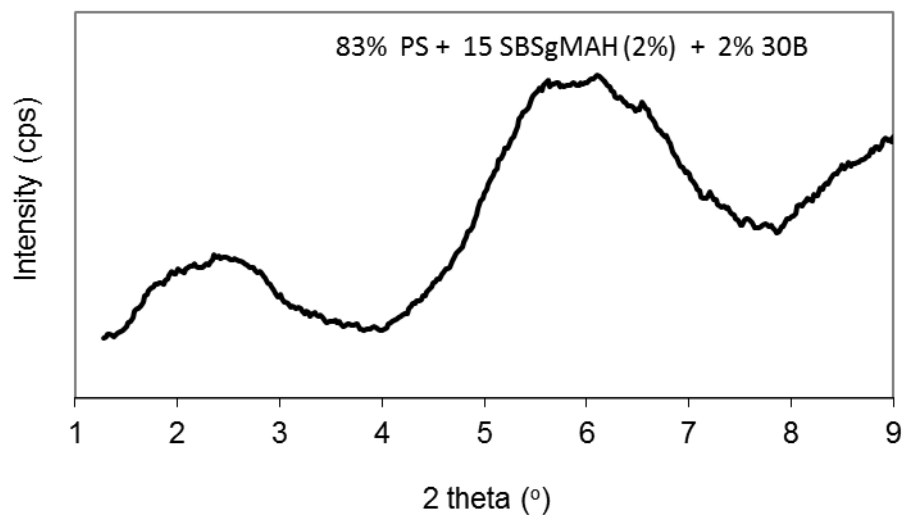
Figure A.29 XRD pattern of PS / 15% SBSgMAH (2%) / Cloisite ® 30B (2%) ternary nanocomposites
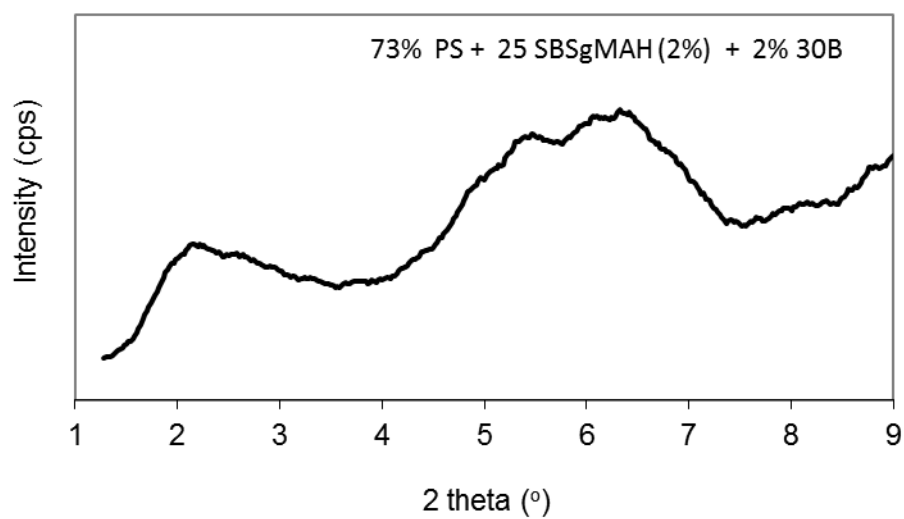

**Figure A.30** XRD pattern of PS / 25% SBSgMAH (2%) / Cloisite ® 30B (2%) ternary nanocomposites
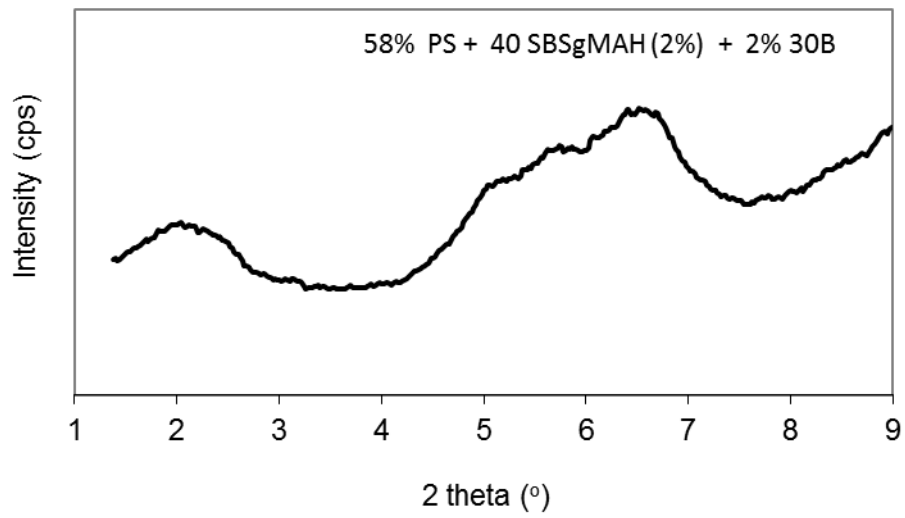
Figure A.31 XRD pattern of PS / 40% SBSgMAH (2%) / Cloisite ® 30B (2%) ternary nanocomposites
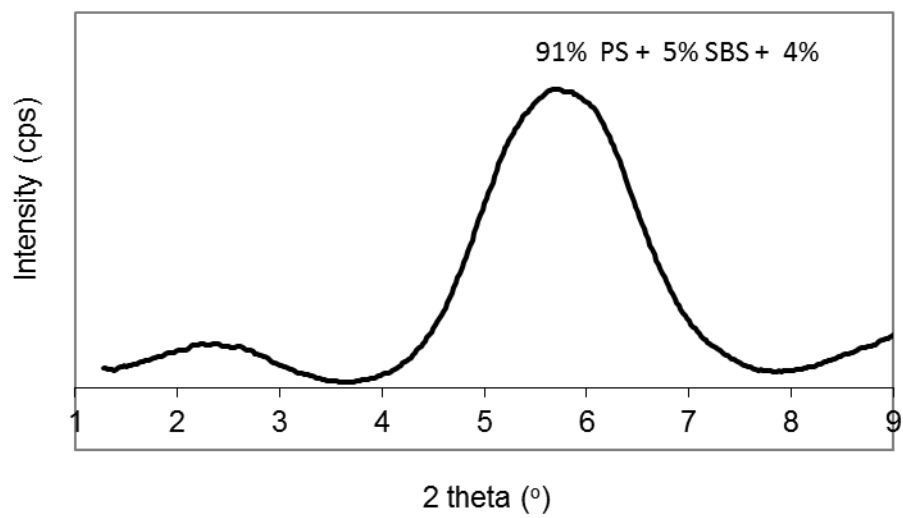

Figure A.32 XRD pattern of PS / 5% SBS / Cloisite ® 30B (4%) ternary nanocomposites
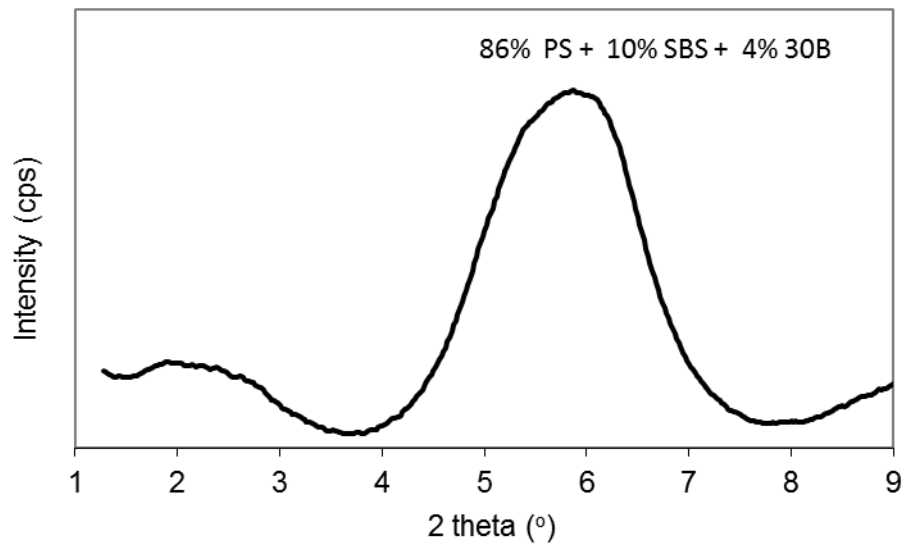
Figure A.33 XRD pattern of PS / 10% SBS / Cloisite ® 30B (4%) ternary nanocomposites
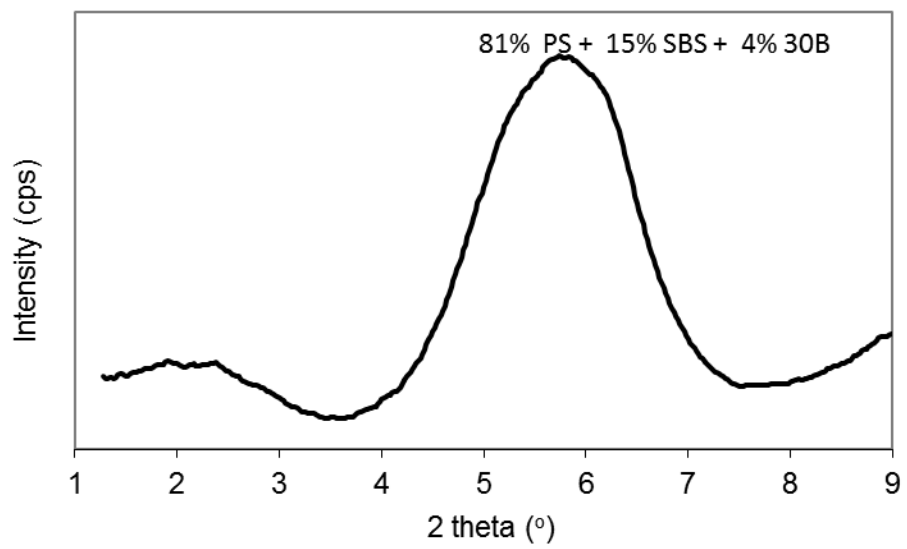

Figure A.34 XRD pattern of PS / 15% SBS / Cloisite ® 30B (4%) ternary nanocomposites
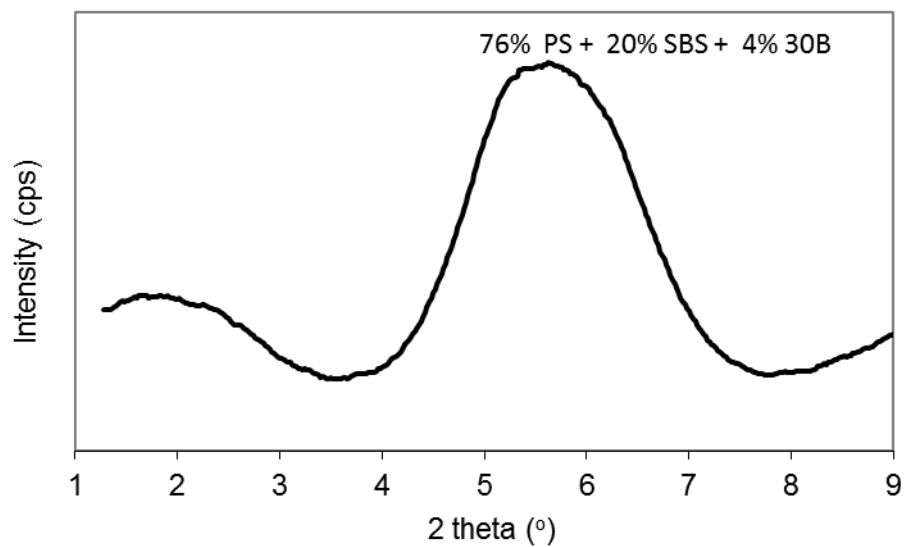
Figure A.35 XRD pattern of PS / 20% SBS / Cloisite ® 30B (4%) ternary nanocomposites
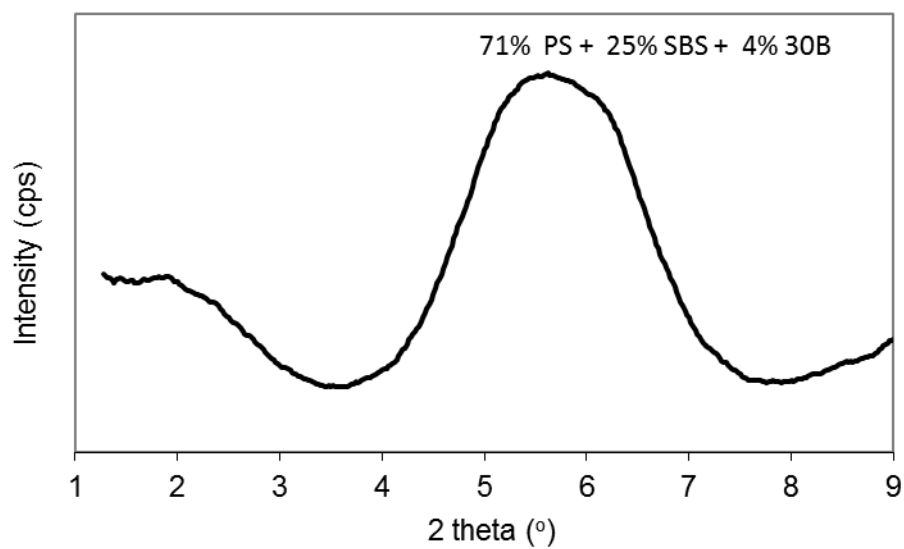
Figure A.36 XRD pattern of PS / 25% SBS / Cloisite ® 30B (4%) ternary nanocomposites
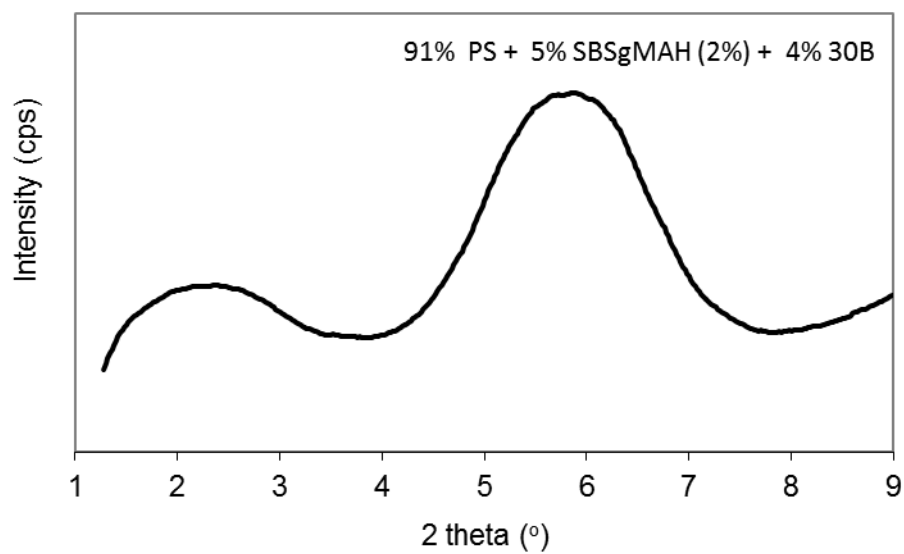
Figure A.37 XRD pattern of PS / 5% SBSgMAH (2%) / Cloisite ® 30B (4%) ternary nanocomposites
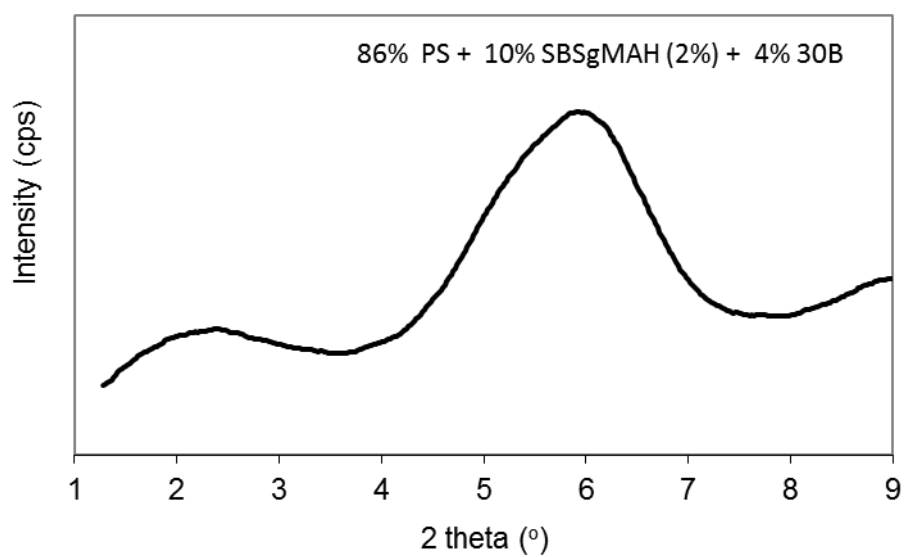
Figure A.38 XRD pattern of PS / 10% SBSgMAH (2%) / Cloisite ® 30B (4%) ternary nanocomposites
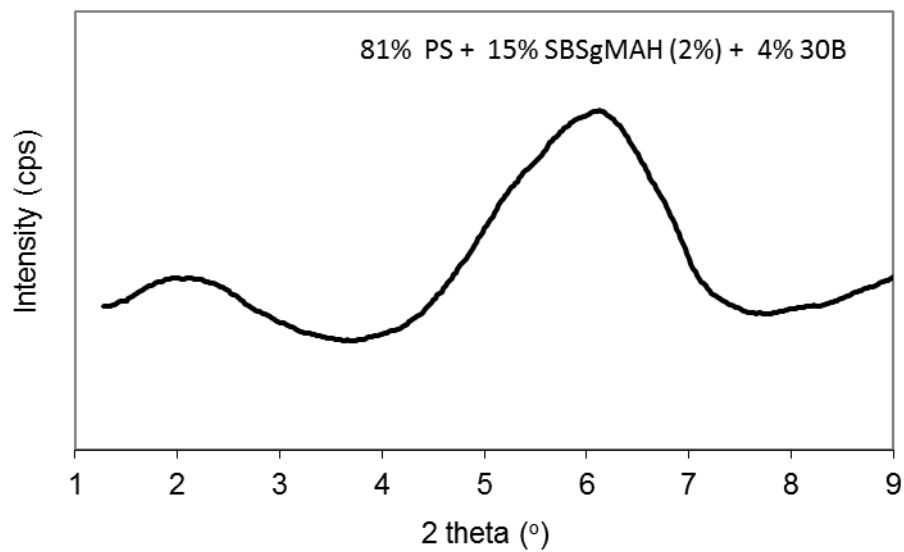
Figure A.39 XRD pattern of PS / 15% SBSgMAH (2%) / Cloisite ® 30B (4%) ternary nanocomposites
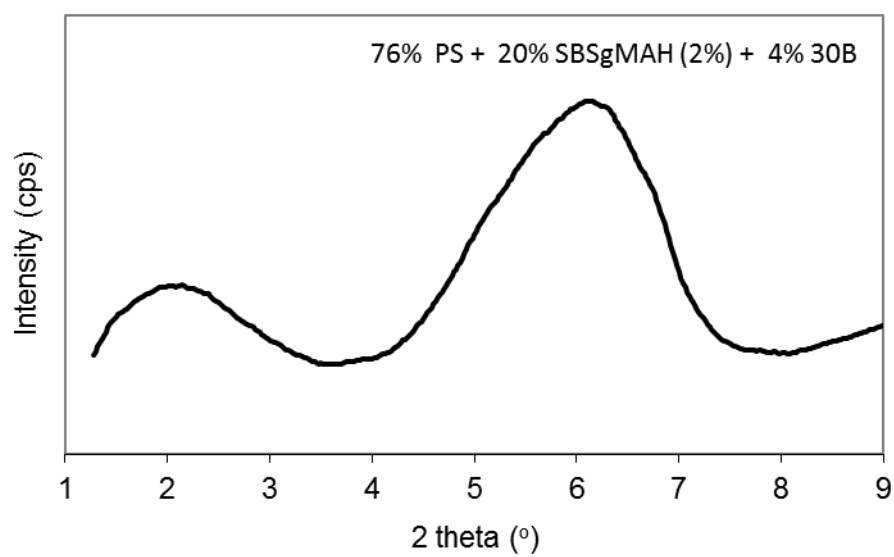

**Figure A.40** XRD pattern of PS / 20% SBSgMAH (2%) / Cloisite ® 30B (4%) ternary nanocomposites
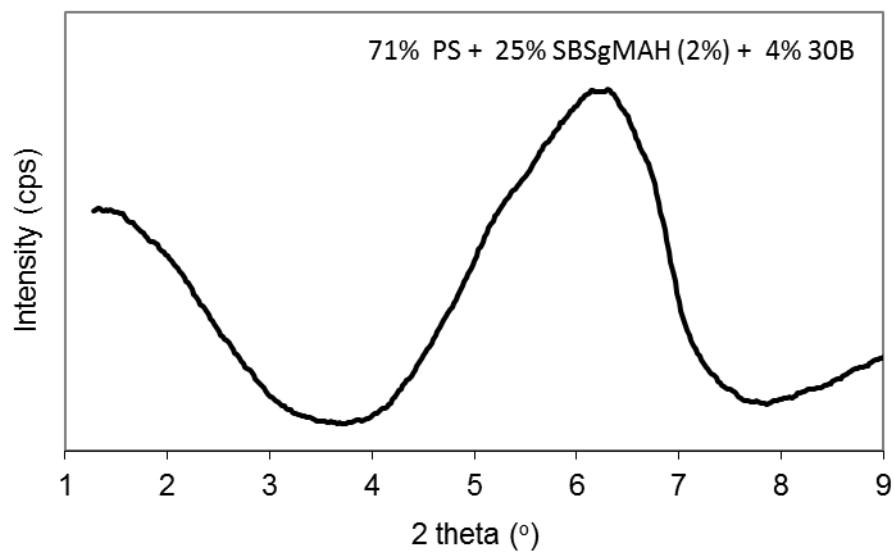
Figure A.41 XRD pattern of PS / 25% SBSgMAH (2%) / Cloisite ® 30B (4%) ternary nanocomposites

MECHANICAL PROPERTIES

Table B.1 Tensile strength (MPa) of all compositions

Composition	Concentration		Tensile Strength (MPa)	Standard deviation
	Elastomer (wt %)	Organoclay (wt %)		
PS	---	---	33.18	1.8
PS / Organoclay Binary Nanocomposites				
PS + 15A	---	2	30.82	0.7
PS + 25A	---	2	32.57	1.1
PS + 30B	---	2	34.29	1.2
PS + 30B	---	4	37.71	0.9
PS / Aliphatic Elastomer / Organoclay Ternary Nanocomposites				
PS + 2210 + 30B	5	2	29.52	1.7
PS + 8840 + 30B	5	2	32.24	1.3
PS + 8900 + 30B	5	2	37.14	0.9
PS + 2210 + 15A	5	2	32.98	1.6
PS + 8840 + 15A	5	2	32.36	1.5
PS + 8900 + 15A	5	2	33.35	2.1
PS + 2210 + 25A	5	2	30.88	1.8
PS + 8840 + 25A	5	2	30.11	1.9
PS + 8900 + 25A	5	2	33.18	1.4
PS / Aromatic Elastomer Binary Blends				
PS + SBS	5	---	41.18	2.1
PS + SBS	10	---	31.3	1.9
PS + SBS	15	---	27.02	1.3
PS + SBS	25	---	20.08	1.6
PS + SBS	40	---	15.89	2.3
PS + SBSgMAH (1%)	5	---	36.04	2.2
PS + SBSgMAH (1%)	10	---	27.91	1.8
PS + SBSgMAH (1%)	15	---	24.9	1.6

Table B.1 Tensile strength (MPa) of all compositions (continued)

PS + SBSgMAH (1%)	25	---	18.42	1.9
PS + SBSgMAH (1%)	40	---	12.93	1.8
PS + SBSgMAH (2%)	5	---	37.17	1.6
PS + SBSgMAH (2%)	10	---	25.42	1.1
PS + SBSgMAH (2%)	15	---	21.69	0.9
PS + SBSgMAH (2%)	25	---	15.96	1.8
PS + SBSgMAH (2%)	40	---	13.18	1.3
PS / Aromatic Elastomer / Organoclay Ternary Nanocomposites				
PS + SBS + 30B	5	2	43.81	1.2
PS + SBS + 30B	10	2	33.5	1.4
PS + SBS + 30B	15	2	27.78	2.1
PS + SBS + 30B	25	2	22.8	1.5
PS + SBS + 30B	40	2	15.7	1.9
PS+ SBSgMAH(1%) + 30B	5	2	40.16	1.6
PS+ SBSgMAH(1%) + 30B	10	2	34.67	2.3
PS+SBSgMAH(1%) + 30B	15	2	26.89	1.4
PS+SBSgMAH(1%) + 30B	25	2	22.23	2.1
PS+SBSgMAH(1%) + 30B	40	2	15.73	1.6
PS+ SBSgMAH(2%) + 30B	5	2	42.57	1.8
PS+ SBSgMAH(2%) + 30B	10	2	32.53	1.3
PS+SBSgMAH(2%) + 30B	15	2	26.47	0.9
PS+SBSgMAH(2%) + 30B	25	2	16.25	2.1
PS+SBSgMAH(2%) + 30B	40	2	14.51	1.6
PS + SBS + 30B	5	4	48.19	1.4
PS + SBS + 30B	10	4	36.85	1.6
PS + SBS + 30B	15	4	30.56	1.1
PS + SBS + 30B	25	4	25.08	1.3
PS+ SBSgMAH(2%) + 30B	5	4	47.68	1.1
PS+ SBSgMAH(2%) + 30B	10	4	36.43	1.8
PS+SBSgMAH(2%) + 30B	15	4	29.65	1.2
PS+SBSgMAH(2%) + 30B	25	4	18.2	1.4

Table B.2 Elongation at break (%) of all compositions

Composition	Concentration		Elong. at break (%)	Standard deviation
	Elastomer (wt %)	Organoclay (wt %)		
PS	---	---	1.112	0.08
PS / Organoclay Binary Nanocomposites				
PS + 15A	---	2	0.85	0.06
PS + 25A	---	2	0.95	0.07
PS + 30B	---	2	0.94	0.04
PS + 30B	---	4	0.87	0.12
PS / Aliphatic Elastomer / Organoclay Ternary Nanocomposites				
PS + 2210 + 30B	5	2	2.09	0.16
PS + 8840 + 30B	5	2	1.68	0.11
PS + 8900 + 30B	5	2	1.42	0.13
PS + 2210 + 15A	5	2	2.07	0.18
PS + 8840 + 15A	5	2	2.02	0.20
PS + 8900 + 15A	5	2	1.36	0.13
PS + 2210 + 25A	5	2	1.79	0.11
PS + 8840 + 25A	5	2	1.69	0.16
PS + 8900 + 25A	5	2	1.26	0.09
PS / Aromatic Elastomer Binary Blends				
PS + SBS	5	---	3.72	0.23
PS + SBS	10	---	6.33	0.31
PS + SBS	15	---	12.55	0.45
PS + SBS	25	---	14.82	0.51
PS + SBS	40	---	15.86	0.87
PS + SBSgMAH (1%)	5	---	2.46	0.09
PS + SBSgMAH (1%)	10	---	2.38	0.11
PS + SBSgMAH (1%)	15	---	15.42	0.32
PS + SBSgMAH (1%)	25	---	18.86	0.76
PS + SBSgMAH (1%)	40	---	21.86	0.81
PS + SBSgMAH (2%)	5	---	2.74	0.30
PS + SBSgMAH (2%)	10	---	4.17	0.45
PS + SBSgMAH (2%)	15	---	8.10	0.41
PS + SBSgMAH (2%)	25	---	9.40	0.63
PS + SBSgMAH (2%)	40	---	20.73	1.09

Table B.2 Elongation at break (%) of all compositions (continued)

PS / Aromatic Elastomer / Organoclay Ternary Nanocomposites				
PS + SBS + 30B	5	2	4.12	0.73
PS + SBS + 30B	10	2	10.53	0.96
PS + SBS + 30B	15	2	16.33	1.03
PS + SBS + 30B	25	2	16.34	1.11
PS + SBS + 30B	40	2	17.12	0.98
PS+ SBSgMAH(1%) + 30B	5	2	2.10	0.31
PS+ SBSgMAH(1%) + 30B	10	2	10.15	1.10
PS+SBSgMAH(1%) + 30B	15	2	16.8	1.21
PS+SBSgMAH(1%) + 30B	25	2	21.46	1.63
PS+SBSgMAH(1%) + 30B	40	2	24.16	1.87
PS+ SBSgMAH(2%) + 30B	5	2	2.16	0.23
PS+ SBSgMAH(2%) + 30B	10	2	7.52	0.74
PS+SBSgMAH(2%) + 30B	15	2	16.88	1.52
PS+SBSgMAH(2%) + 30B	25	2	18.28	1.71
PS+SBSgMAH(2%) + 30B	40	2	23.01	1.93
PS + SBS + 30B	5	4	3.77	0.51
PS + SBS + 30B	10	4	9.64	1.23
PS + SBS + 30B	15	4	14.94	1.64
PS + SBS + 30B	25	4	14.95	1.42
PS+ SBSgMAH(2%) + 30B	5	4	2.00	0.16
PS+ SBSgMAH(2%) + 30B	10	4	6.95	0.85
PS+SBSgMAH(2%) + 30B	15	4	15.61	1.23
PS+SBSgMAH(2%) + 30B	25	4	16.91	1.11

Table B.3 Young's modulus (MPa) of all compositions

Composition	Concentration		Young's Modulus (MPa)	Standard deviation
	Elastomer (wt %)	Organoclay (wt %)		
PS	---	---	1695	156
PS / Organoclay Binary Nanocomposites				
PS + 15A	---	2	1775	125
PS + 25A	---	2	1872	117
PS + 30B	---	2	1905	164

Table B.3 Young's modulus (MPa) of all compositions (continued)

PS + 30B	---	4	2067	141
PS / Aliphatic Elastomer / Organoclay Ternary Nanocomposites				
PS + 2210 + 30B	5	2	1170	98
PS + 8840 + 30B	5	2	1353	106
PS + 8900 + 30B	5	2	1533	112
PS + 2210 + 15A	5	2	1283	128
PS + 8840 + 15A	5	2	1244	109
PS + 8900 + 15A	5	2	1487	118
PS + 2210 + 25A	5	2	1230	93
PS + 8840 + 25A	5	2	1988	175
PS + 8900 + 25A	5	2	1516	118
PS / Aromatic Elastomer Binary Blends				
PS + SBS	5	---	2469	187
PS + SBS	10	---	2477	173
PS + SBS	15	---	2362	168
PS + SBS	25	---	2173	161
PS + SBS	40	---	1575	141
PS + SBSgMAH (1%)	5	---	2410	181
PS + SBSgMAH (1%)	10	---	2279	163
PS + SBSgMAH (1%)	15	---	2313	166
PS + SBSgMAH (1%)	25	---	1985	184
PS + SBSgMAH (1%)	40	---	1360	135
PS + SBSgMAH (2%)	5	---	2498	183
PS + SBSgMAH (2%)	10	---	2226	112
PS + SBSgMAH (2%)	15	---	2102	117
PS + SBSgMAH (2%)	25	---	1918	161
PS + SBSgMAH (2%)	40	---	1551	145
PS / Aromatic Elastomer / Organoclay Ternary Nanocomposites				
PS + SBS + 30B	5	2	2481	133
PS + SBS + 30B	10	2	2613	175
PS + SBS + 30B	15	2	2438	143
PS + SBS + 30B	25	2	2117	155
PS + SBS + 30B	40	2	1501	132
PS+ SBSgMAH(1%) + 30B	5	2	2583	189
PS+ SBSgMAH(1%) + 30B	10	2	2424	119
PS+SBSgMAH(1%) + 30B	15	2	2101	112
PS+SBSgMAH(1%) + 30B	25	2	1879	145

Table B.3 Young's modulus (MPa) of all compositions (continued)

PS+SBSgMAH(1%) + 30B	40	2	1418	102
PS+ SBSgMAH(2%) + 30B	5	2	2612	144
PS+ SBSgMAH(2%) + 30B	10	2	2456	132
PS+SBSgMAH(2%) + 30B	15	2	2304	128
PS+SBSgMAH(2%) + 30B	25	2	1846	136
PS+SBSgMAH(2%) + 30B	40	2	1525	118
PS + SBS + 30B	5	4	2691	188
PS + SBS + 30B	10	4	2835	137
PS + SBS + 30B	15	4	2645	143
PS + SBS + 30B	25	4	2296	154
PS+ SBSgMAH(2%) + 30B	5	4	2905	191
PS+ SBSgMAH(2%) + 30B	10	4	2731	146
PS+SBSgMAH(2%) + 30B	15	4	2562	119
PS+SBSgMAH(2%) + 30B	25	4	2053	120

Table B.4 Impact strength (kJ/mm^2) of all compositions

Composition	Concentration		Impact strength (kJ/mm^2)	Standard deviation
	Elastomer (wt %)	Organoclay (wt %)		
PS	---	---	7.80	0.36
PS / Organoclay Binary Nanocomposites				
PS + 15A	---	2	5.41	0.31
PS + 25A	---	2	4.13	0.33
PS + 30B	---	2	4.57	0.25
PS + 30B	---	4	3.89	0.27
PS / Aliphatic Elastomer / Organoclay Ternary Nanocomposites				
PS + 2210 + 30B	5	2	9.59	1.02
PS + 8840 + 30B	5	2	8.33	0.78
PS + 8900 + 30B	5	2	10.83	1.09
PS + 2210 + 15A	5	2	8.04	0.65
PS + 8840 + 15A	5	2	8.01	0.74
PS + 8900 + 15A	5	2	8.57	0.41
PS + 2210 + 25A	5	2	8.71	0.82
PS + 8840 + 25A	5	2	7.45	0.64
PS + 8900 + 25A	5	2	10.89	0.97
PS / Aromatic Elastomer Binary Blends				
PS + SBS	5	---	2.17	0.21
PS + SBS	10	---	4.00	0.32
PS + SBS	15	---	4.81	0.51
PS + SBS	25	---	8.38	0.36
PS + SBS	40	---	5.54	0.38
PS + SBSgMAH (1%)	5	---	9.03	0.84
PS + SBSgMAH (1%)	10	---	8.39	0.93
PS + SBSgMAH (1%)	15	---	9.64	0.74
PS + SBSgMAH (1%)	25	---	9.83	0.69
PS + SBSgMAH (1%)	40	---	9.71	0.54
PS + SBSgMAH (2%)	5	---	5.2	0.39
PS + SBSgMAH (2%)	10	---	8.37	0.74
PS + SBSgMAH (2%)	15	---	9.31	0.86
PS + SBSgMAH (2%)	25	---	8.14	0.72
PS + SBSgMAH (2%)	40	---	9.27	0.69

Table B.4 Impact strength (kJ/mm^2) of all compositions (continued)

PS / Aromatic Elastomer / Organoclay Ternary Nanocomposites				
PS + SBS + 30B	5	2	4.70	0.41
PS + SBS + 30B	10	2	5.36	0.5
PS + SBS + 30B	15	2	4.81	0.41
PS + SBS + 30B	25	2	10.31	1.16
PS + SBS + 30B	40	2	8.51	0.79
PS+ SBSgMAH(1%) + 30B	5	2	9.57	0.86
PS+ SBSgMAH(1%) + 30B	10	2	10.35	0.99
PS+SBSgMAH(1%) + 30B	15	2	10.42	1.10
PS+SBSgMAH(1%) + 30B	25	2	11.24	1.23
PS+SBSgMAH(1%) + 30B	40	2	10.79	1.19
PS+ SBSgMAH(2%) + 30B	5	2	6.43	0.54
PS+ SBSgMAH(2%) + 30B	10	2	9.38	0.77
PS+SBSgMAH(2%) + 30B	15	2	10.26	0.69
PS+SBSgMAH(2%) + 30B	25	2	12.86	1.36
PS+SBSgMAH(2%) + 30B	40	2	10.53	1.15
PS + SBS + 30B	5	4	4.28	0.18
PS + SBS + 30B	10	4	5.14	0.76
PS + SBS + 30B	15	4	4.32	0.27
PS + SBS + 30B	25	4	9.18	1.01
PS + SBS + 30B	40	4	10.36	1.13
PS+ SBSgMAH(2%) + 30B	5	4	5.98	0.83
PS+ SBSgMAH(2%) + 30B	10	4	8.82	1.06
PS+SBSgMAH(2%) + 30B	15	4	9.95	1.17
PS+SBSgMAH(2%) + 30B	20	4	11.83	1.32
PS+SBSgMAH(2%) + 30B	25	4	13.65	1.24

APPENDIX C

DIFFERENTIAL SCANNING CALORIMETRY THERMOGRAMS
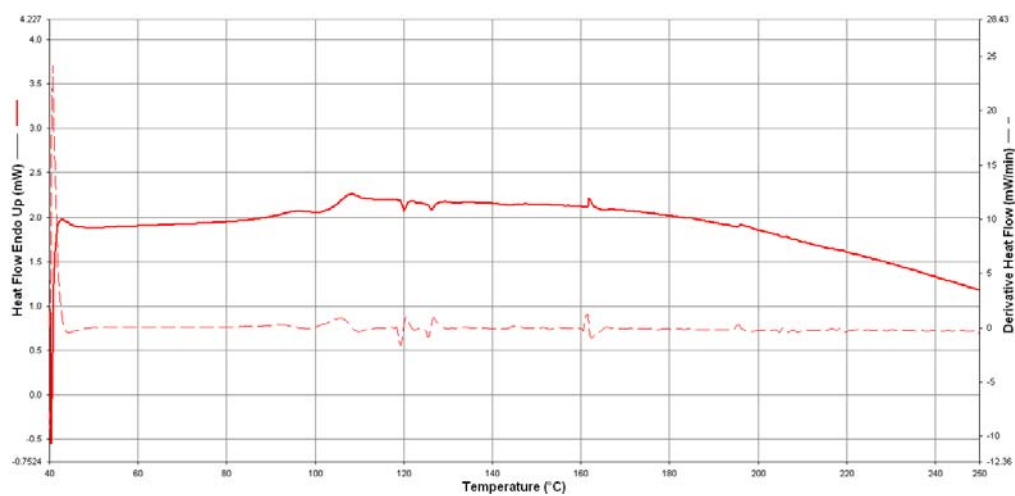
Figure C.1 DSC thermogram of PS
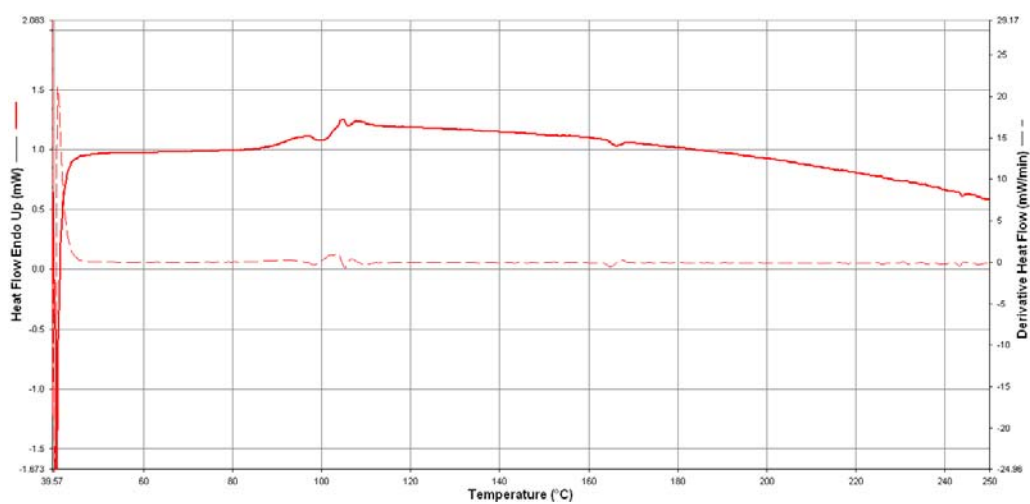
Figure C.2 DSC thermogram of PS / Cloisite ® 15A (2%) binary nanocomposite
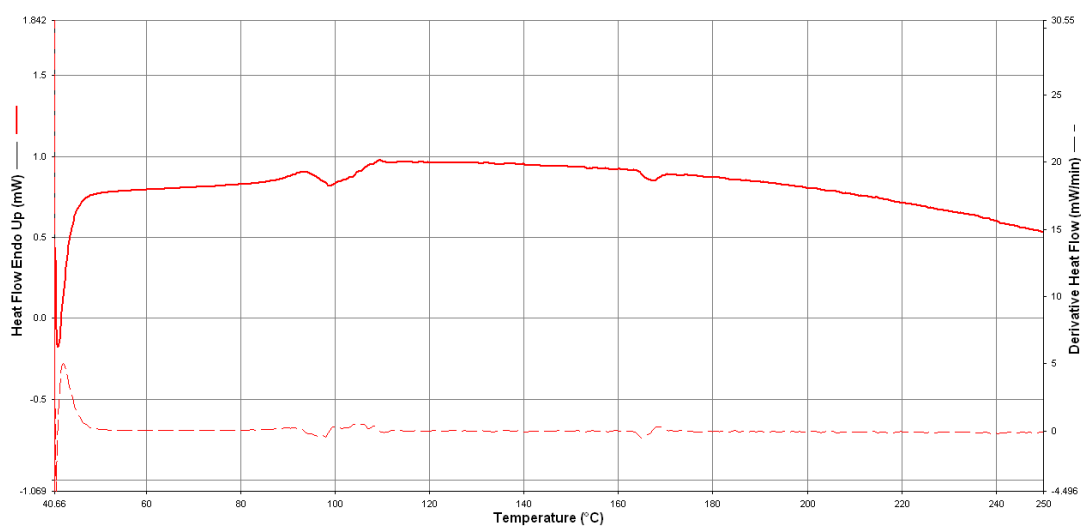
Figure C.3 DSC thermogram of PS / Cloisite ® 25A (2%) binary nanocomposite
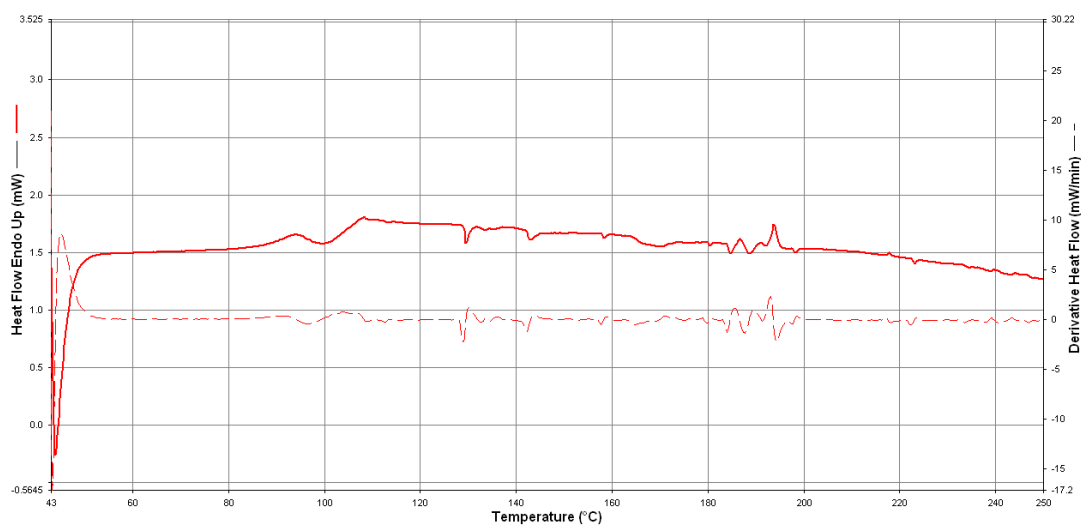
Figure C.4 DSC thermogram of PS / Cloisite ® 30B (2%) binary nanocomposite

177
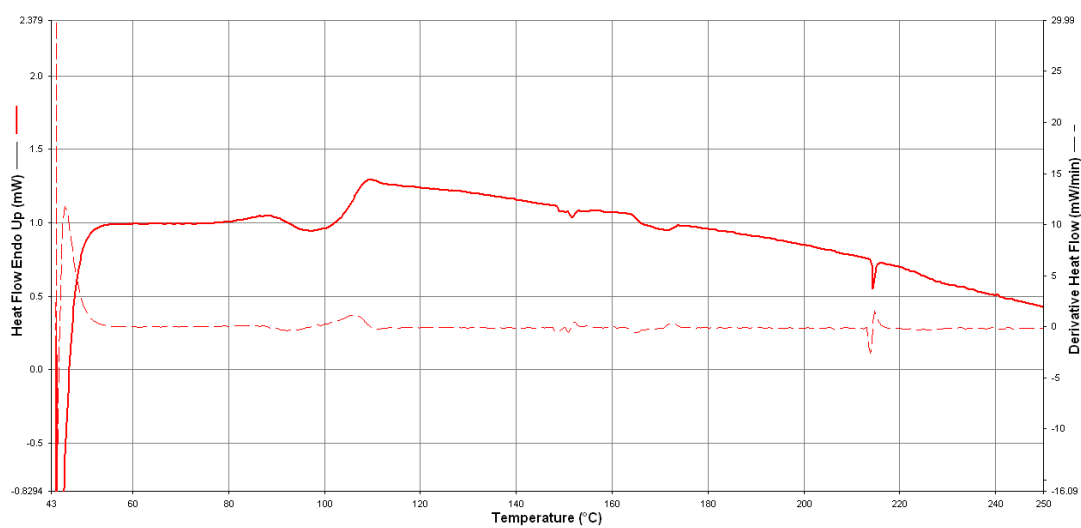
**Figure C.5** DSC thermogram of PS / Cloisite ® 30B (4%) binary nanocomposite
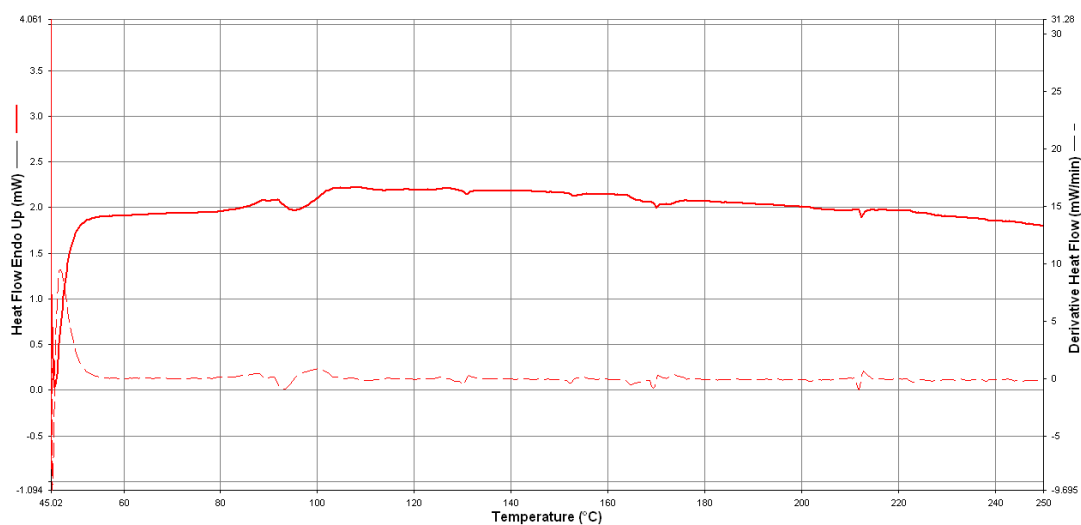

Figure C.6 DSC thermogram of PS / Cloisite ® 30B (2%) / Lotader 8900 (5%) ternary nanocomposite
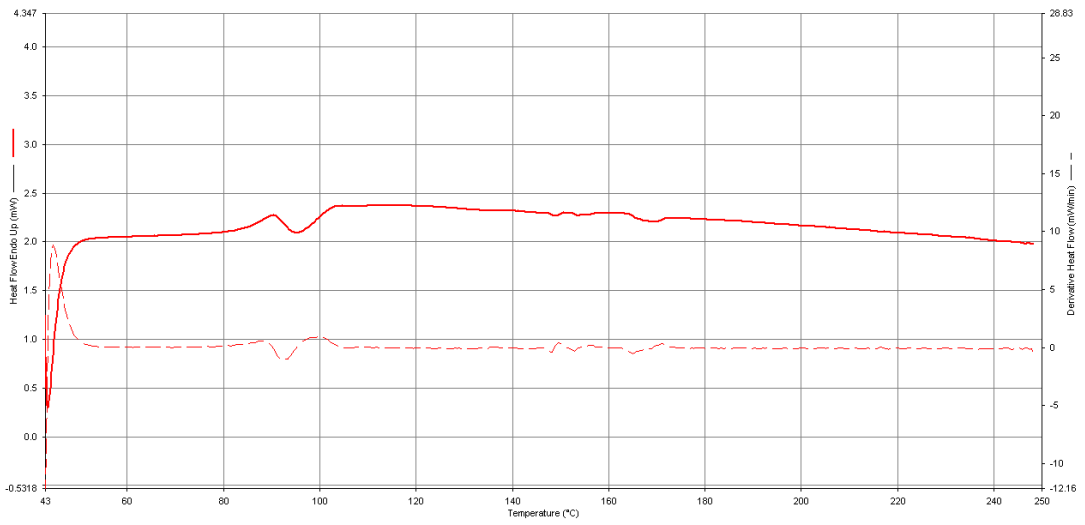
Figure C.7 DSC thermogram of PS / Cloisite ® 30B (2%) / Lotader 8840 (5%) ternary nanocomposite
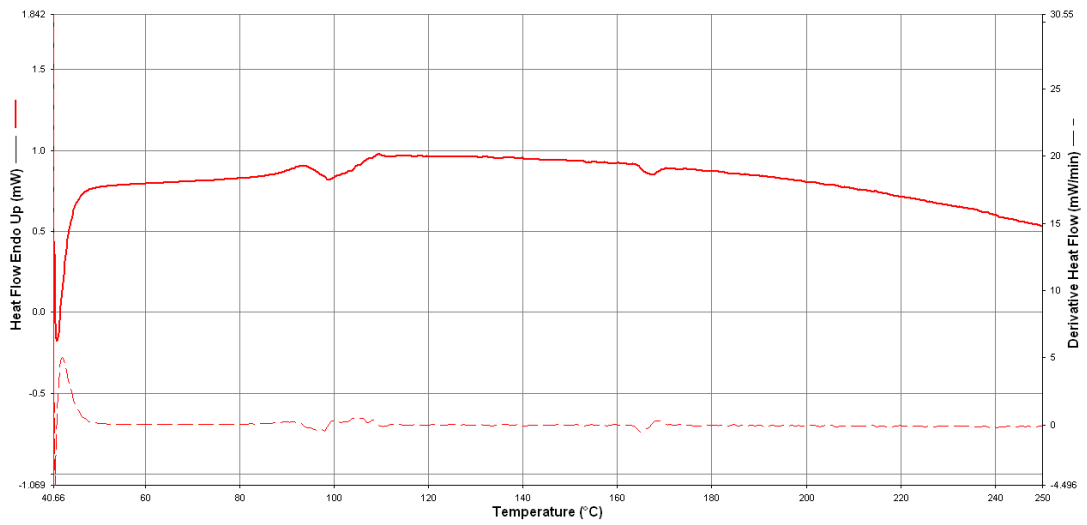
Figure C.8 DSC thermogram of PS / Cloisite ® 30B (2%) / Lotader 2210 (5%) ternary nanocomposite
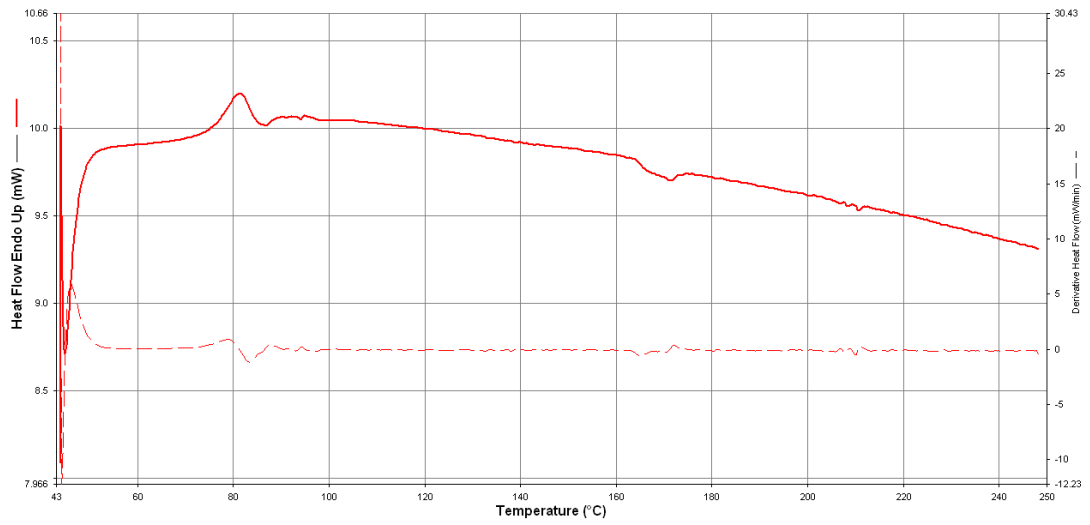
Figure C.9 DSC thermogram of PS / SBS (5%) binary blend
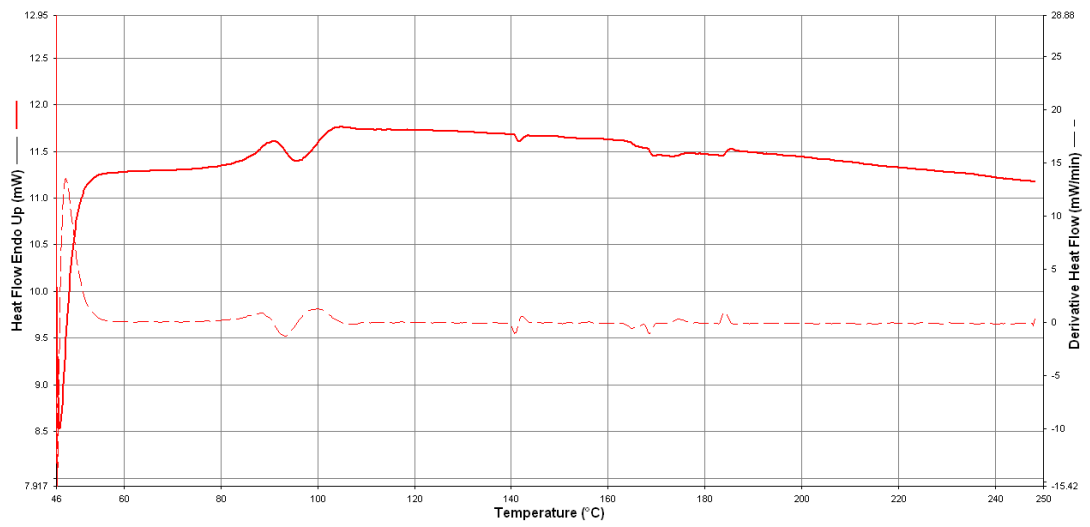
Figure C.10 DSC thermogram of PS / SBS (25%) binary blend
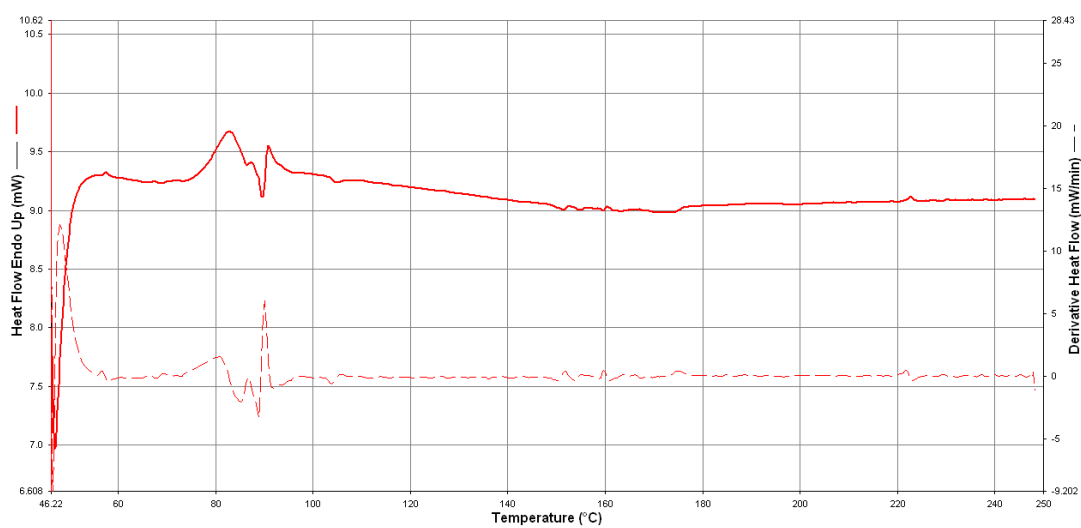
Figure C.11 DSC thermogram of PS / SBSgMAH (1%) (5%) binary blend
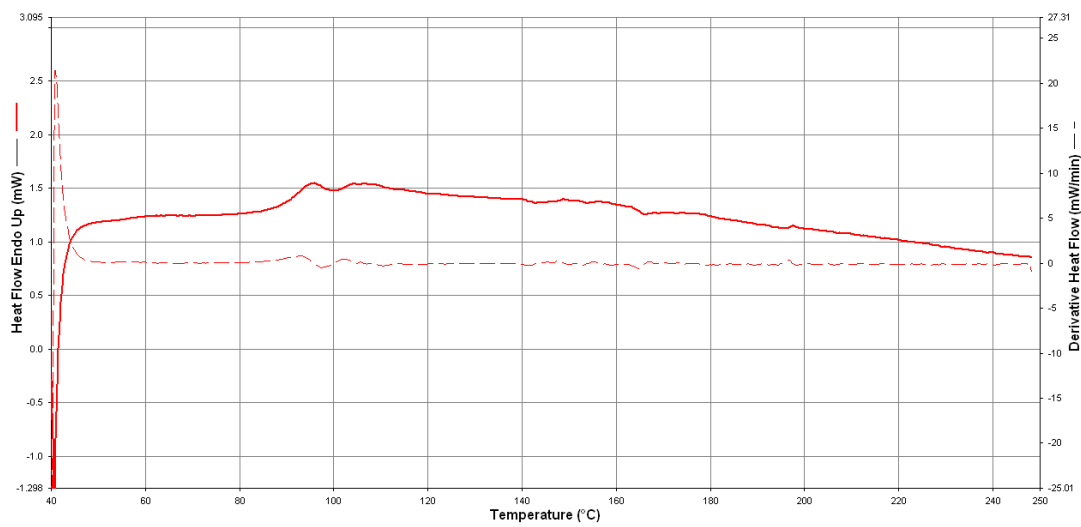
Figure C.12 DSC thermogram of PS / SBSgMAH (1%) (25%) binary blend
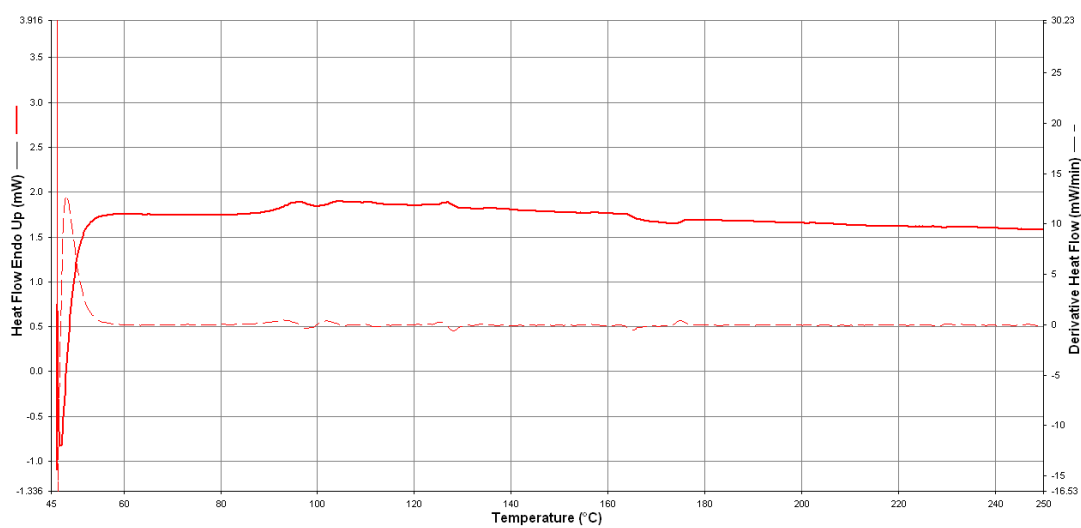
Figure C.13 DSC thermogram of PS / SBSgMAH (2%) (5%) binary blend
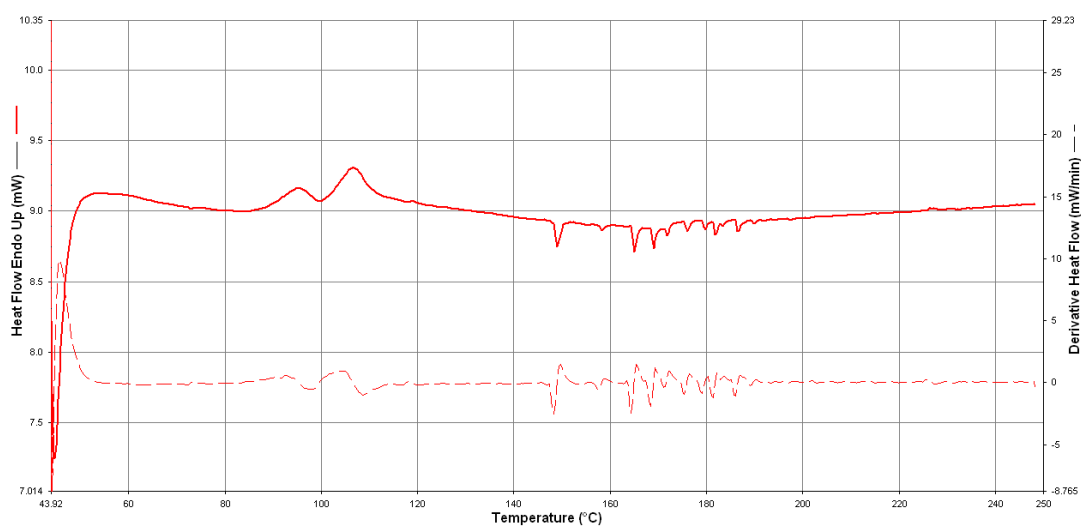
Figure C.14 DSC thermogram of PS / SBSgMAH (2%) (25%) binary blend

182
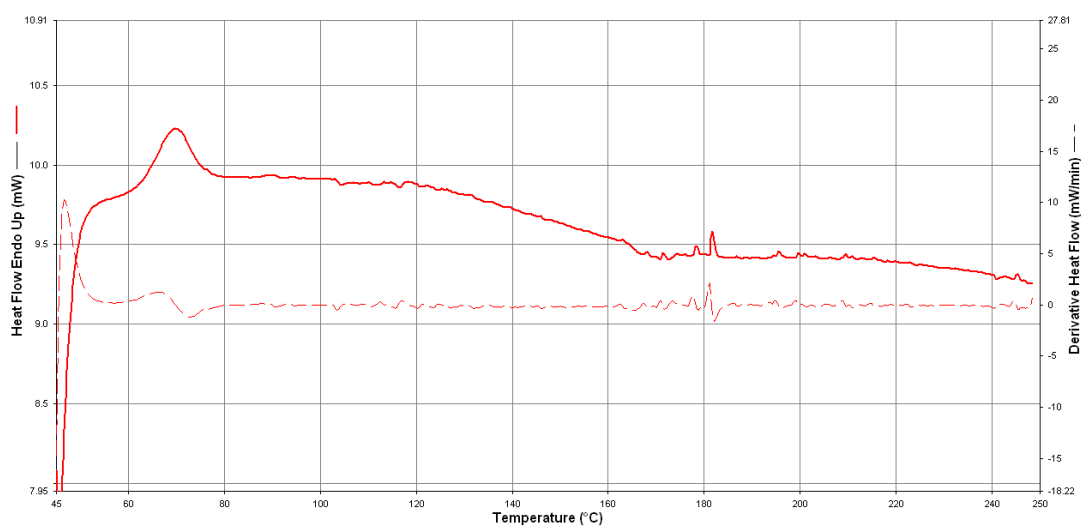
Figure C.15 DSC thermogram of PS / Cloisite ® 30B (2%) / SBS (5%) ternary nanocomposite
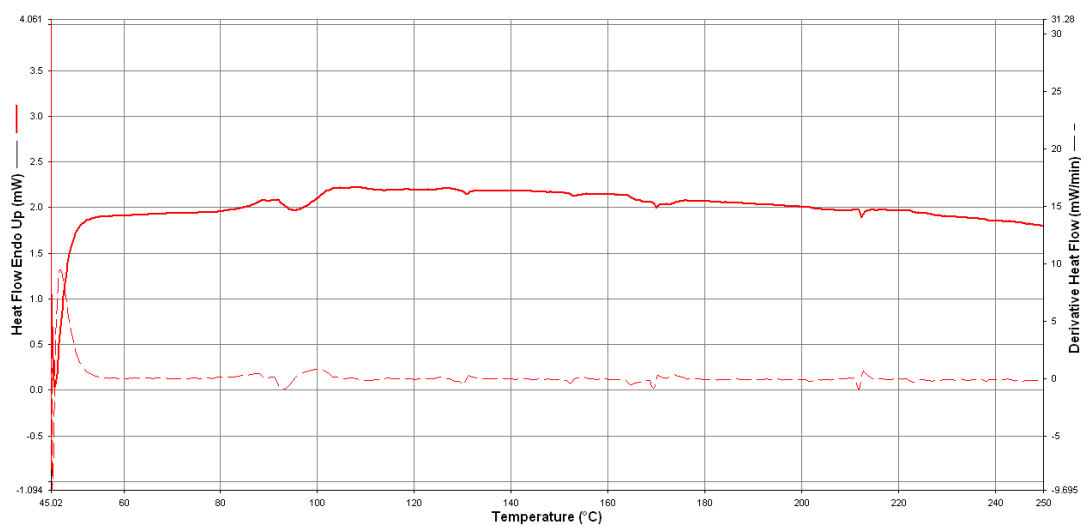
Figure C.16 DSC thermogram of PS / Cloisite ® 30B (2%) / SBS (25%) ternary nanocomposite
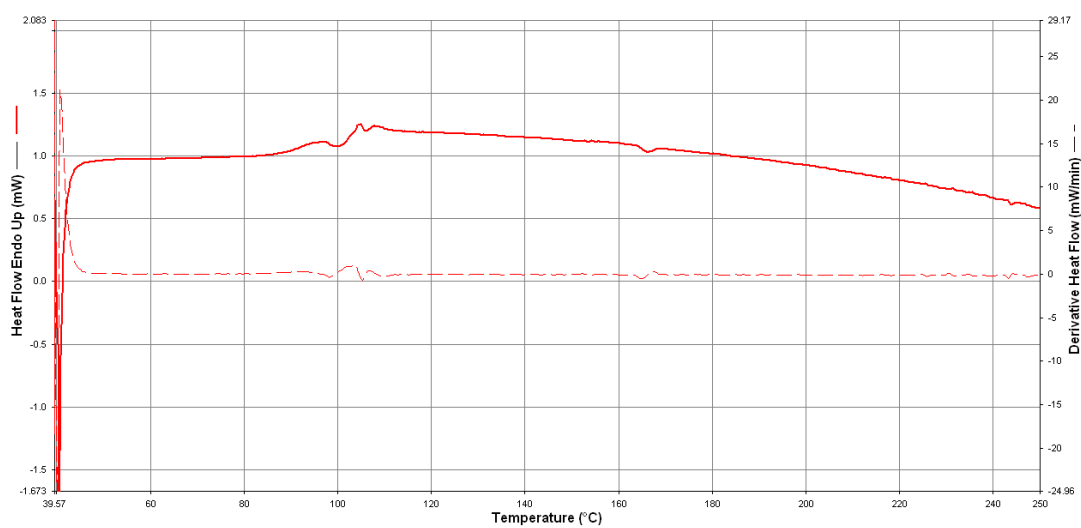
Figure C.17 DSC thermogram of PS / Cloisite ® 30B (4%) / SBS (5%) ternary nanocomposite
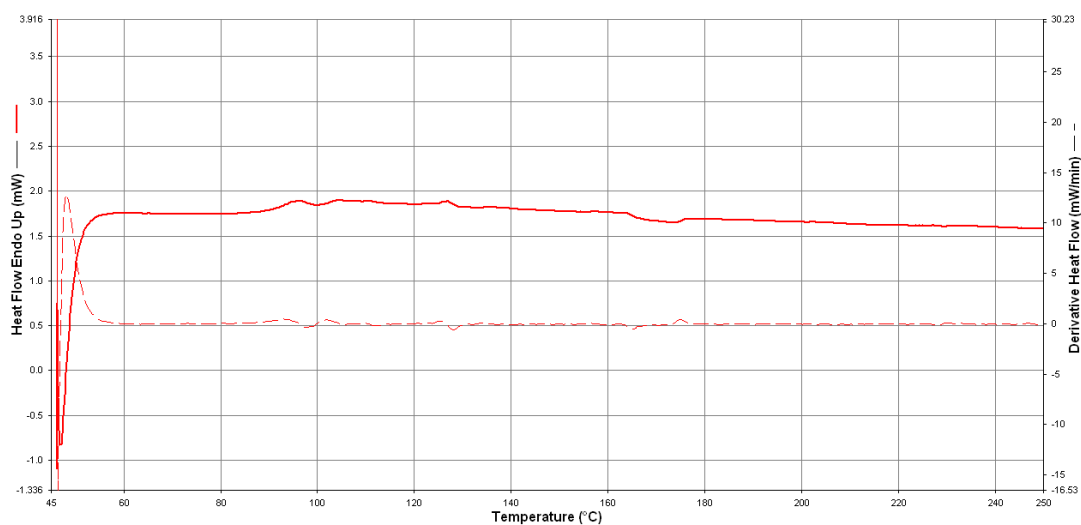

**Figure C.18** DSC thermogram of PS / Cloisite ® 30B (4%) / SBS (25%) ternary nanocomposite
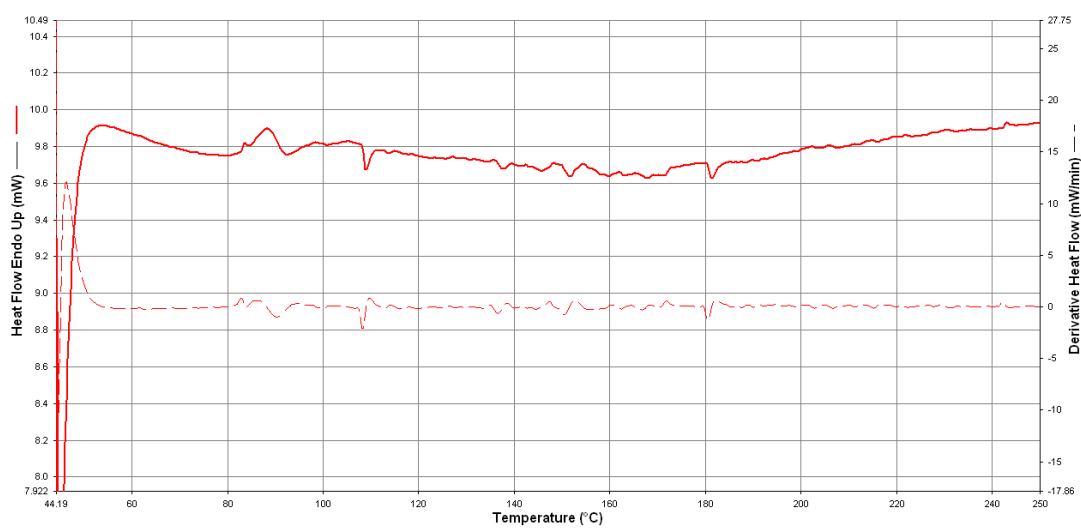
Figure C.19 DSC thermogram of PS / Cloisite ® 30B (2%) / SBSgMAH (1%) (5%) ternary nanocomposite
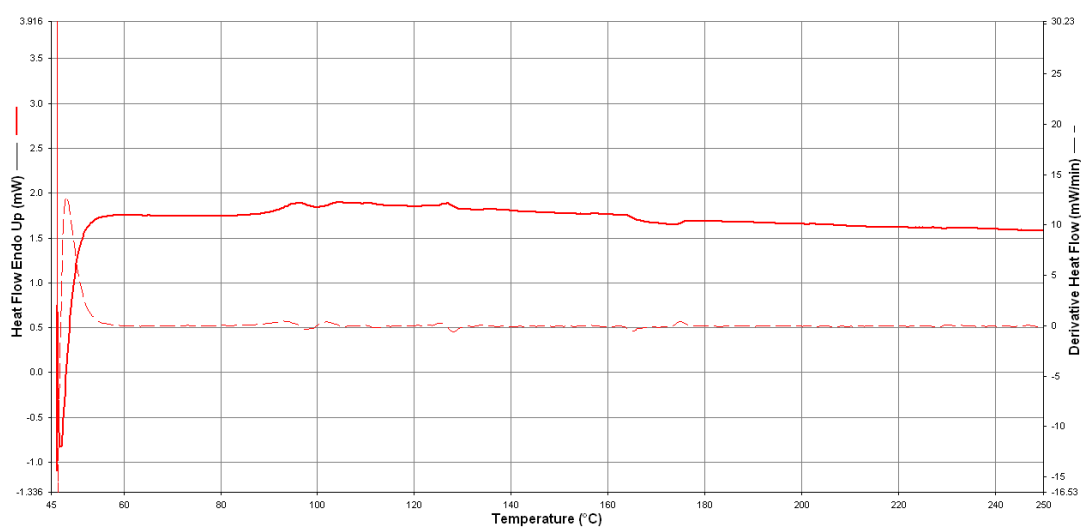

Figure C.20 DSC thermogram of PS / Cloisite ® 30B (2%) / SBSgMAH (1%) (25%) ternary nanocomposite
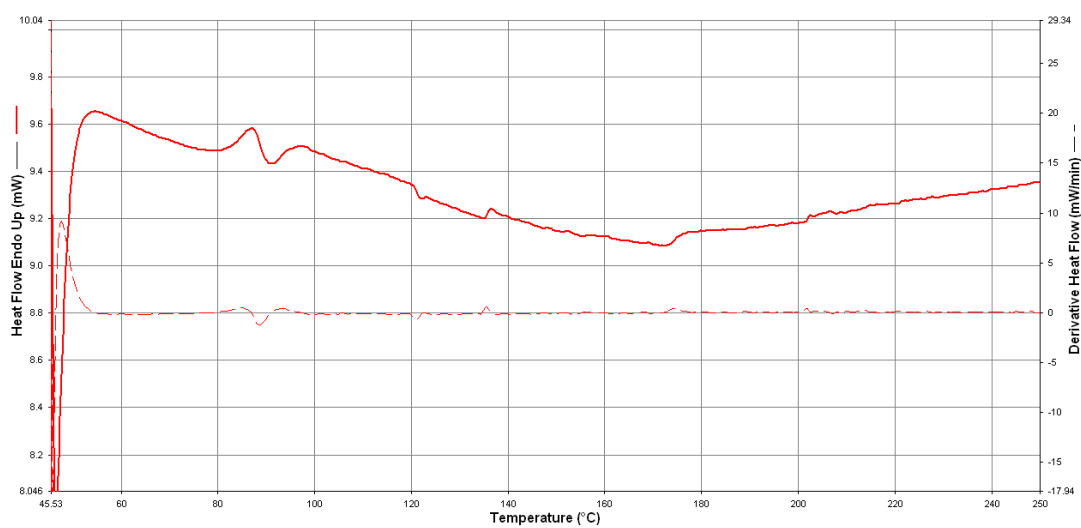
Figure C.21 DSC thermogram of PS / Cloisite ® 30B (2%) / SBSgMAH (2%((5%) ternary nanocomposite
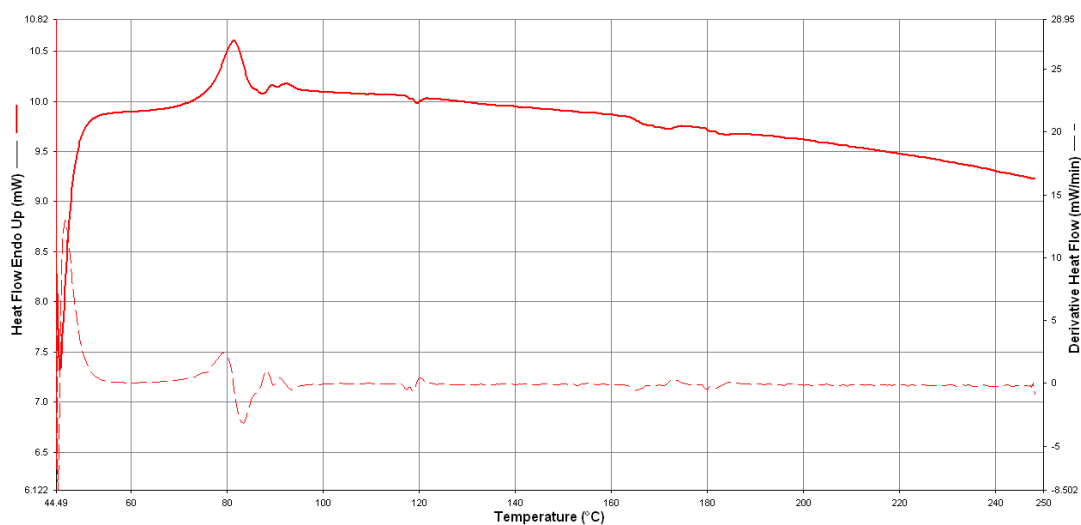

Figure C.22 DSC thermogram of PS / Cloisite ® 30B (2%) / SBSgMAH (2%((25%) ternary nanocomposite
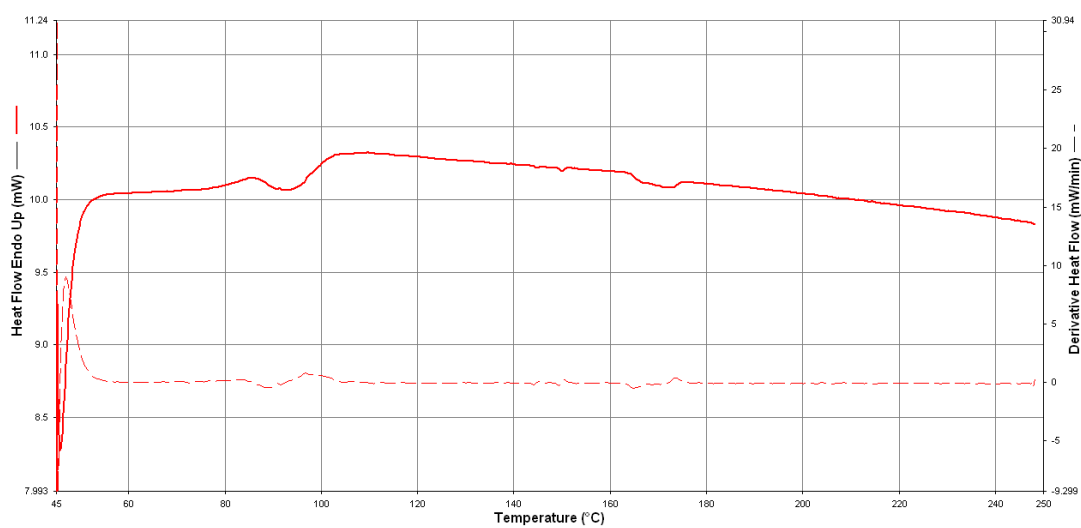
**Figure C.23** DSC thermogram of PS / Cloisite ® 30B (4%) / SBSgMAH (2%((5%) ternary nanocomposite
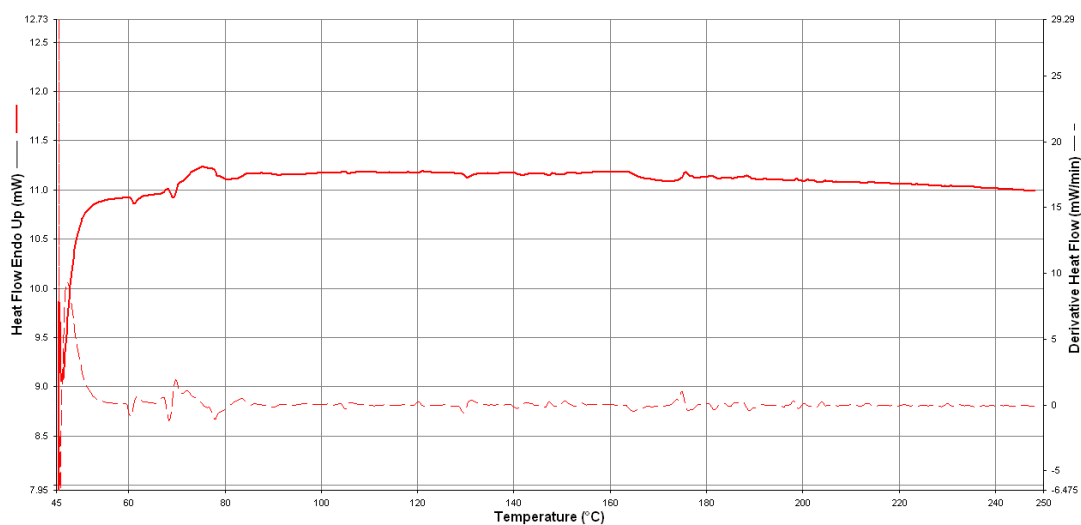
Figure C.24 DSC thermogram of PS / Cloisite ® 30B (4%) / SBSgMAH (2%((25%) ternary nanocomposite

APPENDIX D

DETERMINATION OF MALEIC ANHYDRIDE CONTENT

Maleic anhydride content of SBSgMAH (1%) and SBSgMAH (2%) were determined by the back titration method. 1.0 g of purified sample was dissolved in 100 mL chloroform, and then 50 mL ethanol solution of KOH (0.5 mol/L) was added. The mixed solution was refluxed for 60 minutes with stirring, and then back titrated with 0.1 M HCl, with bromothymol blue as an indicator. Content of maleic anhydride as a percentage of SBS was calculated by following equation.

$$MAH\% = (V_0-V_1) \times 10^{-3} \times C \times M \times (2W)^{-1} \times 100$$

where V_0 is the amount of HCl consumed by using pure SBS as reference (mL), V_1 is the amount of HCl consumed by the grafted sample (mL), C is the molar concentration of HCl (mol/L), M is the molecular weight of maleic anhydride, and W is the weight of sample (g).

HCl Consumed for %2 SBSgMAH = 1 ml (V_1)
HCl Consumed for %1 SBSgMAH = 3 ml (V_1)
HCl Consumed for pure SBS = 5 ml (V_0)

According to this procedure and values, maleic anhydride contents of SBSgMAH (1%) and SBSgMAH (2%) were found as 0.98% and 1.96%, respectively.

CURRICULUM VITAE

PERSONAL INFORMATION

Name & Surname	**:** Ali Sinan Dike
Nationality	**:** Turkish
Date and Place of Birth	**:** 28.12. 1975 - Kırıkhan

EDUCATION

Degree	Institution	Year
Ph.D.	METU, Polymer Science and Technology	2011
B.Sc.	Atatürk Univ. Chemical Engineering	2000
High School	Kırıkhan Lisesi	1992

WORK EXPERIENCE

Place	Position	Year
METU, Dept. of Polymer Sci. & Tech.	Research Asistant	2003-2011
Atatürk.Univ. Dept. of Metallurgical & Materials Eng.	Research Asistant	2002-2003
SETAŞ Kimya A.Ş.	Chemical Engineer	2001-2002

FOREIGN LANGUAGE

English